Phase Equilibria Measurements and Modelling of CO_2–Rich Fluids/Brine Systems

By

Seyed Ramin Mousavi Belfeh Teymouri

Submitted for the Degree of Doctor of Philosophy in Petroleum Engineering

Heriot-Watt University
Institute of Petroleum Engineering
School of Energy, Geoscience, Infrastructure and Society

September 2016

ABSTRACT

An attractive option for reducing the emissions of CO_2 to the atmosphere is CCS[1] processes which is capturing and transporting the captured CO_2 to large storage sites, e.g., saline aquifers. However, to achieve this goal there are several economic barriers and challenging engineering problems that cannot be taken care of without having a precise knowledge of thermo-physical properties of such systems. Robust models validated with precise experimental data are probably the most important part of the above-mentioned knowledge.

In this study the PC-SAFT equation of state was applied to calculate thermo-physical properties and phase equilibria of CCS and flow assurance systems of interest. The model was tuned for numerous binary systems containing common gases and hydrocarbons by adjusting the BIPs[2] to experimental VLE or LLE[3] data. The PC-SAFT pure compound parameters of water, glycols and alcohol were also optimised using saturation data and their BIPs with non-polar substances were adjusted to experimental data. Second order derivatives of the PC-SAFT model contributions to Helmholtz free energy were also derived analytically to calculate second order thermodynamics properties of a few pure compounds.

To experimentally study the phase equilibria of CO_2-brine systems, solubilities of CO_2 in different concentrations of NaCl, KCl, $CaCl_2$ and $MgCl_2$ aqueous solutions were measured over a wide range of temperatures and pressures. The water content of CO_2-rich phases in equilibrium with sodium chloride aqueous solutions and pure water were also measured over a broad range of temperature and pressures up to 550 bar. To validate the experimental data, the CPA[4] and the PC-SAFT equation of states were tuned to literature data and the developed model calculations were compared with the experimental data measured in this work.

[1] Carbon Capture and Storage
[2] Binary Interaction Parameter
[3] Vapour-Liquid or Liquid-Liquid Equilibria
[4] Cubic Plus Association equation of state

Dedicated to my beloved mother *Zahra* and father *Sadegh*.

I will always remember how much you love me and how much you support me.

ACKNOWLEDGMENTS

This thesis is submitted in partial fulfilment of the requirements for the Ph.D. degree at Heriot-Watt University. This research work has been conducted at the Institute of Petroleum from November 2012 to November 2016 under the supervision of Professor Bahman Tohidi, Dr Antonin Chapoy and Dr Rod Burgass.

The project has been financed by grants by a Joint Industrial Project (JIP) conducted at the Institute of Petroleum Engineering, Heriot-Watt University which is gratefully acknowledged.

I would like to express my sincere gratitude to Professor Bahman Tohidi who gave me this opportunity to be a part of his esteem research team in Centre for Gas Hydrate and Flow Assurance group and his advisory comments and suggestions are gratefully appreciated. I also would like to thank Dr Antonin Chapoy for his continuous help and great advices during my studies specially his ideas and support on the modelling part of my PhD. Special thanks to Dr Rod Burgass for his great help and support in the laboratory. His valuable ideas, comments and suggestions through this work are gratefully appreciated. I wish to express my thanks to all the staff of Institute of Petroleum Engineering, Heriot-Watt University.

At the end but not at the least, words cannot express my respect and gratitude to my beloved parents for all their sacrifices and help. My beloved father who passed away and was always the greatest help, reliance and inspiration in my life. Countless and infinite thanks and appreciation to my dear mother whose love, patience and support made me whole. This was not possible without their help and efforts.

ACADEMIC REGISTRY

Research Thesis Submission

Name*:*	Seyed Ramin Mousavi Belfeh Teymouri		
School:	EGIS / Institute of Petroleum Engineering		
Version: *(i.e. First, Resubmission, Final)*		Degree Sought:	PhD of Petroleum Engineering

Declaration

In accordance with the appropriate regulations I hereby submit my thesis and I declare that:

1) the thesis embodies the results of my own work and has been composed by myself
2) where appropriate, I have made acknowledgement of the work of others and have made reference to work carried out in collaboration with other persons
3) the thesis is the correct version of the thesis for submission and is the same version as any electronic versions submitted*.
4) my thesis for the award referred to, deposited in the Heriot-Watt University Library, should be made available for loan or photocopying and be available via the Institutional Repository, subject to such conditions as the Librarian may require
5) I understand that as a student of the University I am required to abide by the Regulations of the University and to conform to its discipline.
6) I confirm that the thesis has been verified against plagiarism via an approved plagiarism detection application e.g. Turnitin.

* *Please note that it is the responsibility of the candidate to ensure that the correct version of the thesis is submitted.*

Signature of Candidate*:*		Date:	

Submission

Submitted By *(name in capitals):*	SEYED RAMIN MOUSAVI BELFEH TEYMOURI
Signature of Individual Submitting:	
Date Submitted:	

For Completion in the Student Service Centre (SSC)

Received in the SSC by *(name in capitals):*			
Method of Submission *(Handed in to SSC; posted through internal/external mail):*			
*E-thesis Submitted (**mandatory for final theses)***			
Signature:		Date	

Please note this form should be bound into the submitted thesis.

Table of Contents

List of Figures

List of Tables

List of publications under preparation by the candidate

1- R.Mousavi, A.Chapoy and B.Tohidi, “Phase equilibria modelling of glycol containing systems using PC-SAFT equation of state”.

2- R.Mousavi, A.Chapoy and B.Tohidi, “Application of PC-SAFT equation of state in phase equilibria modelling of alcohol containing systems”.

3- R.Mousavi, A.Chapoy, R.Burgass and B.Tohidi, “Phase equilibria modelling and measurements of CO_2 and aqueous solutions of NaCl at temperatures below 25 °C”.

4- R.Mousavi, A.Chapoy, R.Burgass and B.Tohidi, “Phase equilibria modelling and measurements of CO_2 and aqueous solutions of KCl, $CaCl_2$ and $MgCl_2$ at elevated temperatures and pressures”.

5- R.Mousavi, A.Chapoy and B.Tohidi, “Application of PC-SAFT equation of state in calculating the second derivative properties”.

List of Symbols

A	Helmholtz free energy	J
A^r	Residual Helmholtz free energy	J
A^{ideal}	Helmholtz free energy of ideal gas	J
a^{res}	Molar residual Helmholtz free energy	J/mol
a_{01}, a_{02}, a_{03}	Model Constants defined in Eq. 2.17	-
b_{01}, b_{02}, b_{03}	Model Constants defined in Eq. 2.18	-
$a_{01,x_i}, a_{02,x_i}, a_{03,x_i}$	Model Constant derivatives defined in Eq. 2.51	-
A^{DH}	Debye-Hückel model parameter defined in Eq. 2.136	-
$b_{01,x_i}, b_{02,x_i}, b_{03,x_i}$	Model Constants derivatives defined in Eq. 2.52	-
B^{DH}	Debye-Hückel model parameter defined in Eq. 2.136	-
$C_{1,2}$	Abbreviations defined in Eq. 28 and Eq. 2.35	-
C_{1,x_i}	Abbreviation derivative defined in Eq. 2.48	-
C_P	Isobaric heat capacity	J/K
C_V	Isochoric heat capacity	J/K
d_i	Temperature dependant segment diameter of component i	Å
d_m	Density of salt free mixture	mol/m^3
g_{ij}^{hs}	Site-Site radial distribution function of hard-sphere fluid	-
h_{is}	Binary interaction parameter of Debye-Hückel model	-
$I_{1,2}$	Abbreviations defined by Eq. 2.15, Eq. 2.16	-
$I_{1,2,x_i}$	Abbreviation derivatives defined by Eq. 2.49, Eq. 2.50	-
I_s	Ionic strength	mol/m^3
k_{ij}	Binary interaction parameter	-
k_B	Boltzmann constant	$\frac{J}{K}$

k_T	Isothermal compressibility coefficient	Pa^{-1}
m_i	Segment number of component i	-
$\bar{m}$	Mean segment number	-
M_w	Molecular weight	$\frac{gr}{mol}$
M_m	Molecular weight of salt free mixture	$\frac{gr}{mol}$
N_{AV}	Avogadro number	-
P	Pressure	Pa
R	Universal gas constant	$\frac{J}{mol\ K}$
r	Reduced radial distance	-
T	Temperature	K
$u(r)$	Pair potential	J
V	Volume	m^3
v	Volume	$Å^3$
x_i	Mole fraction of component i	-
Y_i	Mole fraction of component i in light phase	-
Z	Compressibility factor	-

Greek letters

ρ	Number density	$1/Å^3$
σ_i	Segment diameter of component i	Å
ε_i	Depth of pair potential of component i	J
η	Packing fraction	-
ζ_n	Abbreviation (n = 0, 1, 2, 3), see Eq. 2.8	$Å^{n-3}$
$\zeta_{n,T}$	Abbreviation derivatives (n = 1, 2, 3), see Eq. 2.86	$\frac{Å^{n-3}}{K}$
$\zeta_{n,T2}$	Abbreviation second derivatives (n = 1, 2, 3), see Eq. 2.99	$\frac{Å^{n-3}}{K^2}$

ζ_{n,x_i}	Abbreviation derivative (n = 1, 2, 3), see Eq. 2.43	$Å^{n-3}$
λ	Reduced well width of the square-well potential	-
ε^{AB}	Association energy between sites A and B	J
κ^{AB}	Effective association volume	-
Δ^{AB}	Association strength between site A and B	$Å^3$
$\overline{m^2\varepsilon\sigma^3}$	Abbreviation defined in Eq. 2.25	$JÅ^3$
$\overline{m^2\varepsilon^2\sigma^3}$	Abbreviation defined in Eq. 2.26	$J^2Å^3$
μ_i^{res}	Residual chemical potential of component i	J
α	Thermal expansion coefficient	K^{-1}
μ_{JT}	Joule-Thomson coefficient	K/Pa
ϕ_i	Fugacity coefficient of component i	-
γ^{DH}	Debye-Hückel activity coefficient	-
η^d	Dielectric constant	-

List of abbreviations

AAD	Absolute average deviation
PC-SAFT	Perturbed chain statistical association fluid theory
CPA	Cubic plus association
EoS	Equation of state
DH	Debye-Hückel model
VLE	Vapour-Liquid equilibria
LLE	Liquid-Liquid equilibria
VLHE	Vapour-Liquid-Hydrate equilibria
SAFT	Statistical association fluid theory
EXP	Experimental
res	Residual property

hs	Hard-Sphere contribution
ch	Chain contribution
hc	Hard-Chain contribution
disp	Dispersion contribution
assoc	Association contribution
OBJ	Objective function
GC	Gas chromatograph
CM	Chilled mirror

Chapter 1

1-Introduction

One of the greatest problem we face nowadays is global warming. The so-called "greenhouse effect" which is the cause of global warming is a danger to life on the earth. Global warming has several effects on the nature. Examples are killing the species which cannot tolerate the temperature rise or causing an increase in sea level due to melting the polar ice sheets. Animal extinction or dramatic changes in the normal routine of the nature will affect the human life as well. The area of the deserts will also be increased and dramatic agriculture decline and sever food crisis will happen consequently. Atmosphere contains a few greenhouse gases which absorb solar radiations reflected from earth and traps the heat inside the atmosphere causing the warming up of earth. However different greenhouse gas types produced by human activities have changed the natural balance of atmosphere concentration and increased the amount of those gases in the atmosphere.

Carbon dioxide is considered as the main and the most important substance categorized as greenhouse gases which is mainly produced by fossil fuels consumption to supply the global energy demand. Due to the current population growth and changes in life styles in the past few decades' energy demand has increased substantially. Consequently, a constant rise is observed in the carbon dioxide concentration in the atmosphere as fossil fuels are the main source of energy throughout the world in both household and industrial usage sectors. Figure 1.1 shows the percentage of the greenhouse gas emissions from 2010 and the main producer of each gas reported by IPCC on 2014. As shown in the figure, 65% of the greenhouse gas emission is carbon dioxide which is produced by fossil fuel consumption. The highest CO_2 emissions growth rate has been observed in developing countries, such as China while a relatively constant increasing rate was observed in the "*carbon intensity of energy*" for both developed and developing countries [1]. According to the data reported by National Oceanic and Atmospheric Administration (NOAA), the CO_2 concentration in the atmosphere has been increasing from around 390 ppm to more than 401 ppm from 2012 to 2015 [2].

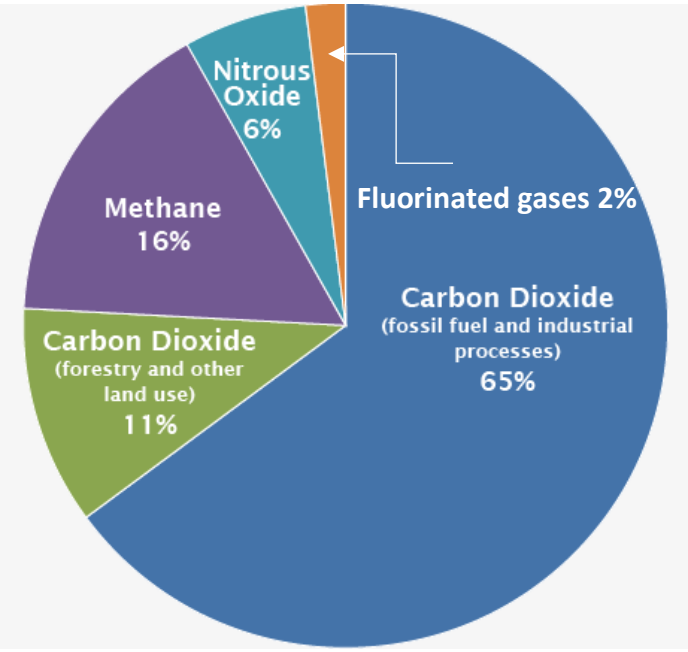

Figure 1.1 Global greenhouse gas emissions by gas reported by IPCC (2014)

To prevent global warming and the resulting climate change it is necessary to capture CO_2 from the large emission sources rather than emitting to the atmosphere and transport them to a suitable platform wherein CO_2 is securely stored deep down in a geological formation. The CO_2 capture and separation from the combustion product which is the first step toward CCS can be performed in three recommended procedures including post-combustion capture, pre-combustion capture and oxylfuel (O_2/CO_2 recycle combustion) capture [3] where CO_2 is separated chemically or physically [3]. After CO_2 was separated from the industrial outlet gases, it will be compressed and transported to storage sites or utilized.

CO_2-rich liquid or supercritical state are transported through pipelines from the emission sources to the suitable geological storage sites. Fluids coming from capture facilities contains mainly CO_2 and some impurities such as N_2, H_2, O_2, H_2S, CH_4, SO_3, NO, NO_2, CO and water. Long distance transportation together with physical and chemical properties of such compounds requires challenging engineering. The moisture content can cause several flow assurance issues, e.g. corrosion, ice and/or gas hydrate formation and pipeline blockage. Therefore, the fluid system should meet certain dehydration requirements. Furthermore, the stream is generally compressed and transported as liquid or dense-phase to avoid two-phase flow, as well as increasing the mass flow rate of the system. There is limited or no reliable experimental data on water content and dehydration requirements in such systems, in particular, at low temperature conditions that hydrate formation may occur during transport and storage.

IPCC report suggests three main storage options including geological storage, ocean storage and mineral carbonation [4]. The storage in the ocean involves dissolving CO_2 in sea water by injecting CO_2 deep down in the ocean or to form hydrate that because of the greater density than sea water can sink into the ocean [4]. The mineral carbonation process consists of chemically conversion of CO_2 in stable inorganic materials and storing them for a long time [4]. So far, the most advanced option among all storage methods reported by IPCC is CO_2 injection for Enhanced Oil Recovery purposes that has gained most attractions because of its economic advantages [4]. Table 1.1 summarized different methods of CO_2 storage and their development status until 2005.

Table 1.1 Maturity of CO_2 storage options [4]

Method	Development
Geological storage Enhanced Oil Recovery (EOR)	Mature market
Gas or oil fields	Economically feasible under specific conditions
Saline formations	Economically feasible under specific conditions
Enhanced Coal Bed methane recovery (ECBM)	Demonstration phase
Ocean storage Direct injection (dissolution type)	Research phase
Direct injection (lake type)	Research phase
Mineral carbonation Natural silicate minerals	Research phase
Waste materials	Demonstration phase

The most important concern in storage sector is possible CO_2 leakage to ocean and/or atmosphere [4] which could seriously damage the marine ecology due to natural ocean circulation and the movement of the dissolved CO_2 [4] as well as compromising CCS as a climate change reduction option. The necessities of a suitable geological storage have been summarized by Solomon et al. as follow [5]:

- ✓ *"Adequate porosity and thickness (storage capacity) and permeability (injectivity)".*
- ✓ *"Satisfactory sealing caprock".*
- ✓ *"A stable geological environment to avoid compromising the integrity of the storage site."*

Each method of storage has its own disadvantages, for instance the cost of chemically conversion of CO_2 is relatively high [3]. Furthermore, despite the security and the long term storage capability that can be provided by this method, stored CO_2 can have serious

effect on the oceans and endanger marine environment [3]. Saline aquifers are large brine bearing formation which have a high CO_2 storage capacity. At formation conditions CO_2 exists in supercritical state. Therefore, high amount of CO_2 can be stored deep underground. Adequate knowledge of the phase equilibria of CO_2 and water system and the effect of impurities are therefore crucial.

Solubility of CO_2 is highly governed by interactions between the injected CO_2 and the reservoir fluids. The storage capacity is directly related to the solubility of CO_2 in aqueous phase and thermodynamic properties of such systems at reservoir conditions. As mentioned before, it is favourable in the eyes of industry to transfer CO_2 in supercritical state which provides a high mass flow rate of CO_2 because of the great density of CO_2 in supercritical state. However, at very high pressure the risk of hydrate formation in the transport pipelines which could result in pipeline blockage and massive economical loss can be existed. In this case the solubility of water in rich CO_2 phase becomes very important.

In general, engineering and control of CO_2 storage and transportation processes require a good understanding of the thermodynamics and physical properties of CO_2/brine systems. As fluid phase behaviour of the above mentioned systems with the help of new experimental approaches is well understood, the correlations can complement with theoretical methods.

Furthermore, simulation and modelling softwares are inseparable requirements of engineering especially in oil and gas industry. There has been always an urgent need for state of the art and reliable models to be implemented in fast and reliable computer applications. On the other hand, developing a reasonable and trustable model capable of producing reliable results fast and accurate simultaneously over a wide range of conditions is not achievable without accurate and proper experimental data in hand. Once a complete set of reliable experimental data is available then models can be tuned and enhance the capabilities of engineering softwares. In this thesis, the Perturbed Chained Statistical Association Fluid Theory, known as the PC-SAFT model was used to calculate the thermodynamics properties and phase equilibria of oil and gas systems of interest. The PC-SAFT model was proposed by Gross and Sadowski [6] is an extension of the SAFT model developed by Chapman et al. [7]. The performance of PC-SAFT equation of state in predicting the fluid density even in the near critical region in very good and because of its capability in modelling the long chain molecules like polymers, it has been

widely used for modelling of the asphaltene precipitation. However, the focus of the modelling section of this thesis will be on tuning the PC-SAFT model for flow assurance and carbon dioxide capture, transport and storage systems of concern.

In flow assurance, water has a great deal of importance as it is the main reason of gas hydrates formation. Because of the lack of good descriptive model for water which can predicts the unique properties of water like its density below 4 °C, a new set of PC-SAFT pure parameters has been developed and reported in Chapter 2. The binary interaction parameters of various components with water using experimental measurements performed in this work and available experimental data were tuned and summarized afterward. Because of the importance of organic inhibitors in hydrate dissociation point calculation and also the significant role of glycol solvents in gas dehydration or CO_2 absorption processes, new sets of PC-SAFT pure component parameters were optimized using open literature data. The binary interaction parameters between organic inhibitors have been tuned using either available literature or in-house experimental data. The second derivative properties of noted systems were also calculated using analytical differentiation of PC-SAFT equation of state and predictions were compared to open experimental data in the literature.

In this study, the solubility of CO_2 in aqueous solutions of different salts has been measured and reported in Chapter 3. The detailed description of the solubility measurement experimental setup as well as the experimental procedure and material used are presented in this chapter. The experimental solubility measurements are divided into two main categories. The first one is the solubility measurements of pure CO_2 in 10 wt% and 20 wt% sodium chloride aqueous solutions, at low temperatures of -5 °C, 0 °C, 5 °C, 10 °C, 15°C and 25 °C and up to 300 bar pressures. The second category involves solubility measurement of pure CO_2 in demineralized water as well as aqueous solutions of several salts including sodium chloride, potassium chloride, calcium chloride and magnesium chloride in different salt concentrations at elevated temperatures of 50 °C, 100 °C and 150 °C and elevated pressures up to 550 bar to simulate deep geological conditions and produce reliable data for CO_2/brine phase equilibria at those conditions. In addition to the CO_2 solubility measurements in single salt aqueous solutions, solubilities were also measured in a mixture of salts aqueous solution at the same elevated temperatures and pressures. The experimental uncertainties for all measurements have been calculated and results were compared to the available experimental data reported in the literature by adjusting the CPA and PC-SAFT equation of states to the available

literature data and compare the model calculation with experimental data obtained in this study. The CPA equation of state was used in addition to the PC-SAFT model to be able to justify the validity of the experimental measurements regardless of the PC-SAFT model.

To account for cases in which the risk of hydrate formation is high in CO_2 transportation sector, the solubility of water in the CO_2-rich phases has been studied experimentally and reported in Chapter 4. The water contents measurements were performed using 10 wt% and 20 wt% aqueous solutions of sodium chloride at pressures up to 390 bar and low temperatures from 0 °C to 25 °C for 10 wt% brine and -5 °C to 25 °C for 20 wt% solution. The water contents of CO_2-rich fluids as well as pure CO_2 were also experimentally investigated at elevated temperatures and pressures to study the water content behaviour of CO_2-rich systems at high pressures and temperatures. For water content measurements at elevated temperatures Gas Chromatograph method was used as the water content of at above mentioned conditions is quite high. To check the reliability and capability of gas chromatography method for the water content measurements at elevated temperatures, the solubility of water in methane at 50 °C, 100 °C and 150 °C temperatures and elevated pressures were measured and compared against available experimental data and model calculations. The experimental setup descriptions and procedure adopted for water content measurements as well as the GC calibration details are presented in Chapter 4 as well.

Chapter 2

2-Phase Equilibria Modelling Using PC-SAFT Equation of State

2.1 Introduction and Model Background

Equations of states are referred as the equations which correlate the volume, temperature and pressure of a system. The simplest equation of state is the classical ideal gas law where the energy of a system (PV) is linearly correlated with temperature. The van der Waals equation of state proposed in 1873 showed considerably better results than the ideal gas equation. Due to the correction in the energy term of the classical ideal gas equation which accounts for attraction forces between molecules and the correction to the volume of the system by considering the volume of the molecules, the van der Waals EoS[1] was capable of predicting the liquid formation. Following by the van der Waals EoS the next generation of equation of states that could be rearranged in a cubic polynomial equation form were emerged.

The most commonly used cubic EoSs in engineering are the Peng-Robinson [8] and the Soave-Redlich-Kwong [9] EoSs that have been extensively used in phase equilibria modelling studies as well as industrial simulation applications. These models that are sometimes referred as engineering equation of states, show promising results for predicting the phase equilibria behaviour and PVT properties of conventional fluids like small molecules present in the atmosphere (CO_2, O_2, N_2, etc.) and heavier and more complex structural molecules of petroleum fluids. Those equations of states have two main terms, a repulsion contribution accounting for the repulsive forces between molecules and an attraction term to account for the van der Waals intermolecular attractions or the weak momentary polarizations. These forces are main interactions within the organic molecules like non-polar hydrocarbons and inorganic molecules.

However, cubic EoSs fail to produce satisfactory results for more complex fluids such as polar solvents, electrolytes, heavy petroleum residual fluids like asphaltenes, polymers, and surface active agents wherein either more sophisticated molecular interactions or more complicated molecular structure and characteristics contribute to the microscopic and macroscopic fluid properties. As the key to model macroscopic properties of a fluid is the ability to describe microscopic properties and to account for the abovementioned

[1] Short for Equation of State

complications involve in intermolecular and intramolecular interactions of real complex fluids, the molecular-based equation of states were introduced.

Chapman et al. proposed an equation of state by applying the Wertheim thermodynamic perturbation theory [10], [11] referred as SAFT, an acronym for Statistical Association Fluid Theory [7], [12]. In the original SAFT approach, molecules are considered as single (spherical particles) or multiple chained hard-sphere segments (non-spherical molecules) with or without association sites depending on whether the molecule can form hydrogen bonding or not. The SAFT EoS is expressed as the sum of three intermolecular interactions contributions to the residual Helmholtz free energy, segment (hard-sphere repulsion and dispersion attraction), chain and association contributions. The residual Helmholtz free energy is defined as the difference between total and ideal Helmholtz free energy of a system at specified temperature and density (Eq. 2.1).

$$A^{res}(T,\rho,x) = A(T,\rho,x) - A^{ideal\ gas}(T,\rho,x) \quad \text{Eq. 2.1}$$

$$A^{res}(T,\rho,x) = A_{Segment}(T,\rho,x) + A_{Chain}(T,\rho,x) + A_{Association}(T,\rho,x) \quad \text{Eq. 2.2}$$

Eq. 2.2 represents the original SAFT approach toward calculating the residual Helmholtz free energy of a system where the segment contribution accounts for the repulsion forces and attraction interaction between segments. The chain contribution accounted for the increment of the residual Helmholtz free energy due to the formation of segment chains and the association term which covers the intramolecular association forces between hydrogen bonding sites of polar molecules.

For instance, as illustrated in Figure 2.1, with the SAFT equation of state, 1-hexanol alcohol is treated as a chain of six spherical segments (CH_2 groups) where the hydrogen bonding sites of oxygen and hydrogen are placed on one segment at the end of the chain. The repulsion and attraction forces between CH_2 groups are calculated by the segment term, and the increment of the residual Helmholtz free energy due to the formation of the CH_2 segments chains is calculated by the chain term followed by association forces calculation due to the hydrogen bonding between oxygen and hydrogen atoms.

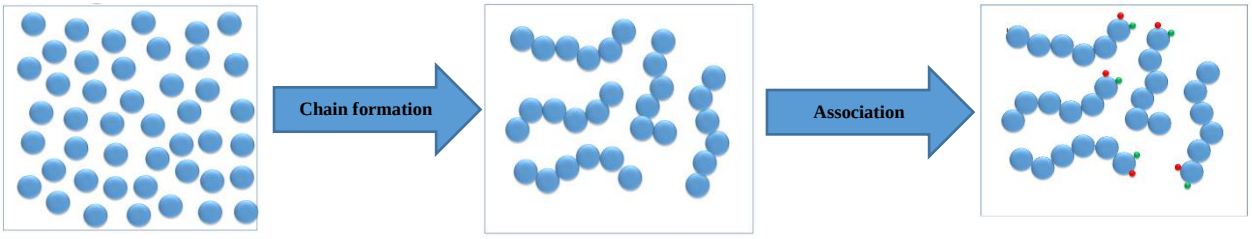

Figure 2.1 Contributions to the Helmholtz free energy in SAFT equation of state

In 2000 Gross and Sadowski developed an equation of state for square-well chain fluids by applying the second-order perturbation theory of Barker and Henderson to a hard-chain reference fluid (see Eq. 2.3) [13]. In this approach the residual free Helmholtz energy is sum of the Hard-Chain and Perturbation contributions. The above mentioned equation of state proposed by Gross and Sadowski [13] is described here in general.

$$\frac{a^{res}}{RT} = \frac{a_{Hard-Chain}}{RT} + \frac{a_{Perturbation}}{RT} \qquad \text{Eq. 2.3}$$

The hard-chain contribution (reference fluid) in Eq. 2.3 is sum of the hard-sphere and chain contributions

$$\frac{a_{Hard\ chain}}{RT} = m\frac{a_{Hard\ sphere}}{RT} + \frac{a_{chain}}{RT} \qquad \text{Eq. 2.4}$$

where based on the equation derived by Chapman et al. [7], the chain contribution to the residual Helmholtz free energy is obtained using the expression below.

$$\frac{a_{chain}}{RT} = \sum_i x_i(m_i - 1) ln\, g_{ii}^{hs} \qquad \text{Eq. 2.5}$$

In Eq. 2.5, x_i is the component mole fraction, m_i is the segment number of component i and g_{ii}^{hs} is the radial pair distribution function of segments of component i in the hard sphere system. The hard sphere contribution to the Helmholtz free energy and the radial distribution function are given by Eq. 2.6 and Eq. 2.7 which are calculated using the radial distribution function and compressibility factor (see Eq. 2.32) of a hard sphere mixture proposed by Boublik [14] and Mansoori et al. [15]

$$\frac{a_{hs}}{RT} = \frac{1}{\zeta_0}\left[\frac{3\zeta_1\zeta_2}{(1-\zeta_3)} + \frac{{\zeta_2}^3}{\zeta_3(1-\zeta_3)^2} + \left(\frac{{\zeta_2}^3}{{\zeta_3}^2} - \zeta_3\right) ln(1-\zeta_3)\right] \qquad \text{Eq. 2.6}$$

$$g_{ij}^{hs} = \frac{1}{(1-\zeta_3)} + \left(\frac{d_i d_j}{d_i + d_j}\right)\frac{3\zeta_2}{(1-\zeta_3)^2} + \left(\frac{d_i d_j}{d_i + d_j}\right)^2 \frac{2{\zeta_2}^2}{(1-\zeta_3)^2} \qquad \text{Eq. 2.7}$$

where ζ abbreviation is calculated using the equation below.

$$\zeta_n = \frac{\pi}{6}\rho \sum_i x_i m_i \sigma_i{}^n \qquad \text{Eq. 2.8}$$

In the above equation ρ is number density, x_i is the mole fraction of component i and σ_i is the segment diameter of component i. Please note that in the next subsequent work [6] (will be discussed in section 2.2) Gross and Sadowski used a temperature dependent segment diameter to describe the soft repulsive interactions between molecules which is calculated using the following equation.

$$d(T) = \int_0^\sigma \left[1 - exp(-\frac{u(r)}{kT})\right] dr = \sigma_i[1 - 0.12exp(\frac{3\varepsilon_i}{kT})] \qquad \text{Eq. 2.9}$$

The perturbation section can be obtained after the reference fluid has been defined. In the perturbation approach the Helmholtz free energy is expanded in inverse temperature around the free energy of a reference system [6]. "*The perturbations expansion is fast convergent and can be truncated after the second term*" [13], [16]. Therefore, the perturbation term in Eq. 2.3 is calculated using the expression below

$$\frac{A_{Perturbation}}{kTN} = \frac{A_{First\ Term}}{kTN} + \frac{A_{Second\ Term}}{kTN} \qquad \text{Eq. 2.10}$$

where k is the Boltzman`s constant and N is the number of molecules. As the shape segments of a chain molecules are considered spherical in the SAFT approach, Gross and Sadowski extended the perturbation theory of Baker and Henderson which was proposed for spherical molecules to chain molecules [13]. Therefore, the interaction between two chain molecules must be calculated as sum of the interactions between all segments of the chain molecules. Gross and Sadowski employed the average radial distribution function proposed by Chiew et al. [17]. Therefore, the first and second terms of the perturbation contribution using square-well chains are expressed as [16]

$$\frac{A_{First\ Term}}{NkT} = -2\pi\rho m^2(\frac{\varepsilon}{kT})\sigma^3 \int_1^\lambda g^{hc}(m; x, \rho)x^2 dx \qquad \text{Eq. 2.11}$$

$$\frac{A_{Second\ Term}}{NkT} = -\pi\rho m(Z^{hc} + \rho\frac{\partial Z^{hc}}{\partial\rho})^{-1}(\frac{\partial\rho}{\partial P^{hs}})m^2(\frac{\varepsilon}{kT})^2\sigma^3\frac{\partial}{\partial\rho}(\int_1^\lambda \rho g^{hc}(m; x, \rho)x^2 dx) \qquad \text{Eq. 2.12}$$

In the above equations, ρ is number density of the reference fluid, x is the reduced radial distance from a molecule and g^{hc} is the average segment-segment radial distribution function at the density of the reference fluid at specified temperature. The well-square potential parameters σ, ε and λ are defined as segment diameter, depth of the potential well and the reduced well-width respectively. To numerically calculate the integrals in Eq. 2.11 and Eq. 2.12, a sort of similar approach to the one proposed by Gulati and Hall

[18] was adopted by Gross and Sadowski [13] in which the integrals were calculated by simple power series (I_1 and I_2) that are functions of density and segment number. The first and second term of the perturbation contribution for pure fluid were then calculated using Eq. 2.13 and Eq. 2.14 (refer to Eq.23 and Eq.24 of their article [13]).

$$\frac{A_{First\ Term}}{NkT} = -2\pi\rho I_1(\eta,\bar{m})m^2(\frac{\varepsilon}{kT})\sigma^3 \qquad \text{Eq. 2.13}$$

$$\frac{A_{Second\ Term}}{NkT} = -\pi\rho\bar{m}(1+Z^{ref}+\rho\frac{\partial Z^{ref}}{\partial\rho})^{-1}I_2(\eta,\bar{m})m^2(\frac{\varepsilon}{kT})^2\sigma^3 \qquad \text{Eq. 2.14}$$

where η is packing fraction representing reduced segment density, Z^{ref} is the compressibility factor of the reference fluid, ε and σ are the depth of pair potential and segment diameter. As stated before, $I_1(\eta,\bar{m})$ and $I_2(\eta,\bar{m})$ are the substitutes of the perturbation theory integrals in the forms of simple power series. The details of the mathematical simplification and solving the first and second term integrals can be found elsewhere [13], [18]. The power series and the mixing rules are given by Eq. 2.15- Eq. 2.18.

$$I_1(\eta,m) = \sum_{n=1}^{6} a_i(m)\eta^n \qquad \text{Eq. 2.15}$$

$$I_2(\eta,m) = \sum_{n=1}^{6} b_i(m)\eta^n \qquad \text{Eq. 2.16}$$

$$a_i(m) = a_{0i} + \frac{m-1}{m}a_{1i} + \frac{m-1}{m}\frac{m-2}{m}a_{2i} \qquad \text{Eq. 2.17}$$

$$b_i(m) = b_{0i} + \frac{m-1}{m}b_{1i} + \frac{m-1}{m}\frac{m-2}{m}b_{2i} \qquad \text{Eq. 2.18}$$

Unlike other previously represented power series of I_1 and I_2 which were function of density, for specified segment number, Gross and Sadowski used two power series of six order as the functions of segment number and density. The segment dependent coefficients $a_i(m)$ and $b_i(m)$ were proposed by Liu et al. and are calculated by Eq. 2.17 and Eq. 2.18 [19]. The constants in the above mentioned equation were then optimized to the calculated values of I_1 and I_2 using molecular dynamics simulation of hard-chain molecules with segments number from 1 to 1000 and packing fractions up to 0.6 [13]. The van der Waals one fluid mixing rules were then applied to account for the unlike segment number, segment diameter and potential depths to extend the model for mixtures. The average segment number of the mixture is used in the Eq. 2.17 and Eq. 2.18 for calculation of the power series coefficients [13].

$$\frac{A_{First\ Term}}{NkT} = -2\pi\rho I_1(\eta,\bar{m})\sum_i\sum_j x_i x_j m_i m_j(\frac{\varepsilon_{ij}}{kT})\sigma_{ij}{}^3 \qquad \text{Eq. 2.19}$$

$$\frac{A_{Second\ Term}}{NkT} = -\pi\rho\bar{m}(1 + Z^{hc} + \rho\frac{\partial Z^{hc}}{\partial\rho})^{-1} I_2(\eta, \bar{m}) \sum_i \sum_j x_i x_j m_i m_j (\frac{\varepsilon_{ij}}{kT})^2 {\sigma_{ij}}^3$$

Eq. 2.20

The conventional mixing rules used in the first and second terms of the perturbation contribution are obtained using Eq. 2.21 and Eq. 2.22.

$$\sigma_{ij} = \frac{\sigma_i + \sigma_j}{2} \qquad \text{Eq. 2.21}$$

$$\varepsilon_{ij} = \sqrt{\varepsilon_i \varepsilon_j}(1 - k_{ij}) \qquad \text{Eq. 2.22}$$

2.2 PC-SAFT Equation of State

In 2001, Gross and Sadowski published an extension of their previous work on the application of the perturbation theory of Barker and Henderson [20] for a hard-chain reference fluid [6] wherein the equation of state was extended to real fluids by optimizing the constants of power series to the experimental vapour pressures and vapour, liquid and supercritical densities of n-alkanes. Before tuning the model constants, the pure component parameters for n-alkane compounds had to be obtained. To do this, a Lennard-Jones perturbing potential was assumed by Gross and Sadowski in Eq. 2.11 and Eq. 2.12 and an expression for the average radial distribution function $g(r)^{hc}$ for hard chains suggested by Chiew [17] was used. They determined the power series I_1 and I_2 for Lennard-Jones-like chains in the next step. The three pure compound parameters m, σ and ε of the n-alkanes were subsequently optimised by fitting the EoS to the vapour pressures and saturate liquid densities of n-alkanes. The coefficients a_{0i}, a_{1i}, a_{2i}, b_{0i}, b_{1i} and b_{2i}were then adjusted to the vapour pressures and liquid, vapour, and supercritical densities of n-alkanes using the optimised pure compound parameters [6].

The final form of the equation of state is expressed as Eq.2.23 which has two contributions to the free Helmholtz energy, hard-chain (or reference fluid) and dispersion contributions.

$$\frac{a^{res}}{RT} = \frac{a_{Hard\ chain}}{RT} + \frac{a_{Dispersion}}{RT} \qquad \text{Eq. 2.23}$$

where the hard chain contribution to the residual Helmholtz free energy is obtained from Eq. 2.4-2.8 and the dispersion term is calculated using the equation below:

$$\frac{a_{Dispersion}}{RT} = -2\pi\rho I_1(\eta, \bar{m})\overline{m^2\varepsilon\sigma^3} - \pi\rho\bar{m}C_1 I_2(\eta, \bar{m})\overline{m^2\varepsilon^2\sigma^3} \qquad \text{Eq. 2.24}$$

The van der Waals mixing rules are applied to account for unlike segments interactions in $\overline{m^2\varepsilon\sigma^3}$ and $\overline{m^2\varepsilon^2\sigma^3}$ abbreviations. I_1 and I_2 expressions are calculated using Eq. 15 and Eq. 2.16.

$$\overline{m^2\varepsilon\sigma^3} = \sum_i \sum_j x_i x_j m_i m_j \left(\frac{\varepsilon_{ij}}{kT}\right) {\sigma_{ij}}^3 \quad \text{Eq. 2.25}$$

$$\overline{m^2\varepsilon^2\sigma^3} = \sum_i \sum_j x_i x_j m_i m_j \left(\frac{\varepsilon_{ij}}{kT}\right)^2 {\sigma_{ij}}^3 \quad \text{Eq. 2.26}$$

$$\bar{m} = \sum_i x_i m_i \quad \text{Eq. 2.27}$$

The C_1 abbreviation is calculated using the following equation

$$C_1 = \left(1 + Z^{hc} + \rho \frac{\partial Z^{hc}}{\partial \rho}\right)^{-1}$$

$$= (1 + \bar{m}\frac{8\eta - 2\eta^2}{(1-\eta)^4} + (1-\bar{m})\frac{20\eta - 27\eta^2 + 12\eta^3 - 2\eta^4}{(1-\eta)^2(2-\eta)^2})^{-1} \quad \text{Eq. 2.28}$$

The compressibility factor is then calculated using the thermodynamic relation below:

$$Z = 1 + \eta \frac{\partial}{\partial \eta}\left(\frac{\partial a^{res}}{\partial \eta}\right)_{T,x} \quad \text{Eq. 2.29}$$

As expressed in Eq. 2.30, the compressibility factor of the system is the summation of the hard-chain and dispersion contributions and compressibility factor of an ideal gas.

$$Z = 1 + Z^{hard\ chain} + Z^{dispersion} \quad \text{Eq. 2.30}$$

where the hard chain and dispersion terms in the Eq. 2.30 are calculated using the expressions below.

$$Z^{hc} = \bar{m} Z^{hs} - \sum_i x_i (m_i - 1)\,(g_{ii}^{hs})^{-1} \rho \frac{\partial g_{ii}^{hs}}{\partial \rho} \quad \text{Eq. 2.31}$$

The hard sphere contribution to the compressibility factor and the derivative of the radial distribution function are obtained using Eq. 2.32 and Eq. 2.33.

$$Z^{hs} = \frac{\zeta_3}{(1-\zeta_3)} + \frac{3\zeta_1\zeta_2}{\zeta_0(1-\zeta_3)^2} + \frac{3{\zeta_3}^3 - 3\zeta_3{\zeta_2}^3}{\zeta_0(1-\zeta_3)^3} \quad \text{Eq. 2.32}$$

$$\rho \frac{\partial g_{ij}^{hs}}{\partial \rho} = \frac{\zeta_3}{(1-\zeta_3)^2} + \left(\frac{d_i d_j}{d_i + d_j}\right)\left(\frac{3\zeta_2}{(1-\zeta_3)^2} + \frac{6\zeta_2\zeta_3}{(1-\zeta_3)^3}\right) + \left(\frac{d_i d_j}{d_i + d_j}\right)^2 \left(\frac{4{\zeta_2}^2}{(1-\zeta_3)^3} + \frac{6{\zeta_2}^2\zeta_3}{(1-\zeta_3)^4}\right) \quad \text{Eq. 2.33}$$

In the PC-SAFT equation of state, a temperature dependant segment diameter (Eq. 2.9)) is used for calculation of ζ_n which is given by given by $\zeta_n = \frac{\pi}{6}\rho \sum_i x_i m_i {d_i}^n$ where d_i is calculated using Eq. 2.9.

The dispersion term is calculated using

$$Z^{disp} = -2\pi\rho \frac{\partial(\eta I_1)}{\partial \eta} \overline{m^2\varepsilon\sigma^3} - \pi\rho\bar{m}\left[C_1 \frac{\partial(\eta I_2)}{\partial \eta} + C_2 \eta I_2 \overline{m^2\varepsilon^2\sigma^3}\right] \quad \text{Eq. 2.34}$$

where the abbreviations $\overline{m^2\varepsilon\sigma^3}$ and $\overline{m^2\varepsilon^2\sigma^3}$ are calculated using Eq. 2.25 and Eq. 2.26. The new abbreviation $C_2 = \frac{\partial C_1}{\partial \eta}$ is introduced and obtained from

$$C_2 = -{C_1}^2(\bar{m}\frac{-4\eta^2+20\eta+8}{(1-\eta)^5} + (1-\bar{m})\frac{2\eta^3+12\eta^2-48\eta+40}{(1-\eta)(2-\eta)^3}) \quad \text{Eq. 2.35}$$

The derivatives perturbation integrals with respect to η is calculated through the expressions

$$\frac{\partial I_1(\eta,m)}{\partial \eta} = \sum_{n=1}^{6} a_i(\bar{m})(n+1)\eta^n \quad \text{Eq. 2.36}$$

$$\frac{\partial I_2(\eta,m)}{\partial \eta} = \sum_{n=1}^{6} b_i(m)(n+1)\eta^n \quad \text{Eq. 2.37}$$

Note that the densities used in the equations are the number densities of the fluid with the unit of $\frac{N}{\text{Å}^3}$ which is converted to $\frac{mol}{m^3}$ units by multiplying to $\frac{10^{30}\ \text{Å}^3}{N_{AV}} = \frac{1}{6.022\times10^{-7}}$. Therefore, pressure is calculated in Pa unit through the general PVT relation:

$$P = Z(6.022\times10^{-7})\rho RT \quad \text{Eq. 2.38}$$

Similarly, the density of fluid must be calculated numerically using appropriate root finding algorithms with initial guess of $\eta = 10^{-12}$ for vapour phase and $\eta = 0.5$ for liquid phases. The obtained value of η is then converted to the molar density using the following equation:

$$\rho[\frac{mol}{m^3}] = \frac{6}{\pi}\eta\left(\sum_i x_i m_i {d_i}^3\right)^{-1}(\frac{1}{6.022\times10^{-7}}) \quad \text{Eq. 2.39}$$

For phase equilibria calculation, the fugacity of all components must be equal in all phases in equilibrium. The chemical potential using the PC-SAFT equation of state is calculated using the equation below:

$$\frac{\mu_i^{res}}{kT} = \frac{a^{res}}{RT} + (Z-1) + \frac{\partial}{\partial x_i}\left(\frac{a^{res}}{RT}\right) - \sum_{j=1}^{Ncomp} x_j(\frac{\partial}{\partial x_i}\left(\frac{a^{res}}{RT}\right)) \quad \text{Eq. 2.40}$$

where Z is the total compressibility factor of the system at the specified temperature and density and the derivatives of the residual Helmholtz free energy with respect to the mole fractions is calculated regardless of the $\sum_i x_i = 1$ meaning that different mole fractions cannot be written in terms of the other mole fraction for differentiation. The derivatives of the contributions to the free Helmholtz free energy are calculated through the expressions below. Here for simplicity a new abbreviation $\tilde{a}$ is shown instead of $\frac{a}{RT}$.

$$\left(\frac{\partial \tilde{a}^{hc}}{\partial x_i}\right)_{T,\rho,x_{i\neq j}}$$

$$= m_i\tilde{a}^{hs} + \bar{m}\left(\frac{\partial \tilde{a}^{hs}}{\partial x_i}\right)_{T,\rho,x_{i\neq j}} - (m_i - 1)lng_{ii}^{hs} - \sum_i x_i(m_i - 1)g_{ii}^{hs^{-1}}\left(\frac{\partial g_{ii}^{hs}}{\partial x_i}\right)_{T,\rho,x_{i\neq j}}$$

Eq. 2.41

where the derivative of the hard sphere contribution is obtained via

$$\left(\frac{\partial \tilde{a}^{hs}}{\partial x_i}\right)_{T,\rho,x_{i\neq j}} =$$

Eq. 2.42

$$\frac{\zeta_{0,xi}}{(\zeta_0)}\tilde{a}^{hs} + \frac{1}{\zeta_0}\left[\frac{3(\zeta_{1,xi}\zeta_2+\zeta_1\zeta_{2,xi})}{(1-\zeta_3)} + \frac{3\zeta_1\zeta_2\zeta_{3,xi}}{(1-\zeta_3)^2} + \frac{3{\zeta_2}^2\zeta_{2,xi}}{\zeta_3(1-\zeta_3)^2} + \frac{{\zeta_2}^3\zeta_{3,xi}(3\zeta_3-1)}{{\zeta_3}^2(1-\zeta_3)^3} + \left(\frac{3{\zeta_2}^2\zeta_{2,xi}\zeta_3-2{\zeta_2}^3\zeta_{3,xi}}{{\zeta_3}^3} - \zeta_{0,xi}\right)\ln(1-\zeta_3) + \left(\zeta_0 - \frac{{\zeta_2}^3}{{\zeta_3}^2}\right)\frac{\zeta_{3,xi}}{(1-\zeta_3)}\right]$$

$$\zeta_{n,xi} = \frac{\pi}{6}\rho m_i {d_i}^n$$

Eq. 2.43

$\zeta_{n,xi}$ is the derivative of ζ_n with respect to the mole fraction of component i.

$$\left(\frac{\partial g_{ii}^{hs}}{\partial x_i}\right)_{T,\rho,x_{i\neq j}} =$$

Eq. 2.44

$$\frac{\zeta_{3,xi}}{(1-\zeta_3)^2} + \left(\frac{d_i d_j}{d_i + d_j}\right)\left(\frac{3\zeta_{2,xi}}{(1-\zeta_3)^2} + \frac{6\zeta_2\zeta_{3,xi}}{(1-\zeta_3)^3}\right) + \left(\frac{d_i d_j}{d_i + d_j}\right)^2\left(\frac{4\zeta_2\zeta_{2,xi}}{(1-\zeta_3)^3} + \frac{6{\zeta_2}^2\zeta_{3,xi}}{(1-\zeta_3)^4}\right)$$

The derivative of the dispersion contribution is

$$\left(\frac{\partial \tilde{a}^{dis}}{\partial x_i}\right)_{T,\rho,x_{i\neq j}} =$$

Eq. 2.45

$$-2\pi\rho\left[I_{1,xi}\overline{m^2\varepsilon\sigma^3} + I_1\left(\overline{m^2\varepsilon\sigma^3}\right)_{xi}\right] - \pi\rho\left\{\left[m_i C_1 I_2 + \bar{m}C_{1,xi}I_2 + \bar{m}C_1 I_{2,xi}\right]\overline{m^2\varepsilon^2\sigma^3}\ \bar{m}C_1 I_2\left(\overline{m^2\varepsilon^2\sigma^3}\right)_{xi}\right\}$$

with

$$\left(\overline{m^2\varepsilon\sigma^3}\right)_{xi} = 2m_i\sum_j x_i m_i\left(\frac{\varepsilon_{ij}}{kT}\right){\sigma_{ij}}^3$$

Eq. 2.46

$$\left(\overline{m^2\varepsilon^2\sigma^3}\right)_{xi} = 2m_i\sum_j x_i m_i\left(\frac{\varepsilon_{ij}}{kT}\right)^2{\sigma_{ij}}^3$$

Eq. 2.47

$$C_{1,xi} = C_2\zeta_{3,xi} - {C_1}^2\left\{m_i\frac{8\eta-2\eta^2}{(1-\eta)^4} - m_i\frac{20\eta-27\eta^2+12\eta^3-2\eta^4}{(1-\eta)^2(2-\eta)^2}\right\}$$

Eq. 2.48

$$I_{1,xi} = \sum_{n=1}^{6}[a_n(m)i\zeta_{3,xi}\eta^{n-1} + a_{n,xi}(m_i)]$$

Eq. 2.49

$$I_{2,xi} = \sum_{n=1}^{6}[b_n(m)i\zeta_{3,xi}\eta^{n-1} + b_{n,xi}(m_i)] \quad \text{Eq. 2.49}$$

$$a_{n,xi} = \frac{m_i}{\bar{m}^2}a_{1n} + \frac{m_i}{\bar{m}^2}(3 - \frac{4}{\bar{m}})a_{2n} \quad \text{Eq. 2.50}$$

$$b_{n,xi} = \frac{m_i}{\bar{m}^2}b_{1n} + \frac{m_i}{\bar{m}^2}(3 - \frac{4}{\bar{m}})b_{2n} \quad \text{Eq. 2.51}$$

As mentioned before the chain and association terms in the PC-SAFT equation of state are the same as the chain and association terms of the SAFT equation of states. The association contribution to Helmholtz free energy is obtained using the equation below.

$$\frac{a^{assoc}}{RT} = \sum_i x_i \sum_{A_i}(lnX_{A_i} - \frac{X_{A_i}}{2} + \frac{1}{2}) \quad \text{Eq. 2.52}$$

where X_{A_i} is the mole fraction of molecule i not bonded to site A in mixture with other components which is given by:

$$X_{A_i} = \frac{1}{\sum_i \sum_{B_j} x_j X_{B_j} \Delta^{A_i B_j}} \quad \text{Eq. 2.53}$$

with

$$\Delta^{A_i B_j} = g_{ij}^{hs} exp(\frac{\varepsilon_{AB}}{kT} - 1){d_{ij}}^3 \kappa^{A_i B_j} \quad \text{Eq. 2.54}$$

where $d_{ij} = \frac{d_i + d_j}{2}$

X_{A_i}in Eq. 2.53 must be calculated numerically for all components in a mixture, however, for pure components, the non-bonded fractions can be calculated analytically. The pure component equations for X_{A_i} can be found elsewhere [21]. Tan et al. proposed a method for calculation of non-bonded fraction, X_{A_i} and its derivatives with respect to the density, mole fraction and temperature [22]. The contribution of association to the compressibility factor and the chemical potential are obtained using the following equations.

$$Z^{assoc} = \rho \sum_i x_i \sum_{A_i}\left(\frac{1}{X_{A_i}} - \frac{1}{2}\right)\frac{\partial X_{A_i}}{\partial \rho} \quad \text{Eq. 2.55}$$

Or according to the equation A.10 of Chapman et al. [23]

$$Z^{assoc} = \sum_i x_i \frac{\mu_i^{assoc}}{RT} - \frac{a^{assoc}}{RT} \quad \text{Eq. 2.56}$$

The contribution to the chemical potential is given by

$$\frac{\mu_i^{assoc}}{RT} = \sum_{A_i}\left(lnX_{A_i} - \frac{1}{X_{A_i}} + \frac{1}{2}\right) + \sum_j x_j \sum_{A_j}\left(\frac{1}{X_{A_i}} - \frac{1}{2}\right)\frac{\partial X_{A_i}}{\partial x_i} \quad \text{Eq. 2.57}$$

2.3 Binary Systems of Non-Associating Components

The PC-SAFT equation of state was used in this study to model the phase equilibria and thermodynamics properties of fluids involved in CO_2 capture and storage as well as flow assurance engineering. Pure compound parameters of the PC-SAFT EoS are optimized using the volumetric data and phase behaviour of pure compounds to predict the thermodynamic properties and VLE behaviour of pure systems as accurately as possible. However, real systems involved in the subject of this work, are mixtures of at least two or more associating and non-associating components wherein different types of molecules are present. Gross and Sadowski [6] regressed pure compound parameters of several substances including normal alkanes, branched alkanes, cyclic alkanes, alkenes, aromatics, chlorinated hydrocarbons, permanent gases, ethers, and esters. They showed that using the pure compound parameters reported in their work, the PC-SAFT model is capable of correlating the VLE of several binary systems including, methane/n-butane, propane/benzene and diethyl ether/ethane with excellent agreement with experimental data without further tuning of the model. However, even though PC-SAFT is a robust model for predicting the fluid phase behaviour of pure components and several non-associating binary systems, the need for optimizing the model for many binary or multicomponent systems is inevitable.

This is done by adjusting the one binary interaction parameter k_{ij} in the dispersion term of the model wherein the attraction interactions between two molecules is adjusted with experimental VLE data of the corresponding binary systems. Gross and Sadowski reported the binary interaction parameter of 24 binary systems [6]. The binary systems of supercritical CO_2 and hydrocarbon mixtures were investigated by Dong Fu et al. [24]. They reported the binary interaction parameters of CO_2 and normal alkanes (up to nC_{34}) and benzene. The binary interaction parameters of nitrogen binary mixtures with 29 common oil components were also reported by Sanchez et al. [25]. They proposed a relation for calculating the k_{ij} of N_2 and paraffin components based on molecular weight of methane and molecular weight of n-alkanes.

$$k_{N_2-nAlkane} = 0.0307 + 0.03094\left(\frac{M_{nAlkane}-M_{methane}}{M_{nAlkane}}\right) + 0.12204\left(\frac{M_{nAlkane}-M_{methane}}{M_{nAlkane}}\right)\left(\frac{M_{nAlkane}-2M_{methane}}{M_{nAlkane}}\right) \quad \text{Eq. 2.58}$$

In this section, the tuning approach and results for binary mixtures of several components with emphasis on the components relevant to CO_2 capture and storage and flow assurance are reported. For non-associating binary mixtures, a single temperature independent

binary interaction parameters have been tuned and are reported. The pure parameters of the non-associating compounds involved in the binary mixtures to be tuned have been taken from different references listed in Table 2.1. The conventional Berthelot-Lorentz mixing rule is applied to determine the potential parameters of unlike segments pairs in the dispersion term of the PC-SAFT EoS.

$$\sigma_{ij} = \frac{1}{2}\,(\sigma_i + \sigma_j) \qquad \text{Eq. 2.59}$$

$$\varepsilon_{ij} = \sqrt{\varepsilon_i \varepsilon_j}\,(1 - k_{ij}) \qquad \text{Eq. 2.60}$$

To obtain an optimized k_{ij}, the Nelder-Mead version of SIMPLEX method [26] was applied to minimize the following objective function using experimental VLE data obtained from literature:

$$OBJ = \sum_{i=1}^{N_{exp}} \left(\left(\frac{P_i^{EoS} - P_i^{Exp}}{P_i^{Exp}} \right)^2 + \left(\frac{y_i^{EoS} - y_i^{Exp}}{y_i^{Exp}} \right)^2 \right) \qquad \text{Eq. 2.61}$$

where P_i^{EoS} and Y_i^{EoS} are the calculated bubble point pressure of the mixture and the composition of the vapour phase, respectively. Likewise, P_i^{Exp} and Y_i^{Exp} are the corresponding experimental bubble point pressure and the experimental vapour composition, respectively.

The binary interaction parameters of ***82*** binary systems were tuned using either experimental VLE data obtained from literature or in-house measured data. The optimized k_{ij} of each binary systems together with the references of experimental datasets used, the AAD %[1] of the tuned model with corresponding experimental data, the total temperature and pressure ranges covered, the total number of data point used and the AAD % values of each binary system are summarized through Table 2.2 to Table 2.5. The binary systems were categorized into five binary groups where each group represents the binary systems to be made by one of methane, ethane, CO_2, nitrogen and SO_2 and other components.

[1] Absolute Average Deviation

Table 2.1 Pure compound parameters for PC-SAFT from the literature for non-associating compounds

Compound	m	σ (Å)	ε/k_B (K)	Reference
methane	1.0000	3.7039	150.03	[6]
ethane	1.6069	3.5206	191.42	[6]
propane	2.002	3.6184	208.11	[6]
n-butane	2.3316	3.7086	222.88	[6]
n-pentane	2.6896	3.7729	231.2	[6]
n-hexane	3.0576	3.7983	236.77	[6]
n-heptane	3.4831	3.8049	238.4	[6]
n-octane	3.8176	3.8373	242.78	[6]
n-nonane	4.2079	3.8448	244.51	[6]
n-decane	4.6627	3.8384	243.87	[6]
n-dodecane	5.306	3.8959	249.21	[6]
n-tetradecane	5.9002	3.9396	254.21	[6]
n-pentadecane	6.2855	3.9531	254.14	[6]
n-hexadecane	6.6485	3.9552	254.14	[6]
n-octadecane	7.3271	3.9668	256.2	[6]
n-eicosane	7.9849	3.9869	257.75	[6]
n-octacosane	10.7117	4.0783	270.6104	[6]
n-triacontane	11.3889	4.0997	273.394	[6]
n-dotriacontane	12.0661	4.1211	276.1776	[6]
n-hexatriacontane	13.4205	4.1639	281.7448	[6]
n-tetratetracontane	16.1293	4.2495	292.8792	[6]
CO_2	2.0729	2.7852	169.21	[6]
H_2S	1.7163	3.009	224.96	[27]
argon	0.9285	3.4784	122.23	[6]
SO_2	2.8611	2.6826	205.35	[6]
N_2	1.2053	3.313	90.96	[6]
O_2	1.1217	3.21	114.96	[27]
CO	1.3097	3.2507	92.15	[6]

Table 2.2 Optimized binary interaction parameters of binary systems containing methane

	Binary System	k_{ij}	T-range (K)	P-range (bar)	N points	AAD % P_{bubble}	AAD % y_{vapour}	Ref.
Methane	ethane	-0.0056	122.04-283.15	0.1079-66.571	147	3.12%	1.84%	[28]–[37]
	propane	0.0033	90-360.93	0.107-101.63	156	2.44%	1.29%	[28], [32], [38]–[44]
	nC_8	0.0205	223.15-423.15	10.35-288.78	92	6.53%	0.76%	[45]
	nC_9	0.0192	223.15-423.16	10.133-323.23	124	5.57%	0.37%	[46], [47]
	nC_{12}	0.0306	323.15-373.15	13.3-103.8	12	2.21%	-	[48]
	nC_{14}	0.0248	294.8-447.6	19.9-95-4	24	3.53%	-	[49]
	nC_{16}	0.0619	189.3-623.15	4.9-249.3	14	3.63%	0.14%	[50]
	nC_{18}	0.0297	323-447.6	19.9-95-9	24	4.02%	-	[49]
	nC_{20}	0.0398	323.2-573.15	0.95-10.69	35	4.73%	-	[51]–[53]
	nC_{28}	0.0275	348.2-423.2	0.93-7.09	19	3.53%	-	[51]
	nC_{32}	0.0256	343.15	15.85-66.3	10	4.9%	-	[51]
	nC_{36}	0.0341	373.2-423.2	8.7-79.3	14	2.74%	-	[51]
	nC_{44}	0.0322	373.2-423.3	6.8-55.7	15	2.27%	-	[51]
	N_2	0.0320	88.71-183.15	0.212-44	550	2.54%	6.12%	[42], [54]–[62]
	H_2S	0.0539	222.2-352.98	7.1-134.38	131	5.60%	5.89%	[63]–[66]
	N_2O	0.0911	273.15-298.15	20.26-83.15	19	10.86%	47.47%	In-house Data

The binary interaction parameter for binary systems containing methane was tuned to experimental VLE data from various references except for the methane/N_2O system which was tuned to in-house VLE measured data. The P-xy diagrams of a few selected binary systems are plotted in Figure 2.2 to Figure 2.4. The highest deviation from experimental data was observed for nitrous oxide/methane where the AAD % value of calculated vapour phase composition is 47% while the model calculation for the bubble point pressure of the mixture shows a reasonable deviation from experimental data. As can be seen from Figure 2.2 to Figure 2.4 at each temperature the deviation from experimental data is higher close to the critical composition region of the system.

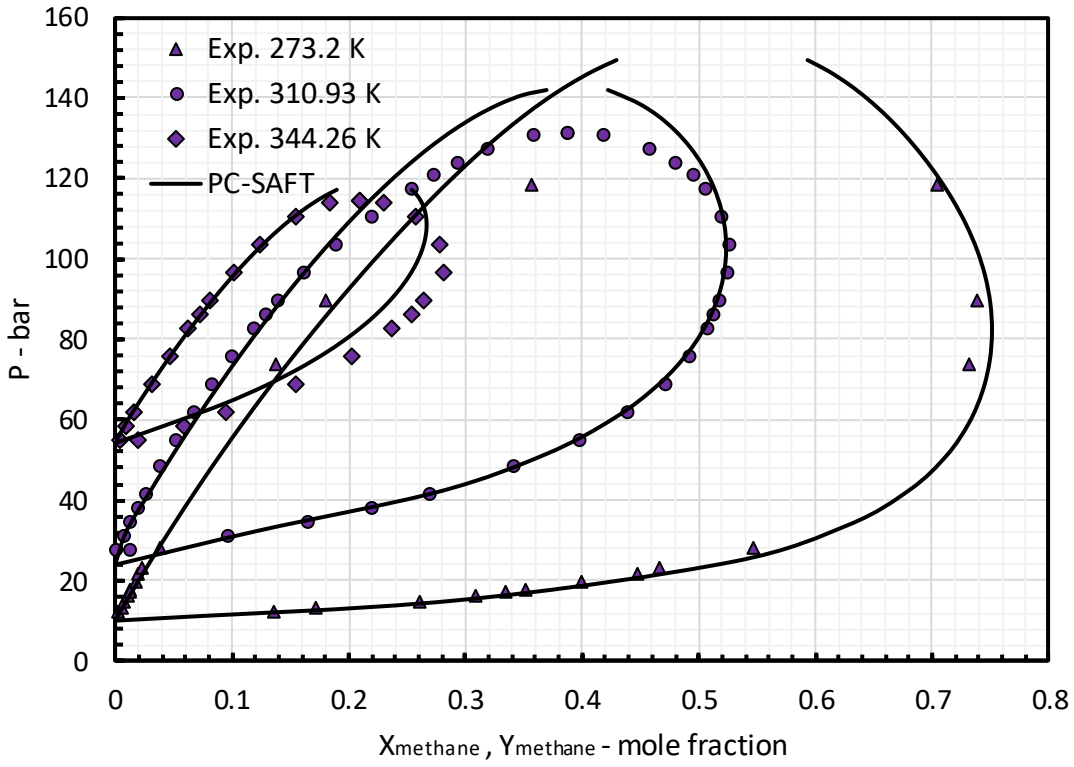

Figure 2.2 P-xy diagram of methane-H_2S system at 273.2 K, 310.93K and 344.26K: Comparison with tuned PC-SAFT model and experimental data (273.2: [66]**, 310.93:**[64] **, 344.26:** [63]**)**

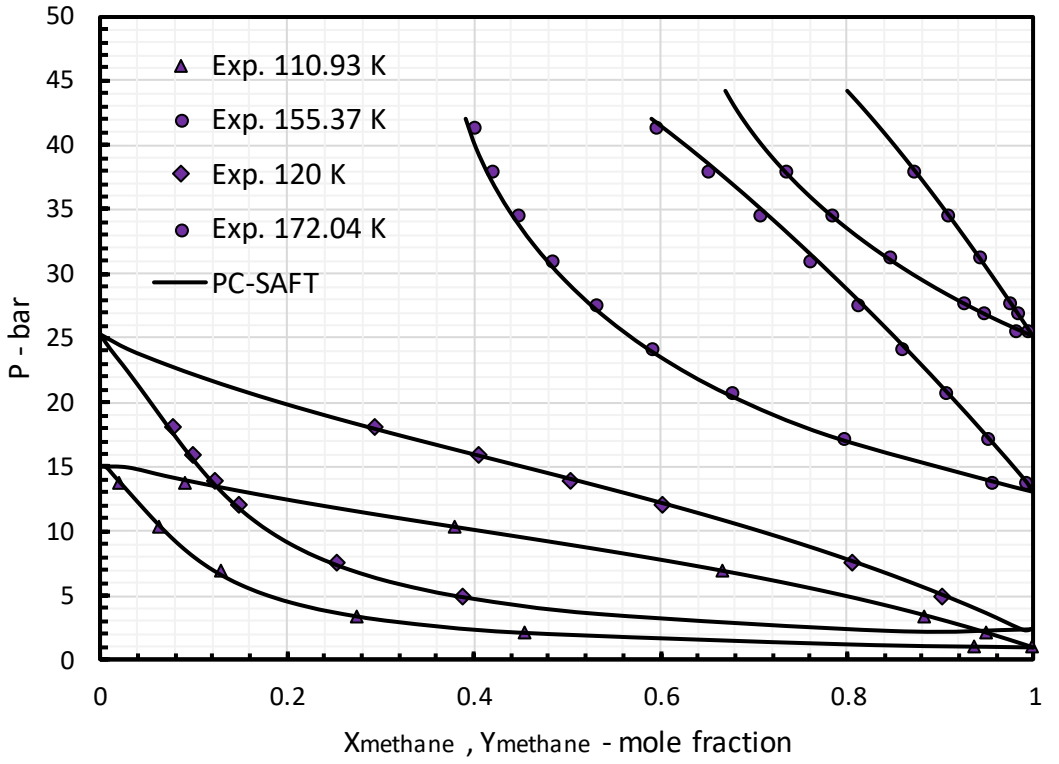

Figure 2.3 P-xy diagram of methane-nitrogen system at 110.93 K, 155.37 K, 172.04 K and 120 K: Comparison with tuned PC-SAFT model and experimental data (110.93 K: [54] **, 155.37 K:** [54]**, 172.04 K:** [57] **, 120 K:** [67]**)**

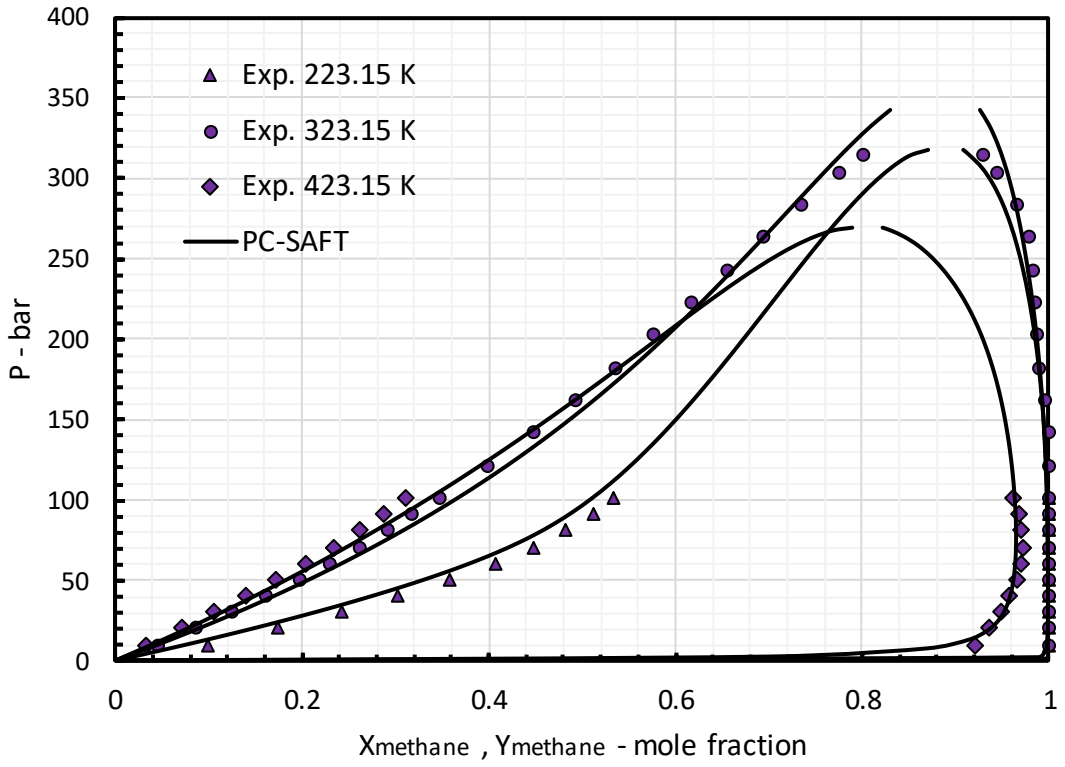

Figure 2.4 P-xy diagram of methane-n-nonane system at 223.15 K, 323.015 K and 423.15 K: Comparison with tuned PC-SAFT model and experimental data (223.15 K: [47]**, 323.15 K:**[47]**, 423.15 K:**[47]**)**

Detailed information of the k_{ij} optimisation of CO_2 binary mixtures are listed in Table 2.3 and the experimental and calculated VLE of a few systems are plotted together in the Figure 2.5 and Figure 2.6. Several datasets were used for tuning of CO_2 binary systems to cover all the available data reported for these systems while for CO_2/CO and CO_2/N_2 systems, in-house dataset were used. For CO_2/n-butane binary system around 457 data points were used for adjusting the k_{ij} over a wide range of temperature and pressure. Considering the number of data used for this system the AAD % value of 6.8 for bubble point pressure and 6.92 for vapour phase composition, seem to be within the variance of the experimental data reported.

Table 2.3 Optimized binary interaction parameter of binary systems containing CO_2

	Binary System	k_{ij}	T-range (K)	P-range (bar)	N points	AAD % P_{bubble}	AAD % y_{vapour}	Ref.
Carbon dioxide	propane	0.1063	224.36-361-15	3.3-66.7	308	5.16%	4.31%	[68]–[74]
	n-butane	0.1333	227.98-418.48	0.33-81.6	457	6.8%	6.92%	[70], [72], [75]–[84]
	n-pentane	0.1257	252.67-458.54	1.5-96.3	202	5.01%	1.85%	[70], [78], [85]–[88]
	n-hexane	0.1294	273.15-393.15	8-117	124	4.32%	0.69%	[89]–[92]
	n-heptane	0.1252	310.65-477.21	1.8-133.1	134	4.42%	1.42%	[75], [93], [94]
	n-octane	0.1336	304.15-348.15	15-113.5	103	7.35%	0.38%	[95]–[97]
	n-nonane	0.1215	298.2-343.25	5.2-118.	38	8.78%	0.55%	[98], [99]
	n-decane	0.1269	277.59-594.2	3.44-188	207	10.42%	1.15%	[94], [98], [100]–[104]
	nC_{14}	0.1710	344.3	110.7-163.6	18	10.24%	-	[105]
	nC_{16}	0.1674	463.05-663.75	20.4-51.8	16	2.85%	0.65%	[106]
	nC_{19}	0.1629	313.15-333.15	11.1-79.5	35	6.94%	-	[107]
	nC_{20}	0.1551	310.15-573.35	0.5-33.5	109	5.75%	-	[52], [108]–[110]
	C_{22}	0.1470	323.2-473.2	63.7-373	20	8.04%	-	[108], [111]
	C_{24}	0.1607	373.2-473.2	94-389	15	5.98%	-	[112]
	C_{28}	0.1418	373.2-473.3	89-229	9	11.3%	-	[108], [110]
	benzene	0.0989	273.15-393.2	4.36-77.2	175	5.08%	1.06%	[89], [92], [110], [113]–[118]
	toluene	0.1145	290.8-477.04	2.5-152.9	252	6.95%	1.42%	[116], [119]–[127]
	oxygen	0.0609	273.15-298.15	38-115	82	3.94%	4.32%	[128]–[130]
	carbon monoxide	-0.0325	245.61-298.15	28-110	33	3.34%	2.83%	In-house Data
	argon	0.04822	233.15-299.21	15-156	76	3.42%	2.35%	[131]–[133]
	nitrogen	-0.0264	283.15-298.15	46-99.8	20	1.90%	1.05%	In-house Data
	H_2S	0.0653	258.41-313.02	10.0-54.7	139	1.05%	3.99%	[134], [135]

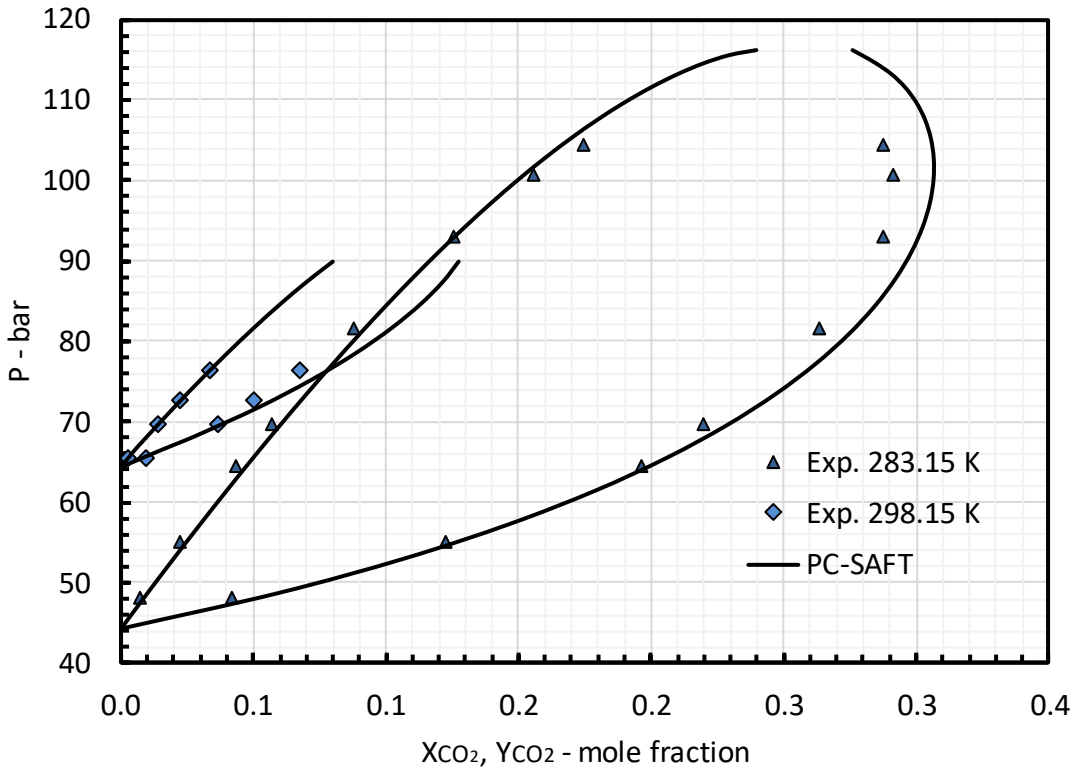

Figure 2.5 P-xy diagram of carbon dioxide-nitrogen system at 283.15 K, and 298.15.15 K: Comparison with tuned PC-SAFT model and experimental data (in-house Data)

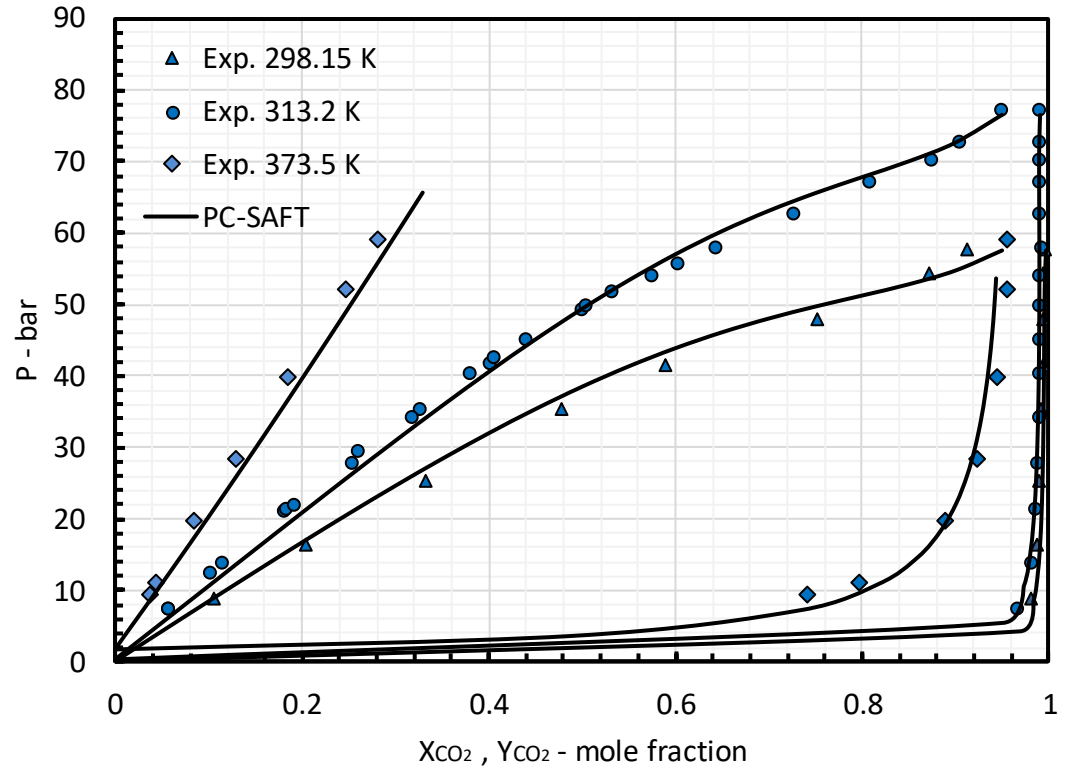

Figure 2.6. P-xy diagram of carbon dioxide-benzene system at 298.15 K, 313.2 K and 373.5 K: Comparison with tuned PC-SAFT model and experimental data (298.15:[89] **, 313.2:**[113], [114] **, 373.5:**[116] **)**

As shown in Figure 2.5 model calculation and experimental data are in good agreement for the CO_2/N_2 system where AAD % of 1.90 and 1.05 were calculated using 24 data points. Very good agreement with experimental vapour phase composition was found for the CO_2/benzene system with 1.06 AAD %, and as illustrated in Figure 2.6, the model accurately predicts the solubility of CO_2 in the benzene-rich phase over a reasonably wide range of temperature from 273.15 K to 393.2K.

In Table 2.4 the optimized BIPs and the optimization details of H_2S compromising binary systems as well as two binary systems including SO_2, binary systems of N_2O/propane and O_2/argon are reported. In-house datasets were used for tuning the model for N_2O/propane, SO_2/CO and SO_2/ethane systems. As expected, an excellent agreement with the experimental data was found for simple spherical molecule gas mixture of O_2/argon using 140 data point with 0.39% and 1.21% AAD values for mixture bubble point pressure and vapour phase composition respectively. The highest deviation from experimental vapour composition was found for N_2O/propane the AAD of 6.35% was observed between model calculation and experimental data. The calculated and experimental VLE of SO_2 and CO binary system is also displayed in Figure 2.7.

Table 2.4 Optimized binary interaction parameter of binary systems containing H_2S, SO_2, N_2O and O_2

	Binary System	k_{ij}	T-range (K)	P-range (bar)	N points	AAD % P_{bubble}	AAD % y_{vapour}	Ref.
H_2S	propane	0.0811	217.04-358	1.379-57.22	224	3.29%	5.78%	[136]–[139]
	pentane	0.0764	277.59-444.26	1.379-89.77	56	2.28%	2.46%	[140]
	hexane	0.0760	322.95-422.65	4.3-75.4	25	3.32%	0.76%	[95], [141]
	heptane	0.0863	310.9-394.3	6.06-95.4	19	4.58%	-	[142]
	octane	0.0842	288.15-303.15	1.01	4	0.52%	-	[95]
	nonane	0.0888	310.93-477.59	1.3-27.6	15	2.10%	0.97 %	[143]
	decane	0.0865	277.59-523.15	1.37-133.4	71	4.56%	0.19%	[144], [145]
	nC_{15}	0.0759	422.6	11.3-112.1	8	2.25%	-	[141]
	nC_{20}	0.0825	322.9-423.3	4-76.7	28	6.12%	-	[146]
SO_2	carbon monoxide	0.0028	324.47-385.71	29.3-19.4	25	3.48%	4.19%	In-house Data
	ethane	0.0825	303.15-323.15	8-74.4	24	3.3%	1.99%	In-house Data
N_2O	propane	0.1625	263.85-348.15	7.1-65.1	34	6.99%	6.35%	In-house Data
O_2	argon	0.0104	84-118.32	0.6-10.3	140	0.39%	1.21%	[147], [148]

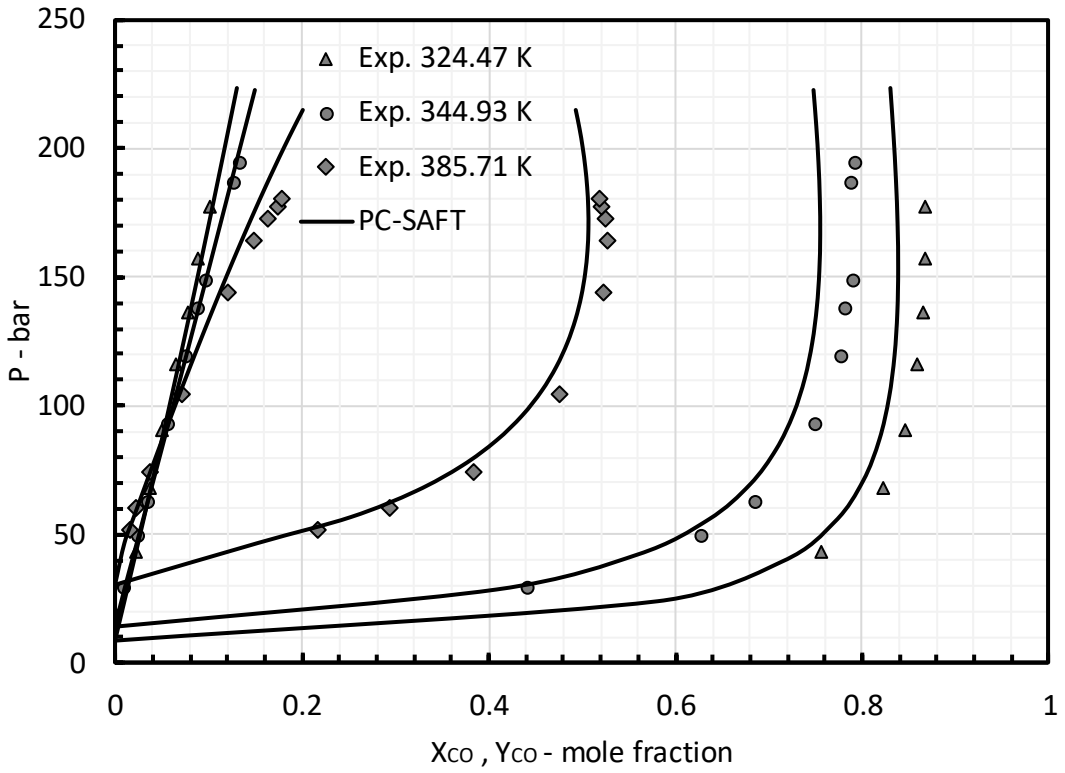

Figure 2.7. P-xy diagram of SO_2-CO system at K, 324.47 K, 344.93 K and 385.71 K: Comparison with tuned PC-SAFT model and experimental data (In-house Data)

The binary interaction parameters of 13 binary mixtures containing nitrogen were adjusted to literature and in-house VLE experimental data. For those systems, which the composition of the vapour phase was not available, only the bubble point pressure of the mixture was used in the objective function. The calculated P-xy diagrams of nitrogen-argon system have been plotted against the experimental data in the Figure 2.8 at 83.82 K, 99.98 K and 119.98 K. The BIP optimization details for binary systems containing nitrogen are reported in Table 2.5. Like the argon/O_2 system, excellent agreement between calculated and experimental VLE data was found at 83.82 K, 99.98 K and 119.98 K for argon/N_2 system. Figure 2.9 compares the calculated solubilities of nitrogen in normal eicosane at 323 K to 423 K and experimental data where 3.22% deviation was calculated between calculated and experimental solubilities at the whole range of temperature and pressure covered.

Table 2.5 Optimized binary interaction parameter of binary systems containing nitrogen

	Binary System	k_{ij}	T-range (K)	P-range (bar)	N points	AAD % P_{bubble}	AAD % y_{vapour}	Ref.
Nitrogen	propane	0.0872	114.1-353.15	1.50-219.1	131	10.55%	-	[149]–[153]
	butane	0.0991	153.15-422.04	4.05-285.1	113	9.73%	13.46%	[77], [82], [154]–[157]
	pentane	0.1001	144.3-377.59	2.5-310.7	37	5.23%	1.10%	[158]
	heptane	0.1242	298.15-455.37	19.6-998.5	108	4.64%	4.95%	[121], [159]–[164]
	octane	0.1437	233.15-373.35	2.02-350.4	67	11.51%	-	[163], [165], [166]
	nonane	0.1335	322-344.3	37.2-347.4	12	2.72%	-	[163]
	decane	0.1045	310.93-410.93	17.2-346.4	101	7.8%	0.19%	[163], [167]
	nC_{12}	0.1545	344.15-410.9	12.9-95.5	25	3.27%	-	[17f2]
	nC_{16}	0.1395	323.15-473.15	49-294	15	7.10%	-	[168]
	nC_{20}	0.1634	323.2-423.2	38.3-172.3	20	3.22%	-	[168]
	nC_{28}	0.1617	348.2-423.2	43-164.7	19	2.22%	-	[168]
	nC_{36}	0.1637	373.15-423.15	53-171.1	12	2.04%	-	[168]
	argon	-0.0053	85.03-122.89	0.8-28.3	453	1.02%	0.62%	[55], [169]–[177]

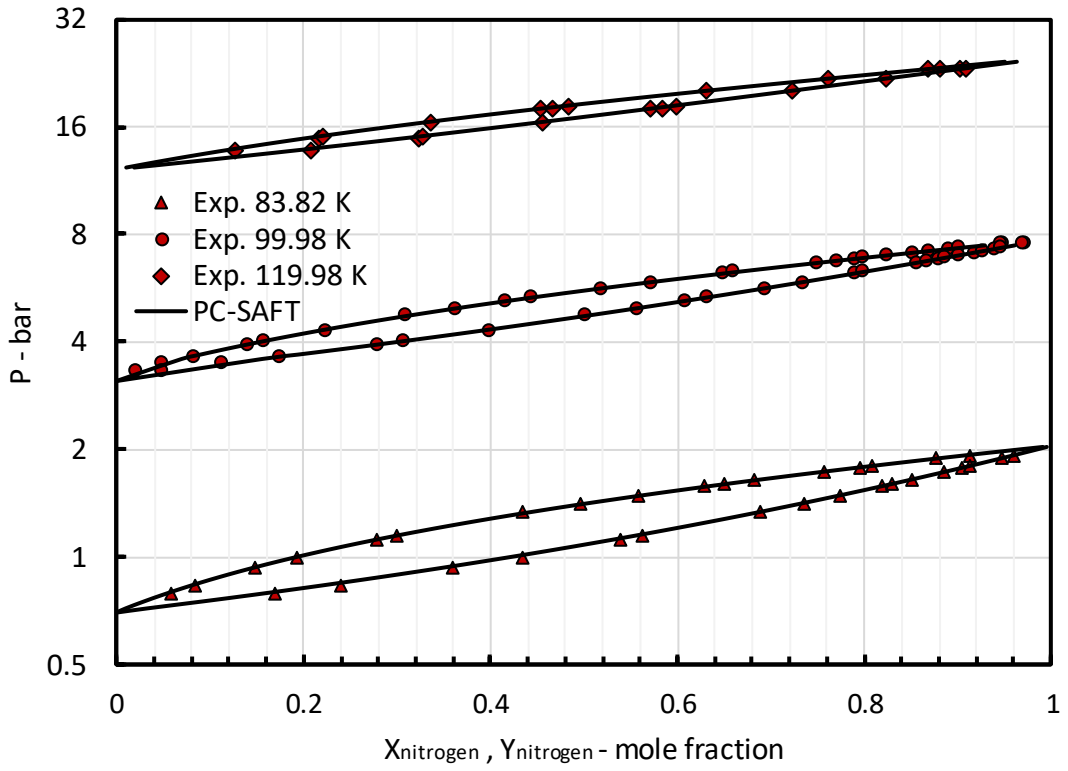

Figure 2.8 P-xy diagram of Ar-N_2 system at K, 83.82 K, 99.98 K and 119.98 K: Comparison with tuned PC-SAFT model and experimental data (83.82: [169]**, 99.98:**[174]**, 119.98:** [174]**)**

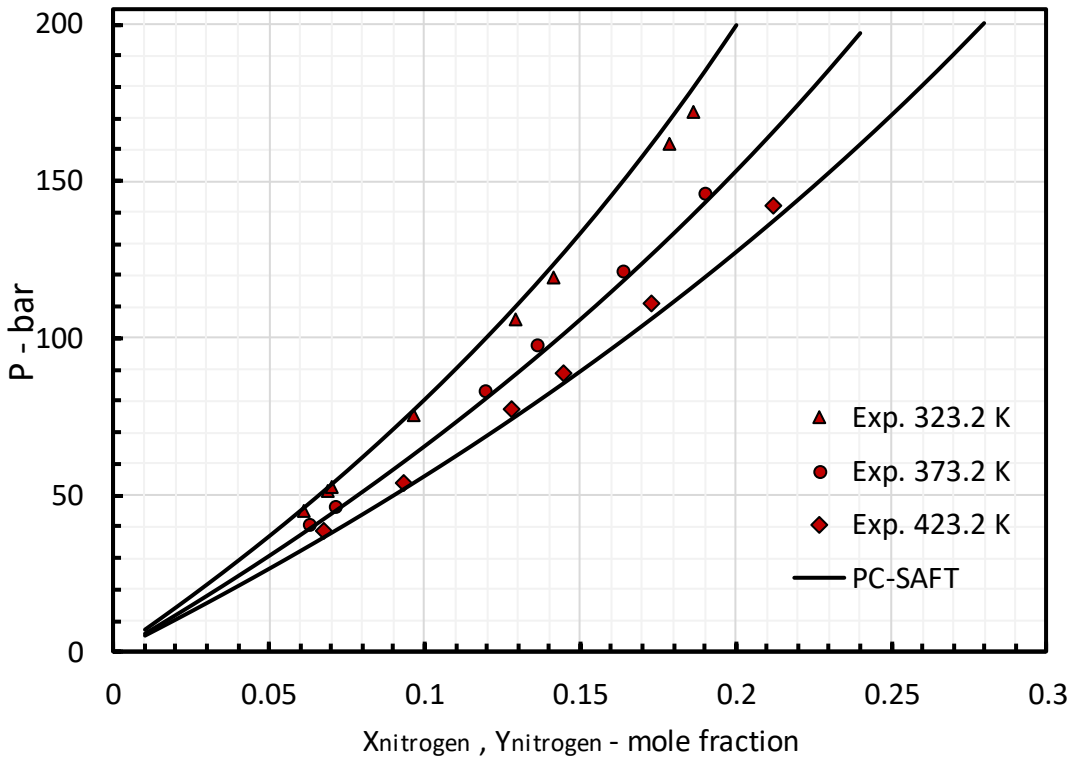

Figure 2.9 P-x diagram of N_2-nC_{20} system at K, 323.2 K, 373.2 K and 432.2K: Comparison with tuned PC-SAFT model and experimental data ([168]**)**

Binary mixtures of ethane and N_2, CO_2, H_2S, N_2O and a number of normal alkanes have been investigated, and the optimised binary interaction parameters are reported in Table 2.6. AAD of 3.56% was found from experimental bubble point pressure for the ethane/decane system while the predictions for vapour phase composition agree well with experimental data.

Table 2.6 Optimized binary interaction parameter of binary systems containing ethane

	Binary System	k_{ij}	T-range (K)	P-range (bar)	N points	AAD % P_{bubble}	AAD % y_{vapour}	Ref.
Ethane	propane	-0.0041	127.59-369.18	0.0002-51.849	314	3.12%	3.39%	[44], [178]–[186]
	butane	0.0087	235.35-419.25	1.613-57.9	79	2.93%	1.85%	[187]–[191]
	pentane	0.0119	277.59-44.56	3.477-682457	80	2.08%	1.32%	[192]
	hexane	0.0044	310.9-449.82	1.7237-79.015	84	6.00%	-	[187], [193]
	heptane	0.0083	234.85-524.25	6.89-88.185	141	2.33%	1.28%	[187], [194]
	octane	0.0208	273.15-373.15	4.0527-68	77	2.37%	0.66%	[97], [195]
	decane	0.0198	277.59-510.93	3.4474-118.25	93	3.56%	0.66%	[196]–[198]
	nC_{12}	0.0202	298.15-373.15	2.9-58.4	77	3.38%	-	[46], [162], [199]
	nC_{14}	0.0244	323.2-422.7	20.2-80	21	3.5%	-	[200]
	nC_{18}	0.0241	323.3-422.5	9.4-81.7	22	3.26%	-	[201]
	nC_{20}	0.0207	323.15-572.85	5.05-76.87	30	4.32%	-	[52]
	nC_{36}	0.0242	373.15-473.15	3.68-47.6	13	1.21%	-	[202]
	nC_{44}	0.0234	373.15-423.16	3.87-31.07	15	3.48%	-	[202]
	N_2	0.0412	110.93-290	1.965-134.66	260	7.23%	13.03%	[31], [33], [41], [57], [150]–[152], [203], [204]
	CO_2	0.0954	222.04-298.15	6.24-66.3	301	1.03%	5.28%	[30], [37], [71], [72], [150], [191], [205]–[209]
	H_2S	0.0685	199.93-357.87	0.6516-82.73	56	1.59%	1.97%	[210]
	N_2O	0.1514	273.15-293.05	16.47-43.43	37	8.79%	12.57%	In-house Data

Figure 2.10 shows the calculated and experimental P-xy diagram of the nitrogen-ethane system at 149.82 K, 194.26 K and 122.04 K where the agreement between model calculations and experimental data appeared to be excellent at both temperatures. Furthermore, as seen in Figure 2.10, a liquid-liquid immiscibility is observed at 122.04 K between nitrogen-rich and ethane-rich phases where with increasing the mole fraction of ethane in the system, the boiling point pressure of the system remains constant at roughly the bubble pressure of pure nitrogen at 122.04 K. This means that, at this temperature with increasing the amount of nitrogen in the system two immiscible phases are formed and with further increasing the nitrogen content of the system only molar phase fraction of the nitrogen-rich phase increases and the bubble point on the mixture remains almost constant at around the bubble pressure of pure nitrogen at 122.04 K. The calculated VLE of ethane-n-dodecane is plotted in Figure 2.11 together with experimental data at 308.15 K to 373.15 K. Calculated and experimental data of CO_2/ethane system are compared in Figure 2.12 where shown that model correlates the experimental data very well at 230 K, 283.15 K and 250 K and predicts the azeotrope composition of the system at those temperatures accurately.

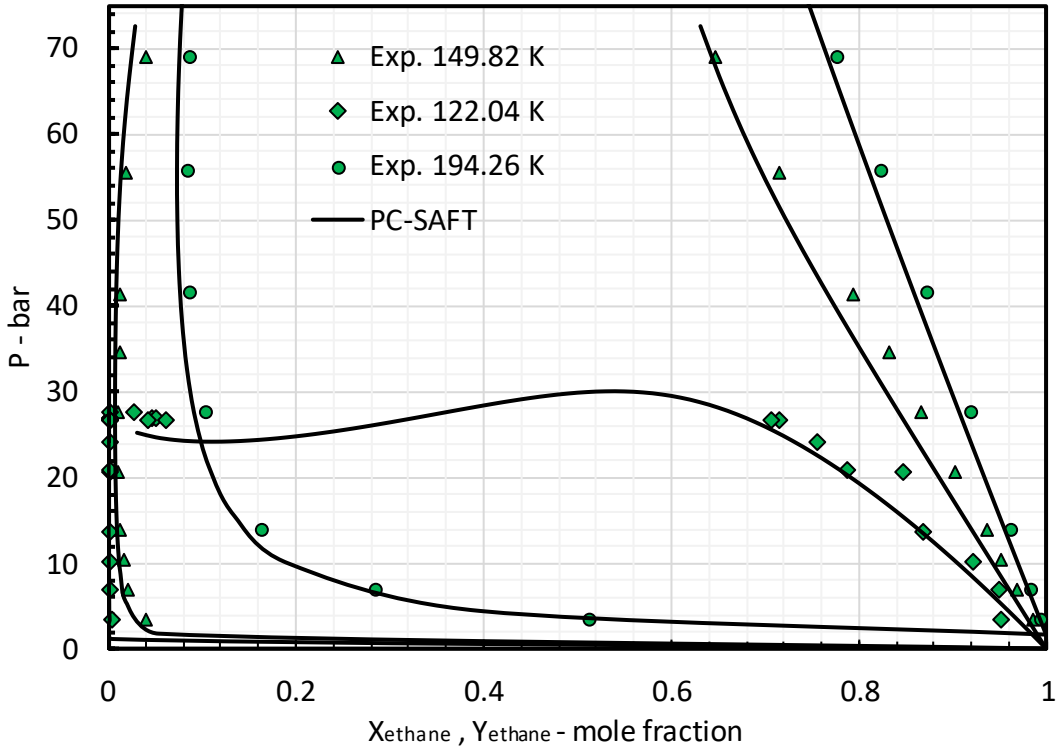

Figure 2.10 Vapour-liquid and liquid-liquid equilibria of N_2-ethane system at K, 149.82 K, 194.26 K and 122.04 K: Comparison with tuned PC-SAFT model and experimental data (149.82 and 194.26: [57]**, 122.04:** [33]**)**

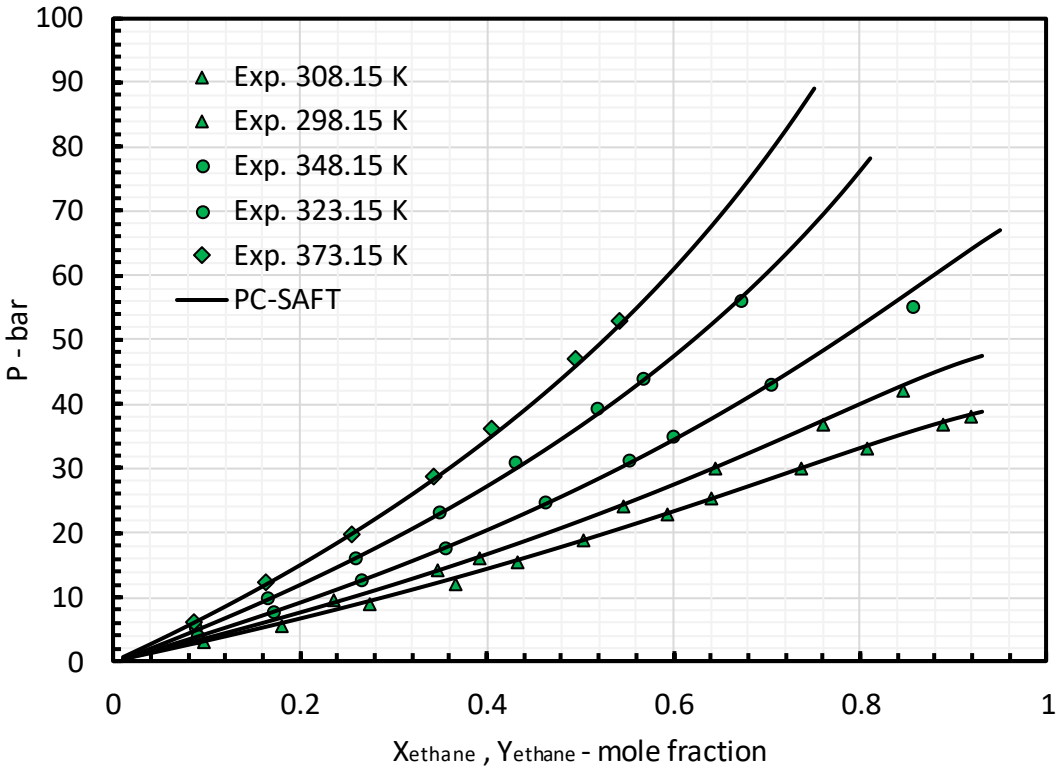

Figure 2.11 P-xy diagram of nC_{12}-ethane system at 308.15 K, 298.15 K, 348.15 K, 323.15 K and 373.15 K: Comparison with tuned PC-SAFT model and experimental data (298.15 K, 348.15K, 323.15 K, 373.15 K: [162]**, 308.15 K:** [199]

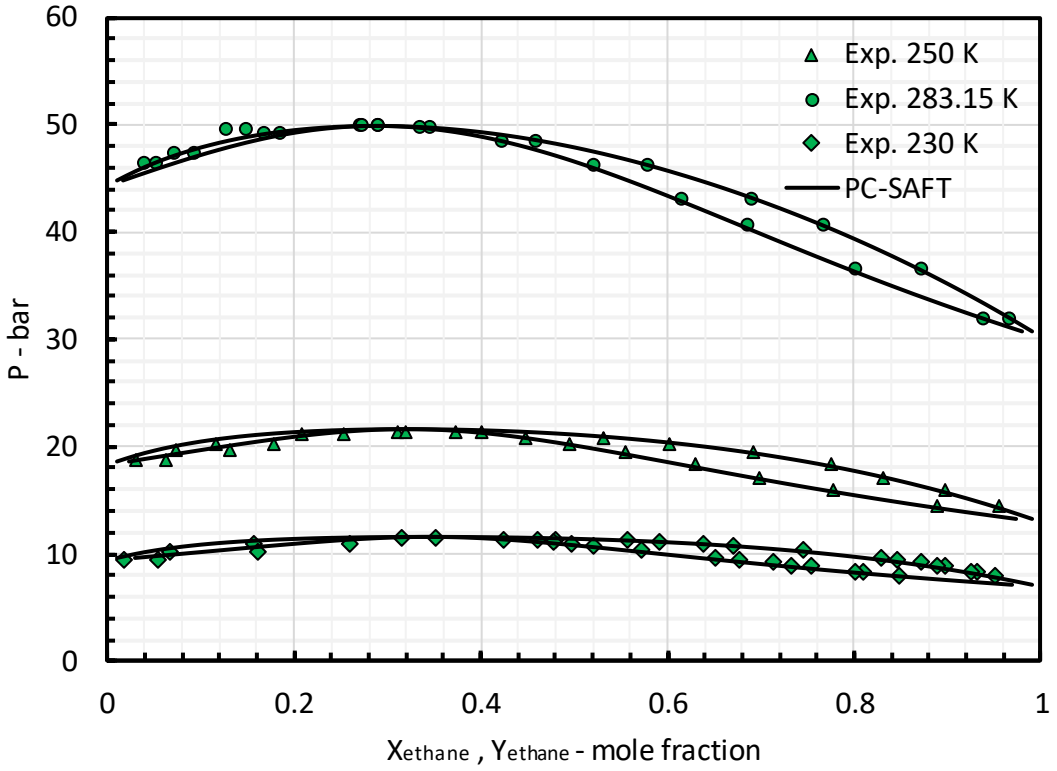

Figure 2.12 P-x diagram of CO_2-ethane system at 250 K, 283.15 K and 230 K: Comparison with tuned PC-SAFT model and experimental data (230K: [206]**, 283.15:** [209]**, 250 K:** [30]**)**

2.4 Modelling of Pure Water

Natural gases are in equilibrium with brines at reservoir conditions. In multi-phase transportation pipelines or downstream natural gas treatment facilities natural gas may be saturated with water or brine. A small moisture content in the transportation pipelines can results in hydrate formation and pipeline blockage, damage to the pipeline facilities and severe disruption in the operation. To assess the risk of hydrate formation using modelling approach, an accurate thermodynamic model is required to precisely predict the hydrate stability zone of the fluid.

Polar fluids or associating compounds in which hydrogen bonding and electrostatic interactions are prominent such as water, methanol, ethanol and glycols, play a significant role in flow assurance systems of concern. Therefore, a robust model which is capable of predicting the phase behaviour of such systems is needed. Five pure compound parameters are required for the PC-SAFT equation of state, and as mentioned before, two of which characterise the interaction between associating molecules. The pure component parameters for such compounds are usually obtained by tuning the model with experimental vapour pressure and saturated liquid density data of the pure compound. However, more properties may be considered in the objective function depending on the

expectation from the model in predicting a particular property within a desired conditions or accuracy.

In this work, a new set of PC-SAFT EoS pure compound parameters was tuned to model the phase equilibria and PVT behaviour of water accurately. To do this, based on von Solms et al. conclusion [211], the 4C association scheme was selected to describe the associating site structure of the water molecule. Saturated liquid density and vapour pressure of water were simultaneously tuned to smoothed data taken from NIST [212]. To account for the unique behaviour of water density at the temperature range 0 °C-4 °C and also to increase the capability of the model in calculating the water fugacity needed for phase equilibria calculation, a temperature dependent dispersion energy parameter $\frac{\varepsilon}{k_B}$ and a temperature dependant segment diameter parameter σ were introduced in this work. All parameters were adjusted to experimental saturated liquid densities and vapour pressures of pure water at 273.15 to 523.15 K. The resulting optimized $\frac{\varepsilon}{k_B}$ and σ values were then regressed to a third order polynomial equation to correlate the pure compound parameters with temperature. A temperature independent objective function was adopted to optimize the segment number m and association parameters, $\frac{\varepsilon_{AB}}{k}$ and κ^{AB} and then a temperature dependent objective function was applied to further adjust the temperature dependant parameters with experimental data.

$$OBJ = \sum_1^{Nexp}\left(\left(\frac{VP_i^{EoS}-VP_i^{Exp}}{VP_i^{Exp}}\right)^2+\left(\frac{\rho_i^{EoS}-\rho_i^{Exp}}{\rho_i^{Exp}}\right)^2\right) \quad \text{Eq. 2.62}$$

$$OBJ(T) = \left(\left(\frac{VP_T^{EoS}-VP_T^{Exp}}{VP_T^{Exp}}\right)^2+\left(\frac{\rho_T^{EoS}-\rho_T^{Exp}}{\rho_T^{Exp}}\right)^2\right) \quad \text{Eq. 2.63}$$

The resulting correlations for temperature dependent $\frac{\varepsilon_{water}}{k_B}$ and σ_{water} are:

$$\frac{\varepsilon_w}{k_B}(T) = A_3T^3 + A_2T^2 + A_1T + A_0 \quad \text{Eq. 2.64}$$

$$\sigma_w(T) = B_3T^3 + B_2T^2 + B_1T + B_0 \quad \text{Eq. 2.65}$$

Optimized PC-SAFT pure water parameters, as well as the coefficients of the polynomial equation, are listed in Table 2.7.

Table 2.7 Optimum PC-SAFT parameters for pure water

m	1.53	
$\frac{\varepsilon_w}{k_B}(K)$	A_0	2.3845E+02
	A_1	- 4.0452E-01
	A_2	+ 1.0124E-03
	A_3	-7.6782E-07
σ_w(Å)	B_0	2.9526
	B_1	- 2.6247E-03
	B_2	+ 5.7815E-06
	B_3	-3.8066E-09
$\frac{\varepsilon_{AB}}{k_B}(K)$	1804.17	
κ_{AB}	0.0948	

To check the predictive capability of the model using the new set of parameter, the vapour pressure and saturated liquid density of pure water together with water freezing point at atmospheric pressure were tested against experimental data. von Solms et al. presented seven sets of pure compound parameters for water using the 4C scheme and incorporated measured monomer fractions using spectroscopy [211]. According to their publication, using the adjusted pure compound parameters, better predictions were obtained for the monomer fraction, without compromising the prediction accuracy of the liquid density and vapour pressure [211]. A temperature dependent segment diameter was also introduced by Held et al. to account for the unique behaviour of water density with respect to temperature changes below 4 °C [213]. This parameter set was adjusted at 273.16 to 373.15 K. Table 2.8 summarizes the water pure parameter reported in the literature. Table 2.9 also compares the calculated freezing points and the AAD % values of calculated and experimental vapour pressure and saturated liquid density at 273.14 K to 520 K using the pure parameter set adjusted in this work and those reported by others.

Table 2.8 This work and literature PC-SAFT pure compound parameters for water

Associating Scheme	Reference	m	σ_w(Å)	$\frac{\varepsilon_w}{k_B}(K)$	$\frac{\varepsilon_{AB}}{k_B}(K)$	κ_{AB}
2B	[214]	1.0656	3.0007	366.51	2500.7	0.034868
4C	[211]	2	2.3533	207.84	1506.4	0.1550
4C	[211]	3	2.0135	182.92	1259	0.4287
2B	[213]	1.204659	Eq. (7)	353.9449	2425.6714	0.0450989
4C	***This work***	***1.53***	***Eq. 2.65***	***Eq. 2.66***	***1804.17***	***0.0948***

Table 2.9 Calculated freezing point and AAD % of calculated vapour pressure and saturated liquid density of water using the pure parameters reported in the literature and the those adjusted in this work

Reference	Calculated Vapour pressure AAD %	Calculated saturated liquid density AAD %	Calculated Freezing Point (K)	Deviation from Experimental $\Delta T_{freezing\ poitn}$ (K)
[214]	3.92%	7.50%	281.766	8.616
[211]	10.49%	0.95%	282.101	8.951
[211]	12.97%	1.20%	282.834	9.684
[213]	2.05%	0.42%	274.818	1.668
This work	***0.08%***	***0.16%***	***273.201***	***0.051***

As presented in Table 2.9, the calculated freezing point using the pure compound parameters regressed in this work deviates 0.051 K from the experimental data while the best deviation obtained using the literature sets of parameters is the one calculated by Held et al. set of parameters with 1.668 K deviation from pure water freezing point at atmospheric pressure. Using the parameters reported by von Solms et al. the freezing point of water is calculated around 8 °C which can lead to significant error in hydrate calculations. The vapour pressure and saturated liquid density of water are plotted versus temperature in the Figure 2.13 and Figure 2.14 together with the vapour pressure and saturated liquid density of water using the parameters reported in the literature. The AAD % of saturated liquid density calculated using Gross and Sadowski set of parameters [214] is 7.5% while the vapour pressure is predicted reasonably well using this set of parameter where with AAD % value of 3.92.

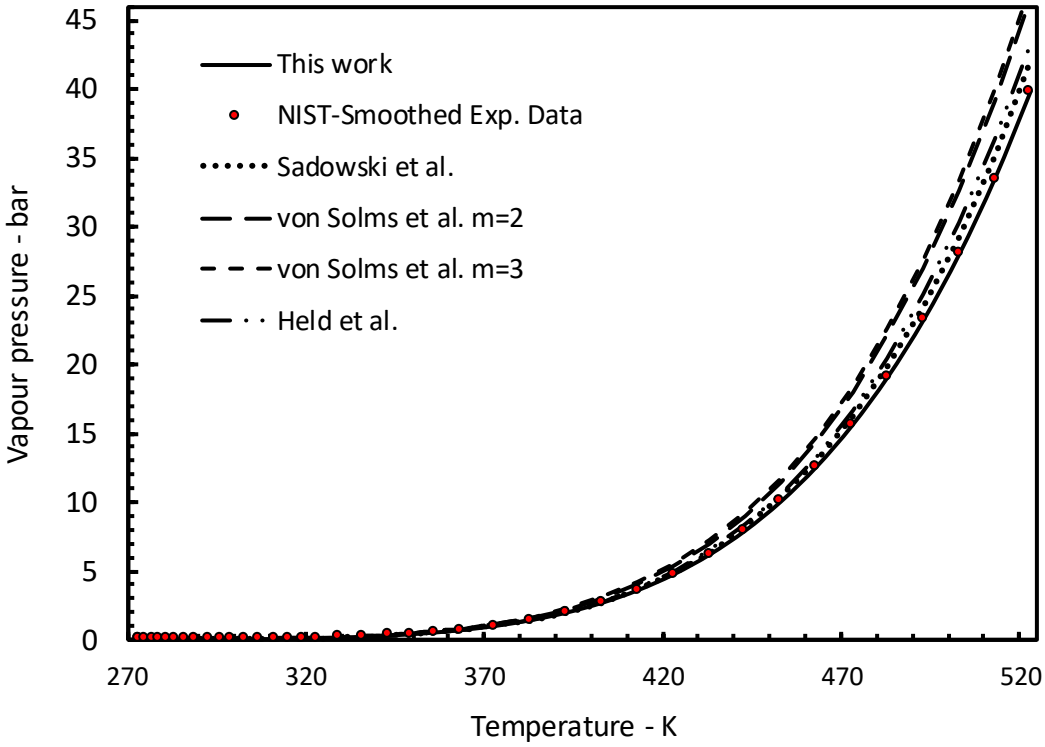

Figure 2.13 Calculated vapour pressure of water with PC-SAFT model using different sets of pure compound parameters (Applied pure parameters from Gross and Sadowski [214]**, von Solms et al.** [211] **and Held et al.** [213]**)**

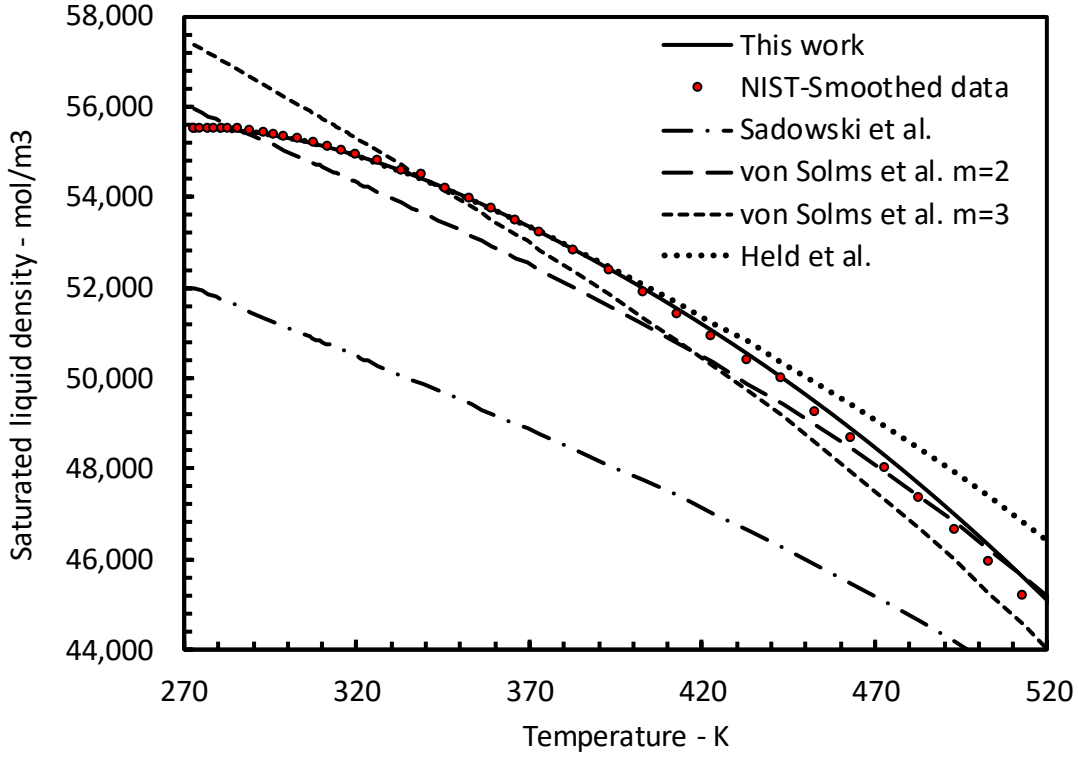

Figure 2.14 Calculated saturated liquid density of water using PC-SAFT model and different sets of pure compound parameters (Applied pure parameters from Gross and Sadowski [214]**, von Solms et al.** [211] **and Held et al.** [213]**)**

The calculated vapour pressures and saturated liquid density using Held et al. set of parameters also shows a very good agreement with experimental data over a wide range of temperature despite the fact that the parameters were adjusted to saturation data of water between 273.15 to 373.15 K [213]. Excellent agreement with experimental data was found for the parameters developed in this work where the vapour pressure and liquid density of water are calculated with 0.08% and 0.16% average deviation from experimental data respectively.

2.5 Binary Systems of Water and Non-Associating Components

Using the new developed PC-SAFT pure compound parameters for water, binary interaction parameters between water and non-associating components must be optimized using experimental solubility data. For 37 water and non-associating binary systems, temperature dependent k_{ij} were introduced and adjusted with experimental VLE or LLE data to increase the ability of the model in phase equilibria behaviour modelling of such systems. It is worth noting that even though temperature dependant pure compound parameters were introduced, the optimized BIPs for non-associating molecules are highly temperature dependant. Conventional Lorentz-Berthelot mixing rules were employed here where the tuned binary interaction parameters (k_{ij}) is introduced to adjust the dispersive interactions between a pair of unlike molecules of a mixture. Association volumes and energies were combined arithmetically and geometrically respectively in the association contribution calculations. No additional parameter was introduced for tuning the association energies. The following objective function was chosen to minimized by the Nelder-Mead version of SIMPLEX algorithm [26].

$$OBJ = \sum_{i=1}^{N_{exp}} \left(\left(\frac{X_i^{EoS} - X_i^{Exp}}{X_i^{Exp}} \right)^2 \right) \qquad \text{Eq. 2.66}$$

where x_i is the solubility of the non-associating component in pure water at specified temperature and pressure. All the temperature dependent binary interaction parameters were fitted to a polynomial equation of second order (Eq. 2.67) which the coefficients are reported in Table 2.10.

$$k_{ij}(T) = A_2 T^2 + A_1 T + A_0 \qquad \text{Eq. 2.67}$$

Table 2.10 Coefficients of the temperature dependent BIP polynomial function

	Binary system	A_0	A_1	A_2
Water	methane	-7.0477	3.6599	-4.2038
	ethane	-5.5634	3.2466	-3.9384
	propane	-4.8241	2.9925	-3.8098
	iso-butane	-17.9951	12.0075	-19.2017
	n-butane	-7.3857	4.9239	-7.3076
	iso-pentane	-10.3372	6.9431	-10.6951
	argon	-9.6993	4.9145	-5.5884
	n-hexane	-4.8564	3.1718	-4.1279
	n-octane	-3.2583	2.2943	-2.9489
	n-nonane	-6.5025	4.1820	-5.5976
	benzene	-1.1752	1.0391	-1.4584
	carbon monoxide	-9.9497	4.8389	-6.0950
	cyclo-pentane	-2.3783	1.8058	-2.1350
	hydrogen sulphide	-0.4558	0.4996	-1.1768
	ethyl benzene	-2.1620	1.6189	-2.1891
	hydrogen	-4.5166	-0.0128	1.2204
	krypton	-4.5272	2.4753	-2.3257
	methyl cyclo hexane	-4.3926	3.0959	-4.1080
	methyl cyclo pentane	2.6474	-0.8548	0.8506
	nitrous oxide	-10.0552	6.5201	-10.7829
	nitrogen	-6.3417	3.2008	-3.7119
	oxygen	-8.0269	3.9697	-4.1975
	toluene	-1.3367	1.1065	-1.4763
	xenon	-4.4317	2.4913	-2.6629
	p-xylene	-1.7249	1.3916	-1.9802
	m-xylene	-2.5863	1.9197	-2.7801
	o-xylene	1.2724	-0.5631	1.2810
	cyclo-hexane	-2.4374	1.7991	-2.3004
	n-decane	0.104233	0	0
	n-C_{12}	-1.5088	1.3433	-1.7101
	n-C_{14}	-0.5722	0.6522	-0.6273
	n-C_{16}	-0.1887	0.3362	-0.1444
	n-C_{18}	0.4617	0	0
	n-C_{20}	-1.3035	0.6871	-0.4034
	n-C_{30}	0.0102	0	0
	n-C_{36}	-0.0844	0	0

For binary systems of water and decane, nC_{18}, nC_{30} and nC_{36} where only one single experimental solubility point was available, non-temperature dependent BIPs are reported. Table 2.11 summarized the temperature and pressure ranges of the experimental data used for tuning BIPs together with the resulting total AAD % of each system. In Figure 2.15 PC-SAFT and Duan [215] model calculations for solubilities of methane in

pure water are plotted where the AAD % of 3.51% was obtained at 273.15 K to 523.15 K temperature range and 1 to 2000 bar pressures. The calculated solubilities of H_2S in pure water using PC-SAFT and Duan model [216] were compared in Figure 2.16 at 303.15 K to 483.15 K. As shown in Figure 2.16 the agreement between model calculations is relatively good except for the solubilities at 483.15 K where a higher deviation, i.e. AAD % of 8.04% was calculated due to proximity to the critical region. Solubilities of heavy normal alkanes are also plotted against experimental solubility data of normal tetradecane, normal hexadecane and normal eicosane at the fixed pressure of 50 bar in Figure 2.17. Results show very good agreement with the experimental data for all three normal alkanes. However, some deviations are observed at low temperatures for solubility of normal eicosane in water.

Table 2.11 Details of the experimental data used for binary interaction parameter of water/non-associating binary system as well as the resulting average absolute deviations for these systems

	Binary System	T-range (K)	P-range (bar)	N Points	AAD % $X_{soluete}$	References
Water	methane	273.15-523.15	1.0-2000.0	231	3.51%	[217]
	ethane	273.15-444	1.0-1000.0	201	2.14%	[218]
	propane	273.15-422.04	0.1-192	219	5.07%	[219]–[235]
	iso-butane	278.15-318.15	1.01	14	5.86%	[227], [228], [231]
	n-butane	273.15-363.15	1.01	100	5.93%	[140], [221]–[224], [227]–[230], [236]–[245]
	iso-pentane	273-333.15	1.01	18	3.68%	[246]–[250]
	argon	283.15-453.7	1.01-25.26	61	2.89%	[251]–[258]
	n-hexane	273.15-443.15	0.1-50	33	10.89%	[220], [223], [247], [249], [250], [259]–[266]
	n-octane	273.15-456.15	1.01	21	9.14%	[246], [247], [249], [265]
	n-nonane	293.15-409.95	1.01	23	29.02%	[246], [250], [261], [265], [267]
	benzene	273.15-473.15	1.01	129	4.69%	[246], [247], [249], [250], [262], [263], [266], [268]–[290]
	carbon monoxide	273.15-477.59	1.01-137.9	119	4.52%	[96], [291]–[294]
	carbon dioxide	293.15-513.15	1-1000	220	1.42%	[295]
	cyclo-pentane	276.45-373	1.01	12	9.68%	[246], [249], [286]
	hydrogen sulphide	303-513.15	1-200	79	6.80%	[216]
	hydrogen	273.15-616.48	3.4-1013	99	8.55%	[296]–[303]
	krypton	277.15-523.5	1.01-67	35	6.84%	[251], [254], [257], [304]–[306]
	methyl-cyclo-hexane	298-423	1.01	12	4.69%	[231], [246]
	methyl-cyclo-pentane	298.15-457.15	1.01	8	3.55%	[231], [246], [249], [250], [307]
	nitrous oxide	278.15-355.4	1.01	79	3.65%	[308]–[315]
	nitrogen	393-573	10-600	84	6.29%	[316]
	oxygen	273-603	1.01-1000	162	9.56%	[317]
	toluene	273-485	1.01-68	118	5.03%	[224], [228], [246], [247], [249], [259], [263], [269], [271], [274], [275], [278], [279], [318], [319]
	xenon	277.15-476.3	1.01-54.2	25	8.08%	[251], [254], [257], [304], [306]
	p-xylene	273-363	1.01	35	0.15%	[246], [247], [250], [272], [318], [320], [321]
	m-xylene	273-343	1.01	9	4.25%	[246], [247], [250], [272], [321]–[323]
	o-xylene	273-318	1.01	16	13.45%	[228], [246], [247], [250], [272], [320], [321], [323]
	cyclo-hexane	274-424	1.01	31	4.75%	[228], [231], [246], [250], [262]–[264], [271], [287], [290]
	n-decane	293-298	1.01	4	7.53%	[261], [267], [324], [325]
	nC_{12}	298-423	1.01	6	7.57%	[246], [326], [327]
	nC_{14}	298-472	1.01-50	6	17.24%	[326], [327]
	nC_{16}	298-473	1.01-50	6	0.57%	[326], [327]
	nC_{18}	298	1.01	1	22.49%	[327]
	nC_{20}	298.15-473.15	1.01-50	6	1.25%	[326], [327]
	nC_{30}	298.15	1.01	1	2.57%	[328]
	nC_{36}	298.15	1.01	1	3.51%	[328]

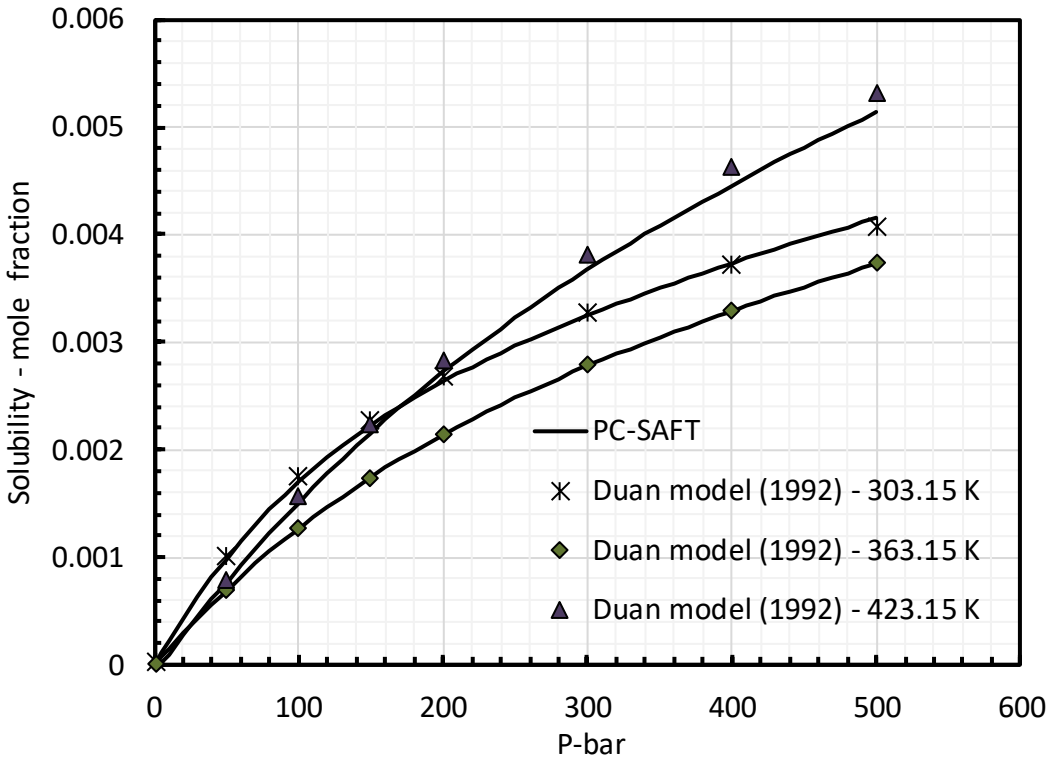

Figure 2.15 P-x diagram of methane-water system at 303.15 K, 363.15 K and 423.15 K, Comparison with tuned PC-SAFT model and Duan model ([217]**)**

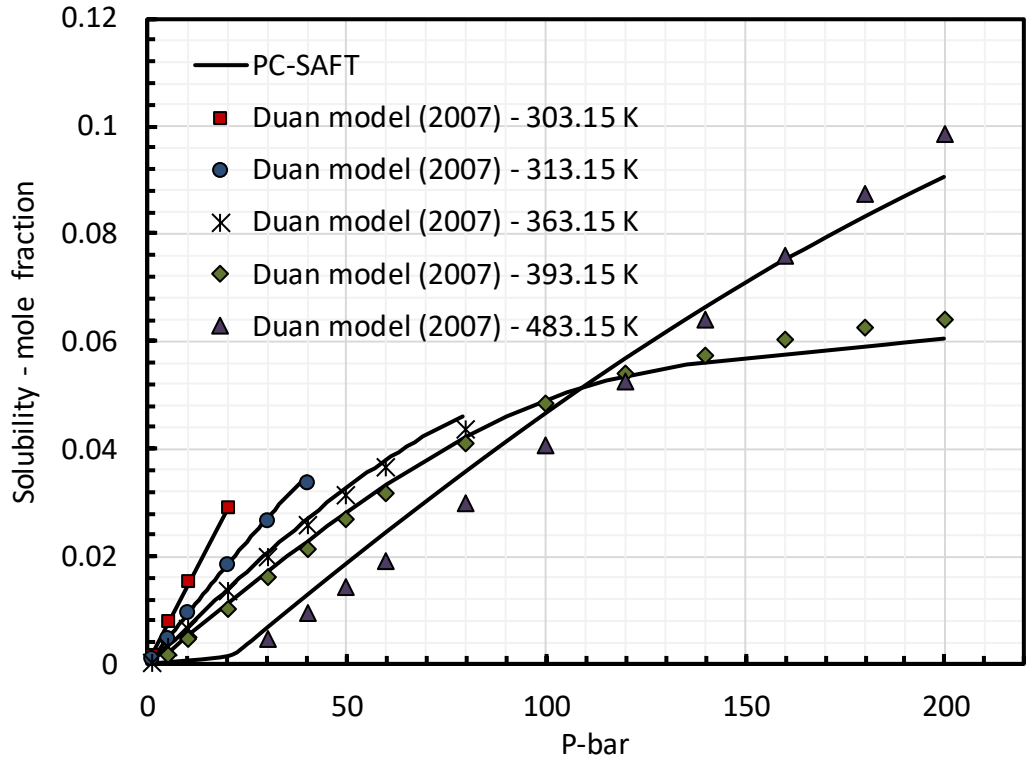

Figure 2.16 P-x diagram of H_2S-water system at 303.15 K, 313.15 K, 363.15 K and 393.15 K and 483.15 K, Comparison with tuned PC-SAFT model and Duan model predictions ([216]**)**

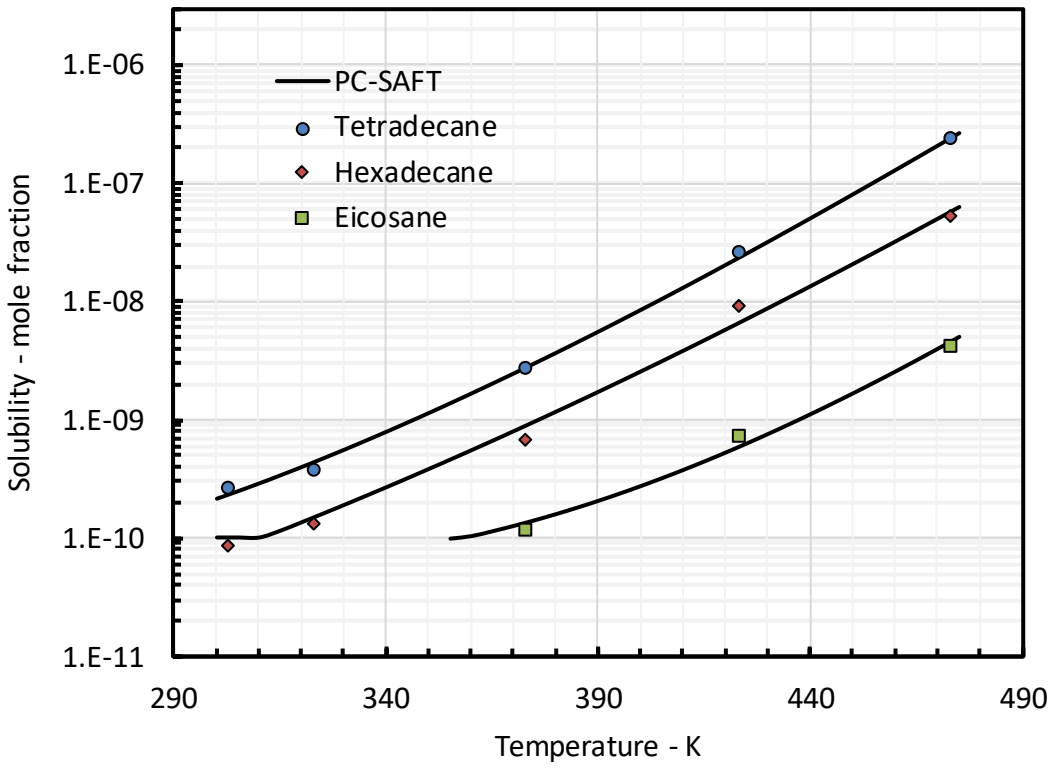

Figure 2.17 T-x diagram of heavy normal alkanes-water systems at P=50 bar: Comparison with tuned PC-SAFT model and experimental data ([326]**)**

For CO_2-water system, another parameter was introduced to correlate the pseudo-retrograde behaviour of water solubility in the CO_2-rich phase. A similar approach to the one proposed by Austegard et al. [329] was adopted in this work where the association strength of the CO_2-water molecules are described as the association strength proportional to the association strength between water molecules. Both parameters were then simultaneously adjusted to experimental solubilities and water content data using the following objective function:

$$OBJ = \sum_{i=1}^{N_{exp}} \left(\left(\frac{X_i^{EoS} - X_i^{Exp}}{X_i^{Exp}} \right)^2 + \left(\frac{Y_i^{EoS} - Y_i^{Exp}}{Y_i^{Exp}} \right)^2 \right) \qquad \text{Eq. 2.68}$$

where X_i^{EoS}, X_i^{Exp} are calculated and experimental solubilities of CO_2 in water and Y_i^{EoS}, Y_i^{Exp} are calculated and experimental water content of the CO_2-rich phase respectively. Duan model [295] was used to adjust the BIP and the experimental water content data were taken from several references here [330]–[338]. The optimum temperature dependent dispersion and association BIPs are presented here.

$$k_{Solvation} = 6.12150664\text{e}-08T^3 - 6.81401597\text{e}-05T^2 + 2.64147810\text{e}-02\text{T} - 3.30480229$$

$$k_{ij} = 2.46105561e-08T^3 - 3.07478777e-05T^2 + 1.27089464e-02T - 1.67616684$$

Figure 2.18 shows the calculated solubilities of CO_2 in water using Duan [295] and PC-SAFT models at 288.15 K, 298.15 K, 363.15 K and 423.15 K. As the available experimental data below 293.15 K were limited, the tunings were performed at 293.15 K to 423.15 K temperature range. However, around 5.5% AAD was found between the model calculations at 273.15 K to 513.15 K temperature range. The model calculations and experimental water content in the CO_2-rich phase at T<50 °C and T>100 °C are compared in Figure 2.19 and Figure 2.20. The AAD % of 11.08% was obtained between the model calculation and experimental water content data at 278.15 K to 603.15 K.

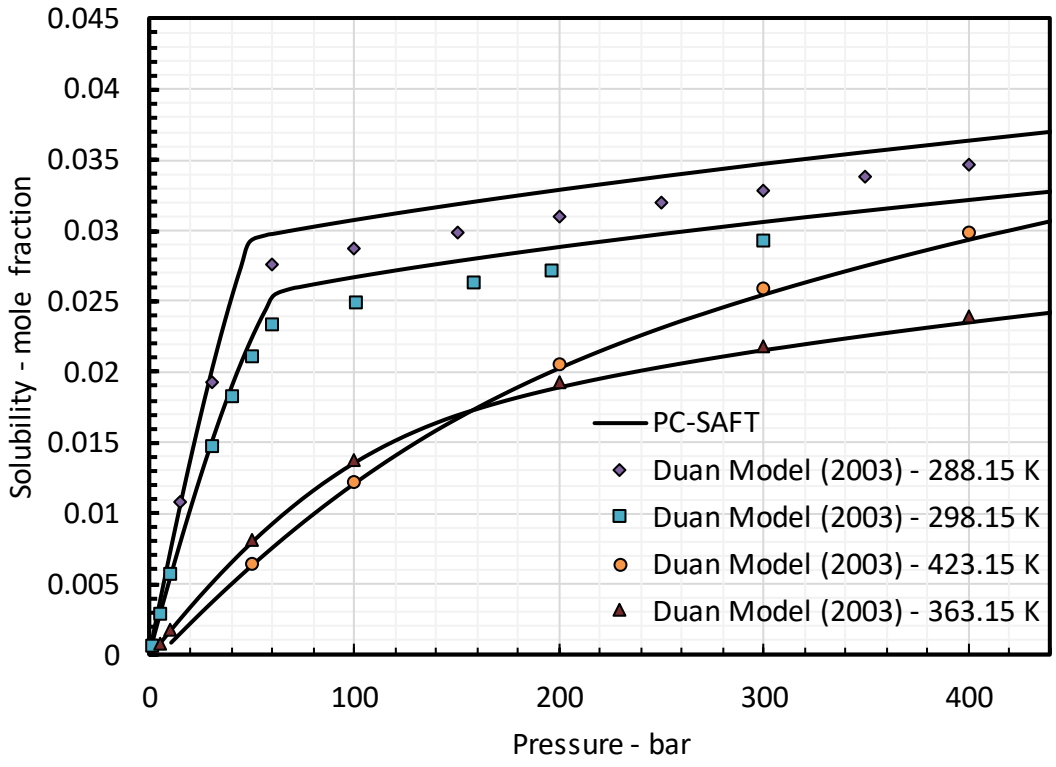

Figure 2.18 VLE and LLE diagram of CO_2-water system at 288.15 K, 298.15 K, 363.15 K and 423.15 K: Comparison between tuned PC-SAFT model and Duan model ([295]**)**

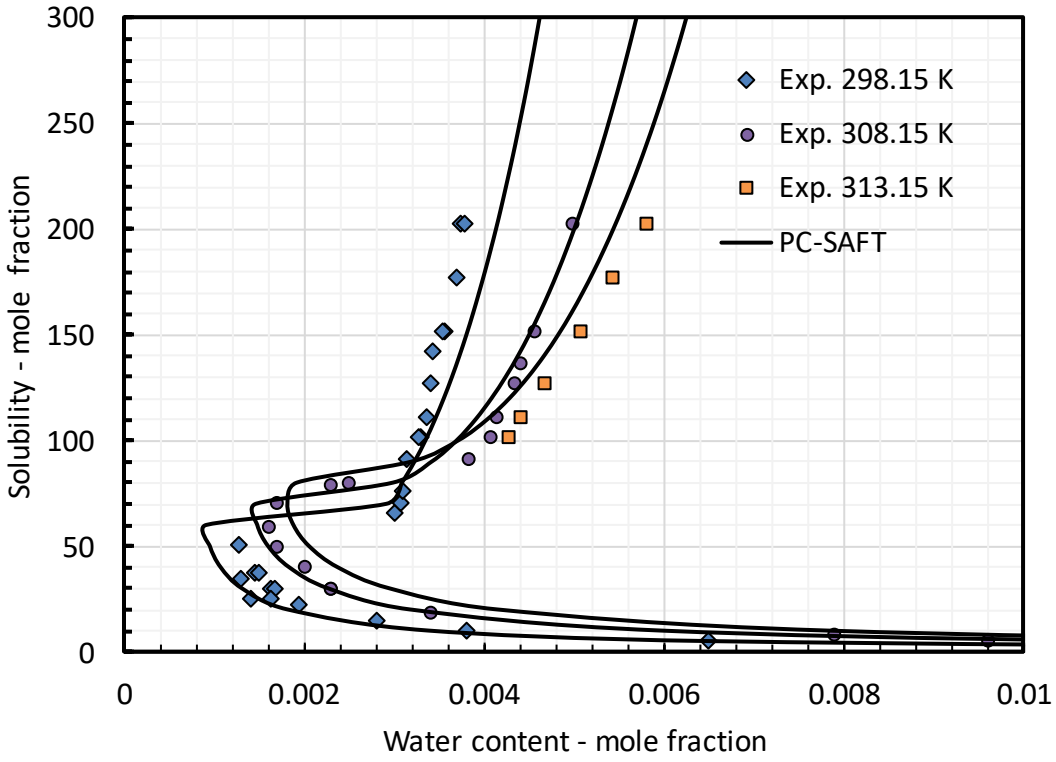

Figure 2.19 P-y diagram of CO_2-water system at 298.15 K, 308.15 K, 313.15 K: Comparison with PC-SAFT model and experimental data (298.15 K: [339]–[342]**, 308.15:** [340], [341]**, 313.15:**[341]**)**

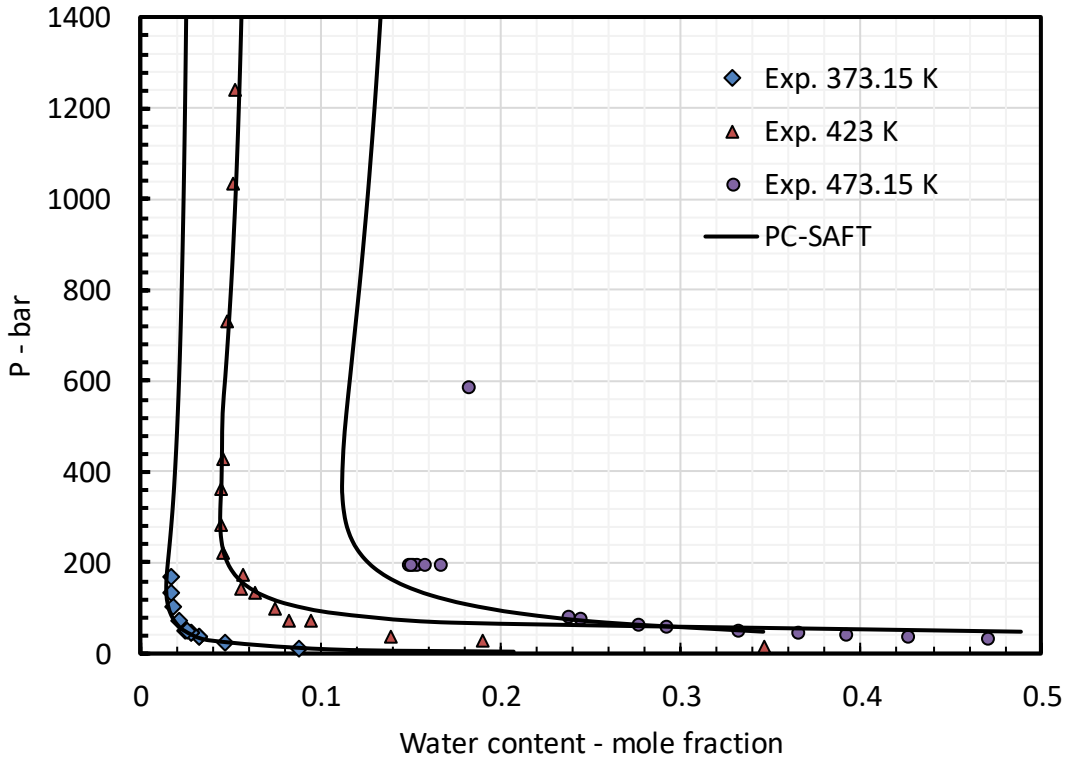

Figure 2.20 P-y diagram of CO_2-water system at 373.15 K, 423 K, 473.15 K: Comparison with PC-SAFT model and experimental data (373.15: [336], [342]**, 423:** [336]**, 473.15:** [338]**)**

2.6 PC-SAFT Pure Compound Parameter Optimization for Glycols

Natural gas is transferred to the natural gas processing units from reservoirs via pipelines at in some cases high pressures and low temperatures whereas the risk of hydrate formation is considerably high. To prevent hydrate formation in such systems, one option is to inject thermodynamic hydrate inhibitors. Alcohol based chemicals have been extensively used as thermodynamic hydrate inhibitors. In theory, thermodynamic hydrate inhibitors weaken the hydrogen bonding between water molecules and make the solid phase unstable at freezing point or hydrate formation conditions [343]. Methanol has been used extensively as thermodynamic inhibitor; however, because of some environmental considerations, it has been replaced by glycols recently. Glycols are organic alcohols wherein two hydroxyl groups are attached to a hydrocarbon chain making different types of glycols i.e. MEG (Mono Ethylene Glycol), DEG (Di Ethylene Glycol) and TEG (Tri Ethylene Glycol) and etc… glycols are usually used as antifreeze agents, thermodynamic hydrate inhibitors and absorbents in the natural gas industries.

Mono-Ethylene glycol or MEG is widely used as an anti-freezing agent and hydrate formation inhibitor in chemical and natural gas industries. DEG[1] is also used as hydrate inhibitor in transportation pipeline between gas production and processing facilities. Tetra-ethylene glycol or TeEG is used as an absorption agent in the extraction column of aromatic hydrocarbons purification processes [344].

To design and control the abovementioned processes, modelling and simulation applications equipped with reliable models are needed to accurately predict the thermophysical properties and phase behaviour of such systems. The cubic plus association (CPA) equation of state has been extensively used for modelling of binary mixtures of glycol containing systems [345]–[347]. However, a few studies have been reported on thermodynamic modelling of glycol containing systems using SAFT and its extensions. Li et al. used SAFT equation of state presented by Radosz et al. [348] to model the VLE of CO_2, some hydrocarbons, water and alcohol binary and ternary mixtures systems [349]. SAFT-VR was applied to model a closed loop liquid-liquid phase equilibria of a system containing water and poly(ethylene glycol) [350]. SAFT-VR EoS was also employed for hydrate phase boundary calculation in the presence of hydrate inhibitors [351]. Pedrosa et al. studied the effect of the molecular structure on the solubility of several compounds in glycols using the soft-SAFT equation of state [352].

[1] Di-Ethylene glycol

They correlated the equation of state pure compound parameters which have been fitted to VLE experimental data, with molecular weights of glycols. They presented a correlation for the chain length, size, and energy of interaction parameters with the molecular weight of the compounds with fixed association parameters [352]. The phase equilibria modelling of polyethylene glycol binary mixtures was then studied by Pedrosa et al. using the soft-SAFT equation of state in another publication [353]. The pure compound parameters for polyethylene glycol were obtained by extrapolation from the correlation suggested in their previous work [352]. A simplified model of PC-SAFT has been introduced by von Solms et al. [354] which can reduce the computational cost without affecting the model performance and accuracy. The simplified PC-SAFT EoS was used by Grenner et al. for VLE and LLE modelling of glycol and water mixtures where they presented new sets of pure compound parameters for glycols using experimental vapour pressures and saturated liquid densities [344]. In that publication, binary interaction parameters of glycols and some gases and aromatic hydrocarbons were then optimised using the literature phase equilibria data [344]. Taffazol et al. employed sPC-SAFT EoS to predict the thermo-physical properties of some associating fluid which are frequently used in oil and gas industries [355].

In this study, new sets of pure compound parameters were optimized for MEG, DEG, TEG and PG by fitting the original PC-SAFT EoS to experimental vapour pressures and saturate liquid densities. Because the experimental data in the literature are only available over a limited range of temperature, data correlations available in the DIPPR database were used for optimization. To our knowledge, there is no study published in the literature on modelling of glycol containing systems using the original PC-SAFT equation of state. Binary interaction parameters were then adjusted to experimental VLE data of glycols binary mixtures. By minimizing the following objective function, new sets of pure molecular parameters were optimized and are reported in Table 2.12.

$$OBJ = \sum_{i=1}^{N} \left| \frac{P_i^{sat.exp} - P_i^{sat.calc}}{P_i^{sat.exp}} \right| + \sum_{j=1}^{N} \left| \frac{\rho_j^{liq.sat.exp} - \rho_j^{liq.sat.calc}}{\rho_j^{liq.sat.exp}} \right| \quad \text{Eq. 2.69}$$

Table 2.12 PC-SAFT pure compound parameters used in this work for glycols.

Compound	m	σ (Å)	ε/k (K)	ε^{AB}(K)	κ^{AB}	P^{sat} (AAD %)	ρ^{liq} (AAD %)	T (K)	Scheme	Ref.
MEG	**1.92591**	**3.57018**	**326.09**	**2050.27**	**0.02564**	**0.56**	**1.54**	**273 -475**	**4C**	**This Work**
DEG	**2.65502**	**3.79877**	**333.92**	**2313.71**	**0.01196**	**3.72**	**0.53**	**275 - 486**	**4C**	**This Work**
TEG	**3.40309**	**3.92111**	**324.78**	**2148.16**	**0.01963**	**3.58**	**0.44**	**273 -477**	**4C**	**This Work**
TeEG	**5.16867**	**3.6241**	**265.877**	**2118.96**	**0.09424**	**2.01**	**3.83**	**294 - 477**	**4C**	**This Work**
PG	**2.08682**	**3.7845**	**297.9**	**2104.09**	**0.02210**	**2.52**	**1.28**	**275 - 475**	**4C**	**This Work**
MEG	1.90878	3.5914	325.23	2080.03	0.0235	5.77	2.43	273 -475	4C	[344]
DEG	3.05823	3.6143	310.29	2080.03	0.0235	12.12	0.24	275 - 486	4C	[344]
TEG	3.18092	4.0186	333.17	2080.03	0.0235	17.89	0.51	273 -477	4C	[344]
TeEG	4.7509	3.8138	309.22	2080.03	0.0235	9.04	1.05	294 - 477	4C	[344]
PG	2.33917	3.6351	284.62	2080.03	0.0235	6.92	1.19	275 - 475	4C	[344]
MEG	1.6912	3.5951	102.56	3165.30	0.029	46.25	0.87	273 -475	4C	[355]
DEG	2.9418	3.6787	320.90	1842.10	0.0334	45.52	1.19	275 - 486	4C	[355]
TEG	3.5520	3.7122	160.70	3300.00	0.0607	89.83	0.24	273 -477	4C	[355]

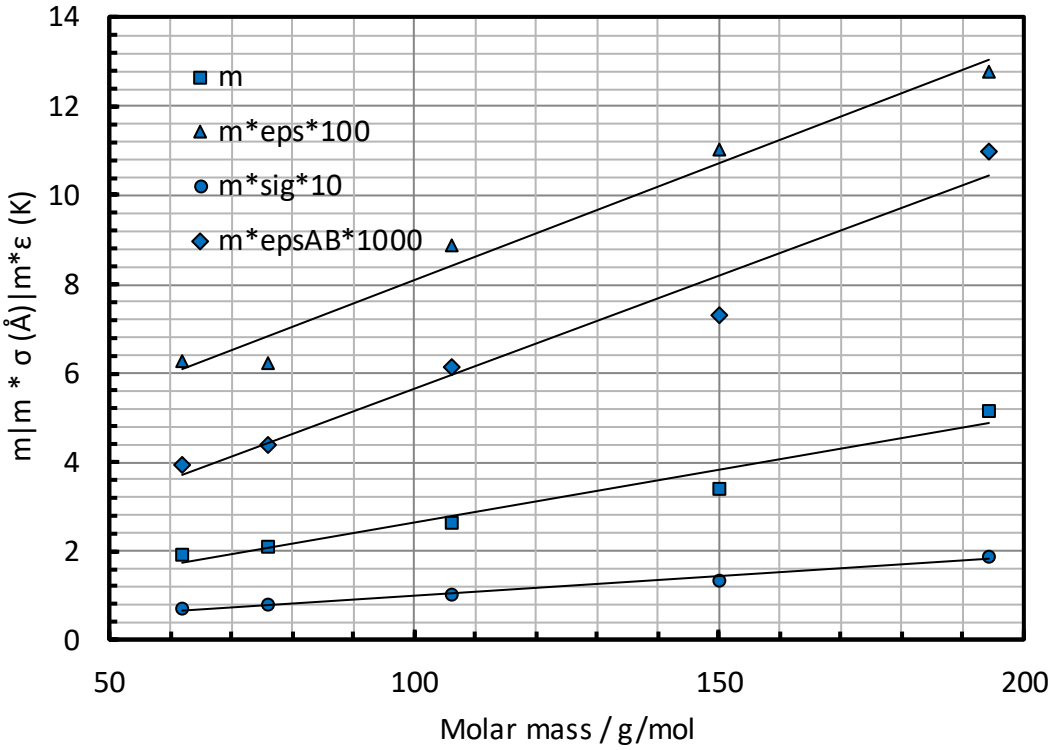

Figure 2.21 m, mε and mσ values versus molar masses of MEG, DEG, TEG, TeEG and PG.

As reported in Table 2.12, small AAD % from experimental data were obtained at a relatively broad range of temperatures using the new sets of parameters optimized in this work for both vapour pressure and saturate liquid density. However, because of the very small vapour pressure values of TeEG at low temperatures, pure compound parameters were tuned to a smaller range of temperature.

The AAD % of calculated and experimental vapour pressures and saturate liquid densities of glycols using pure compound parameters reported in the literature are also reported in Table 2.12. As seen in Table 2.12, using the sets of parameters suggested by Taffazol et al. [355], calculated vapour pressures of glycols deviate significantly from experimental data while the model shows a very good performance in predicting the saturated liquid densities. Using Grenner et al. [344] set of parameters, higher deviations from experimental data were obtained with respect to those calculated using this work sets of parameters for vapour pressures while the model shows relatively similar performance in calculating saturate liquid densities using all sets of parameters. A linear correlation was found between the molecular weight of glycols and pure compound parameters adjusted in this work. Figure 2.21 shows the trends of m and scaled $m\varepsilon$, $m\sigma$ and $m\varepsilon^{AB}$ values versus molar weight of glycols.

Figure 2.22 and Figure 2.23 compare calculated and experimental vapour pressure and saturated liquid density of MEG. The best agreements with experimental saturated liquid density was found using the pure component parameters suggested by Tafazzol et al. [355] with AAD of 0.87% from experimental data while the AAD % obtained using the parameters developed in this work and the one reported by Grenner et al. [344] are 1.54% and 2.53%. Despite a good agreement obtained for saturated liquid density using Tafazzol et al. [355] sets of parameters, the model shows very weak performance in calculation of vapour pressure with around 40% AAD from experimental data while the average deviation using Grenner et al. [344] and this work set of parameters is 5.77% and 0.56% respectively. Figure 2.24 shows the model calculations using three sets of parameters for vapour pressure of DEG at relatively low temperatures of 274 K to 304 K. The AAD % obtained for vapour pressure of DEG is 3.72% using the parameters developed in this work and 12.12% and 45.52% for parameters reported by Grenner et al. [344] and Tafazzol et al. [355], respectively. As shown in Figure 2.24, the PC-SAFT equation of state after applying the pure parameters optimized in this work exhibits excellent capability in correlating the vapour pressure of DEG even at low temperatures. Figure 2.25 displays the experimental and calculated saturated liquid density.

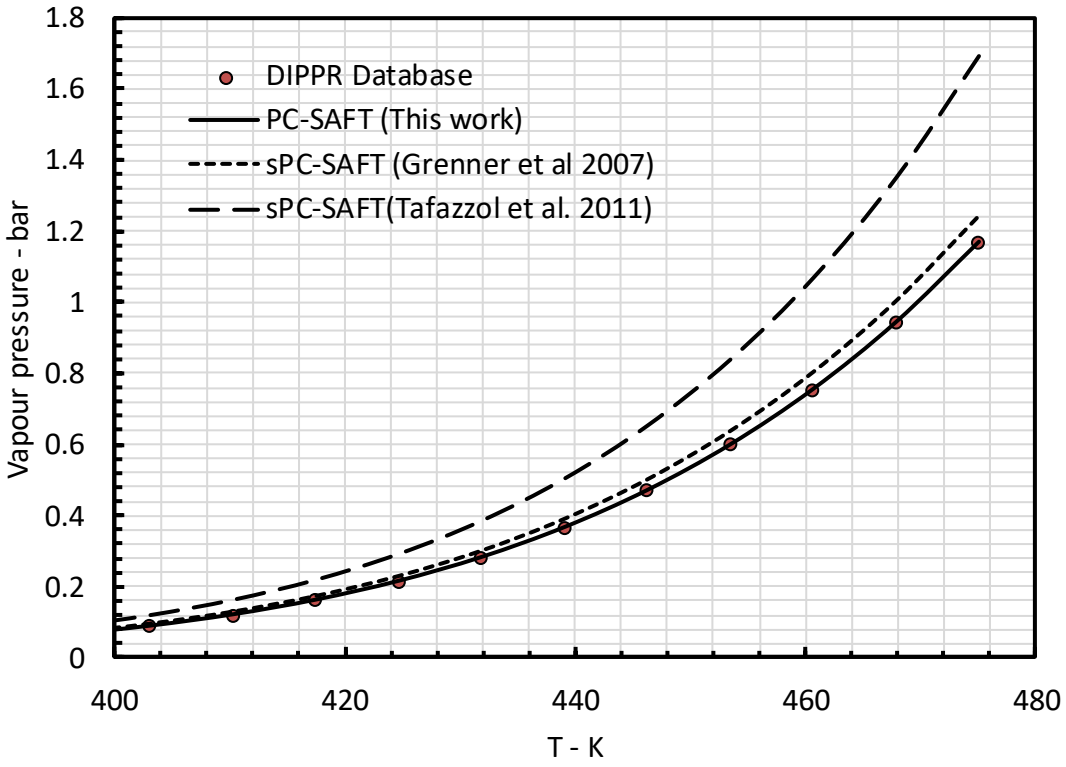

Figure 2.22 Vapour pressure of MEG at 400 K to 472 K: PC-SAFT predictions using sets of pure parameters developed in this work and those reported in the literature.

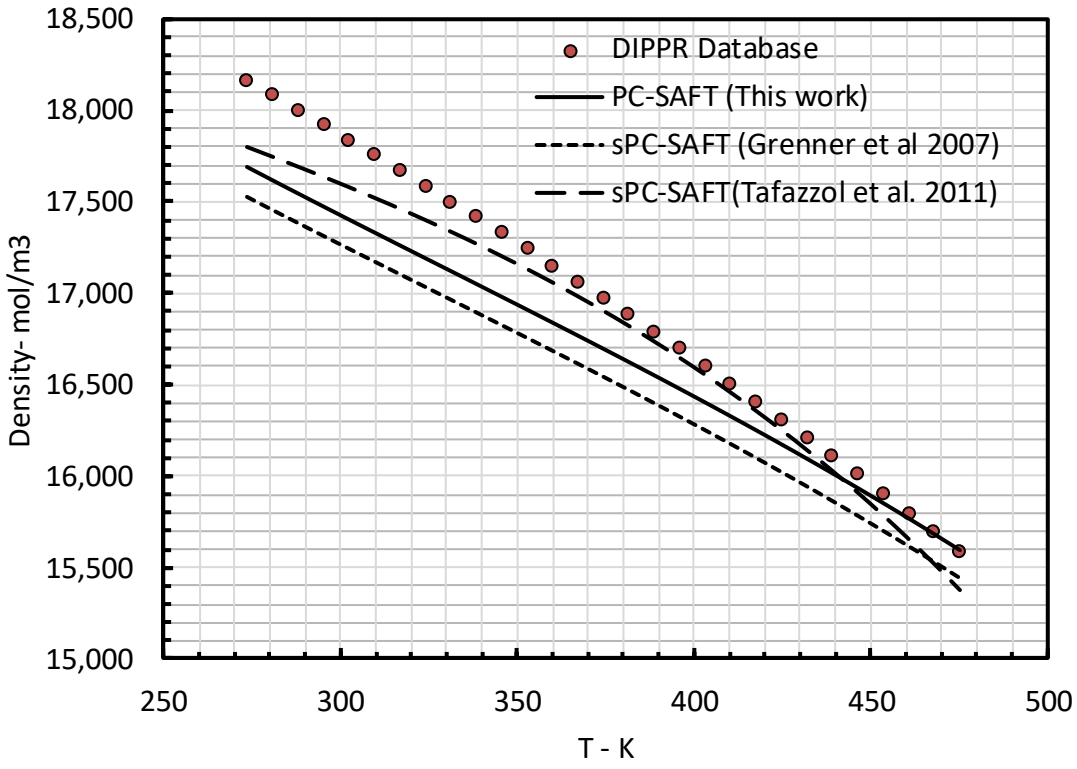

Figure 2.23 Saturated liquid density of MEG at 270 K to 470 K: PC-SAFT predictions using sets of pure parameters developed in this work and those reported in the literature.

Using the pure parameters presented by Grenner et al. [344] PC-SAFT equation of state performs best in liquid density calculation with 0.24% average deviation while the AAD % values using the pure parameters of this work and the one reported by Tafazzol et al. [355] is 0.53% and 1.19%, respectively. Figure 2.26 and Figure 2.27 compare the calculated and experimental values of vapour pressures and saturated liquid density of TEG. As illustrated in Figure 2.26, PC-SAFT calculated properties using this work set of parameters show the best agreement with experimental data. Regarding to saturated liquid density, as shown in Figure 2.27, using the Grenner et al. [344] pure parameters model performs better at moderate temperatures i.e. 300 K to 430 K, but the total AAD % obtained using the parameters optimized in this work is 0.44% which comparing to AAD % value of 0.51% for Grenner et al. parameters depicts a better agreement with experimental data.

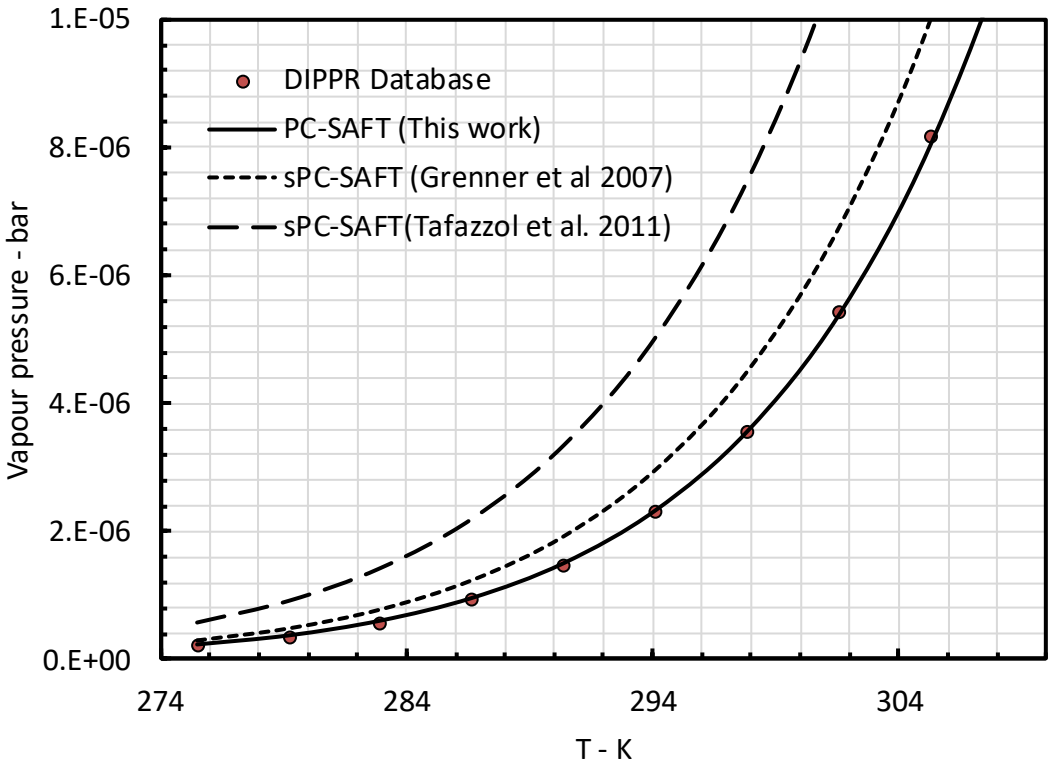

Figure 2.24 Vapour pressure of DEG at 275 K to 307 K: PC-SAFT predictions using sets of pure parameters developed in this work and those reported in the literature.

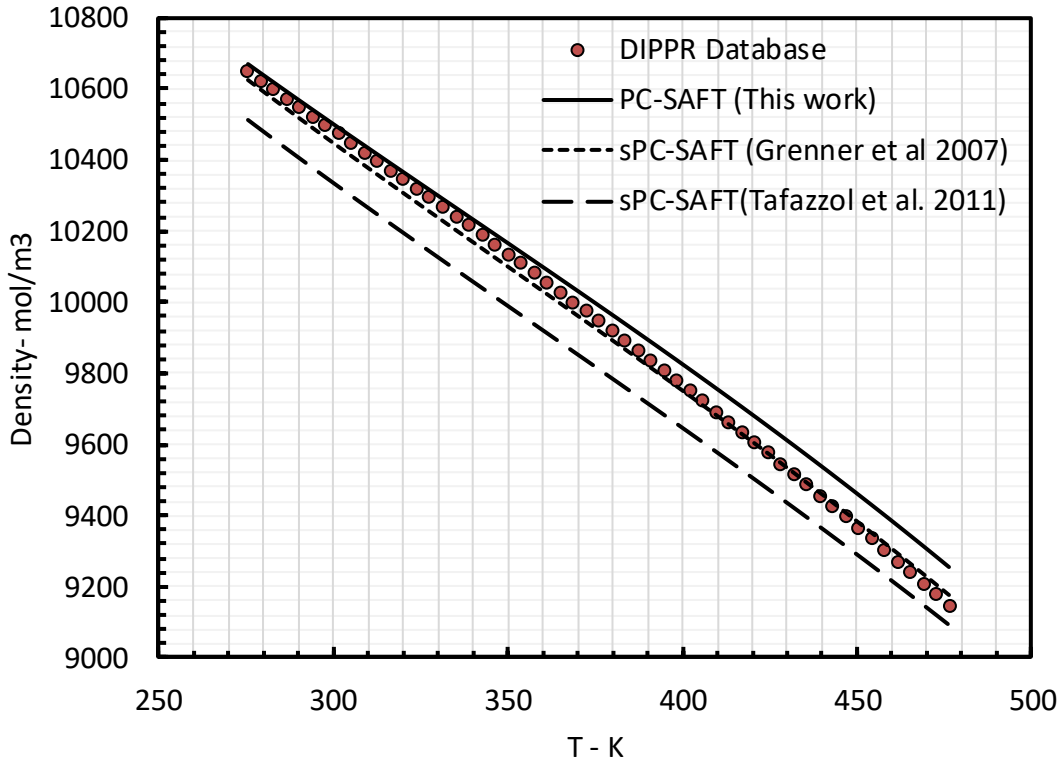

Figure 2.25 Saturated liquid density of DEG at 270 K to 470 K: PC-SAFT predictions using sets of pure parameters developed in this work and those reported in the literature.

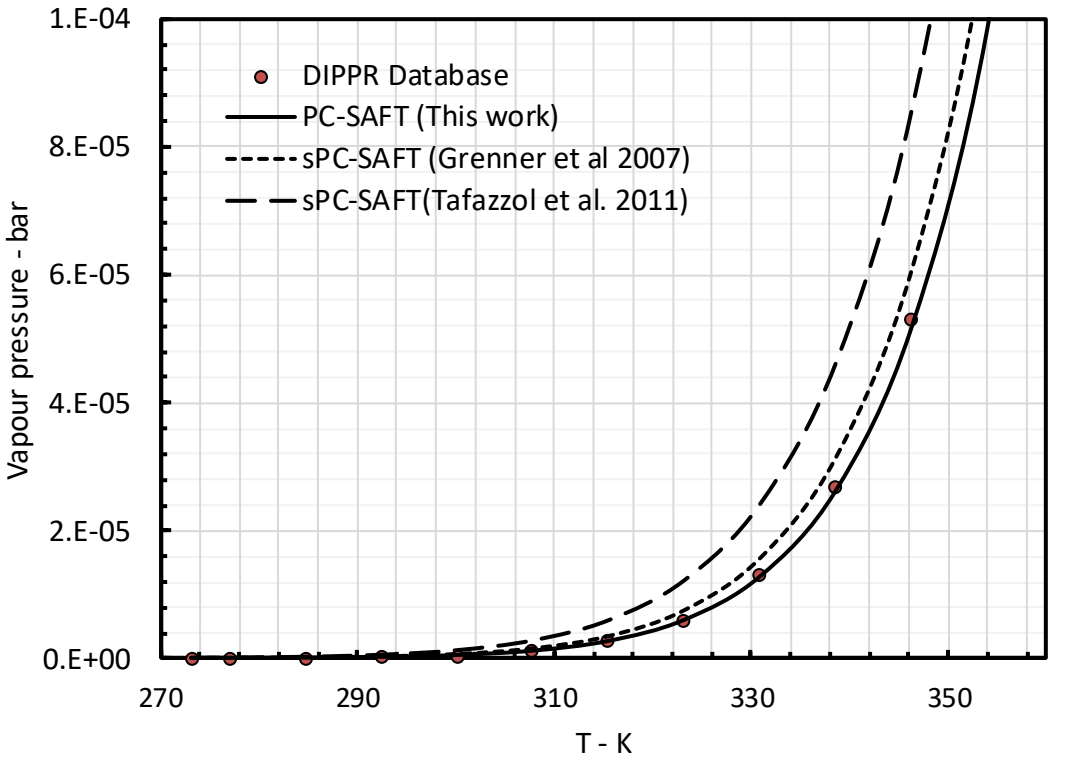

Figure 2.26 Vapour pressures of TEG at 270 K to 350 K: PC-SAFT predictions using sets of pure parameters developed in this work and those reported in the literature.

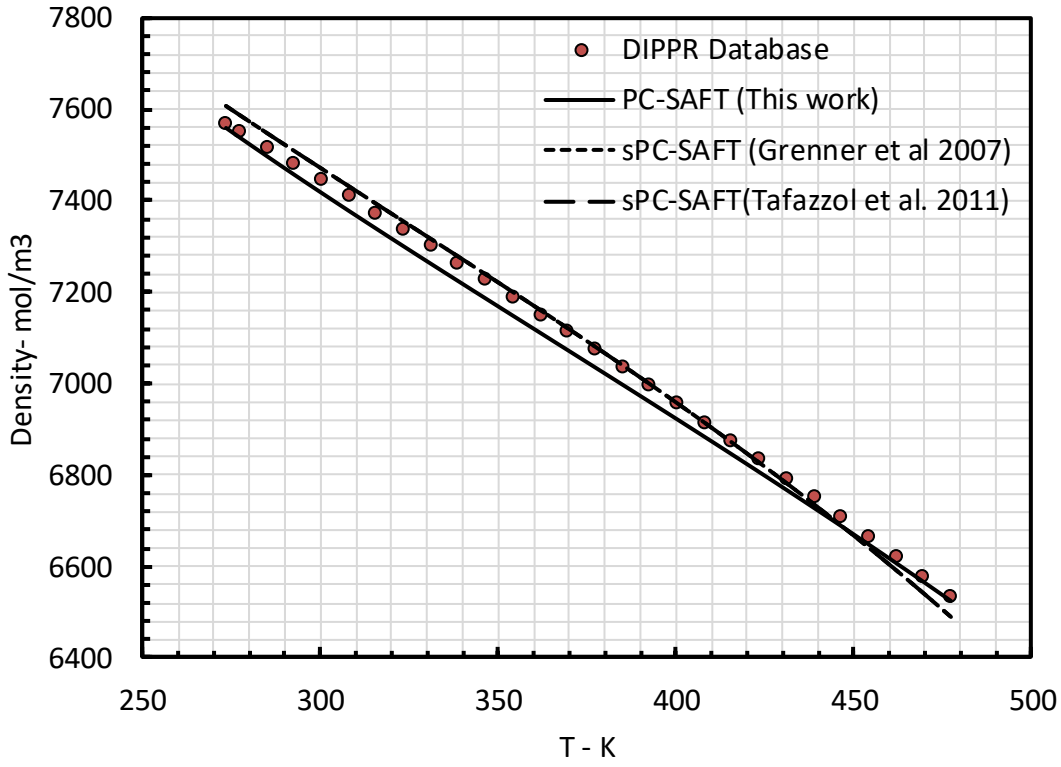

Figure 2.27 Saturated liquid density of TEG at 270 K to 480 K: PC-SAFT predictions using sets of pure parameters developed in this work and those reported in the literature.

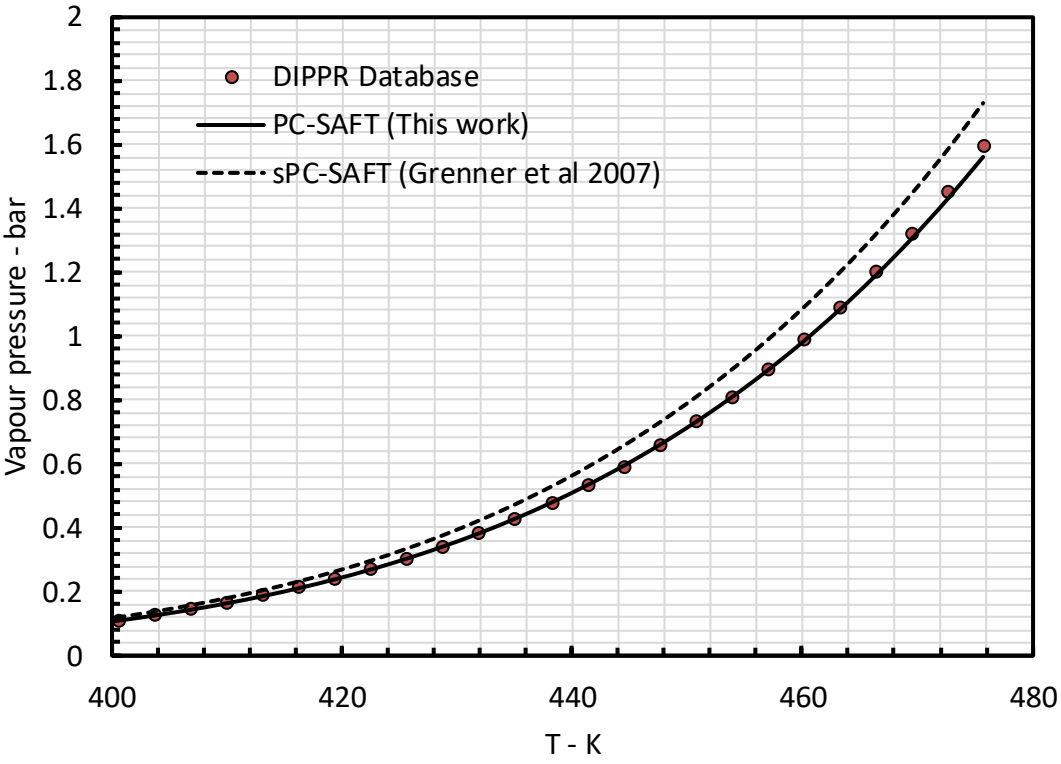

Figure 2.28 Vapour pressure of PG at 400 K to 472 K: PC-SAFT predictions using sets of pure parameters developed in this work and those reported in the literature.

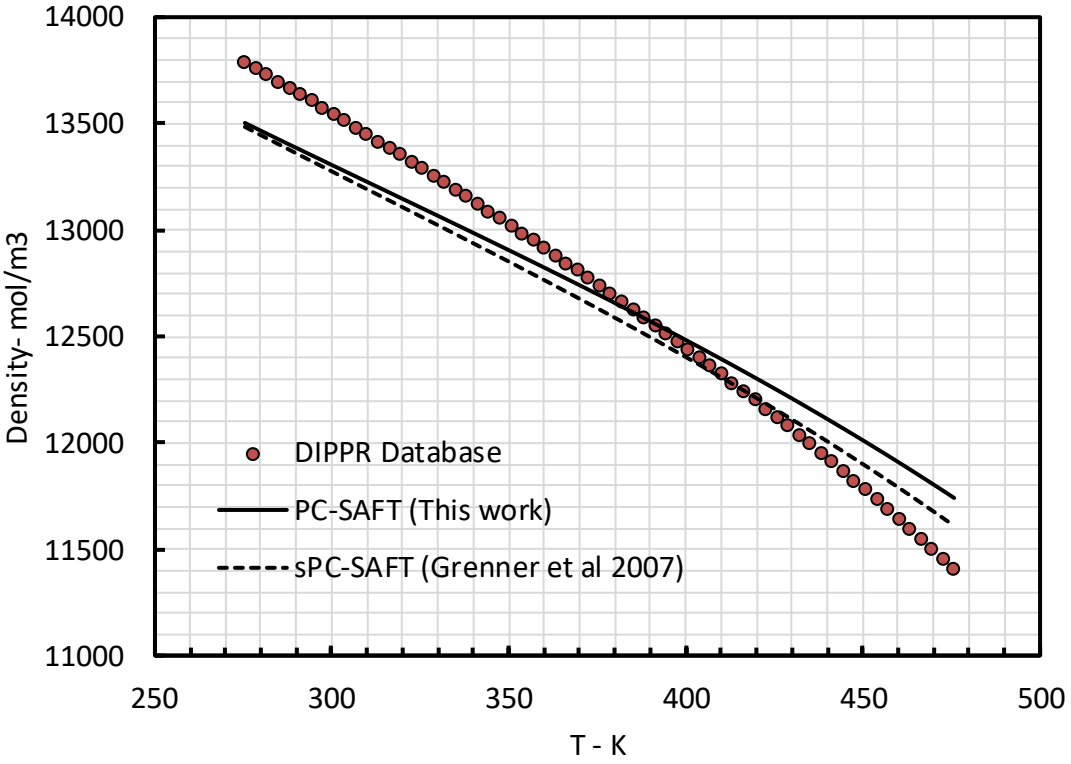

Figure 2.29 Saturated liquid density of PG at 270 K to 480 K: PC-SAFT predictions using sets of pure parameters developed in this work and reported in the literature.

Figure 2.28 and Figure 2.29 compare the calculated and experimental values of vapour pressure and saturate liquid density of poly ethylene glycol (PG). Similar to other glycols, the predicted vapour pressure agrees with the experimental data using the parameters developed in this work with AAD % of 2.52% while this value is 6.92% using Grenner et al. [344] parameters. Despite the good results for calculated vapour pressures using this work parameters compare to one reported by Grenner et al., calculated saturated liquid densities using this study parameters deviate slightly more than those calculated using Grenner et al. parameters with AAD of 1.28% and 1.19% respectively.

2.7 Binary Interaction Parameters for Glycols with Non-Associating Compounds

The binary mixtures of MEG, DEG, TEG and TeEG with several non-associating components are being investigated in this section. Temperature dependent binary interaction parameters are introduced to correlate the VLE/LLE of glycol binary systems as accurately as possible. The tuned temperature dependent k_{ij} were then fitted to a polynomial equation of the second order (Eq. 2.70). However, the BIP of several binary mixtures showed a linear trend with temperature.

$$k_{ij} = A_2 T^2 + A_1 T + A_0 \qquad \text{Eq. 2.70}$$

The tuning details including the coefficients of the polynomial equation of the BIPs, the temperature and pressure ranges of the experimental data covered for each binary system, the total absolute average deviation from experimental data and the dataset(s) used for tunings are summarized in Table 2.13 and Table 2.14. As can be seen from Table 2.13, all the BIPs obtained for MEG binary mixtures except for methane and CO_2 containing systems follow a linear trend with temperature.

Table 2.13 Binary interaction parameters of MEG and several non-associating compounds

Binary System		k_{ij}			T-range	P-range	AAD %	Ref of Data
		A_0	A_1	A_2	K	bar		
MEG	CO_2	3.7244E-01	-2.1546E-03	3.7842E-06	263.15-323.15	1.06-249	6.95%	In-house Data
	methane	-2.1493E-01	1.5438E-03	-2.1172E-06	283.2-398.15	1.05-400.6	4.33%	[356]–[358]
	ethane	2.3962E-01	-4.2678E-04	0	283.2-308.15	1.01-40	6.74%	[356], [359]
	propane	3.3894E-02	3.1743E-05	0	298.15-398.15	0.823-194.8	1.94%	[360]
	N_2	2.5464E-01	-3.2311E-04	0	323.15-398.15	16-396	6.66%	[357]
	toluene	4.0513E-01	-1.0298E-03	0	279.1-361	1.01	1.90%	[361]
	benzene	-1.2054E-03	4.3425E-01	0	279.2-342.1	1.01	0.75%	[361]
	hexane	3.1135E-01	-7.9282E-04	0	307.95-330.35	1.01	5.71%	[362]
	heptane	3.2269E-01	-7.7541E-04	0	315.95-351.85	1.01	6.66%	[362]
	methyl-cyclo -hexane	3.7048E-01	-8.8110E-04	0	312.65-351.85	1.01	6.05%	[362]

Table 2.14 Binary interaction parameters of DEG, TEG and TeEG and several non-associating compounds

Binary System		k_{ij}			T-range	P-range	AAD %	Ref of Data
		A_0	A_1	A_2	K	bar		
DEG	CO_2	-1.285E-01	9.854E-04	-1.18E+00	298.15-398.15	0.39-211	4.28%	[363]
	ethane	2.822E-02	9.000E-05	0	298.15-398.15	0.25-404.5	4.29%	[364]
	H2S	-5.188E-02	1.104E-04	0	298.15-398.15	0.0193-74.8	9.23%	[363]
TEG	CO_2	4.3523E-02	1.3541E-04	0	298.15-398.15	1.05-202.5	2.16%	In-house Data
	methane	2.4432E-02	1.6829E-04	0	298.15-398.15	1.092-196.9	1.63%	[365]
	propane	2.4101E-01	-1.1542E-03	1.8448E-06	298.15-348.15	0.159-17.5	7.71%	[365]
	ethane	5.5717E-02	6.5388E-05	0	298.15-373.15	1.1-101	2.02%	[365]
	H_2S	-1.5914E-01	8.3326E-04	-1.0960E-06	298.15-398.15	0.11-24.68	6.28%	[365]
TeEG	benzene	-1.5706E+00	7.5966E-03	-9.1287E-06	354.24-441.33	1.01	4.64%	[366]
	toluene	-1.2174E+00	5.4851E-03	-6.1503E-06	386.33-454.89	1.01	4.10%	[366]
	O-xylene	-5.6210E+00	2.4699E-02	-2.70608E+00	418.93-461.74	1.01	3.09%	[366]

Figure 2.30 displays the calculated solubilities of CO_2 in MEG using adjusted binary interaction parameter to the experimental VLE data. As shown by Figure 2.30, model

shows to be capable of correlating the CO_2 solubility at temperatures ranging from 263.15 K to 323.15 K.

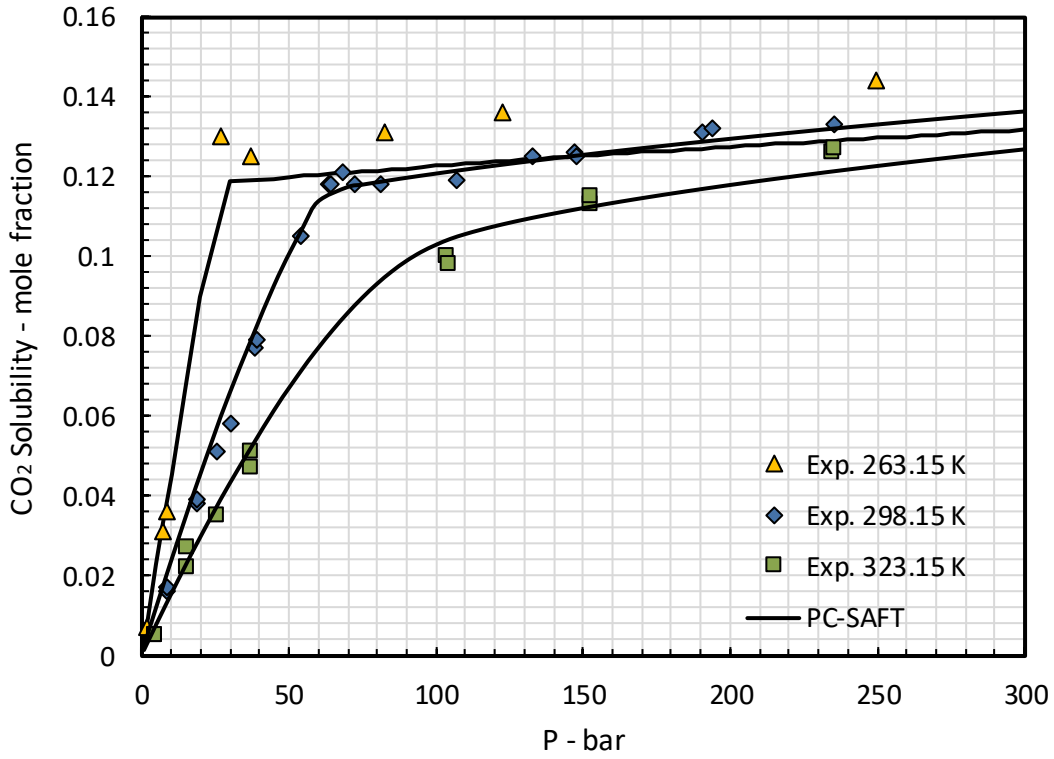

Figure 2.30 Solubility of CO_2 in MEG at 263.15 K, 298.15 K, 323.15 K: Comparison with tuned PC-SAFT model and experimental data (In-house data)

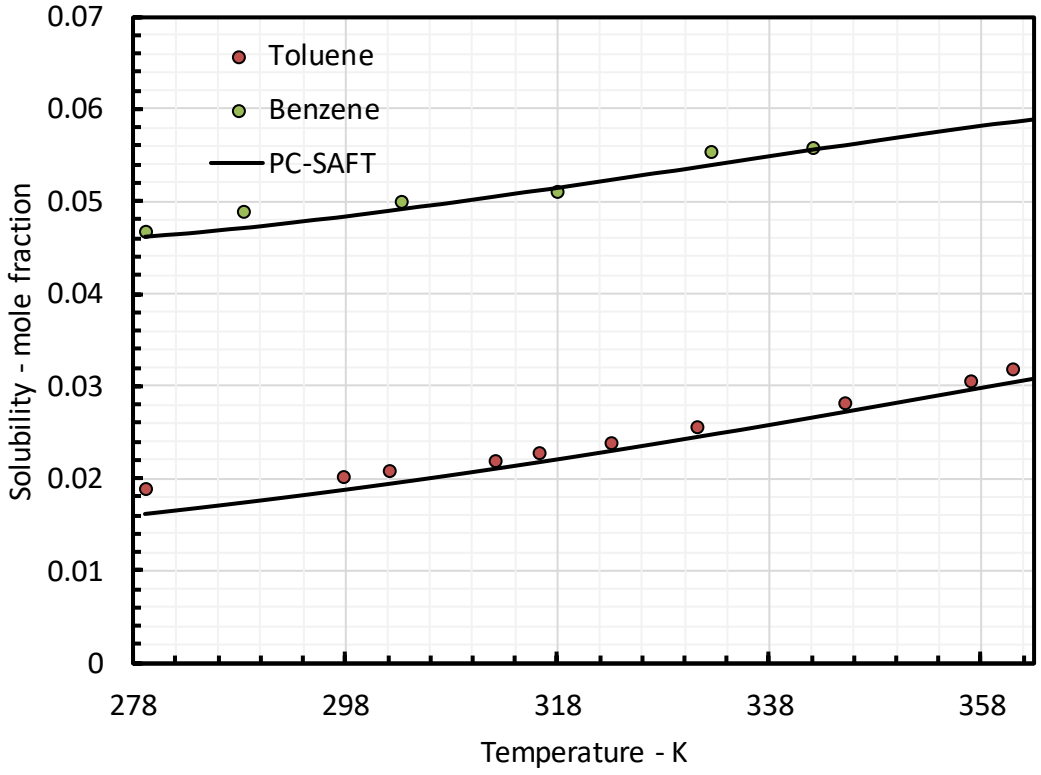

Figure 2.31 Solubility of benzene and toluene in MEG at 1.013 bar: Comparison with tuned PC-SAFT model and experimental data ([361]**).**

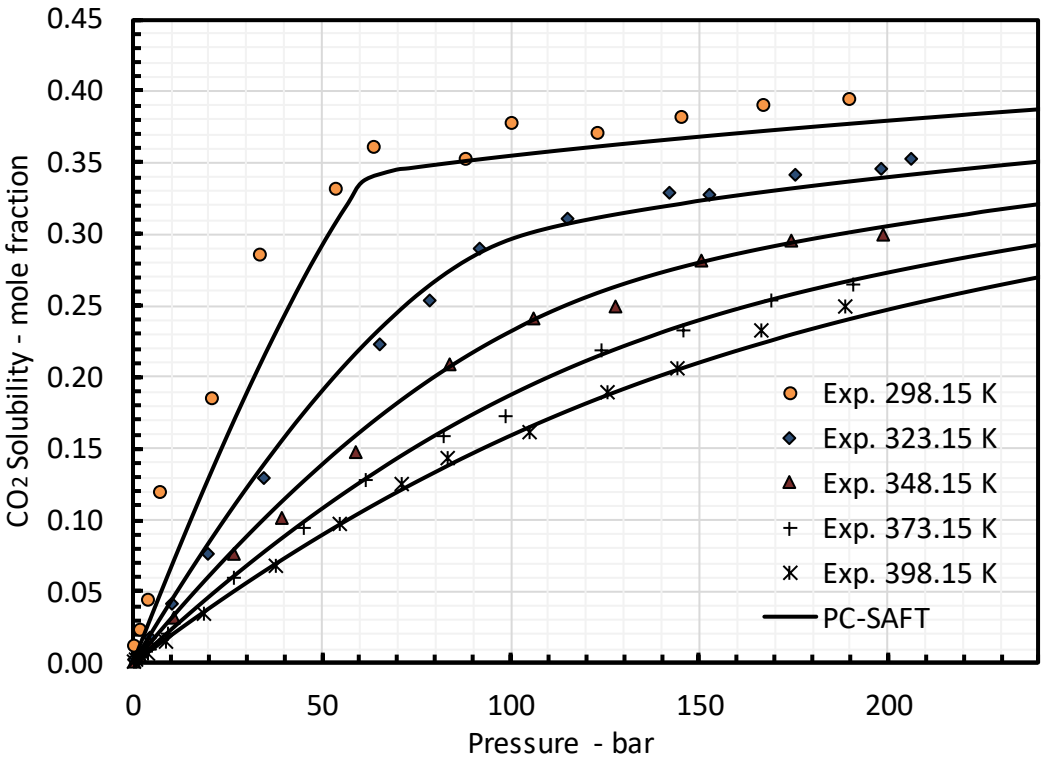

Figure 2.32 Solubility of CO_2 in DEG at 298.15 K, 323.15 K, 348.15 K, 373.15K and 398.15K: Comparison with tuned PC-SAFT model and experimental data (In-house data).

Solubilities of benzene and toluene in MEG are also plotted in Figure 2.31 at 1 atm. Very good agreements were found for both binary mixtures at temperature range of 279 K to 361 K where the AAD % of 1.90 and 0.75 for toluene and benzene respectively were obtained. Calculated CO_2 solubilities in DEG were compared to the experimental data in Figure 2.32 at 5 different temperatures from 298.15 K to 398.15 K. Despite using a temperature dependent BIP, the deviation from calculated CO_2 and experimental data is considerable at 298.15 (5.20 AAD %) while at other temperatures model calculation are in an excellent agreement with experimental data. Figure 2.33 shows the calculated and experimental solubilities of ethane in TEG at 298.15K to 373.15 K where with a total 2.02 AAD %, an excellent agreement is seen between model calculations and experimental data.

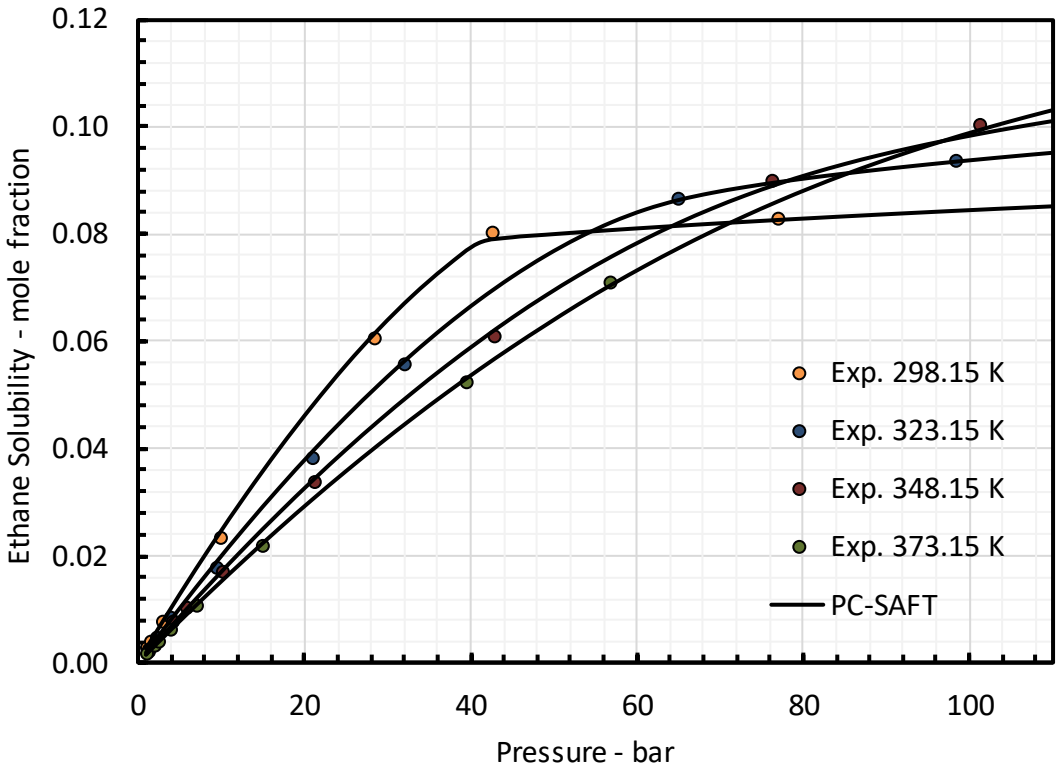

Figure 2.33 Solubility of ethane in TEG at 298.15 K, 323.15K, 348.15K, 373.15 K: Comparison with tuned PC-SAFT model and experimental data ([365]**).**

2.8 PC-SAFT Pure Parameter Optimization for Alcohols

Methanol and ethanol have been in use in natural gas transportation industry as thermodynamic hydrate inhibitor for a long time. They lower the activity of water and act like an antifreeze and shift the hydrate dissociation phase boundary to lower temperatures [367]. As mentioned before, accurate modelling of associating systems using molecular based equation of states is not trivial. Gross and Sadowski [214] reported very good and accurate sets of pure compound parameters for alcohols. They optimized the pure-component parameters for 18 associating compounds over a wide range of temperature e.g. from 200K to 512 K for methanol.

In the studies associated with hydrate dissociation point calculation or in flow assurance engineering scope of work, where hydrate inhibitors like methanol are involved at low temperatures, a robust model is required to model the phase behaviour of such systems with a reliable accuracy. As will be shown in continuance, using the sets of pure compound parameters suggested by Gross and Sadowski [214], model predictions differs considerably from experimental vapour pressure of alcohols despite the fact the parameters were tuned using a wide range of temperatures.

In this study the PC-SAFT model was applied to calculate saturation properties of alcohols including methanol, ethanol, 1-propanol and 2-propanol with emphasis on the temperature and pressure ranges where at most of modelling in flow assurance scope of work is needed to be carried out. Similar to the preceding optimization sections, the following objective function was minimized and new sets of pure compounds parameters were optimized using vapour pressures and saturate liquid densities of alcohols. The new optimized parameter together with the parameters developed by Gross and Sadowski [214] are reported in Table 2.15.

$$OBJ = \sum_{i=1}^{N} \left| \frac{P_i^{sat.exp} - P_i^{sat.calc}}{P_i^{sat.exp}} \right| + \sum_{j=1}^{N} \left| \frac{\rho_j^{liq.sat.exp} - \rho_j^{liq.sat.calc}}{\rho_j^{liq.sat.exp}} \right| \qquad \text{Eq. 2.71}$$

Table 2.15 PC-SAFT pure compound parameters used in this work for Alcohols.

Compound	m	σ (Å)	ε/k (K)	ε^{AB}(K)	κ^{AB}	P^{sat} (AAD %)	ρ^{liq} (AAD %)	T (K)	Scheme	Ref.
methanol	**1.55439**	**3.15333**	**185.234**	**2942.67**	**0.036506**	**2.17%**	**5.27%**	**220-370**	**2B**	**This Work**
ethanol	**2.38267**	**3.17706**	**198.237**	**2649.12**	**0.034662**	**0.16%**	**0.70%**	**250-370**	**2B**	**This Work**
1-propanol	**3.2714**	**3.13885**	**224.143**	**2112.23**	**0.026917**	**1.75%**	**0.31%**	**250-371**	**2B**	**This Work**
2-propanol	**3.09403**	**3.20881**	**208.382**	**2469.64**	**0.013383**	**2.73%**	**0.97%**	**250-372**	**2B**	**This Work**
methanol	1.5255	3.23	188.9	2899.5	0.035176	4.90%	0.45%	220-370	2B	[214]
ethanol	2.3827	3.1771	198.24	2653.4	0.032384	5.02%	0.74%	250-370	2B	[214]
1-propanol	2.9997	3.2522	233.4	2276.8	0.015268	3.22%	1.50%	250-371	2B	[214]
2-propanol	3.0929	3.2085	208.42	2253.9	0.024675	9.26%	0.94%	250-372	2B	[214]

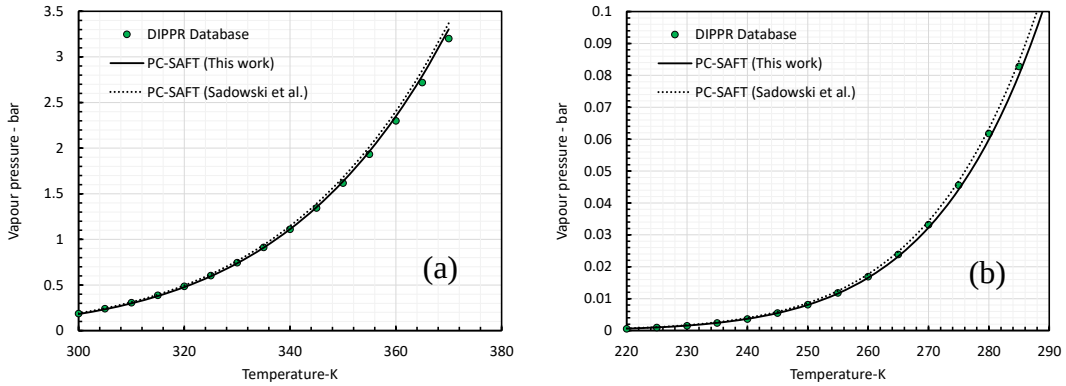

Figure 2.34 Vapour pressure of methanol: PC-SAFT calculation results using pure compound parameters developed in this work and those reported by Gross and Sadowski [214]

Figure 2.34 displays the calculated and experimental vapour pressures of methanol at two temperature ranges, from 300 K to 370 K (Figure 2.34-a) and 220 K to 290 K (Figure 2.34-b). As seen in the Figure 2.34-b, using both sets of pure compound parameters, model performs similar while at higher temperatures using the set of parameters developed in this work, the deviation from experimental data is lower. Although, as reported in Table 2.15, the AAD % of the calculated vapour pressure is lower, the AAD

% of saturate liquid density is higher than those calculated using Gross and Sadowski parameters [214].

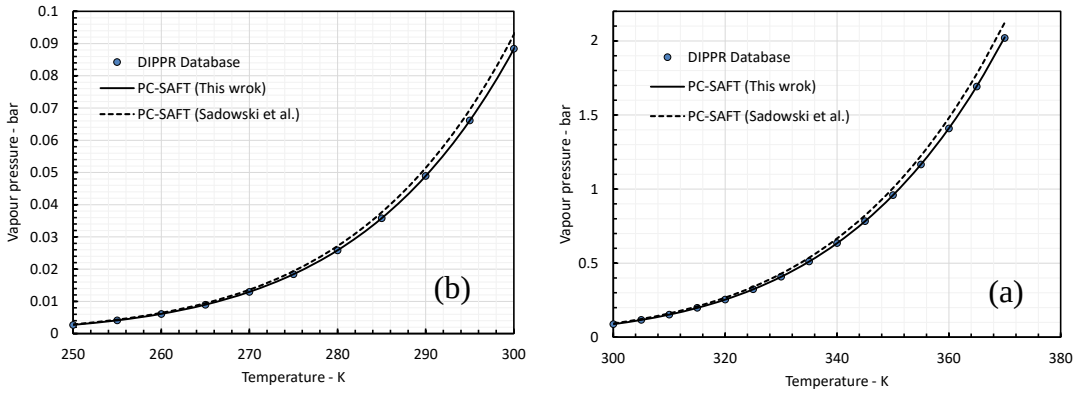

Figure 2.35 Vapour pressure of ethanol: PC-SAFT predictions using pure compound parameters developed in this work and those reported by Gross and Sadowski [214]

Figure 2.35 and Figure 2.36 compare calculated vapour pressure and saturate liquid density of ethanol using two sets of pure compound parameters and experimental data. As displayed in Figure 2.35-a and Figure 2.35-b, using the new optimized set of parameters, model calculated vapour pressures deviation from experimental data is less than those calculated using the one reported by Gross and Sadowski [214], while using both parameters, model performs similar in calculating saturated liquid density (see Figure 2.36).

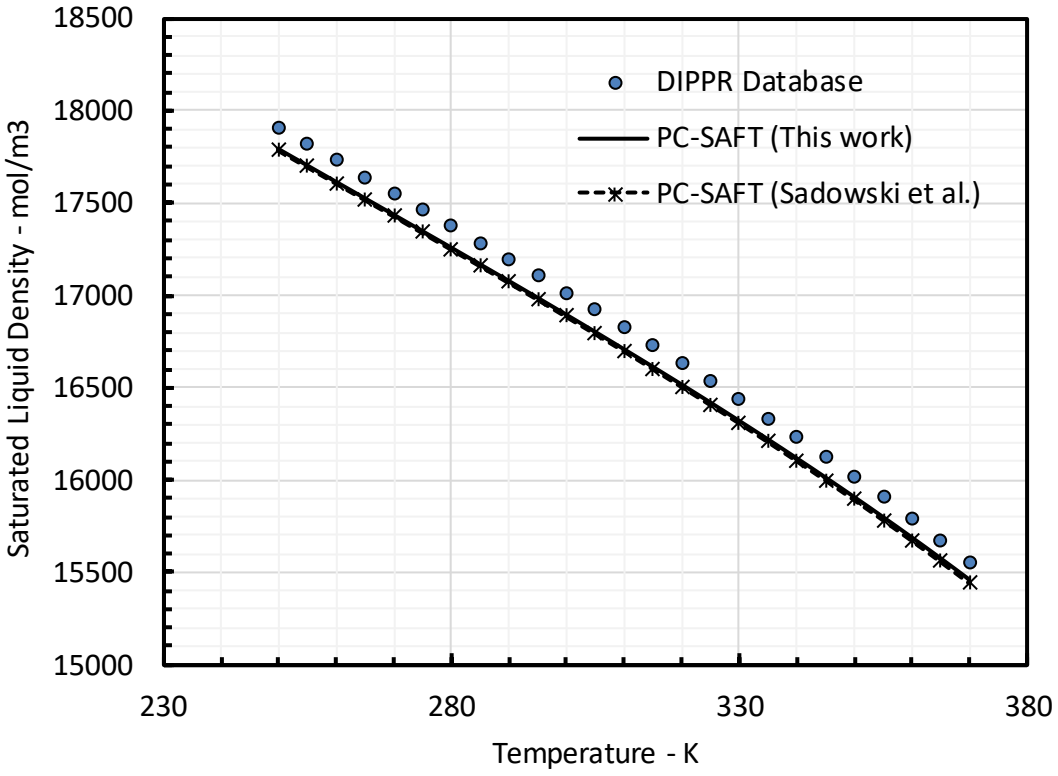

Figure 2.36 Saturated liquid density of ethanol: PC-SAFT predictions using pure parameters developed in this work and those reported by Gross and Sadowski [214]

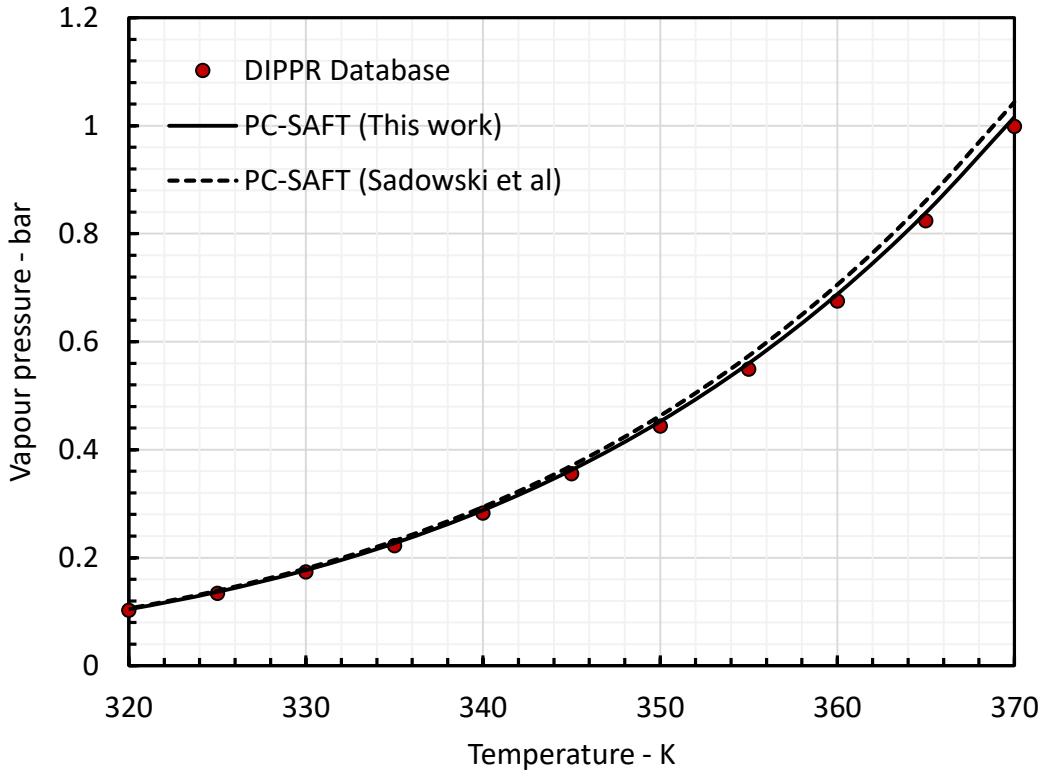

Figure 2.37 Vapour pressure of 1-propanol: PC-SAFT predictions using sets of pure parameters developed in this work and reported by Gross and Sadowski [214]

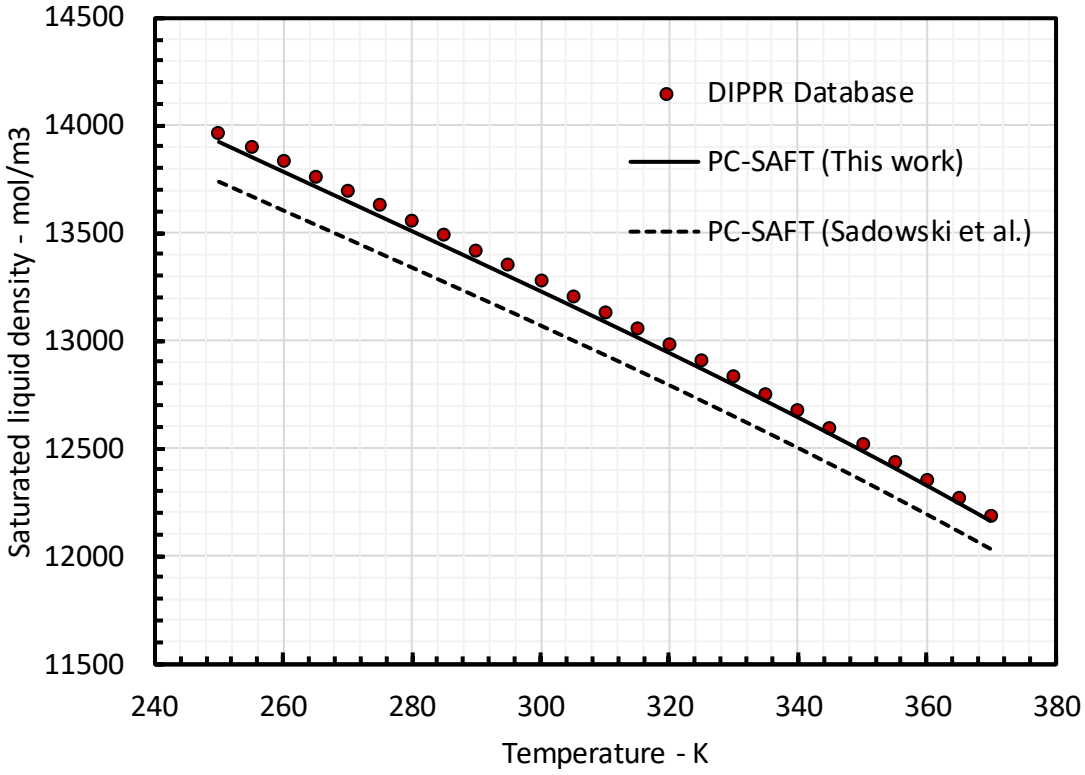

Figure 2.38 Saturated liquid density of 1-propanol: PC-SAFT predictions using pure compound parameters developed in this work and those reported by Gross and Sadowski [214]

The vapour pressure and saturated liquid density of 1-propanol calculated using two sets of parameters are compared with experimental data through Figure 2.37 and Figure 2.38 respectively. PC-SAFT equation of state appears to deliver the same results using both sets of parameters (considering the AAD % value of 1.75 using this work parameters model performs slightly better than when the other set of parameter is used yielding AAD % of 3.22), however, using this work set of parameter the calculated liquid density deviation from experimental is 5 times less than that those calculated using Gross and Sadowski [214] parameters with ADD % values of 0.32 and 1.5 respectively. The calculated vapour pressures and liquid densities of 2-propanol are also plotted together with the experimental values in Figure 2.39. While the AAD % of liquid density predictions are quite the same (See Table 2.15) the resulting AAD % using this work and Gross and Sadowski parameters are 2.73 and 9.26 indicating that the model performs quite better performance using the parameters developed in this work.

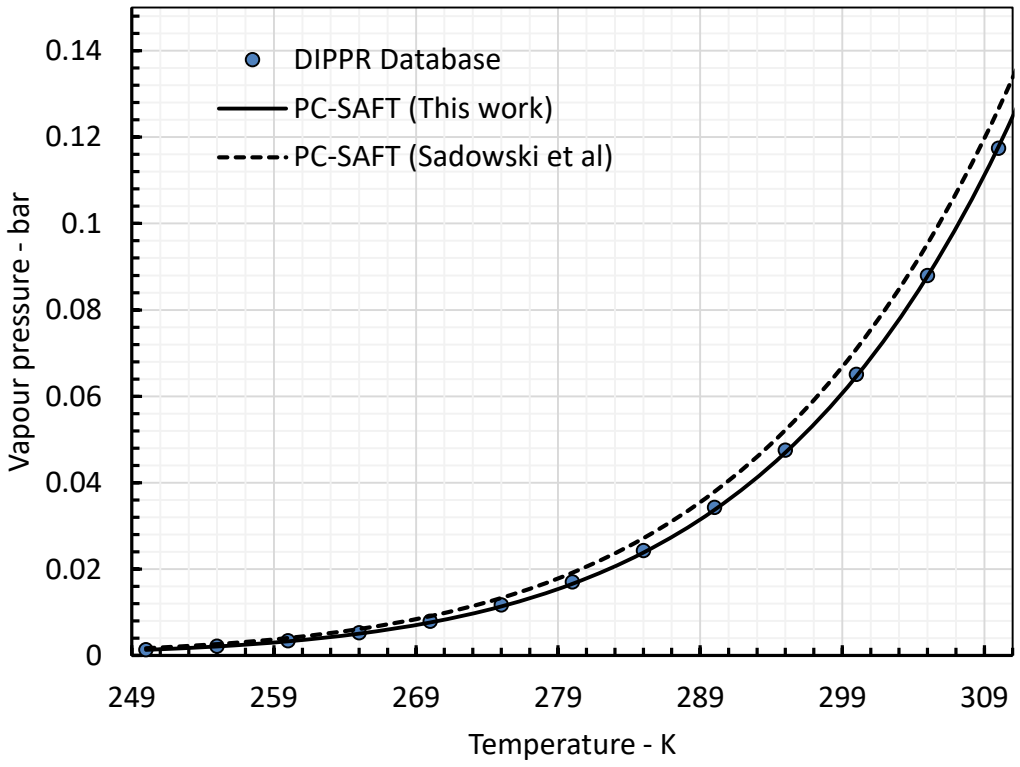

Figure 2.39 Saturated liquid density of 2-propanol: PC-SAFT predictions using pure parameters developed in this work and those reported by Gross and Sadowski [214]

2.9 Calculation of Second Thermodynamic Derivative Properties Using PC-SAFT.

As discussed before, the main objective of thermodynamic models is to predict the phase equilibria and PVT behaviour of simple and complex systems over an extensive range of conditions. Moreover, reliable modelling and simulation softwares that perform fast and

more importantly accurate are crucial necessities in oil and gas industries. Obviously, without implementing robust and fast convergent models developing such computer applications seems not to be possible. In oil and gas industries, accurate description of the second thermodynamic properties such as C_P, C_V, thermal expansion coefficient, Joule-Thomson coefficient and sound velocity is very important as these properties are often required in process and equipment design or engineering and process control sectors.

There are several empirical correlations available in the literature for predicting abovementioned properties which have been developed for a specific system or are suitable at specific conditions. However, employing equation of states to calculate the second derivative properties allows us to predict the properties regardless of conditions and type of the system as long as the equation of state is tuned or applicable for such systems. In this regard, Villiers et al. [368] applied SAFT, CPA and the sPC-SAFT equation of states to test the ability of these models to predict heat capacities, pressure–volume derivative, pressure–temperature derivative and speed of sound of n-alkanes and 1-acohols.

Second derivatives properties are calculated using the first and second derivatives of residual Helmholtz free energy with respect to the temperature and density. To calculate the derivatives one may use numerical differentiation of the Helmholtz free energy where an extra error is imposed to the calculation. From the computational and programming point of view, to perform precise numerical differentiation, higher order formulas must be used whereas the sub-routine responsible for returning the Helmholtz free energy must be called more than 5 or for second derivatives 10 times to reach a reasonable accuracy.

In practical applications, e.g. engineering softwares in which the speed of calculation is very important, using the numerical differentiation for such purposes with higher CPU time and less accuracy is not seemed to be the best idea. However, for simple equation of states like SRK, PR or even sPC-SAFT, the disadvantage of using numerical differentiation might not be valid considering the advanced computing hardware available nowadays. However, in regards to original PC-SAFT equation of state, due to the high non-linearity and complexity of the equations, numerical differentiation is not seemed to be efficient.

Therefore, in this study the analytical expressions needed for second thermodynamic properties calculations are driven (except for those that have been presented by Gross and Sadowski [6]) and presented. At the end of this section, the capability of the PC-SAFT model is evaluated using the driven equations. The formulas for calculating the sec ond derivative properties are summarized below [21].

Constant volume heat capacity:

$$C_V^{res} = -RT^2 \frac{\partial^2}{\partial T^2}\left(\frac{a^{res}}{RT}\right)_{V,n} - 2RT\frac{\partial}{\partial T}\left(\frac{a^{res}}{RT}\right)_{V,n} \quad \text{Eq. 2.72}$$

$$C_v = C_v^{res} + C_v^{ideal} \quad \text{Eq. 2.73}$$

Constant Pressure heat capacity:

$$C_P^{res} = C_v^{res} - T\frac{\left(\frac{\partial P}{\partial T}\right)_{V,n}^2}{\left(\frac{\partial P}{\partial V}\right)_{T,n}} - Rn \quad \text{Eq. 2.74}$$

$$C_P = C_P^{res} + C_P^{ideal} \quad \text{Eq. 2.75}$$

Isothermal compressibility coefficient:

$$k_T{}^{-1} = n\rho\left(\frac{\partial P}{\partial V}\right)_{T,n} \quad \text{Eq. 2.76}$$

Thermal expansion coefficient:

$$\alpha = k_T{}^{-1}\left(\frac{\partial P}{\partial T}\right)_{V,n} \quad \text{Eq. 2.77}$$

Joule-Thomson coefficient:

$$\mu_{JT} = -\frac{1}{C_P}\left(V + T\frac{\left(\frac{\partial P}{\partial T}\right)_{V,n}}{\left(\frac{\partial P}{\partial V}\right)_{T,n}}\right) \quad \text{Eq. 2.78}$$

Sound velocity:

$$u = \sqrt{-V^2\frac{C_P}{C_V}\frac{\left(\frac{\partial P}{\partial V}\right)_{T,n}}{M_w}} \quad \text{Eq. 2.79}$$

The iso-thermal compressibility and thermal expansion values are calculated using the equations below where the second derivative of Helmholtz free energy with respect to the volume and temperatures is needed.

$$\left(\frac{\partial P}{\partial V}\right)_{V,n} = -RT\frac{\partial^2}{\partial V^2}\left(\frac{A^{res}}{RT}\right)_{T,n} - \frac{nRT}{V^2} \quad \text{Eq. 2.80}$$

$$\left(\frac{\partial P}{\partial T}\right)_{V,n} = -RT\frac{\partial^2}{\partial T\partial V}\left(\frac{A^{res}}{RT}\right)_{n} + \frac{P}{T} \quad \text{Eq. 2.81}$$

2.9.1. Calculation of first derivative with respect to the temperature

The first derivatives of hard chain and dispersion contributions with respect to the temperature have been reported by Gross and Sadowski [6] which are presented here. The

first derivative of Helmholtz free energy with respect to the temperature is sum of the derivatives of all contributions

$$\frac{\partial}{\partial T}\left(\frac{a^{res}}{RT}\right)_{v,x_i} = \frac{\partial}{\partial T}\left(\frac{a^{hc}}{RT}\right)_{v,x_i} + \frac{\partial}{\partial T}\left(\frac{A^{dis}}{RT}\right)_{v,x_i} + \frac{\partial}{\partial T}\left(\frac{A^{assoc}}{RT}\right)_{v,x_i} \quad \text{Eq. 2.82}$$

✓ First derivative of Hard-Chain contribution with respect to temperature

$$\frac{\partial}{\partial T}\left(\frac{a^{hc}}{RT}\right)_{v,x_i} = \bar{m}\frac{\partial}{\partial T}\left(\frac{a^{hs}}{RT}\right)_{v,x_i} - \sum_i x_i(m_i - 1)g_{ii}^{hs\,-1}\left(\frac{\partial g_{ii}^{hs}}{\partial T}\right)_{v,x_i} \quad \text{Eq. 2.83}$$

with

$$\left(\frac{\partial g_{ii}^{hs}}{\partial T}\right)_{\rho,x_i} = \frac{\zeta_{3,T}}{(1-\zeta_3)^2} + \left(0.5d_{i,T}\right)\frac{3\zeta_2}{(1-\zeta_3)^2} + (0.5d_i)\left(\frac{3\zeta_{2,T}}{(1-\zeta_3)^2} + \frac{6\zeta_2\zeta_{3,T}}{(1-\zeta_3)^3}\right) + \left(0.5d_i d_{i,T}\right)\frac{2{\zeta_2}^2}{(1-\zeta_3)^3} + (0.5d_i)^2\left(\frac{4\zeta_{2,T}\zeta_2}{(1-\zeta_3)^3} + \frac{6{\zeta_2}^2\zeta_{3,T}}{(1-\zeta_3)^4}\right) \quad \text{Eq. 2.84}$$

And

$$\zeta_{n,T} = \frac{\partial \zeta_n}{\partial T} = \frac{\pi}{6}\rho\sum_i x_i m_i n d_{i,T}(d_i)^{n-1} \quad \text{Eq. 2.85}$$

$$d_{i,T} = \frac{\partial d_i}{\partial T} = \sigma_i\left(3\frac{\varepsilon_i}{kT^2}\right)\left[-0.12exp\left(-3\frac{\varepsilon_i}{kT}\right)\right] \quad \text{Eq. 2.86}$$

First derivative of Hard-Sphere term is calculated using

$$\frac{\partial}{\partial T}\left(\frac{a^{hs}}{RT}\right)_{v,x_i} = \frac{1}{\zeta_0}\left(\frac{3(\zeta_{1,T}\zeta_2+\zeta_{2,T}\zeta_1)}{(1-\zeta_3)} + \frac{3\zeta_1\zeta_2\zeta_{3,T}}{(1-\zeta_3)^2} + \frac{3{\zeta_2}^2\zeta_{2,T}}{\zeta_3(1-\zeta_3)^2} + \frac{{\zeta_2}^3\zeta_{3,T}(3\zeta_3-1)}{{\zeta_3}^2(1-\zeta_3)^3} + \frac{3{\zeta_2}^2\zeta_{2,T}\zeta_3 - 2{\zeta_2}^3\zeta_{3,T}}{{\zeta_3}^3}ln(1-\zeta_3) + \left(\zeta_0 - \frac{{\zeta_2}^3}{{\zeta_3}^2}\right)\frac{\zeta_{3,T}}{(1-\zeta_3)}\right) \quad \text{Eq. 2.87}$$

✓ First derivative of Dispersion contribution with respect to temperature

$$\frac{\partial}{\partial T}\left(\frac{a^{Disp}}{RT}\right)_{v,x_i} = -2\pi\rho\left(\frac{\partial I_1}{\partial T} - \frac{I_1}{T}\right)\overline{m^2\varepsilon\sigma^3} - \pi\rho\bar{m}\left[\frac{\partial C_1}{\partial T}I_2 + C_1\frac{\partial I_2}{\partial T} - 2C_1\frac{I_2}{T}\right]\overline{m^2\varepsilon^2\sigma^3} \quad \text{Eq. 2.88}$$

with

$$\frac{\partial C_1}{\partial T} = \zeta_{3,T}C_2 \quad \text{Eq. 2.89}$$

The first derivatives of the dispersion integral series with respect to temperature is

$$\frac{\partial I_1}{\partial T} = \sum_{i=0}^{6} a_i(\bar{m})i\zeta_{3,T}\eta^{i-1} \quad \text{Eq. 2.90}$$

$$\frac{\partial I_2}{\partial T} = \sum_{i=0}^{6} b_i(\bar{m})i\zeta_{3,T}\eta^{i-1} \quad \text{Eq. 2.91}$$

✓ First derivative of Association contribution with respect to temperature

$$\frac{\partial}{\partial T}\left(\frac{a^{assoc}}{RT}\right)_{v,x_i} = \sum_i\sum_{A_i}\left[\frac{\frac{\partial X_{A_i}}{\partial T}}{X_{A_i}} - 0.5\frac{\partial X_{A_i}}{\partial T}\right] \quad \text{Eq. 2.92}$$

The derivatives of the non-bonded fractions, i.e.$\frac{\partial X_{A_i}}{\partial T}$, is calculated using the procedure suggested by Tan et al. [22] where the derivative of site-site strength is needed. The first derivative of the association strength is calculated using

$$\frac{\partial \Delta^{A_iB_j}}{\partial T} = \frac{\partial g_{ij}^{hs}}{\partial T} exp\left(\frac{\varepsilon_{AB}}{kT} - 1\right) {d_{ij}}^3 \kappa^{A_iB_j} - \frac{\varepsilon_{AB}}{kT^2} g_{ij}^{hs} exp\left(\frac{\varepsilon_{AB}}{kT} - 1\right) {d_{ij}}^3 \kappa^{A_iB_j} + 3 g_{ij}^{hs} exp(\frac{\varepsilon_{AB}}{kT} - 1)\left(\frac{d_{i,T} + d_{j,T}}{2}\right) {d_{ij}}^2 \kappa^{A_iB_j} \quad \text{Eq. 2.93}$$

2.9.2. Calculation of second derivative with respect to the temperature

The first derivative of Helmholtz free energy with respect to the temperature is sum of the derivatives of all contributions

$$\frac{\partial^2}{\partial T^2}\left(\frac{a^{res}}{RT}\right)_{v,x_i} = \frac{\partial^2}{\partial T^2}\left(\frac{a^{hc}}{RT}\right)_{v,x_i} + \frac{\partial^2}{\partial T^2}\left(\frac{a^{dis}}{RT}\right)_{v,x_i} + \frac{\partial^2}{\partial T^2}\left(\frac{a^{assoc}}{RT}\right)_{v,x_i} \quad \text{Eq. 2.94}$$

where n is the number of moles and a^{res} is extensive residual Helmholtz free energy.

✓ Second derivative of Hard-Chain contribution with respect to temperature.

$$\frac{\partial^2}{\partial T^2}\left(\frac{a^{hc}}{RT}\right)_{v,x_i} = \bar{m}\frac{\partial^2}{\partial T^2}\left(\frac{a^{hs}}{RT}\right)_{v,x_i} - \sum_i x_i(m_i - 1)\left[\frac{\frac{\partial^2 g_{ii}^{hs}}{\partial T^2}}{g_{ii}^{hs}} - \left(\frac{\frac{\partial g_{ii}^{hs}}{\partial T}}{g_{ii}^{hs}}\right)^2\right] \quad \text{Eq. 2.95}$$

where

$$\frac{\partial^2 g_{ii}^{hs}}{\partial T^2} = \frac{\zeta_{3,T2}(1-\zeta_3)^2 + 2{\zeta_{3,T}}^2(1-\zeta_3)}{(1-\zeta_3)^4} + \left(\frac{\partial}{\partial T}\left(\frac{d_i d_j}{d_i + d_j}\right)\right)\left(\frac{3\zeta_{2,T}(1-\zeta_3)^2 + 6\zeta_2\zeta_{3,T}(1-\zeta_3)}{(1-\zeta_3)^4}\right) + \left(\frac{\partial^2}{\partial T^2}\left(\frac{d_i d_j}{d_i + d_j}\right)\right)\frac{3\zeta_2}{(1-\zeta_3)^2} + \left(\frac{d_i d_j}{d_i + d_j}\right)\left(\frac{3\zeta_{3,T2}(1-\zeta_3)^2 + 6\zeta_{2,T}\zeta_{3,T}(1-\zeta_3)}{(1-\zeta_3)^4} + \frac{(6\zeta_{2,T}\zeta_{3,T} + 6\zeta_2\zeta_{3,T2})(1-\zeta_3)^3 + 18\zeta_2{\zeta_{3,T}}^2(1-\zeta_3)^2}{(1-\zeta_3)^6}\right) + \left(\frac{\partial}{\partial T}\left(\frac{d_i d_j}{d_i + d_j}\right)\right)\left(\frac{3\zeta_{2,T}}{(1-\zeta_3)^2} + \frac{6\zeta_2\zeta_{3,T}}{(1-\zeta_3)^3}\right) + 2\left(\frac{d_i d_j}{d_i + d_j}\right)\frac{\partial}{\partial T}\left(\frac{d_i d_j}{d_i + d_j}\right)\frac{4\zeta_{2,T}\zeta_2(1-\zeta_3)^3 + 6{\zeta_2}^2\zeta_{3,T}(1-\zeta_3)^2}{(1-\zeta_3)^6} + 2\left(\frac{\partial^2}{\partial T^2}\left(\frac{d_i d_j}{d_i + d_j}\right)\left(\frac{d_i d_j}{d_i + d_j}\right) + \left(\frac{\partial}{\partial T}\left(\frac{d_i d_j}{d_i + d_j}\right)\right)^2\right)\frac{2{\zeta_2}^2}{(1-\zeta_3)^3} + \left(\frac{d_i d_j}{d_i + d_j}\right)^2\left(\frac{(4{\zeta_{2,T}}^2 + 4\zeta_2\zeta_{2,T2})(1-\zeta_3)^3 + 12\zeta_2\zeta_{2,T}\zeta_{3,T}(1-\zeta_3)^2}{(1-\zeta_3)^6} + \frac{(12\zeta_{2,T}\zeta_2\zeta_{3,T} + 6{\zeta_2}^2\zeta_{3,T2})(1-\zeta_3)^4 + 24{\zeta_2}^2{\zeta_{3,T}}^2(1-\zeta_3)^3}{(1-\zeta_3)^8}\right) + 2\left(\frac{d_i d_j}{d_i + d_j}\right)\frac{\partial}{\partial T}\left(\frac{d_i d_j}{d_i + d_j}\right)\left(\frac{4\zeta_2\zeta_{2,T}}{(1-\zeta_3)^3} + \frac{6{\zeta_2}^2\zeta_{3,T}}{(1-\zeta_3)^4}\right) \quad \text{Eq. 2.96}$$

with

$$\frac{\partial^2}{\partial T^2}\left(\frac{d_i d_j}{d_i+d_j}\right)=\frac{\left(d_{i,T2}d_j+2d_{i,T}d_{j,T}+d_i d_{j,T2}\right)(d_i+d_j)+\left(d_{i,T}d_j+d_i d_{j,T}\right)(d_{i,T}+d_{j,T})}{(d_i+d_j)^2}-$$
$$\frac{\left(\left(d_{i,T}d_j+d_i d_{j,T}\right)(d_{i,T}+d_{j,T})+d_i d_j(d_{i,T2}+d_{j,T2})\right)}{(d_i+d_j)^2}+$$
$$\frac{2\left(\left(d_{i,T}d_j+d_i d_{j,T}\right)(d_i+d_j)-d_i d_j(d_{i,T}+d_{j,T})\right)(d_{i,T}+d_{j,T})(d_i+d_j)}{(d_i+d_j)^4} \quad \text{Eq. 2.97}$$

The second derivative of ζ_n with respect to the temperature is calculated via

$$\zeta_{n,T2}=\frac{\pi}{6}\rho\sum_i x_i m_i n\left(d_{i,T}{d_i}^{n-1}+{d_{i,T}}^2(n-1){d_i}^{n-2}\right) \quad \text{Eq. 2.98}$$

where

$$d_{i,T2}=\frac{\partial d_{i,T}}{\partial T}=\sigma_i\left(-6\frac{\varepsilon_i}{kT^3}\right)\left[-0.12\,exp\left(-3\frac{\varepsilon_i}{kT}\right)\right]+\sigma_i\left(9\frac{\varepsilon_i}{kT^2}\right)^2\left[-0.12exp(-3\frac{\varepsilon_i}{kT})\right] \quad \text{Eq. 2.99}$$

Second derivative of Hard-Sphere term is calculated using

$$\frac{\partial^2}{\partial T^2}\left(\frac{a^{hs}}{RT}\right)_{v,x_i}=\frac{1}{\zeta_0}\left[\frac{3\left(\zeta_{1,T2}\zeta_2+2\zeta_{1,T}\zeta_{2,T}+\zeta_1\zeta_{2,T2}\right)(1-\zeta_3)+(3\zeta_{1,T}\zeta_2+3\zeta_1\zeta_{2,T})\zeta_{3,T}}{(1-\zeta_3)^2}+\right.$$
$$\frac{3\left(\zeta_{1,T}\zeta_2\zeta_{3,T}+\zeta_1\zeta_{2,T}\zeta_{3,T}+\zeta_1\zeta_2\zeta_{3,T2}\right)(1-\zeta_3)^2+6\zeta_1\zeta_2{\zeta_{3,T}}^2(1-\zeta_3)}{(1-\zeta_3)^4}+$$
$$\frac{\left(6{\zeta_{2,T}}^2\zeta_2+3{\zeta_2}^2\zeta_{2,T2}\right)\zeta_3(1-\zeta_3)^2-(\zeta_{3,T}(1-\zeta_3)^2-2\zeta_3\zeta_{3,T}(1-\zeta_3))3{\zeta_2}^2\zeta_{2,T}}{(\zeta_3(1-\zeta_3)^2)^2}+$$
$$\frac{(3\zeta_{2,T}{\zeta_2}^2\zeta_{3,T}(3\zeta_3-1)+{\zeta_3}^3\zeta_{3,T2}(3\zeta_3-1)+3{\zeta_2}^3{\zeta_{3,T}}^2)\left({\zeta_3}^2(1-\zeta_3)^3\right)}{({\zeta_3}^2(1-\zeta_3)^3)^2}-$$
$$\frac{\left(2\zeta_{3,T}\zeta_3(1-\zeta_3)^3-3{\zeta_3}^2\zeta_{3,T}(1-\zeta_3)^2\right){\zeta_2}^3\zeta_{3,T}(3\zeta_3-1)}{({\zeta_3}^2(1-\zeta_3)^3)^2}+$$
$$\left(\frac{\left(6{\zeta_{2,T}}^2\zeta_2\zeta_3+3{\zeta_2}^2\zeta_{2,T2}\zeta_3+3{\zeta_2}^2\zeta_{2,T}\zeta_{3,T}-6{\zeta_2}^2\zeta_{2,T}\zeta_{3,T}-2{\zeta_2}^3\zeta_{3,T2}\right){\zeta_3}^3}{{\zeta_3}^6}-\right.$$
$$\left.\frac{3{\zeta_3}^2\zeta_{3,T}\left(3{\zeta_2}^2\zeta_{2,T}\zeta_3-2{\zeta_2}^3\zeta_{3,T}\right)}{{\zeta_3}^6}\right)ln(1-\zeta_3)+\frac{\zeta_{3,T}}{\zeta_3-1}\left(\frac{3{\zeta_2}^2\zeta_{2,T}\zeta_3-2{\zeta_2}^3\zeta_{3,T}}{{\zeta_3}^3}\right)+$$
$$\left.\left(\frac{3{\zeta_2}^2\zeta_{2,T}{\zeta_3}^2-2{\zeta_2}^3\zeta_{3,T}\zeta_3}{{\zeta_3}^4}\right)\frac{\zeta_{3,T}}{1-\zeta_3}+\left(\zeta_0-\frac{{\zeta_2}^3}{{\zeta_3}^2}\right)\left(\frac{\zeta_{3,T2}(1-\zeta_3)+{\zeta_{3,T}}^2}{(1-\zeta_3)^2}\right)\right] \quad \text{Eq. 2.100}$$

✓ Second derivative of Dispersion contribution with respect to temperature.

$$\frac{\partial^2}{\partial T^2}\left(\frac{a^{dis}}{RT}\right)_{v,x_i}=-2\pi\rho\left(\frac{\partial^2 I_1}{\partial T^2}-2\frac{\frac{\partial I_1}{\partial T}}{T}-2\frac{I_1}{T^2}\right)\overline{m^2\varepsilon\sigma^3}-\pi\rho\bar{m}\left(\frac{\partial^2 C_1}{\partial T^2}I_2+\frac{\partial C_1}{\partial T}\frac{\partial I_2}{\partial T}-\right.$$
$$\left.4\frac{\partial C_1}{\partial T}\frac{I_2}{T}+\frac{\partial C_1}{\partial T}\frac{\partial I_2}{\partial T}+C_1\frac{\partial^2 I_2}{\partial T^2}-4\frac{C_1}{T}\frac{\partial I_2}{\partial T}+6C_1\frac{I_2}{T^2}\right)\overline{m^2\varepsilon^2\sigma^3} \quad \text{Eq. 2.101}$$

with

$$\frac{\partial^2 I_1}{\partial T^2}=\sum_{i=0}^{6}a_i(\bar{m})i\left(\zeta_{3,T2}\eta^{i-1}+{\zeta_{3,T}}^2(i-1)\eta^{i-2}\right) \quad \text{Eq. 2.102}$$

$$\frac{\partial^2 I_2}{\partial T^2}=\sum_{i=0}^{6}b_i(\bar{m})i\left(\zeta_{3,T2}\eta^{i-1}+{\zeta_{3,T}}^2(i-1)\eta^{i-2}\right) \quad \text{Eq. 2.103}$$

and

$$\frac{\partial^2 C_1}{\partial T^2} = \zeta_{3,T2} C_2 + \zeta_{3,T} \frac{\partial C_2}{\partial T} \qquad \text{Eq. 2.104}$$

where

$$\frac{\partial C_2}{\partial T} = 2C_1 \frac{\partial C_1}{\partial T} \frac{C_2}{{C_1}^2} - {C_1}^2 \left(\bar{m} \frac{(-8\zeta_{3,T}\zeta_3 + 20\zeta_{3,T})(1-\zeta_3)^5 + 5(4{\zeta_3}^2 + 20\zeta_3 + 8)\zeta_{3,T}(1-\zeta_3)^4}{(1-\zeta_3)^{10}} + (1 - \bar{m}) \left[\frac{(6\zeta_{3,T}{\zeta_3}^2 + 24\zeta_3\zeta_{3,T} - 48\zeta_{3,T})((1-\zeta_3)(2-\zeta_3))^3}{((1-\zeta_3)(2-\zeta_3))^6} - \frac{3(2{\zeta_3}^3 + 12{\zeta_3}^2 - 48\zeta_3 + 40)(-\zeta_{3,T}(2-\zeta_3) - (1-\zeta_3)\zeta_{3,T})((1-\zeta_3)(2-\zeta_3))^2}{((1-\zeta_3)(2-\zeta_3))^6} \right] \right) \qquad \text{Eq. 2.105}$$

✓ Second derivative of association contribution with respect to temperature.

$$\frac{\partial^2}{\partial T^2}\left(\frac{a^{assoc}}{RT}\right) = \sum_i \sum_{A_i} \left[\frac{\frac{\partial^2 X_{A_i}}{\partial T^2}}{X_{A_i}} - \left(\frac{\frac{\partial X_{A_i}}{\partial T}}{X_{A_i}} \right)^2 - 0.5 \frac{\partial^2 X_{A_i}}{\partial T^2} \right] \qquad \text{Eq. 2.106}$$

The second derivatives of the non-bonded fractions, is obtained using Tan et al. [22] procedure where the second derivative of site-site strength is needed. The second derivative of the association strength is calculated using

$$\frac{\partial^2 \Delta^{A_i B_j}}{\partial T^2} = \frac{\partial^2 g_{ij}^{hs}}{\partial T^2} exp\left(\frac{\varepsilon_{AB}}{kT} - 1\right) {d_{ij}}^3 \kappa^{A_i B_j} - \frac{\partial g_{ij}^{hs}}{\partial T} \frac{\varepsilon_{AB}}{kT^2} exp\left(\frac{\varepsilon_{AB}}{kT} - 1\right) {d_{ij}}^3 \kappa^{A_i B_j} + 3\frac{\partial g_{ij}^{hs}}{\partial T} exp\left(\frac{\varepsilon_{AB}}{kT} - 1\right)\left(\frac{d_{i,T} + d_{j,T}}{2}\right) {d_{ij}}^2 \kappa^{A_i B_j} + \left(\frac{\varepsilon_{AB}}{kT^2}\right)^2 g_{ij}^{hs} exp\left(\frac{\varepsilon_{AB}}{kT} - 1\right) {d_{ij}}^3 \kappa^{A_i B_j} + 2\frac{\varepsilon_{AB}}{kT^3} g_{ij}^{hs} exp\left(\frac{\varepsilon_{AB}}{kT} - 1\right) {d_{ij}}^3 \kappa^{A_i B_j} - \frac{\varepsilon_{AB}}{kT^2} \frac{\partial g_{ij}^{hs}}{\partial T} exp\left(\frac{\varepsilon_{AB}}{kT} - 1\right) {d_{ij}}^3 \kappa^{A_i B_j} - 3\frac{\varepsilon_{AB}}{kT^2} g_{ij}^{hs} exp\left(\frac{\varepsilon_{AB}}{kT} - 1\right)\left(\frac{d_{i,T} + d_{j,T}}{2}\right) {d_{ij}}^2 \kappa^{A_i B_j} + 3\frac{\partial g_{ij}^{hs}}{\partial T} exp\left(\frac{\varepsilon_{AB}}{kT} - 1\right)\left(\frac{d_{i,T} + d_{j,T}}{2}\right) {d_{ij}}^2 \kappa^{A_i B_j} - 3 g_{ij}^{hs} exp\left(\frac{\varepsilon_{AB}}{kT} - 1\right)\left(\frac{d_{i,T} + d_{j,T}}{2}\right) {d_{ij}}^2 \kappa^{A_i B_j} + 6\frac{\partial g_{ij}^{hs}}{\partial T} exp\left(\frac{\varepsilon_{AB}}{kT} - 1\right)\left(\frac{d_{i,T} + d_{j,T}}{2}\right)^2 d_{ij} \kappa^{A_i B_j} \qquad \text{Eq. 2.107}$$

2.9.3. Calculation of second derivative with respect to the temperature and volume

$$\frac{\partial}{\partial T \partial V}\left(\frac{A^{res}}{RT}\right) = \frac{\partial}{\partial T \partial v}\left(\frac{a^{res}}{RT}\right) = -\rho^2 \frac{\partial}{\partial \rho}\left(\frac{\partial}{\partial T}\left(\frac{a^{res}}{RT}\right)\right) \qquad \text{Eq. 2.108}$$

✓ Second derivative of Hard-Chain contribution with respect to temperature and density.

$$-\rho^2 \frac{\partial}{\partial \rho}\left(\frac{\partial}{\partial T}\left(\frac{a^{hc}}{RT}\right)\right) = -\bar{m}\rho^2 \frac{\partial}{\partial \rho}\left(\frac{\partial}{\partial T}\left(\frac{a^{hs}}{RT}\right)\right) - \sum_i x_i (m_i - 1) \left[\frac{\rho^2 \frac{\partial g_{ii}^{hs}}{\partial \rho} \frac{\partial g_{ii}^{hs}}{\partial T}}{{g_{ii}^{hs}}^2} - \frac{\rho^2 \frac{\partial}{\partial \rho}\left(\frac{\partial g_{ii}^{hs}}{\partial T}\right)}{g_{ii}^{hs}} \right] \qquad \text{Eq. 2.109}$$

where the $\rho \frac{\partial g_{ii}^{hs}}{\partial \rho}$ and $\frac{\partial g_{ii}^{hs}}{\partial T}$ expressions have been presented before and $\rho \frac{\partial}{\partial \rho}\left(\frac{\partial g_{ii}^{hs}}{\partial T}\right)$ is obtained using the expression below

$$\frac{\partial}{\partial T}\left(\rho\frac{\partial g_{ij}^{hs}}{\partial\rho}\right)=\frac{\zeta_{3,T}(1-\zeta_3)^2+2\zeta_3\zeta_{3,T}(1-\zeta_3)}{(1-\zeta_3)^4}+\left(\frac{d_id_j}{d_i+d_j}\right)\left(\frac{3\zeta_{3,T}(1-\zeta_3)^2+6\zeta_2\zeta_{3,T}(1-\zeta_3)}{(1-\zeta_3)^4}+\frac{(6\zeta_{2,T}\zeta_3+6\zeta_2\zeta_{3,T})(1-\zeta_3)^3-18\zeta_2\zeta_3\zeta_{3,T}(1-\zeta_3)^2}{(1-\zeta_3)^6}\right)+\left(\frac{d_id_j}{d_i+d_j}\right)^2\left(\frac{8\zeta_2\zeta_{2,T}(1-\zeta_3)^3+12{\zeta_2}^2\zeta_{3,T}(1-\zeta_3)^2}{(1-\zeta_3)^6}+\frac{(12\zeta_{2,T}\zeta_2\zeta_3+6{\zeta_2}^2\zeta_{3,T})(1-\zeta_3)^4+24{\zeta_2}^2\zeta_3\zeta_{3,T}(1-\zeta_3)^3}{(1-\zeta_3)^8}\right)+\frac{\partial}{\partial T}\left(\frac{d_id_j}{d_i+d_j}\right)\left(\frac{3\zeta_2}{(1-\zeta_3)^2}+\frac{6\zeta_2\zeta_3}{(1-\zeta_3)^3}\right)+2\left(\frac{d_id_j}{d_i+d_j}\right)\frac{\partial}{\partial T}\left(\frac{d_id_j}{d_i+d_j}\right)\left(\frac{4{\zeta_2}^2}{(1-\zeta_3)^3}+\frac{6{\zeta_2}^2\zeta_3}{(1-\zeta_3)^4}\right)$$ Eq. 2.110

where

$$\frac{\partial}{\partial T}\left(\frac{d_id_j}{d_i+d_j}\right)=\frac{(d_{i,T}d_j+d_id_{j,T})(d_i+d_j)-d_id_j(d_{i,T}+d_{j,T})}{(d_i+d_j)^2}$$ Eq. 2.111

and the second derivate of the Hard-Sphere contribution is

$$-\rho^2\frac{\partial}{\partial\rho}\left(\frac{\partial}{\partial T}\left(\frac{a^{hs}}{RT}\right)\right)=\rho\frac{\partial}{\partial T}\left(\frac{a^{hs}}{RT}\right)-\frac{\rho}{\zeta_0}\left[\frac{3(2\zeta_{1,T}\zeta_2+2\zeta_1\zeta_{2,T})(1-2\zeta_3)+3(\zeta_{1,T}\zeta_2+\zeta_1\zeta_{2,T})\zeta_3}{(1-\zeta_3)^2}+\frac{9(\zeta_1\zeta_2\zeta_{3,T})(1-\zeta_3)^2+6(\zeta_1\zeta_2\zeta_{3,T})(1-\zeta_3)\zeta_3}{(1-\zeta_3)^4}+\frac{12({\zeta_2}^2\zeta_{2,T})\zeta_3(1-\zeta_3)^2-3[\zeta_3(1-\zeta_3)^2-2{\zeta_3}^2(1-\zeta_3)]{\zeta_2}^2\zeta_{2,T}}{(\zeta_3(1-\zeta_3)^2)^2}+\frac{(6{\zeta_2}^3\zeta_{3,T}(3\zeta_3-1)+{\zeta_2}^3\zeta_{3,T}\zeta_3)({\zeta_3}^2(1-\zeta_3)^3)-\left({\zeta_2}^3\zeta_{3,T}(3\zeta_3-1)\right)(2{\zeta_3}^2(1-\zeta_3)^3-3{\zeta_3}^3(1-\zeta_3)^2)}{({\zeta_3}^2(1-\zeta_3)^3)^2}+ln(1-\zeta_3)\frac{(12{\zeta_2}^2\zeta_{2,T}\zeta_3-8{\zeta_2}^3\zeta_{3,T}){\zeta_3}^3-3{\zeta_3}^3(3{\zeta_2}^2\zeta_{2,T}\zeta_3-2{\zeta_2}^3\zeta_{3,T})}{{\zeta_3}^6}-\left(\frac{3{\zeta_2}^2\zeta_{2,T}\zeta_3-2{\zeta_2}^3\zeta_{3,T}}{{\zeta_3}^3}\right)\frac{\zeta_3}{(1-\zeta_3)}+\left(\zeta_0-\frac{3{\zeta_2}^3{\zeta_3}^2-2{\zeta_2}^3{\zeta_3}^2}{{\zeta_3}^4}\right)\left(\frac{\zeta_{3,T}}{1-\zeta_3}\right)+\left(\zeta_0-\frac{{\zeta_2}^3}{{\zeta_3}^2}\right)\left(\frac{\zeta_{3,T}(1-\zeta_3)+\zeta_{3,T}\zeta_3}{(1-\zeta_3)^2}\right)\right]$$ Eq. 2.112

✓ Second derivative of Dispersion contribution with respect to temperature and density.

$$\frac{\partial}{\partial\rho}\left(\frac{\partial}{\partial T}\left(\frac{a^{dis}}{RT}\right)\right)=-2\pi\left[\frac{\partial I_1}{\partial T}-\frac{I_1}{T}+\rho\left(\frac{\partial}{\partial\rho}\left(\frac{\partial I_1}{\partial T}\right)-\frac{\partial}{\partial\rho}\left(\frac{I_1}{T}\right)\right)\right]\overline{m^2\varepsilon\sigma^3}-\pi\bar{m}[\left(\frac{\partial C_1}{\partial T}I_2+C_1\frac{\partial I_2}{\partial T}-2C_1\frac{I_2}{T}\right)+\rho\left(\frac{\partial}{\partial\rho}\left(\frac{\partial C_1}{\partial T}\right)I_2+\frac{\partial C_1}{\partial T}\frac{\partial I_2}{\partial\rho}+\frac{\partial C_1}{\partial\rho}\frac{\partial I_2}{\partial T}+C_1\frac{\partial}{\partial\rho}\left(\frac{\partial I_2}{\partial T}\right)-2\frac{\partial C_1}{\partial\rho}\frac{I_2}{T}-2C_1\frac{\partial}{\partial\rho}\left(\frac{I_2}{T}\right)\right)]\overline{m^2\varepsilon^2\sigma^3}$$ Eq. 2.113

where

$$\rho\frac{\partial}{\partial\rho}\left(\frac{\partial C_1}{\partial T}\right)=\zeta_{3,T}C_2+\zeta_{3,T}\rho\frac{\partial C_2}{\partial\rho}$$ Eq. 2.114

with

$$\rho\frac{\partial C_2}{\partial\rho}=-2C_1C_2\eta\left(\bar{m}\frac{-4\eta^2+20\eta+8}{(1-\eta)^5}+(1-\bar{m})\frac{2\eta^3+12\eta^2-48\eta+40}{[(1-\eta)(2-\eta)]^3}\right)-{C_1}^2\left(\bar{m}\frac{(-8\eta+20)(1-\eta)^5+5(1-\eta)^4(-4\eta^2+20\eta+8)}{(1-\eta)^{10}}+(1-\bar{m})\frac{(6\eta^2+24\eta-48)[(1-\eta)(2-\eta)]^3-3(2\eta-3)[(1-\eta)(2-\eta)]^2(2\eta^3+12\eta^2-48\eta+40)}{[(1-\eta)(2-\eta)]^6}\right)$$ Eq. 2.115

The second derivative of the dispersion integral series with respect to the temperature and density is calculated using

$$\rho\frac{\partial}{\partial\rho}\left(\frac{\partial I_2}{\partial T}\right)=\sum_{i=0}^{6}\left[b_i(\bar{m})i\zeta_{3,T}\eta^{i-1}+b_i(\bar{m})i(i-1)\zeta_{3,T}\eta^{i-1}\right] \quad \text{Eq. 2.116}$$

$$\rho\frac{\partial}{\partial\rho}\left(\frac{\partial I_1}{\partial T}\right)=\sum_{i=0}^{6}\left[a_i(\bar{m})i\zeta_{3,T}\eta^{i-1}+a_i(\bar{m})i(i-1)\zeta_{3,T}\eta^{i-1}\right] \quad \text{Eq. 2.117}$$

✓ Second derivative of association contribution with respect to temperature and density.

$$\frac{\partial^2}{\partial T\partial\rho}\left(\frac{a^{assoc}}{RT}\right)=\sum_i\sum_{A_i}\left[\frac{\frac{\partial^2 X_{A_i}}{\partial T\partial\rho}}{X_{A_i}}-\left(\frac{\frac{\partial X_{A_i}}{\partial T}\frac{\partial X_{A_i}}{\partial\rho}}{X_{A_i}}\right)^2-0.5\frac{\partial^2 X_{A_i}}{\partial T\partial\rho}\right] \quad \text{Eq. 2.118}$$

The derivative of the association strength which is needed in the calculation of non-bonded fraction derivative is obtained using

$$\rho\frac{\partial^2\Delta^{A_iB_j}}{\partial T\partial\rho}=\rho\frac{\partial g_{ij}^{hs}}{\partial T\partial\rho}exp\left(\frac{\varepsilon_{AB}}{kT}-1\right)d_{ij}{}^3\kappa^{A_iB_j}-\frac{\varepsilon_{AB}}{kT^2}\rho\frac{\partial g_{ij}^{hs}}{\partial\rho}exp\left(\frac{\varepsilon_{AB}}{kT}-1\right)d_{ij}{}^3\kappa^{A_iB_j}+$$
$$2\rho\frac{\partial g_{ij}^{hs}}{\partial\rho}exp(\frac{\varepsilon_{AB}}{kT}-1)\left(\frac{d_{i,T}+d_{j,T}}{2}\right)d_{ij}{}^2\kappa^{A_iB_j} \quad \text{Eq. 2.119}$$

2.9.4. Calculation of second derivative with respect to volume

The second derivative of the residual Helmholtz free energy can be written in terms of derivative of compressibility factor with respect to the density.

$$\frac{\partial^2}{\partial V^2}\left(\frac{A^{res}}{RT}\right)_{V,n}=\frac{1}{n}\frac{\partial^2}{\partial v^2}\left(\frac{a^{res}}{RT}\right)_{V,n} \quad \text{Eq. 2.120}$$

$$\frac{\partial^2}{\partial v^2}\left(\frac{a^{res}}{RT}\right)_{V,n}=\left(\frac{\partial Z}{\partial\rho}\rho+Z-1\right)\rho^2 \quad \text{Eq. 2.121}$$

$$\rho\frac{\partial Z}{\partial\rho}=\rho\frac{\partial Z^{hc}}{\partial\rho}+\rho\frac{\partial Z^{dis}}{\partial\rho}+\rho\frac{\partial Z^{assoc}}{\partial\rho} \quad \text{Eq. 2.122}$$

✓ Second derivative of Hard-Chain contribution with respect to density.

$$\rho\frac{\partial Z^{hc}}{\partial\rho}=\bar{m}\,\rho\frac{\partial Z^{hs}}{\partial\rho}-\sum_i x_i(m_i-1)\left[-\frac{\left(\rho\frac{\partial g_{ii}^{hs}}{\partial\rho}\right)^2}{g_{ii}^{hs\,2}}+\frac{\rho\frac{\partial}{\partial\rho}\left(\rho\frac{\partial g_{ii}^{hs}}{\partial\rho}\right)}{g_{ii}^{hs}}\right] \quad \text{Eq. 2.123}$$

with

$$\rho\frac{\partial}{\partial\rho}\left(\rho\frac{\partial g_{ij}^{hs}}{\partial\rho}\right)=\frac{\zeta_3(1-\zeta_3)^2+2\zeta_3{}^2(1-\zeta_3)}{(1-\zeta_3)^4}+\left(\frac{d_id_j}{d_i+d_j}\right)\left(\frac{3\zeta_2(1-\zeta_3)^2+6\zeta_3\zeta_2(1-\zeta_3)}{(1-\zeta_3)^4}+\right.$$
$$\left.\frac{12\zeta_2\zeta_3(1-\zeta_3)^3+18\zeta_2\zeta_3{}^2(1-\zeta_3)^2}{(1-\zeta_3)^6}\right)+\left(\frac{d_id_j}{d_i+d_j}\right)^2\left(\frac{8\zeta_3{}^2(1-\zeta_3)^3+12\zeta_2{}^2\zeta_3(1-\zeta_3)^2}{(1-\zeta_3)^6}+\right.$$
$$\left.\frac{(18\zeta_2{}^2\zeta_3)(1-\zeta_3)^4+24\zeta_2{}^2\zeta_3{}^2(1-\zeta_3)^3}{(1-\zeta_3)^8}\right) \quad \text{Eq. 2.124}$$

and the second derivative of Hard-Sphere is

$$\rho\frac{\partial Z^{hs}}{\partial\rho}=\frac{\zeta_3(1-\zeta_3)+{\zeta_3}^2}{(1-\zeta_3)^2}+\frac{(6\zeta_1\zeta_2)\left(\zeta_0(1-\zeta_3)^2\right)-\left(\zeta_0(1-\zeta_3)^2-2\zeta_0\zeta_3(1-\zeta_3)\right)3\zeta_1\zeta_2}{(\zeta_0(1-\zeta_3)^3)^2}+$$
$$\frac{(9{\zeta_2}^3-\zeta_3{\zeta_2}^3-3\zeta_3{\zeta_2}^3)(\zeta_0(1-\zeta_3)^3)-(\zeta_0(1-\zeta_3)^3-3\zeta_0\zeta_3(1-\zeta_3)^2)(3{\zeta_2}^3-\zeta_3{\zeta_2}^3)}{(\zeta_0(1-\zeta_3)^3)^2} \quad \text{Eq. 2.125}$$

✓ Second derivative of Dispersion contribution with respect to density.

$$\rho\frac{\partial Z^{dis}}{\partial\rho}=-2\pi\overline{m^2\varepsilon\sigma^3}\left(\frac{\partial(\eta I_1)}{\partial\eta}+\rho\frac{\partial}{\partial\rho}\left(\frac{\partial(\eta I_1)}{\partial\eta}\right)\right)-\pi\bar{m}\overline{m^2\varepsilon\sigma^3}\left(C_1\frac{\partial(\eta I_2)}{\partial\eta}+\rho\frac{\partial C_1}{\partial\rho}\frac{\partial(\eta I_2)}{\partial\eta}+\right.$$
$$\left.C_1\rho\frac{\partial}{\partial\rho}\left(\frac{\partial(\eta I_1)}{\partial\eta}\right)+C_2\eta I_2+\rho\frac{\partial C_2}{\partial\rho}\eta I_2+C_2\rho\frac{\partial\eta}{\partial\rho}I_2+\rho C_2\eta\frac{\partial I_2}{\partial\rho}\right) \quad \text{Eq. 2.126}$$

with

$$\rho\frac{\partial}{\partial\rho}\left(\frac{\partial(\eta I_1)}{\partial\eta}\right)=\sum_{j=0}^{6}a_j(\bar{m})(j+1)j\eta^j \quad \text{Eq. 2.127}$$

$$\rho\frac{\partial}{\partial\rho}\left(\frac{\partial(\eta I_2)}{\partial\eta}\right)=\sum_{j=0}^{6}b_j(\bar{m})(j+1)j\eta^j \quad \text{Eq. 2.128}$$

And

$$\rho\frac{\partial C_1}{\partial\rho}=\rho\frac{\partial C_1}{\partial\eta}\frac{\partial\eta}{\partial\rho}=C_2\rho\frac{\partial\eta}{\partial\rho}=C_2\eta \quad \text{Eq. 2.129}$$

$$\rho\frac{\partial C_2}{\partial\rho}=-2C_1C_2\eta\left(\bar{m}\frac{-4\eta^2+20\eta+8}{(1-\eta)^5}+(1-\bar{m})\frac{2\eta^3+12\eta^2-48\eta+40}{[(1-\eta)(2-\eta)]^3}\right)-$$
$${C_1}^2\left(\bar{m}\frac{(-8\eta+20)(1-\eta)^5+5(1-\eta)^4(-4\eta^2+20\eta+8)}{(1-\eta)^{10}}+(1-\right.$$
$$\left.\bar{m})\frac{(6\eta^2+24\eta-48)[(1-\eta)(2-\eta)]^3-3(2\eta-3)[(1-\eta)(2-\eta)]^2(2\eta^3+12\eta^2-48\eta+40)}{[(1-\eta)(2-\eta)]^6}\right) \quad \text{Eq. 2.130}$$

2.9.5 Comparing model calculation with experimental data

After the derivative of the Helmholtz free energy contributions were developed, a number of thermodynamic properties are being compared with the smoothed experimental data available on NIST. Three compounds were chosen to test the capability of the PC-SAFT model in calculating their thermodynamic properties. Propane as a light and dodecane as a heavier hydrocarbon as well as the methanol as an associating compound were selected for this purpose. The derivative properties of methanol were calculated using the PC-SAFT pure compound set of parameters developed in this study and those reported by Gross and Sadowski [214] to compare the performance of each.

The pure compound parameters used for propane and Dodecane are available in Table 2.2.The absolute average deviation of the model calculation from NIST data of isochoric heat capacity (C_V), isobaric heat capacity (C_p), sound velocity (u), and Joule-Thomson coefficients (μ_{JT}), of dodecane are reported in Table 2.16. Experimental and calculated derivative properties of dodecane are also compared in Figure 2.40 to Figure 2.43. As can be seen from the Table 2.16 and Figure 2.40 to Figure 2.43, the is a good agreement between experimental data and model calculation of C_V, C_p and sound velocity of

dodecane at below, proximity and above critical point. However, the calculated Joule-Thompson coefficients at below critical region differ from experimental data by around than 20%. Also, as shown in Figure 2.40, PC-SAFT model is unable to capture the maximum peak of the C_V versus pressure at 270 K despite the fact that the AAD % at this temperature is 5.51. This shortcoming was also reported by Villiers et al. where it was shown that none of the CPA, sPC-SAFT and SAFT models were able to qualitatively predict the maximum peak of the property [368]. As illustrated in Figure 2.42 and Figure 2.43, the PC-SAFT model is capable of predicting the maximum and minimum of the C_p and μ_{JT} properties with very good agreement with experimental data at above critical region with AAD % values of 3.36 and 2.12 respectively.

Table 2.16 Absolute average deviations of calculated second derivative properties of dodecane from experimental data at different temperatures and pressures up to 100 bar.

T - K	C_V	C_P	Speed of sound	Joule-Thomson Coefficient
AAD %				
270	5.51	0.46	0.12	19.58
300	4.71	0.78	1.48	17.09
350	3.26	1.31	3.73	13.49
500	0.29	1.29	8.89	4.19
700	1.81	3.36	27.99	2.12

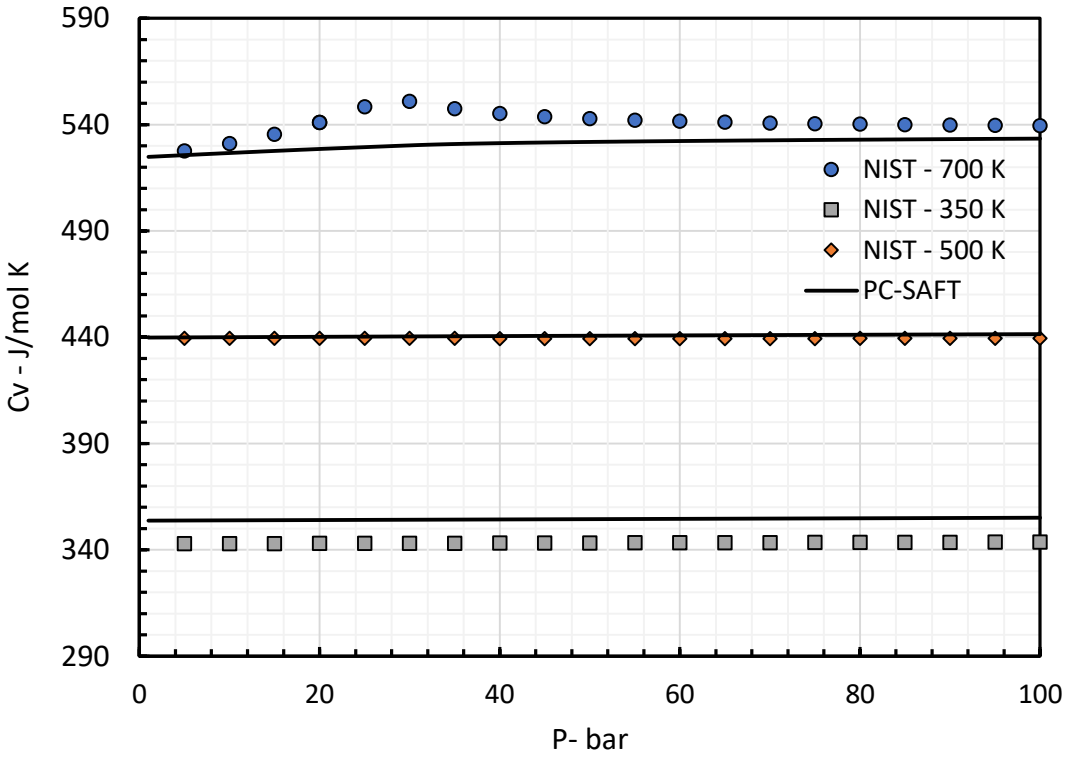

Figure 2.40 Experimental and calculated isochoric heat capacity of dodecane the 350 K, 500 K and 700 K and 1 to 100 bar pressures.

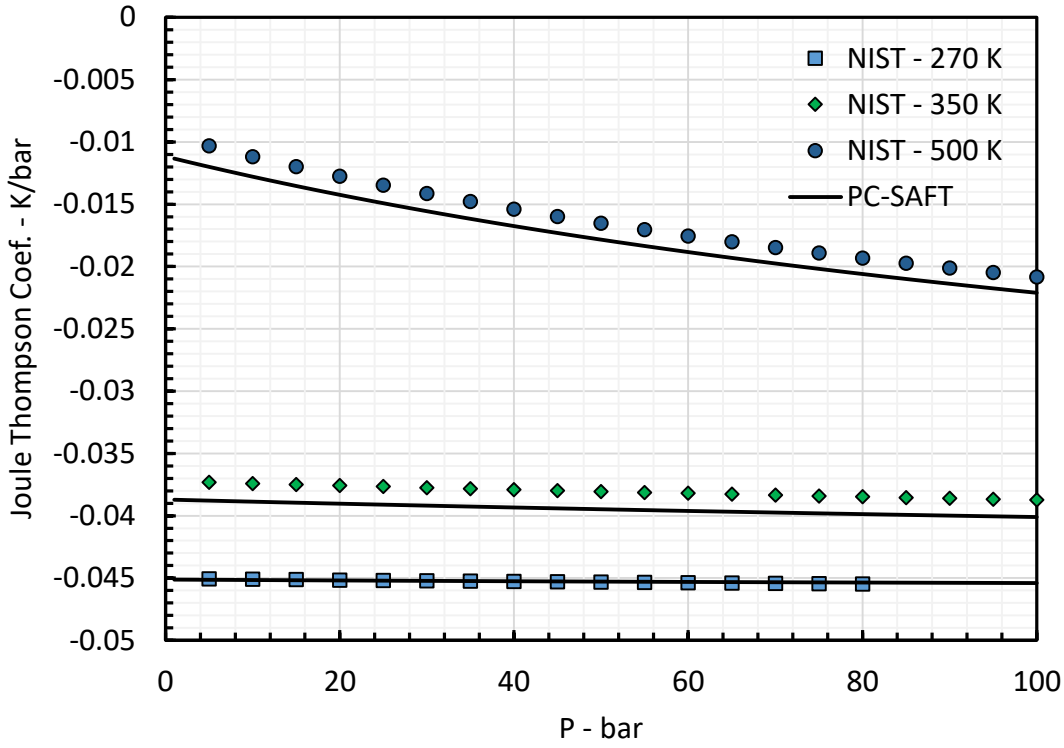

Figure 2.41 Experimental and calculated Joule-Thomson coefficient of dodecane at 270 K, 350 K and 500 K and 1 to 100 bar.

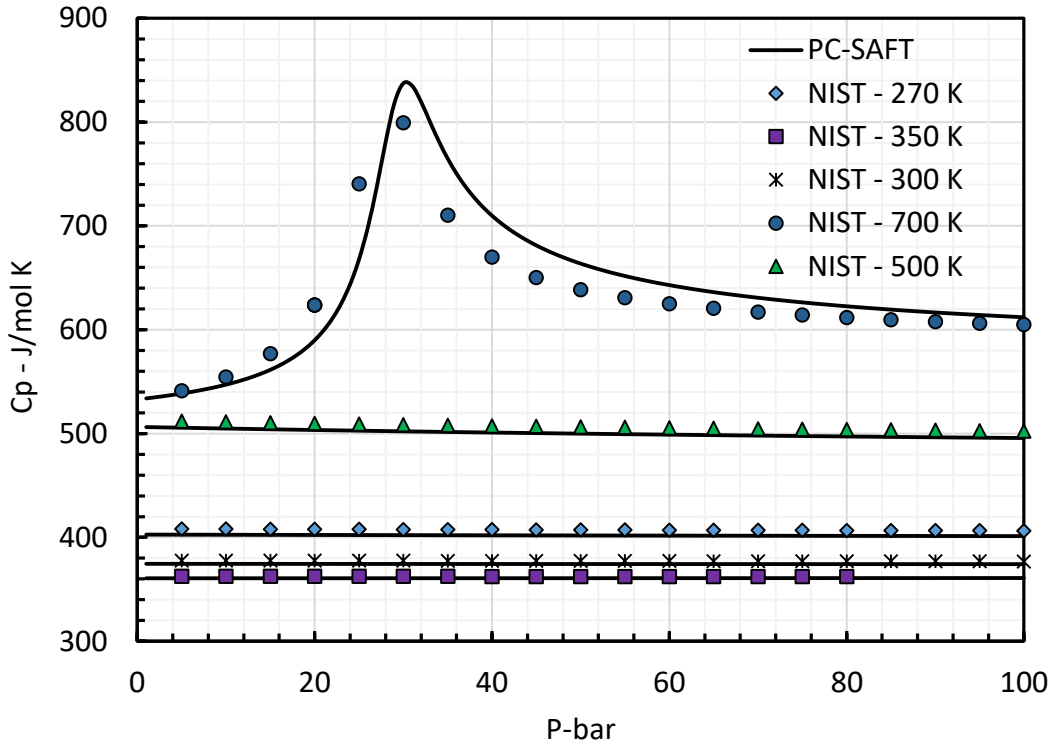

Figure 2.42 Experimental and calculated isobaric heat capacity of dodecane at 270 K, 300 K, 350 K, 500 K and 700 K and pressures up to 100 bar.

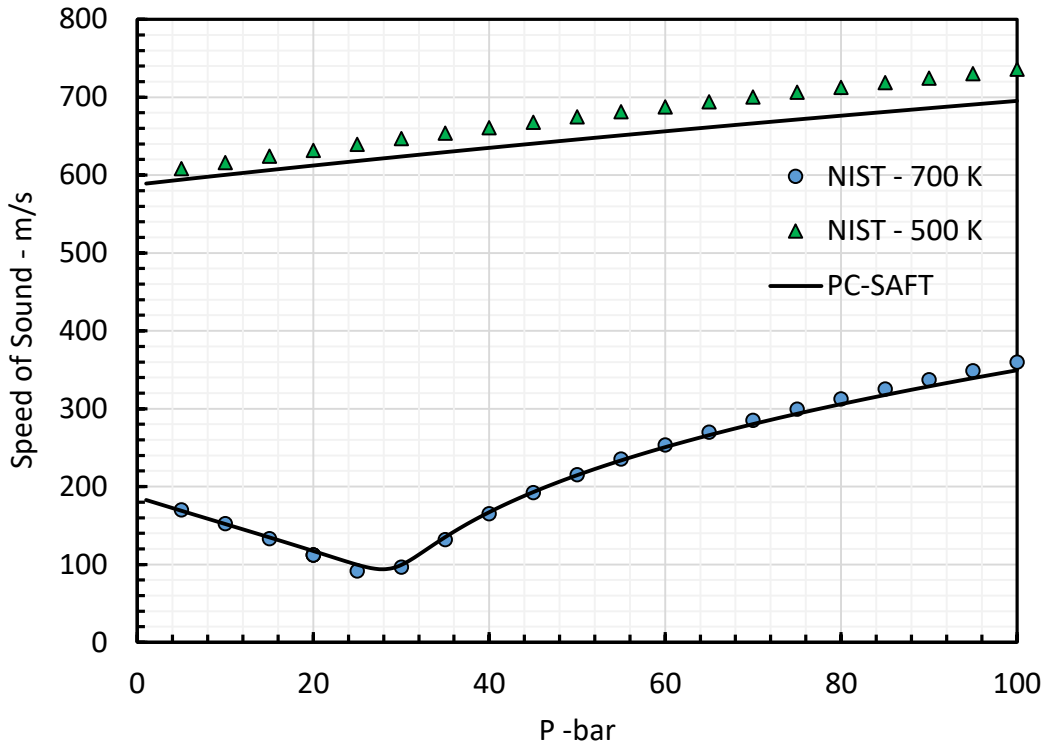

Figure 2.43 Experimental and calculated speed of sound in dodecane at 500 K and 700 K

Average absolute deviation of calculated thermodynamic derivatives of propane is summarised in Table 2.17. Calculated and experimental properties are also plotted together in Figure 2.44 to Figure 2.47 at 300 K and 400 K. Poor model performance was observed in predicting the speed of sound at 200 K with around 48 AAD % value. However, at temperatures higher than 300 K, calculated sound velocity deviation from experimental data are much lesser and as can be seen in Figure 2.45 model captures the extremum point of the sound velocity very well. The calculated isobaric and isochoric heat capacities also agree with the experimental data at 300 K and 400 K, specifically at 400 K where excellent agreement was found in calculating both heat capacities over an extensive pressure range. With respect to the isochoric heat capacity, model is unable to capture the maximum peak of the property similar to that reported for dodecane. As shown in Figure 2.46 model prediction and experimental data of Joule-Thomson coefficient are in a good agreement and the extremum of the curve is captured very well. It is also worth to note that at the extremum region of the Joule-Thomson curve versus pressure, the deviation from the model calculation and experimental data becomes greater as the slope of the curve is high and a small deviation in predicting the location of the extremum could result in a very high difference of the calculated and experimental thermodynamic properties making the average deviation relatively high.

Table 2.17 Average absolute deviations of calculated second derivative properties of propane from experimental data at 200 K, 300 K and 400 K and pressures up to 100 bar.

T - K	C_V	C_P	Speed of sound	Joule-Thomson Coefficient
		AAD %		
200	16.68%	17.17%	48.69%	18.27%
300	0.35%	6.61%	9.42%	3.43%
400	1.46%	2.40%	12.00%	20.75%

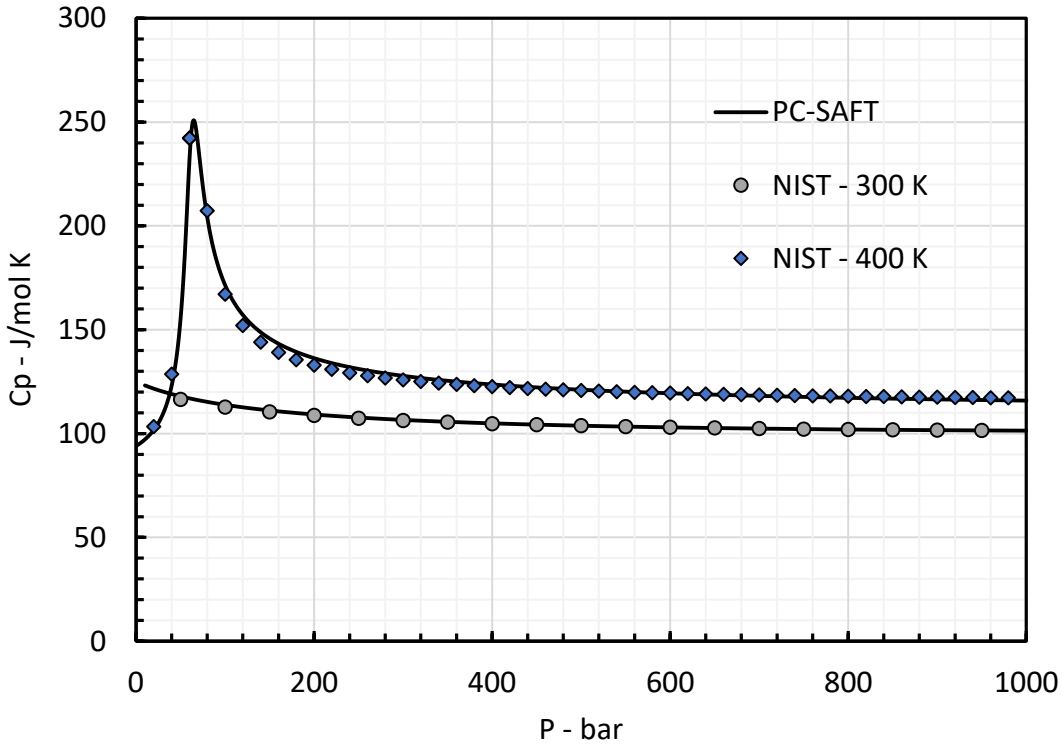

Figure 2.44 Experimental and calculated isobaric heat capacity of propane at 300 K and 400 K and pressures up to 1000 bar.

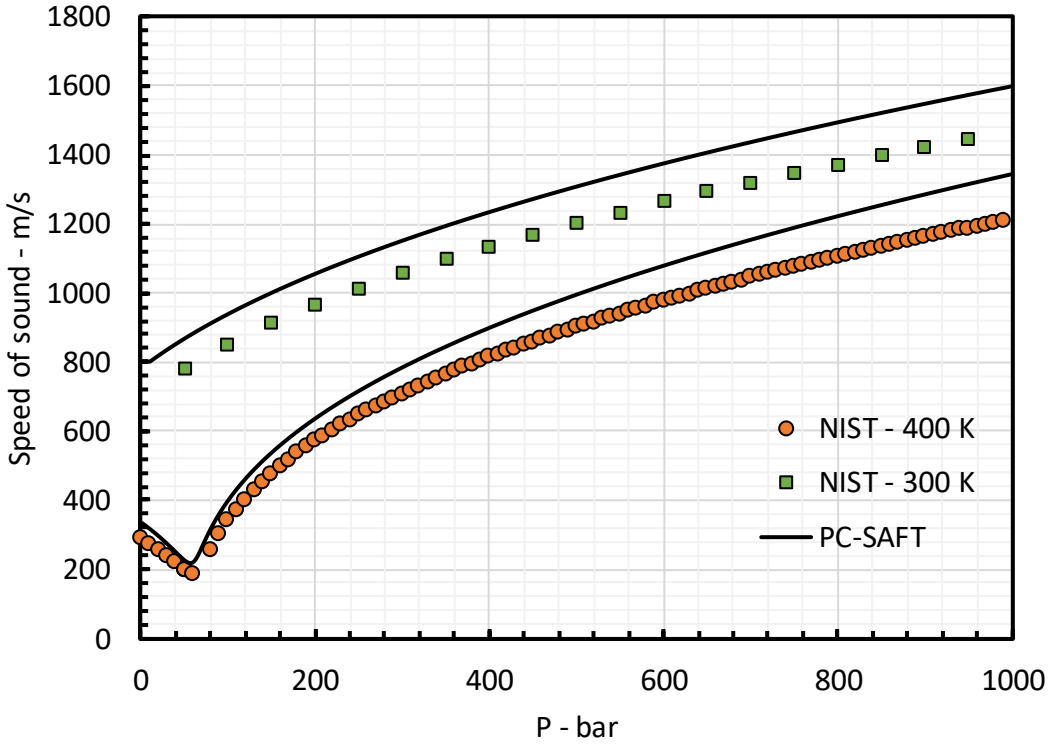

Figure 2.45 Experimental and calculated speed of sound in propane at 300 K and 400 K and pressures up to 1000 bar

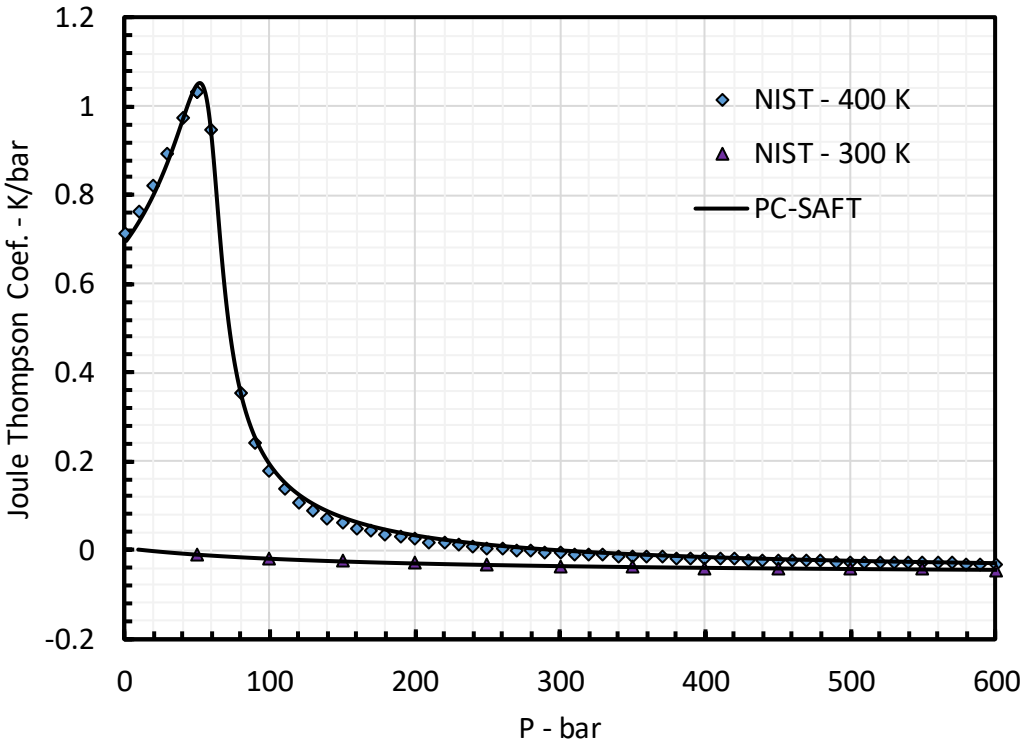

Figure 2.46 Experimental and calculated Joule-Thomson coefficient of propane at 300 K and 400 K and pressures up to 600 bar

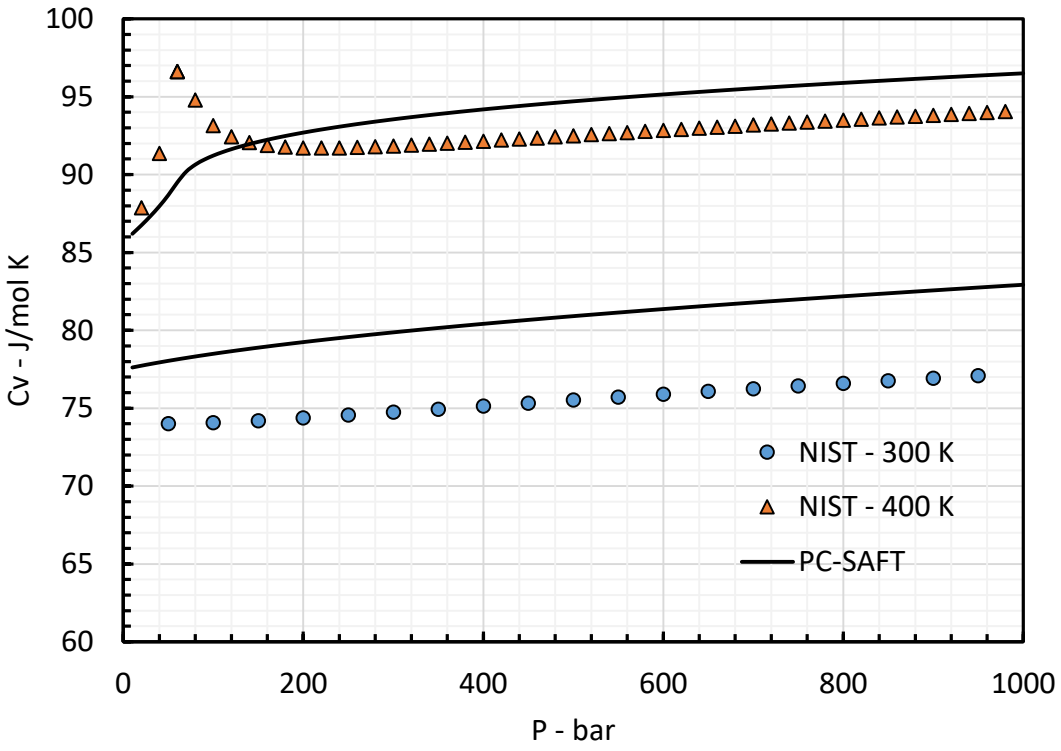

Figure 2.47 Experimental and calculated isochoric heat capacity of propane at 300 K and 400 K and pressures up to 1000 bar

The speed of sound in two typical natural gases were calculated using the PC-SAFT EoS and compared with experimental data reported by Younglove et al. [369]. The binary interaction parameters between components were set to those tuned in this work and presented in Table 2.2 to Table 2.6. The compositions of the fluids are reported in Table 2.18. The AAD % of calculated and experimental speed of sound in the fluids are reported in Table 2.19 at each temperature. Total AAD obtained are 0.73% and 1.02% for Amarillo and Statoil dry gas fluids respectively, which indicates that model performs excellent in calculating the sound velocity in multi-component fluids. Also, as seen in Table 2.19, the deviation from experimental sound velocity in Statoil dry gas increases as temperature decreases.

Table 2.18 Amarillo and Statoil dry gas compositions (mole fraction)

Component	Amarillo gas	Statoil dry gas
methane	0.90708	0.8398
ethane	0.04491	0.13475
propane	0.00815	0.00943
iso-butane	0.00106	0.0004
n-butane	0.00141	0.00067
iso-pentane	0.00027	0.00013
carbon dioxide	0.00500	0.00756
nitrogen	0.03113	0.00718
n-pentane	0.00065	0.00008
n-hexane	0.00034	-

Table 2.19 Average absolute deviation of calculated and experimental sound velocity in Amarillo and Statoil dry gas fluids

Amarillo gas	
T-K	**AAD**
250	1.00%
275	0.32%
298	1.37%
300	0.5%
Total AAD	0.73%
Statoil dry gas	
250	2.05%
275	1.85%
300	0.86%
325	0.34%
350	0.31%
Total AAD	1.02%

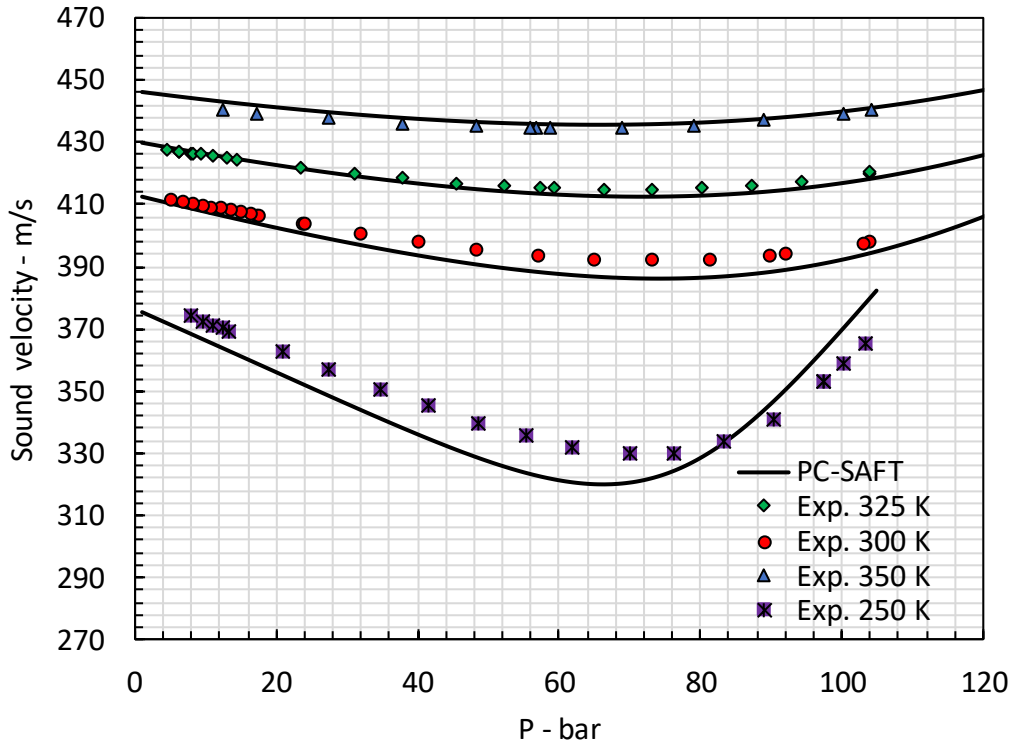

Figure 2.48 Experimental and calculated sound velocity in Statoil dry gas at various temperatures. Experimental data taken from [369]**.**

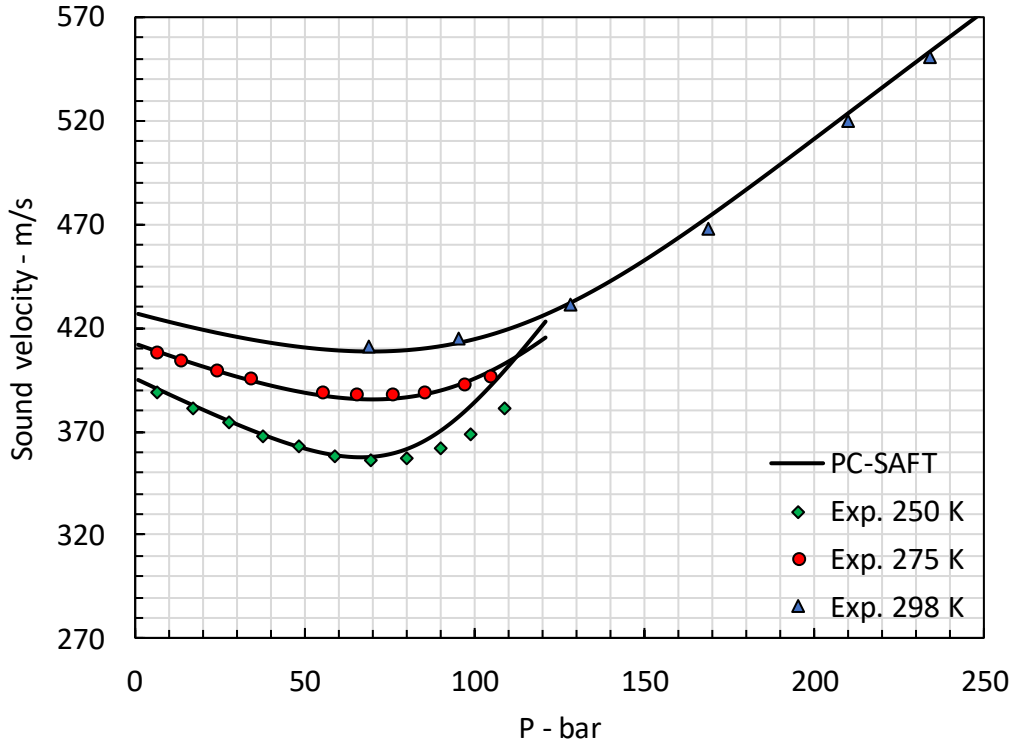

Figure 2.49 Experimental and calculated sound velocity in Amarillo gas at various temperatures. Experimental data taken from [369]

The second derivative properties of methanol were calculated using the pure compound parameters developed in this work and the one reported by Gross and Sadowski [214] to evaluate capability of the PC-SAFT model in predicting second derivative properties and also to compare the performance of the model using two sets of pure compound parameters. The AAD % values of each property at two below and above critical temperatures are summarized in Table 2.20. In general, the model cannot predict the thermodynamic properties of methanol within a reasonable deviation from the experimental data. However, as can be seen from Figure 2.50 and Figure 2.51, the behaviours of the isobaric heat capacity and speed of sound are qualitatively captured by the model but considerable deviations are observed from experimental data. As reported in Table 2.20, PC-SAFT model shows almost the same performance using both sets of parameters for predicting the heat capacities, while a relatively better prediction for speed of sound was observed using the sets of parameters developed in this work with around 2-3% less deviation from experimental data.

Table 2.20 Absolute average deviations of calculated second derivative properties of methanol from experimental data

T-K	Pure compound parameter used	C_V	C_P	Speed of sound
		AAD %		
300	This Work	28.06	23.89	8.72
600	This Work	22.16	9.19	26.57
300	Gross and Sadowski [214]	27.41	23.00	10.57
600	Gross and Sadowski [214]	22.67	9.79	29.04

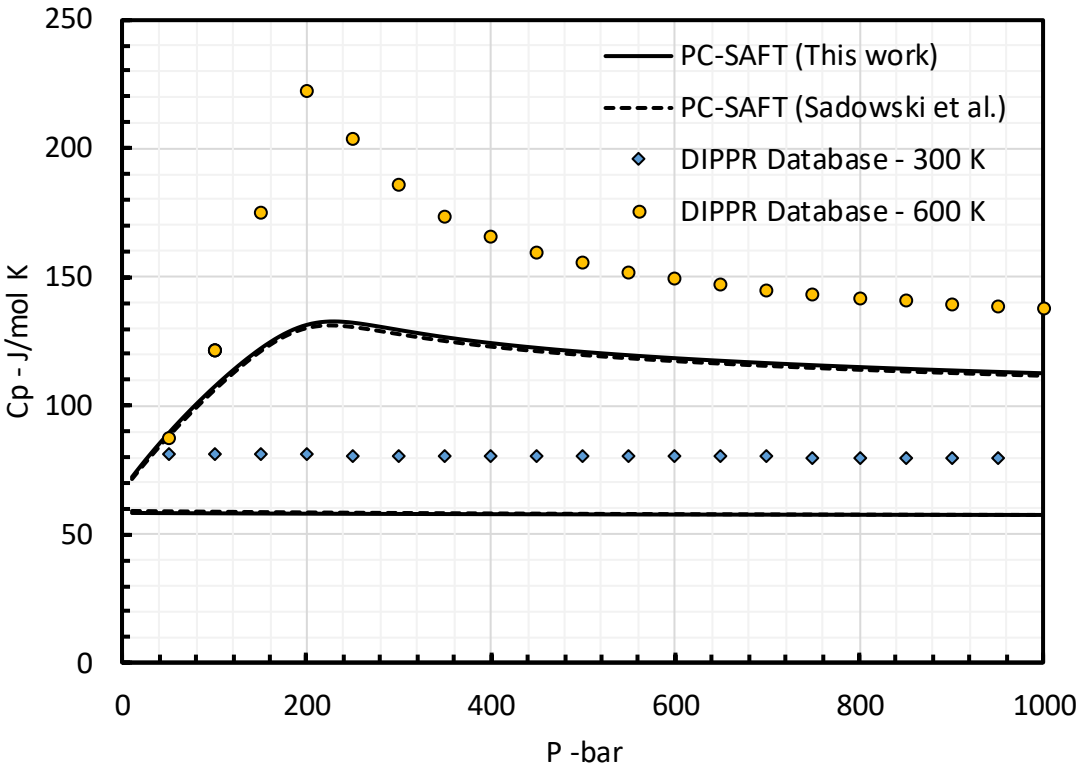

Figure 2.50 Experimental and calculated isobaric heat capacity coefficient of methanol at 300 K and 600 K and pressures up to 1000 bar

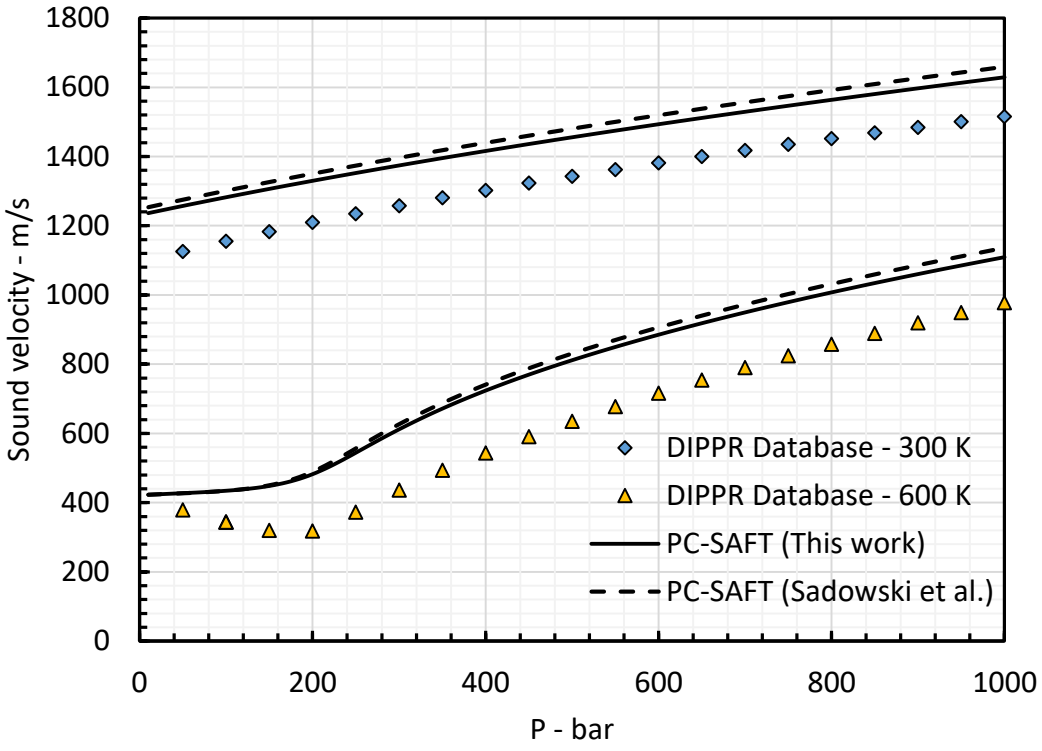

Figure 2.51 Experimental and calculated speed of sound in methanol at 300 K and 600 K and pressures up to 1000 bar

2.10 Modelling of Electrolytes Using PC-SAFT Model

The vapour-liquid and liquid-liquid equilibria of systems with and without presence of associating compounds were extensively investigated in the previous sections using PC-SAFT equation of state. However, when salts are present in the aqueous system the activity of associating compounds is affected and the equilibria of system is changed consequently. When electrolytes are present, the chemical potential of each component in the system is modified by adding the electrolyte contribution to the chemical potential to take into account the effect of the salts in the system.

$$\mu_i = \mu_i^{EoS} + \mu_i^{Electrolyte} \qquad \text{Eq. 2.131}$$

In this study, we used the Debye–Hückel activity coefficient to correct the fugacity coefficients of the components when salts are present in the system. In this approach, we assume that the concentration of salts in the non-aqueous phase is zero and then the fugacity coefficient of each non-electrolyte component in the aqueous phase is corrected using the activity coefficient. The fugacity coefficients of each non-electrolyte component in the aqueous phase is then calculated using

$$ln\phi_i(\mathrm{T},\rho) = ln\phi_i^{EoS}(\mathrm{T},\rho) + ln\gamma_i^{DH}(\mathrm{T},\rho) \qquad \text{Eq. 2.132}$$

where $\phi_i^{EoS}$the fugacity coefficient is calculated using EoS and γ_i^{DH} is Debye–Hückel activity coefficient suggested by Macedo et al. [370] which is calculated via the expression below.

$$\gamma_i^{DH}(\mathrm{T},\rho) = \frac{2A^{DH}M_m h_{is}}{B^{DH^3}} f(B^{DH}{I_s}^{0.5}) \qquad \text{Eq. 2.133}$$

In the above equation, $M_m$the salt-free mixture molecular weight (the molecular weight of the mixture without considering the molecular weight of salt $\frac{kg}{mol}$). As the performance of the simple Debye-Huckel model is good only in low concentration solutions [371] another binary interaction parameter entitled h_{is} is needed to adjust the interaction between salt and non-electrolyte compound. This binary interaction parameter must be tuned with appropriate experimental data i.e. vapour pressure, freezing point and solubility of solutes in aqueous solutions of salts. Haghighi et al. has tuned the binary interaction of salt-water of nine electrolyte systems [372] by adjusting the CPA model to the freezing points and vapour pressures of the electrolytes and reported the h_{ws} parameter (binary interaction parameter of water-salt) as the function of temperature and weight concentration of dissolved salts. $f(B^{DH}{I_s}^{0.5})$ is calculated through

$$f\left(B^{DH}{I_s}^{0.5}\right) = 1 + B^{DH}{I_s}^{0.5} - \frac{1}{1+B{I_s}^{0.5}} - 2ln(1 + B^{DH}{I_s}^{0.5}) \qquad \text{Eq. 2.134}$$

where is the ionic strength based on the salt concentration, and A^{DH} and B^{DH} parameters are obtained using

$$A^{DH} = \frac{1.327757\times10^{5}{d_m}^{0.5}}{(\eta^{d}{}_{m}T)^{1.5}} \quad \text{Eq. 2.135}$$

$$B^{DH} = \frac{6.35969\times{d_m}^{0.5}}{(\eta^{d}{}_{m}T)^{0.5}} \quad \text{Eq. 2.136}$$

where d_m is the density of the salt-free mixture (the density of the aqueous phase at specified temperature and pressure assuming that there is no salt in the aqueous phase $\frac{kg}{m^3}$) and η_m is the dielectric constant of the salt-free mixture

$$\eta^{d}{}_{m} = x_w\eta^{d}{}_{w} \quad \text{Eq. 2.137}$$

where x_w and η_w are the salt-free mole fraction and the dielectric constant of water.

In this work the CPA model of our in-house modelling software (HydraFLASH) was also applied to compare its performance with the PC-SAFT model and further validate the experimental results presented in Chapter 3 and 4. Detail of the CPA model used in this work is available here [373]. To account for the effect of salts in PC-SAFT model, The Debye–Hückel activity coefficient was applied to correct the fugacities of CO_2-brine systems by incorporating the h_{ws} developed by Haghighi et al. [372] and h_{is} adjusted to experimental data of CO_2 solubility in aqueous solutions of salts using PC-SAFT EoS. As the CPA and PC-SAFT models show quite similar performance in calculation of the freezing point (see Table 2.8) and vapour pressures of water over a wide range of temperatures (see Figure 2.52, The AAD % of the CPA and the PC-SAFT model at 273.15 K to 523.15 K temperature range is 0.05%), using the h_{ws}values tuned with CPA model for PC-SAFT equation of state seems to be a reasonable approach. The following objective function was adopted to optimize the electrolyte model for CO_2-brine systems using the experimental solubilities of CO_2 in aqueous solutions of different salts.

$$OBJ = \sum_{i=1}^{N_{exp}} \left(\left(\frac{X_i^{EoS} - X_i^{Exp}}{X_i^{Exp}} \right)^2 \right) \quad \text{Eq. 2.138}$$

Table 2.21 and Table 2.22 present the coefficients of polynomial equation fitted to the tuned temperature dependent $h_{ws}$of the CPA and the PC-SAFT models.

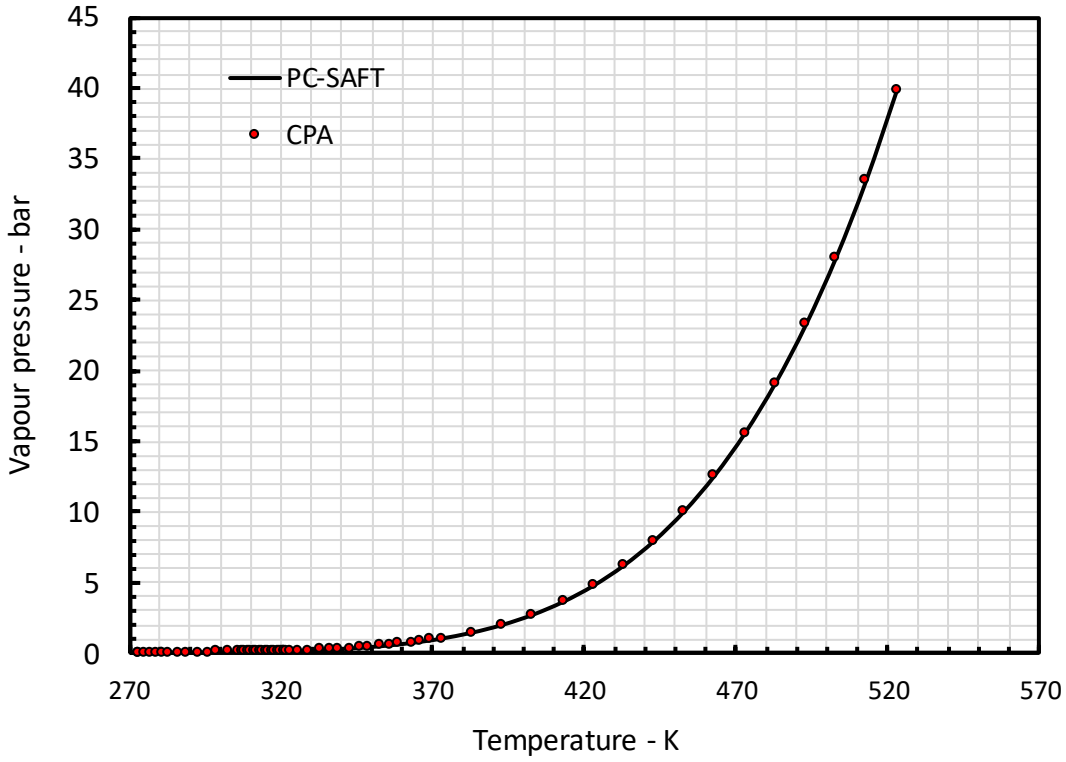

Figure 2.52 Calculated vapour pressure of water using the CPA and PC-SAFT equation of states

Table 2.21 Temperature dependant CO_2 - salt binary interaction parameters of Debye–Hückel activity model tuned using the PC-SAFT equation of state ($h_{ws}(T) = B_2T^2 + B_1T + B_0$)

Salt	T-Range	B_2	B_1	B_0	Experimental Data
NaCl	278.15-423.15	5.41e-5	-0.0428	9.1666	This work
KCl	323.15-423.15	8.07e-5	-0.0574	10.4830	This work
$CaCl_2$	309-424	1.97e-5	-0.0152	3.5700	[374]
$MgCl_2$	309-424	4.27e-5	-0.0321	6.6034	[374], [375]

Table 2.22 Temperature dependant CO_2 - salt binary interaction parameters of Debye–Hückel activity model tuned using the CPA equation of state ($h_{ws}(T) = B_2T^2 + B_1T + B_0$)

Salt	T-Range	B_2	B_1	B_0	Experimental Data
NaCl	278.15-423.15	2.99E-05	-0.0250	5.9356	This work
KCl	323.15-423.15	5.82E-05	-0.0415	7.7347	This work
$CaCl_2$	309-424	1.25E-05	-0.0103	2.7321	[374]
$MgCl_2$	309-424	3.35E-05	-0.0260	5.6132	[374], [375]

2.11 Conclusion

In this chapter a brief review on the SAFT approach and PC-SAFT equation of state was presented. The binary interaction parameters of 82 binary mixtures of non-associating compounds were adjusted to available experimental literature or in-house phase equilibria data. The capability of PC-SAFT EoS in calculating the saturation properties of pure water was improved by introducing the two temperature dependent sets of pure compound parameters and tuning the model to experimental saturation data of water. Comparing the model performance using the new adjusted pure parameters of water showed a significant superiority over all sets of parameter reported in the literature. The dispersive interactions between water and several non-associating compounds were then tuned by adjusting the BIPs of water and non-associating components to the experimental solubility data.

The pure compound parameters of ethylene glycol oligomers, including MEG, DEG, TEG, TeEG and PG were then optimised using the smoothed saturation data of DIPPR database and compared to model calculation results using sets of parameters suggested by others. It was shown that using the sets of pure compound parameters adjusted in this study, calculated saturation properties of all EG-oligomers show better agreement with experimental data. By applying the new sets of pure compound parameters, the binary interaction parameters of glycol and non-associating systems were fitted to available experimental literature or in-house data. New sets of pure compound parameters for methanol, ethanol, 1-propanol and 2-propanol were optimised to experimental vapour pressures and saturated liquid densities and model performance using different sets of pure compound parameters was compared against experimental data. It was shown that calculated saturation properties of studied alcohols correlate the experimental data better using new sets of pure compound parameters comparing to the parameters presented by others. The derivative of Helmholtz free energy contributions of PC-SAFT equation of state were also driven analytically to remove the error of the numerical differentiation from the calculated properties.

Chapter 3

3-Solubility of CO_2 in Pure Water and Aqueous Solution of Salts

3.1 Introduction

Having a precise knowledge on the phase equilibria behaviour of CO_2-pure water or CO_2-aqueous solutions of salts systems and the fluid properties at reservoir conditions where the CO_2 is stored or at transport pipelines conditions is crucial from two major points of views. First, the solubility of CO_2 in brine is directly related to the CO_2 storing capacity of the underground aquifers. The effect of different salt types and different salinity of brine, as well as the effect of temperature and pressure of the formation on the CO_2 solubility in saline water, must be measured accurately to obtain a precise understanding of the behaviour of CO_2-brine systems. Second, as in some cases, thermodynamic or hydrodynamic models used for engineering calculations and simulations, rely heavily on reliable experimental data, accurate experimental phase equilibria data of CO_2-brine systems would be a great help in developing such models.

The phase behaviour of CO_2-aqueous systems has been extensively investigated experimentally and theoretically in the literature. The available literature experimental studies may be divided into three major categories: CO_2 solubility measurement in pure water, solubilities in single salt aqueous solutions and solubilities in multi salts aqueous solutions. The number of experimental data reported on the solubility of CO_2 in pure water is higher than other salt aqueous solutions. Likewise, CO_2 solubility data in aqueous solutions of sodium chloride have been reported more that those reported for calcium chloride, potassium chloride, magnesium chloride and mixed salt aqueous solutions.

Totally 47 datasets were found for solubility data in pure water with more than 1400 solubility points at temperatures from 273.15 K up to 523.15 K and pressures ranging from atmospheric pressure to 3500 bar. Table 3.1 summarises all the datasets gathered from the literature.

Table 3.1 Available experimental data on solubility of CO_2 in pure water

Temperature range / K	Pressure range /bar	Reference
286–348	1.02–1.4	[224]
283-303	1–20	[381]
473–523	98–490	[338]
303–333	100–200	[403]
273–323	1.01–1.14	[34]
374–393	23–703	[380]
348-421	10.2-20.9	[411]
297	1 to 14	[412]
323.15	1.1 - 5.8	[413]
323–623	200–3500	[382]
383–623	100–1500	[383]
303–353	10–39	[384]
298–348	47.9	[385]
298–423	47.9	[386]
303–523	40–126	[387]
323–473	1–54	[388]
323–373	100–800	[389]
288–366	7–203	[390]
283–343	10–160	[391]
323	68–177	[333]
323–348	101–152	[334]
373–473	3–80	[392]
353–471	20–102	[393]
288-298	60-250	[341]
273-285	1-3	[405]
293-333	24-167	[406]
273.15 – 373.15	10– 90	[377]
323 – 373	25 – 71	[378]
285 – 313	25 – 50.7	[379]
294	100–600	[400]
288–298	60–250	[394]
278–293	64–295	[395]
278–338	0.49–0.84	[396]
274–351	2–90	[404]
278–318	5–80	[340]
293.15 – 303.15	5 – 30	[376]
277–283	20–42	[401]
274–288	1–220	[402]

In continuance of Table 3.1		
273-288	1-53	[407]
298-308	25-76	[408]
273-298	1.0-4.6	[409]
273-373	0.1-3.6	[410]
293.15 – 303.15	0.5 – 3	[414]
344	100–1000	[397]
313–353	10–141	[398]
298	21–77	[399]

The data reported by Zel'vinskii et al. [377], Chapoy et al. [404] and Houghton et al. [410] covers a broad range of conditions from temperatures between 273.15 K to 373.15 K and pressures up to 90 bar. The most recent data reported by Jacob et al. [412] at a single temperature of 297K. However, not all the data reported were consistent with each other. Duan et al. [295] gathered a significant number of CO_2 solubility experimental data over wide ranges of temperatures and pressures to tune a thermodynamics-based model. A good review on the consistency of solubility data can be found in their paper.

Several datasets were also found and summarised in Table 3.2 for solubility of CO_2 in aqueous solutions of sodium chloride. Solubility data have been reported in different concentrations of aqueous solutions from 1 wt% to 26.9 wt% NaCl aqueous solutions at temperatures between 273.15 K to 800 K and pressures up to 2800 bar. Drummond et al. have reported the most comprehensive dataset [387] in various concentrations of sodium chloride aqueous solutions at temperatures between 293K to 673K and pressures up to 400 bar. Among all the experimental datasets found in the literature, the most recent one was presented by Tong et al. where the solubility of CO_2 in NaCl aqueous solution was measured to validate the experimental setup and procedures they employed for CO_2 solubility measurements in aqueous solutions of $MgCl_2$ and $CaCl_2$ [374].

Table 3.2 Available experimental data on solubility of CO_2 in NaCl aqueous solutions

Temperature range / K	Pressure range /bar	Salt concentration / wt%	References
313 – 433	1– 100	18.9 –26.9	[413]
313 - 433	2-96	0 – 26	[422]
408 – 800	30 – 2800	5.5 – 20.1	[420]
290 – 673	35 – 400	0 – 27.5	[387]
298 – 348	47.92	0 – 20.8	[419]
298 – 423	47.92	0 – 26	[386]
291.2	1.01	1.16- 26.2	[424]
293	1.01	8.55 - 24.9	[425]
298-318	1.01	0.90	[426]
353 – 473	20 – 100	0 – 1	[421]
313 - 353	1 - 100	0 – 20.1	[423]
423 – 523	100 – 1400	0 – 20	[417]
298	1	0 – 15	[418]
273 – 313	1.02 – 1.09	0 – 18.9	[415]
273 – 323	1.02 – 1.14	0 – 15	[34]
445 – 610	25 – 200	0 – 10.5	[416]
288-333	1.01	2.84 - 21.91	[427]
288-308	1.01	2.84 - 24.32	[428]
273.5-277	8-19	2.84 - 22.26	[429]
273-363	0.04-1	0.58- 26.28	[430]
293-308	1.01	3.93- 14.49	[431]
278-338	0.5-0.9	3.93 - 16.17	[396]
233.15	100	3	[432]
323-373	100-100.4	5.8	[433]

According to Duan et al. [295] a few data points reported by Drummond et al. during pressure increasing and decreasing processes deviates by 8-12%. Also, the data measured by Takenochi et al. [417] at 100 bar is not in agreement with those measured by Drummond et al. [387] and Rumpf et al. [413] at the same conditions [295]. The datasets collected for calcium chloride are presented in Table 3.3. A total number of 10 datasets were found in the literature for solubility of CO_2 in the 1wt% to 43 wt% $CaCl_2$ aqueous solutions at temperatures from 288 K to 423 K and pressures up to 710 bar. As mentioned before, limited number of experimental CO_2 solubility data have been reported in KCl, $CaCl_2$, and $MgCl_2$ aqueous solutions compared to those reported in NaCl aqueous solutions.

Table 3.3 Available experimental data on solubility of CO_2 in $CaCl_2$ aqueous solutions

Temperature Range / K	Pressure Range /bar	Salt concentration /wt%	References
309-424	15-268	10-35.69	[374]
323-423	150	3.53-18.16	[435]
328-375	68.9-206.8	0-34.76	[436]
298 - 308	1	2.2 - 33.8	[428]
373 - 423	47.92	0 - 43.7	[419]
298 - 358	47.92	4.3 - 27.4	[386]
358 -393	15 – 710	0 - 30.2	[380]
288.4	1	1.10-35.69	[424]
298	1	2.17 -20.33	[418]
318	20 - 160	10	[434]

The most comprehensive dataset was reported by Prutton et al. [380] in a wide range of $CaCl_2$ aqueous solution concentrations. Only three experimental datasets were found at elevated temperatures which were reported by Malinin et al. [419], Zhao et al. [435] and Tong et al. [374] except for the dataset reported by Prutton et al. [380], no solubility data were found at pressures higher than 380 bar.

Table 3.4 Available experimental data on solubility of CO_2 in KCl aqueous solutions

Temperature Range / K	Pressure Range /bar	Salt concentration wt%	References
297	10 -160	4.28-9.08	[412]
313-433	1-95	12.98-22.97	[441]
273 – 313	1	0.7 - 23	[437]
313-353	1-105	3.7– 7.5	[438]
318.15	20-160	10	[434]
323-423	150	3.59-25.12	[435]
288-298	1	2.90-7.58	[439]
298	1	1.47-6.94	[440]
298 - 308	1	2.9 - 23.4	[428]

Table 3.4 lists the experimental data found for CO_2-KCl aqueous solutions. Among the total 9 datasets, the datasets reported by Kamps et al. [441] and Zhao et al. [435] covers the elevated temperatures conditions. The solubility data reported by Markham et al. [437] and Yasunishi et al. [428] include wide concentrations of KCl aqueous solutions.

Table 3.5 Available experimental data on solubility of CO_2 in $MgCl_2$ aqueous solutions

Temperature Range / K	Pressure Range /bar	Salt concentration /wt%	References
308-424	12-350	8.69 -32.25	[374]
298	1	0 - 29.99	[442]
323-423	150	3.05 -16	[375]
288 - 318	1	0.9 – 27.1	[428]

Table 3.5 summarises the literature experimental data for CO_2 solubility in magnesium chloride aqueous systems. Tong et al. [374] reported the most comprehensive datasets of CO_2 solubilities in a wide range of salinity at a temperature range, from 308K to 424 K and pressures up to 350 bar. Recently Zhao et al. published a paper on the solubility of CO_2 in aqueous solutions of $CaCl_2$, $MgCl_2$, KCl and Na_2SO_4 at temperatures from 323 K to 423 K and 150 bar pressure [375].

In this work, the main aim is to cover a broad range of temperature, pressure, and salinity for CO_2 solubility measurements. To recognise the gaps in the literature, in terms of covered temperature and pressure ranges, the temperature and pressure ranges of each solubility dataset were presented graphically through Figure 3.1 to Figure 3.4 regardless of the salinity of the tested solution. As seen in Table 3.2 and Figure 3.1, Solubility of CO_2 in sodium chloride has been investigated extensively over a wide range of temperatures and pressures. However, at low temperatures i.e. T <10 °C the solubilities were reported at low pressures. Duan et al. [295] presented a thermodynamic model for the solubility of CO_2 in pure water and aqueous solutions of NaCl at pressure ranges from 1 to 2000 bar, ionic strength from 0 to 4.3 m and temperatures from 273 K to 533 K.

Duan model is capable of correlating the solubility of CO_2 with around 7% deviation from experimental data which is within the experimental data uncertainty [295]. However, because limited data are available at temperatures below 0 °C (the conditions of flow assurance applications concerns), the model is not suitable to use at mentioned conditions. To fill the gap, the solubility of CO_2 at -5 °C < T < 25 °C and -10 °C < T < 25 °C for 10 wt% and 20 wt% NaCl aqueous solutions respectively and pressures up to 200 bar (below hydrate dissociation pressure and freezing point of brine) were measured.

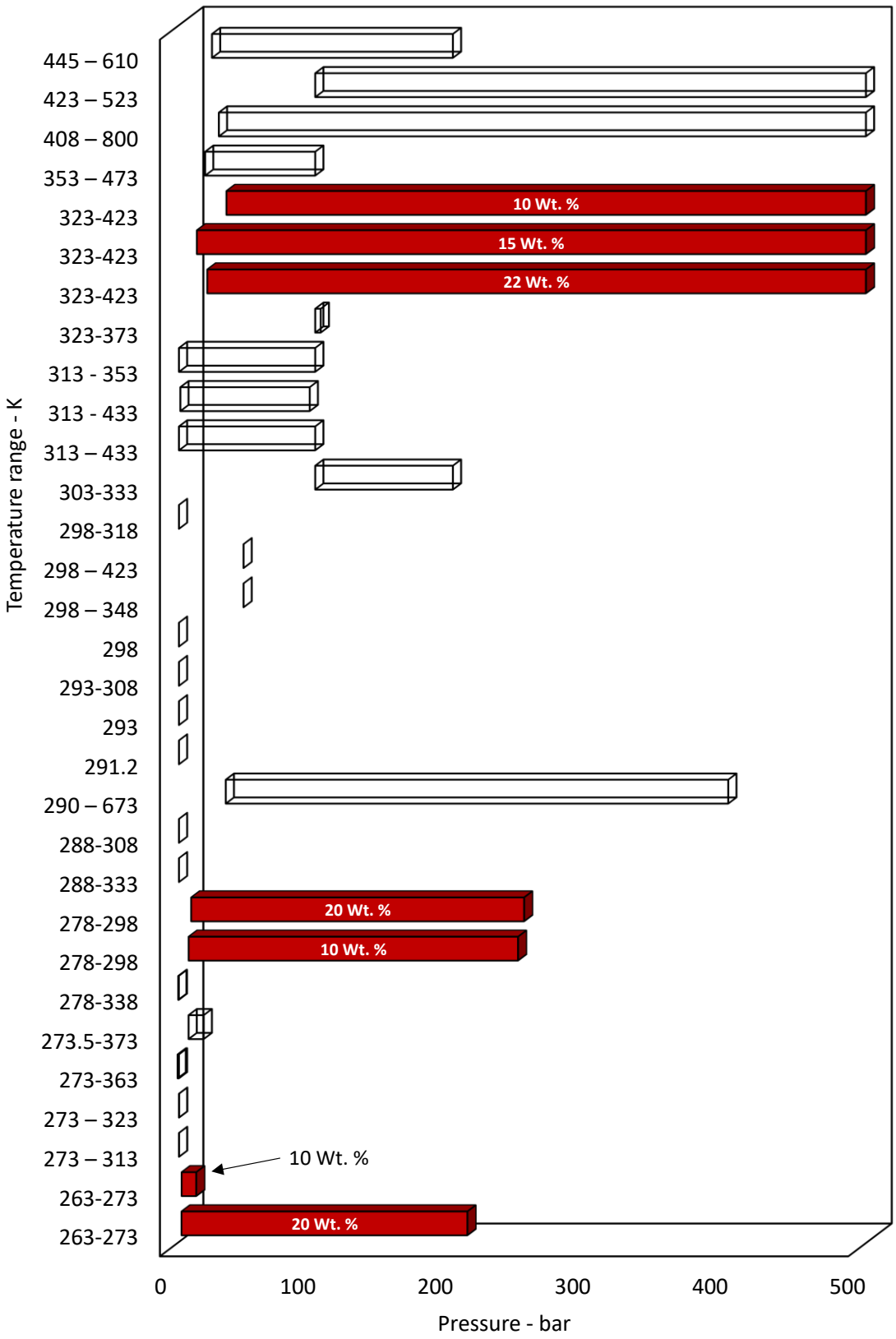

Figure 3.1 Bar chart of temperature and pressure ranges covered in this study (solid bars) and those reported in the literature for solubility of CO_2 in NaCl aqueous solutions

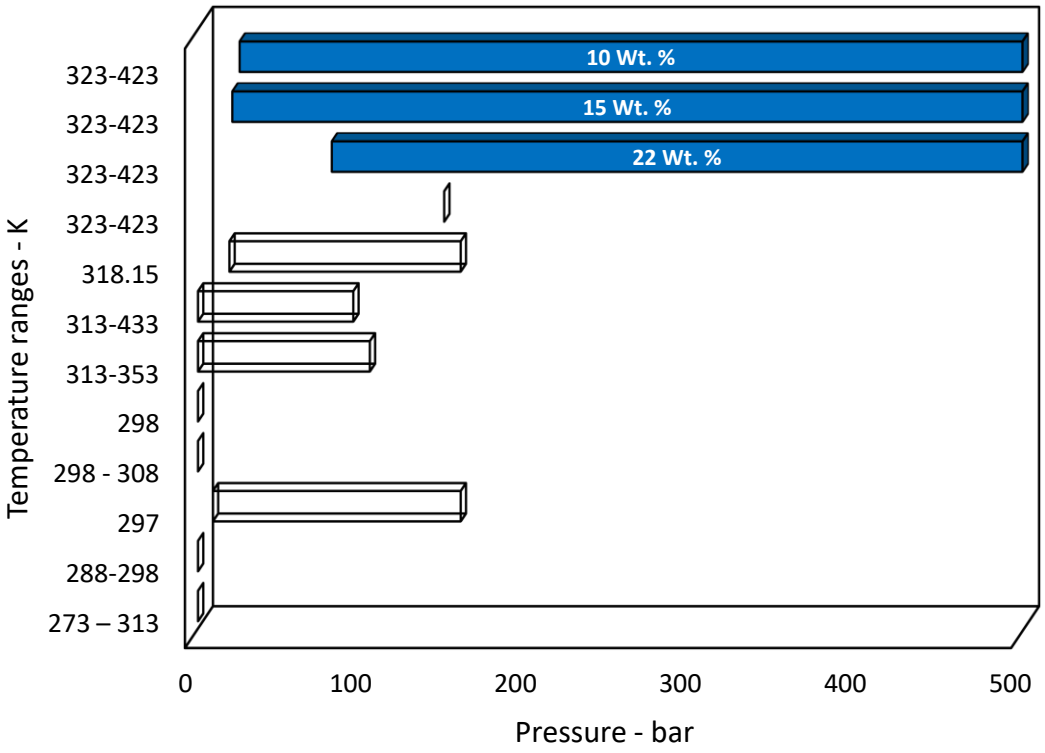

Figure 3.2 Bar chart of temperature and pressure ranges covered in this study (solid bars) and those reported the literature for solubility of CO_2 in KCl aqueous solutions

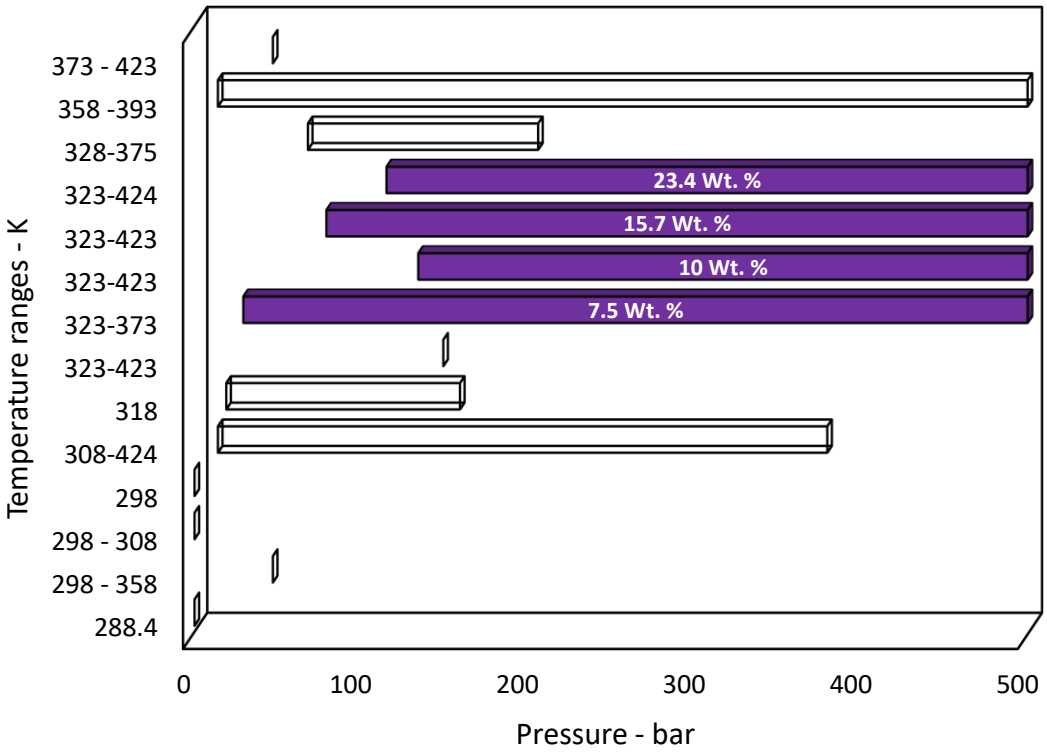

Figure 3.3 Bar chart of temperature and pressure ranges covered in this study (solid bars) and those reported in the literature for solubility of CO_2 in $CaCl_2$ aqueous solutions

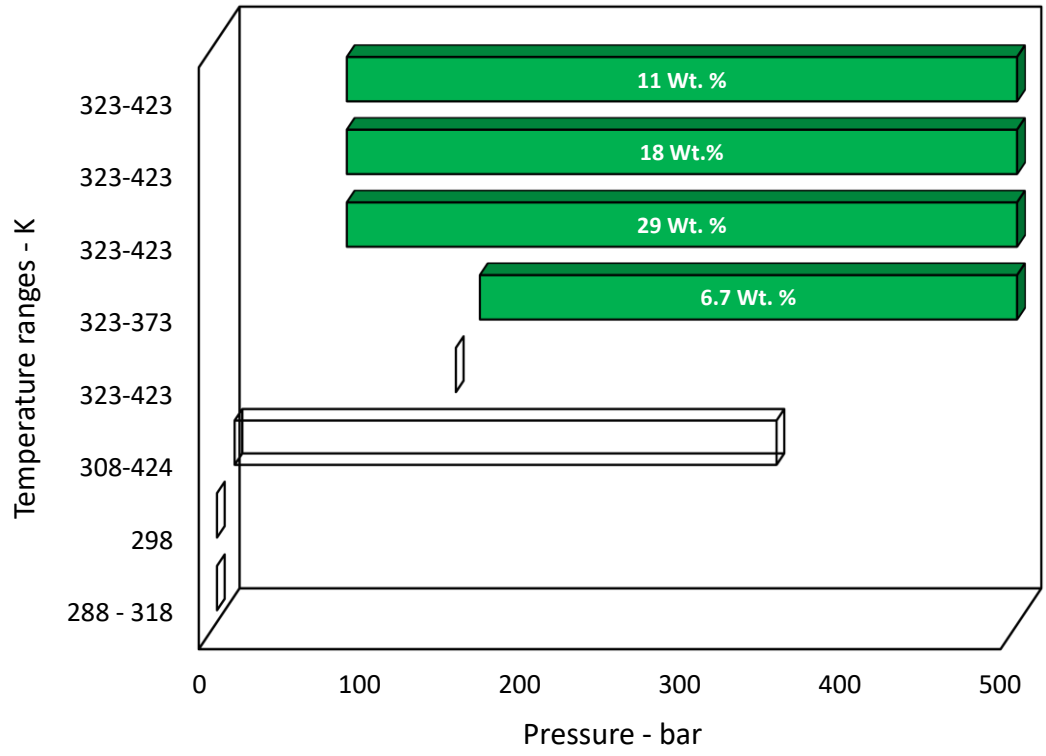

Figure 3.4 Bar chart of temperature and pressure ranges covered in this study (solid bars) and those reported in the literature for solubility of CO_2 in $MgCl_2$ aqueous solutions

3.2 Experimental Equipment, Materials, and Procedures

3.2.1 Materials

1- CO_2: High purity research grade CO_2 (99.995%), with less than 49 ppm of impurities, was purchased from Air Products.

2- NaCl: 0.99 pure sodium chloride was purchased from Fischer Chemistry.

3- KCl: 0.99 pure potassium chloride was purchased from Fischer Chemistry and ALDRICH.

4- $CaCl_2$: 0.99 pure calcium chloride di-hydrate was purchased from Fischer Chemistry.

5- $MgCl_2$: 0.99 pure magnesium chloride hexa-hydrate was purchased from Fischer Chemistry.

3.2.2 Experimental equipment

The solubility measurements in this work were performed using an equilibrium cell mounted on a rocking type rig based on the static-analytical method suggested by Chapoy et al. [443]. Following equipment constitute the experimental setup used in this work for

solubility measurements. A simple process and instrumentation diagram of the setup is shown in Figure 3.5.

1- *The cylindrical cell (R01):* The equilibrium cell used for the phase equilibria measurements was made from titanium, with an effective volume of 300 cm^3, an operating range of 50 – 200 °C and maximum operating pressure of 690 bar.

2- *Metallic jacket:* The R01 cell was placed inside a metallic jacket allowing the bath circulating fluid to envelop the R01 cell and keeping its temperature controlled. The R01 cell is sealed within the metallic jacket so that the valves of the cell can be accessible easily from outside of the jacket. The metallic jacket was insulated using polystyrene foams to prevent heat loss. The pipes connected to the jacket were covered using insulation foam.

3- *Bath (C01):* The temperature of the circulating fluid is controlled by a Julabo FP50 cryostat, for solubility measurements at low temperatures and Julabo MA GB Class III for solubility measurements at elevated temperatures. The baths can pump the fluids through the jacket at constant flow rate of 15 L/min and keeping the circulating fluid temperature within ±0.02 °C and ±0.1 °C respectively.

4- *The cylindrical cell (S01):* The cell S01 used for storing pure CO_2 at 500 bar to load the R01 rig and to keep the pressure of the cell R01 constant during sampling. The cell is made of titanium, with an effective volume of 600 cm^3, an operating range of 50 – 200 °C and rated to 690 bar.

5- *Gasometer (M01):* A manual gasometer provided by VINCI Technology was used to measure the volume of the released gas from the separator vessel at the specified temperature and pressure. The maximum capacity of gasometer is 4000 cm^3, with a volume, temperature and pressure accuracy of 0.1 cm^3, 0.1 °C and 0.01 psi respectively.

6- *Two phase separator (S02):* An Erlenmeyer flask equipped with a magnetic stirrer was used to collect the receiving fluids from the equilibrium cell R01. The flash vessel is sealed and connected to the bottom outlet of the equilibrium cell and the inlet of the gasometer. The stirrer was used to ensure separate the maximum amount of dissolved gas from the liquid. For measurements at 373 and 423 K

measurements, the Erlenmeyer flask is placed within a container filled with chilled water to keep the temperature of the flask low and prevent the vaporisation of the brine. Also, the line between the R01 cell and the separator is long enough to make sure that the fluids are cooled down on its way before entering the separator.

7- *Balance:* The mass of the sampled brine was measured using a Mettler Toledo balance with a capacity range of 0.5 – 3100 g, a resolution of 0.01 g and an accuracy of ±0.01 g.

8- *Temperature probe:* Two temperature monitoring systems were used to control and maintain the rig at a constant temperature. The temperature control system includes a Platinum-Resistant Thermometer (PRT) which measured the temperature of the jacket and the readings were logged using National Instrument LabVIEW 7.1. The temperature sensors were regularly calibrated using known fluid melting points with an accuracy of ± 0.025 °C. The cell pressure was measured using a strain gauge pressure transducer with an accuracy of ± 0.4 bars.

9- *Rocking system:* The cell R01 was placed on a pivotal axis, allowing a horizontal rocking motion, powered by a pneumatic rocking system, connected to a timer unit. The rocking system results in a turbulent movement of the liquid phase on 8.88 second intervals, ensuring complete mixing of fluids within the equilibrium cell and speeding up the equilibrium.

3.2.3 Procedures

- *Loading and experiments start up*

Fresh test brine was made using the demineralized water and precisely weighted salts for each experiment. The equilibrium cell was washed loaded with the fresh test brine from the top afterwards. Around 80% of the volume of the rig was filled with the brine to keep the slight raise in the brine concentration after as minimum as possible, after equilibrium. The air in the cell was then vacuumed using an Edwards IT20 vacuum pump from the valve V04. The pressurised cylinder S01 containing high purity CO_2 was then connected to the same valve, and the rig was initially pressurised after purging the connection line with high purity CO_2. Because the increasing or decreasing the cell temperature from the laboratory conditions results in an unknown greater or lower pressure than the desired

pressure; the cell was initially loaded to 5 bar to avoid releasing the gas from the cell to adjust the cell pressure to the test pressure. After initially pressurising the cell, all fittings and connections were tested for leakage using a foaming liquid. The temperature controlling system was then activated and after the temperature of the cell was stabilised at the desired temperature, the pressure of the cell was increased to a pressure around 20% higher than the test pressure to offset the pressure drop of the cell due to the dissolving of CO_2 in the aqueous phase. The system was allowed to rock for a while until the state of equilibrium i.e. when the dynamic curve of logged temperature and pressure become plateau, is reached. During equilibration, the temperature of the bath was controlled and logged. The cell pressure was also recorded using LabVIEW.

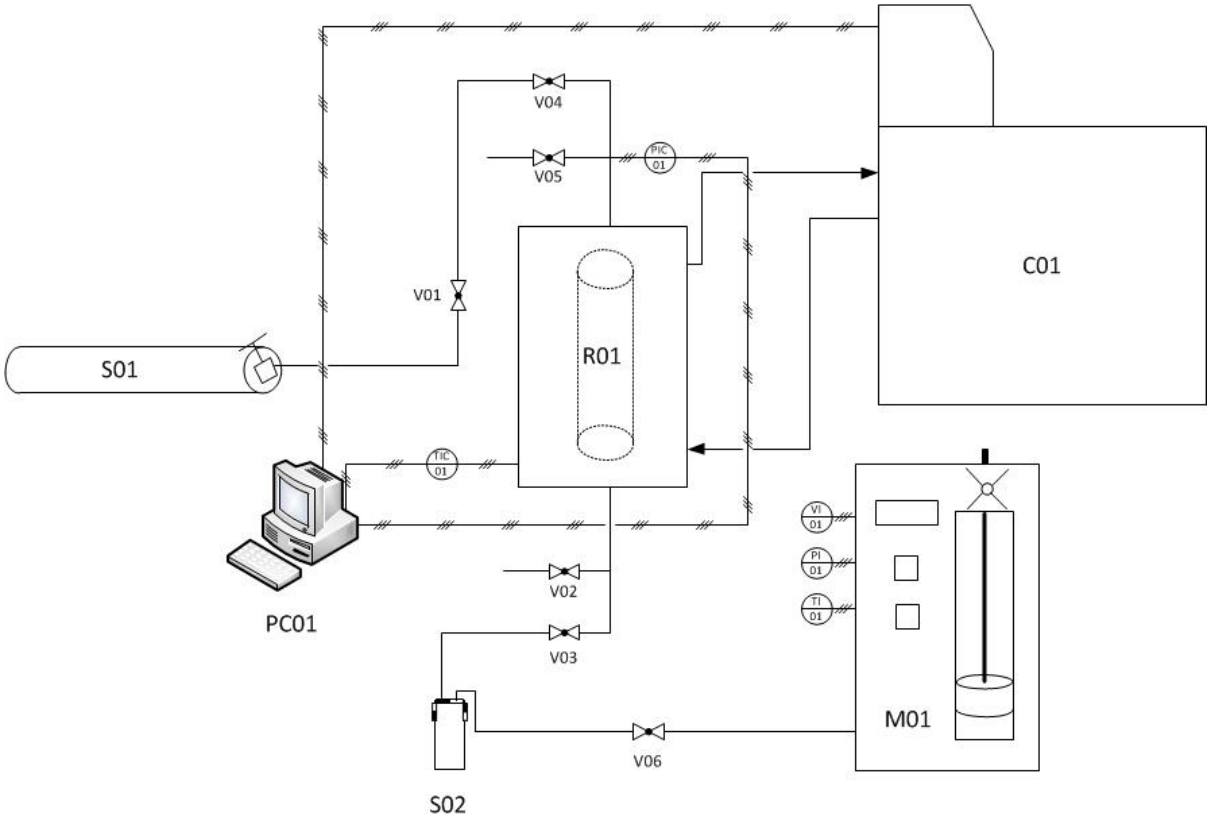

Figure 3.5 Diagram showing the rocking cell setup used for measuring the solubility of CO_2 in brine.

Measurement and sampling

To measure the solubility of CO_2 at the specified pressure and temperature, the rocking system was stopped and the separator vessel S02 was connected to valve V03 at the bottom of the cell R01 using a 250 mm stainless steel pipe with an internal diameter of 1.6 mm. The separator vessel was then connected to the gasometer and pressure of the gasometer was reset to the atmospheric pressure by opening the outlet valve. The initial

conditions of the system including lab pressure and the temperature, the weight of empty separator vessel, and the initial volume of the gasometer cylinder were recorded. To maintain the pressure of the equilibration cell constant during the sampling procedure, the pressurised the cell S01 was connected to the valve V04 and the connecting pipe was purged with CO_2. After ensuring that the pipe was swept completely with CO_2, the connection was tested with foaming liquid to check for any leakage.

The liquid is then sampled by gradually opening the bottom valve V03, and the top valve V04 with care at the same time to keep the pressure of the equilibrium cell constant during sampling. After enough liquid and gas were collected from the equilibrium cell, the sampling valve V03 and CO_2 injection valve V04 were shut. The stirrer was let to work for a few minutes to release all the gas from the sampled liquid. After a few minutes, the volume of the gasometer was adjusted using the manual handle to reach the exact atmospheric pressure that was recorded before sampling. The ultimate volume of the cell and the weight of the separator were then recorded. Having the amount of the CO_2 collected in the gasometer and also the weight of the aqueous phase, the CO_2 solubility in the test liquid at the equilibrium temperature and pressure of the cell was then calculated.

- *Uncertainty calculation*

To calculated the uncertainty of each measurement, we assumed that the measured solubility is a function of lab temperature, lab pressure and the weight of liquid and volume of the released CO_2. Hence, the uncertainties were calculated using the following general formula:

$$Uncertainty = \sqrt{\left(\frac{\partial f}{\partial x}\right)^2 \Delta x^2 + \left(\frac{\partial f}{\partial y}\right)^2 \Delta y^2 + \left(\frac{\partial f}{\partial z}\right)^2 \Delta z^2 + \cdots} \qquad Eq.3.1$$

After each solubility measurements, the volume of the released CO_2 from the liquid at lab temperature and pressure, the weight of sampled liquid is known. The number of moles of CO_2 was calculated using the experimental density of CO_2 at lab conditions and the weight of liquid was measured using a balance with 0.01 g precision. For calculating the error associated with the calculation of released CO_2 number of moles, we assume that the CO_2 at lab conditions follow the ideal gas behaviour and the density can be calculated using the ideal gas equation.

$$\rho = \frac{P}{ZRT} \qquad \textit{Eq.3.2}$$

Using the ideal gas equation, and having the error of pressure gauge and temperature probe of the gasometer, the error associated with the released CO_2 number of moles calculation was calculated using the equation Eq.3.1. The CO_2 mole fraction was then calculated using the definition of fraction which is:

$$x_{CO_2} = \frac{n_{CO_2}}{n_{CO_2} + n_{liquid}} \qquad \textit{Eq. 3.3}$$

3.3 Experimental Results

3.3.1 Solubility of CO_2 in demineralised water

The solubility measurement results are presented in this section. In this dissertation, the CO_2 solubility in the aqueous phase is expressed as the mole fraction of CO_2 in the salt-free aqueous phase. To check whether the experimental setup used and the measurement procedure followed, are reliable for solubility measurements, the solubility of CO_2 in demineralised water was measured at 50 °C and 100 °C. The experimental results were then compared to the PC-SAFT and the CPA models which were adjusted to literature data in Chapter 2. Table 3.6 summarises the measured solubilities and model calculations for CO_2 solubility in pure water at 50 and 100 °C. Figure 3.6 and Figure 3.7 graphically compare the model calculation, literature data and measured CO_2 solubility in pure water at 50 °C and 100 °C respectively. As can be seen, excellent agreements were found between the experimental results, literature and model calculations indicating that the method used for solubility measurements is suitable over the investigated temperature and pressure ranges.

Table 3.6 Measured and calculated solubility of CO_2 in distilled water.

P bara	Measured solubility	Uncertainty	Model Calculation CPA	PC-SAFT	Deviation CPA	PC-SAFT
T = 50 °C						
78.76	0.0180	0.0002	0.0174	0.0185	2.97%	3.19%
208.14	0.0232	0.0002	0.0234	0.0237	0.76%	2.01%
398.55	0.0257	0.0002	0.0269	0.0270	4.52%	5.02%
524.14	0.0276	0.0002	0.0285	0.0287	3.15%	3.97%
AAD %					2.85%	3.55%
T = 100 °C						
80.34	0.0120	0.0001	0.0108	0.0118	10.51%	2.19%
81.03	0.0122	0.0001	0.0108	0.0118	11.32%	3.10%
175.86	0.0185	0.0002	0.0180	0.0188	2.56%	1.81%
400.00	0.0243	0.0003	0.0250	0.0253	3.10%	4.15%
AAD %					6.87%	2.81%

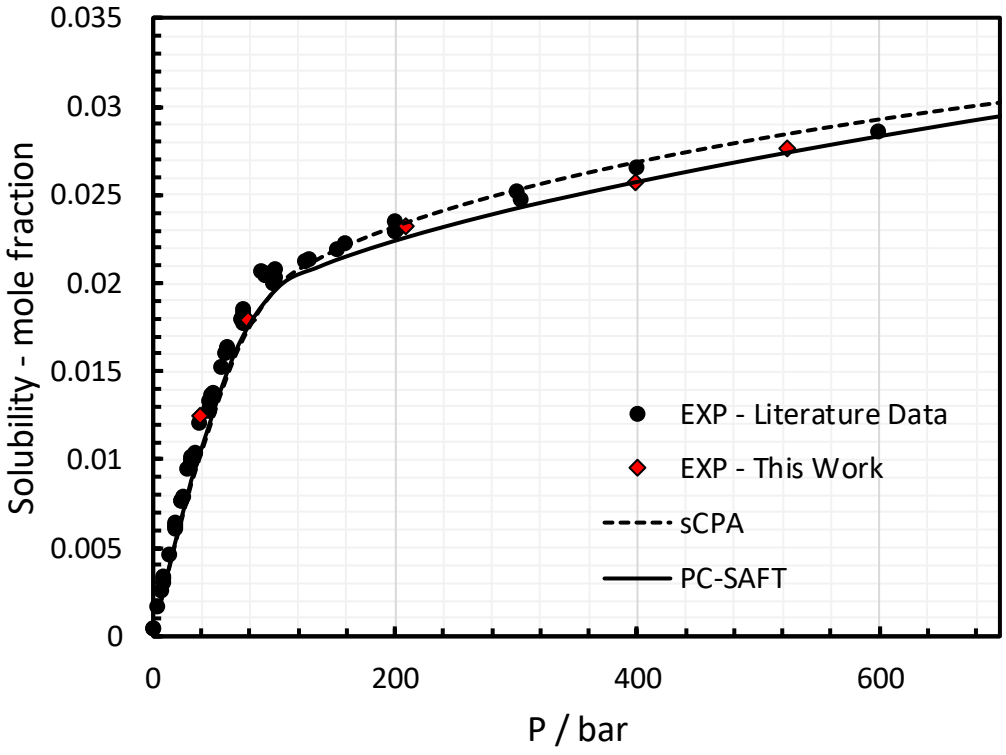

Figure 3.6 Comparison of measured CO_2 solubility in distilled water at 50 °C with literature data and model calculations (literature data taken from: [34], [298], [338], [377], [379], [384], [389], [391], [444]**)**

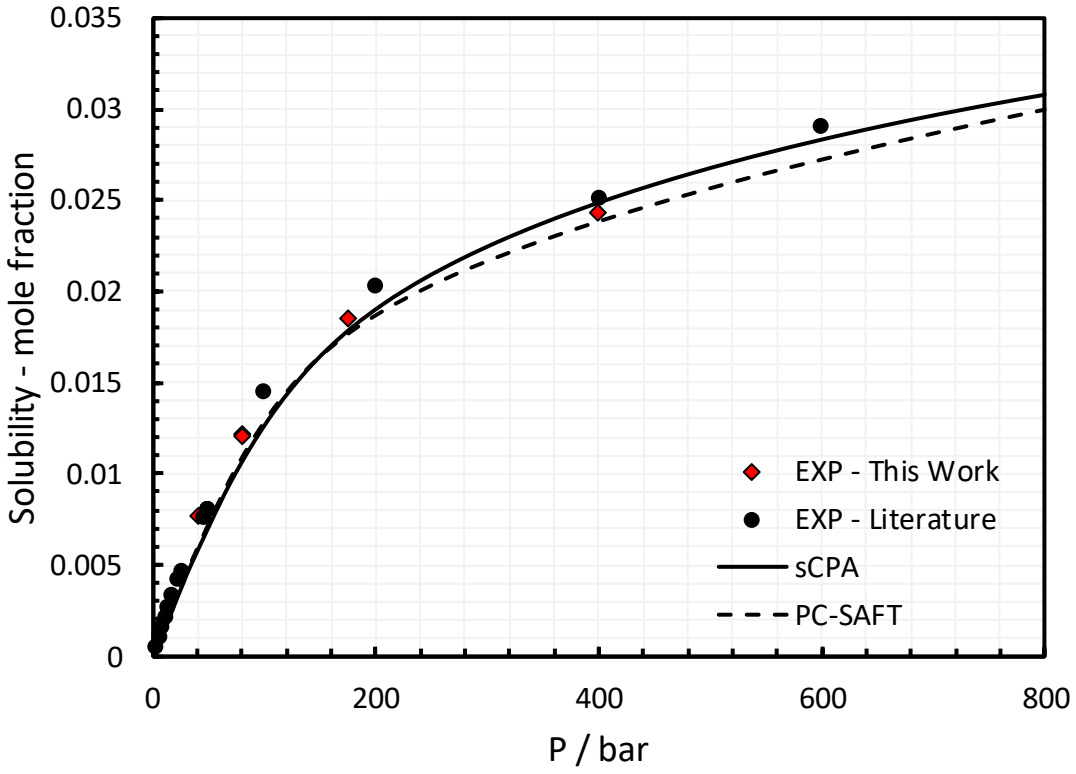

Figure 3.7 Comparison of measured CO_2 solubility in distilled water at 100 °C with literature data and model calculations (literature data taken from: [385], [388], [389], [445] **)**

3.3.2. Solubility of CO_2 in NaCl aqueous solutions at low temperatures (T≤ 25 °C)

In this section, the results of CO_2 solubility measurements in NaCl aqueous solutions are presented. All the measurements were performed at outside the hydrate stability zone of the systems (see Figure 3.8 and Figure 3.9, the test conditions versus the hydrate phase boundary of the CO_2/NaCl aqueous solutions).

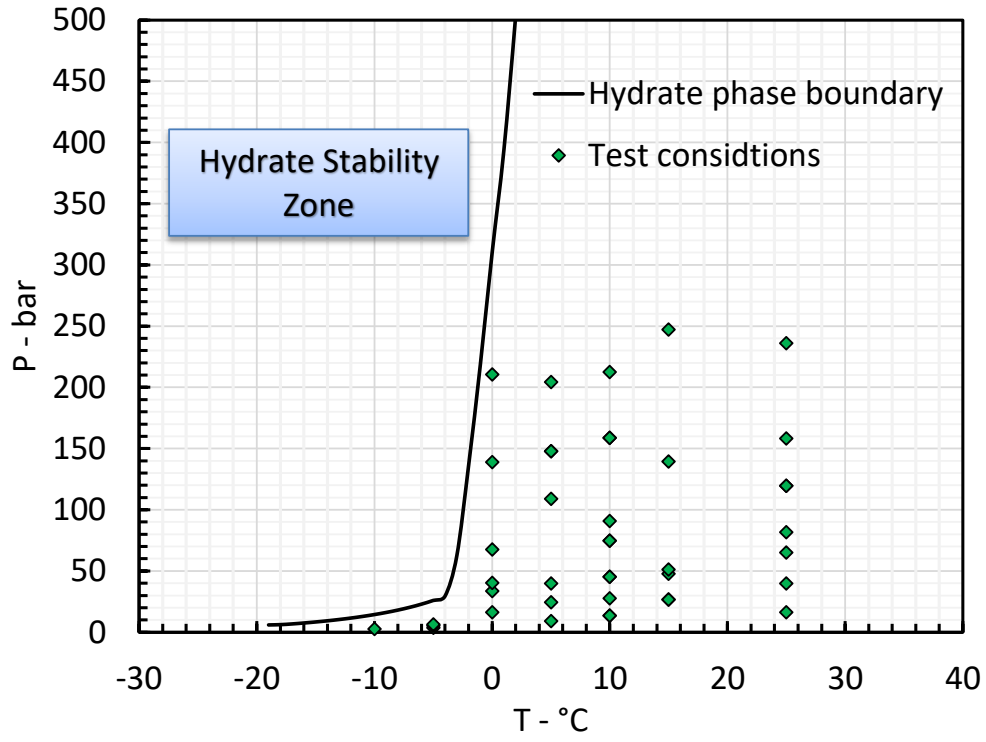

Figure 3.8 Hydrate phase boundary of CO_2 - 20 wt% brine systems and solubility measurement conditions

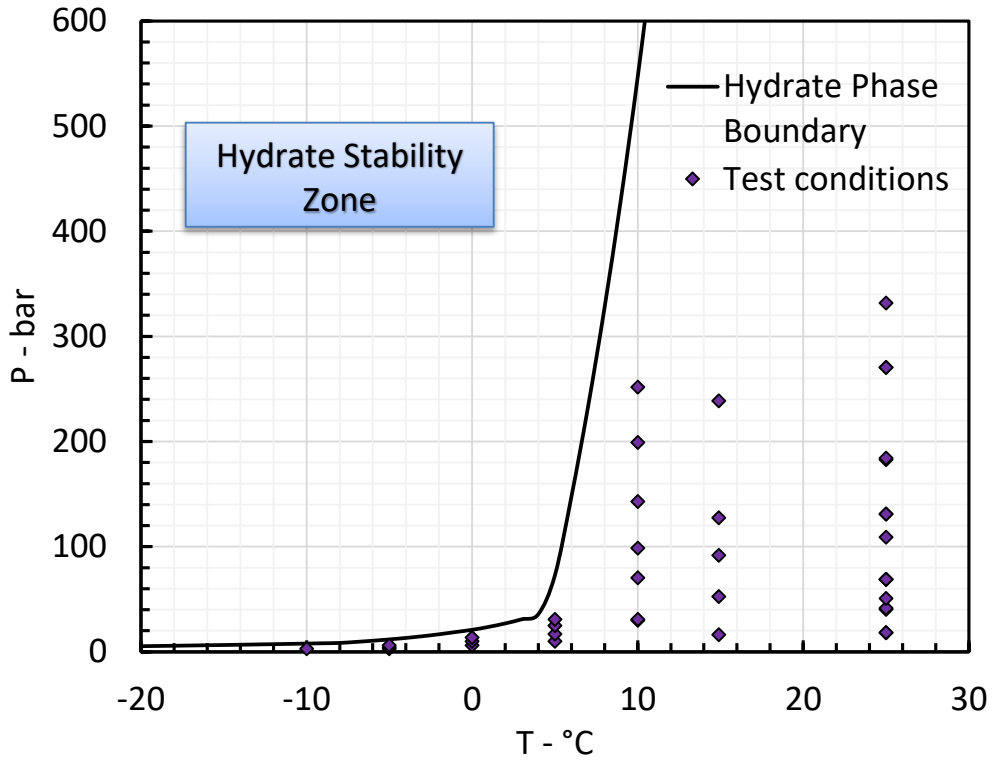

Figure 3.9 Hydrate phase boundary of CO_2 - 10 wt% brine systems and solubility measurement conditions

To validate the experimental results, the CPA and the PC-SAFT models were tuned to the solubility data obtained in this study as they had been measured over a broad range of temperature and salinity, especially at low temperatures (T < 25 °C). The model calculations were then compared to the Duan model predictions.

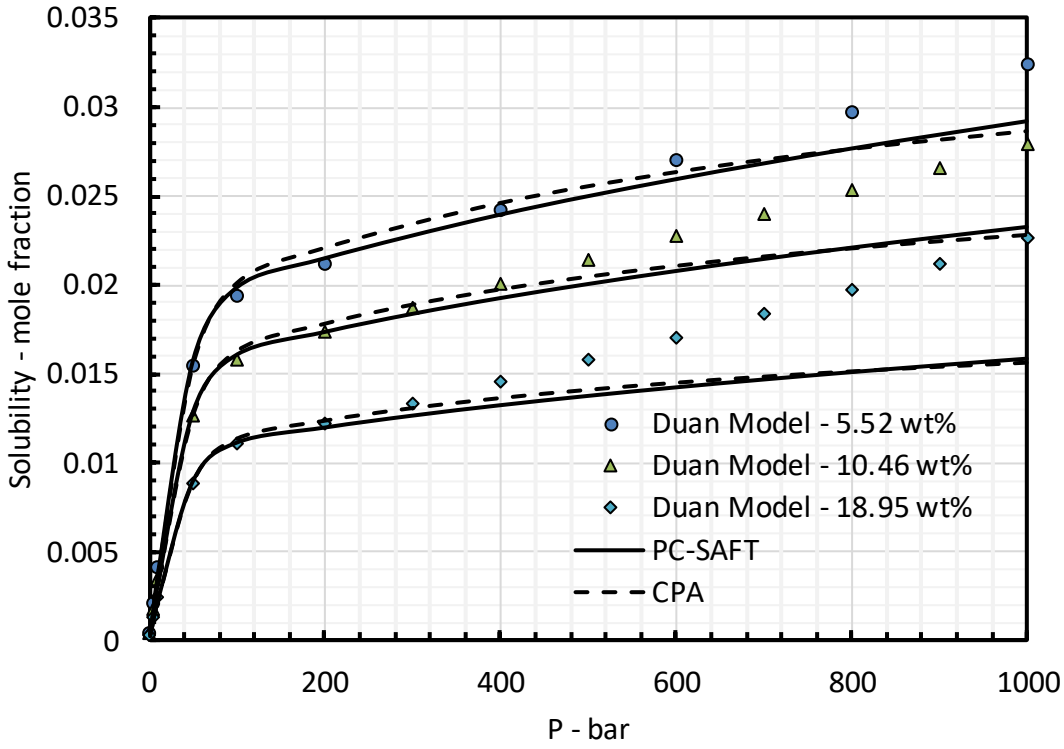

Figure 3.10 Calculated solubility of CO_2 in different concentrations of NaCl aqueous solutions at 303.15 K and pressures up to 1000 bar using the PC-SAFT and the Duan [295] **models**

Figure 3.10 to Figure 3.12 illustrate the calculated CO_2 solubility in various concentrations of NaCl aqueous solutions at 303.15, 363.15 and 423.15 K respectively. As shown in Figure 3.11 and Figure 3.12 the calculated solubilities using the PC-SAFT and the CPA models are in good agreements with the Duan model in different salinities. However as displayed in Figure 3.10, the calculated solubilities using the PC-SAFT and the CPA EoSs deviate considerably at 303.15 K and pressure more than 200 bar. It is suggested that the performances of the PC-SAFT and the CPA models are more accurate and closer to the behaviour of the system at these conditions as the models were tuned to the experimental data at a broader range of temperature and pressure, while the experimental data employed to adjust the Duan model were limited at low temperatures and high pressures.

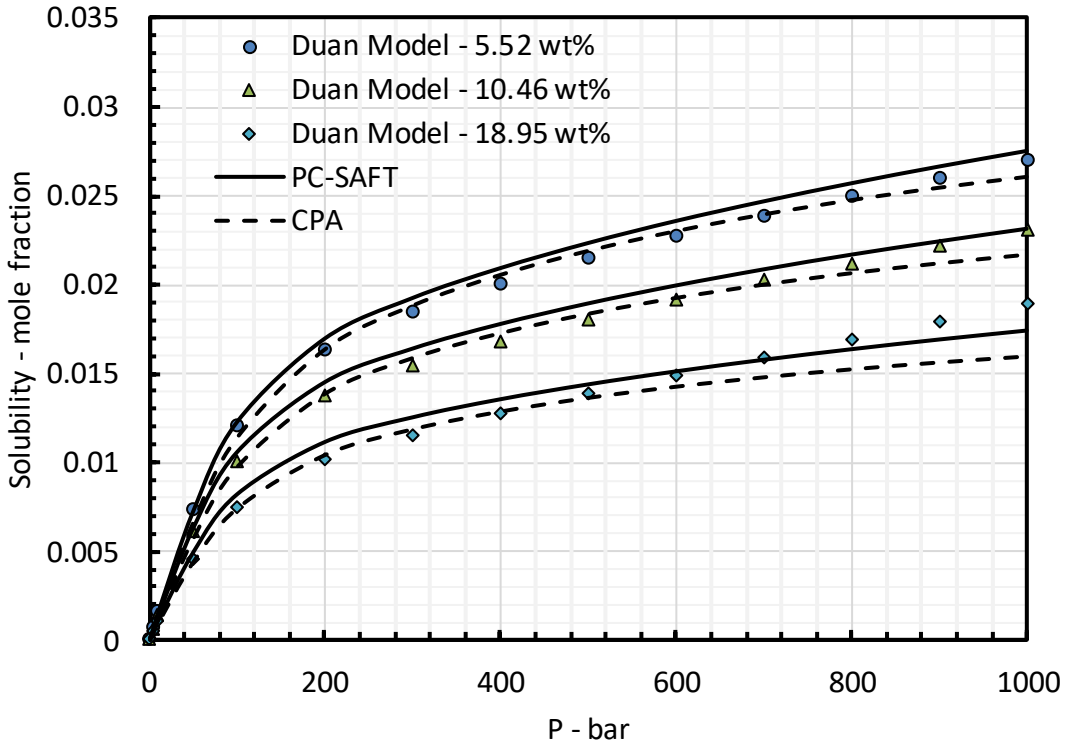

Figure 3.11 Calculated solubility of CO_2 in different concentrations of NaCl aqueous solutions at 363.15 K and pressures up to 1000 bar using the PC-SAFT and the Duan [295] **models**

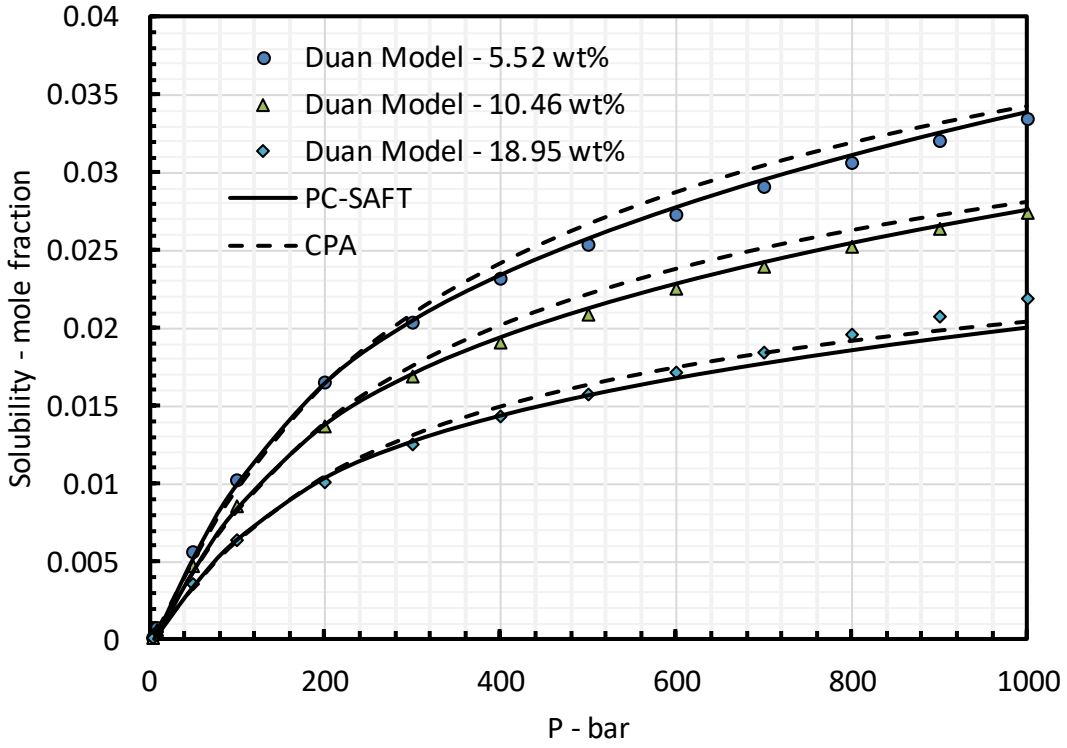

Figure 3.12 Calculated solubility of CO_2 in different concentrations of NaCl aqueous solutions at 423.15 K and pressures up to 1000 bar using the PC-SAFT and the Duan [295] **models**

Experimental results of CO_2 solubility in 10 wt% NaCl aqueous solution at low temperatures together with the model calculation are reported in Table 3.7, Table 3.8 and Table 3.9. Table 3.10, Table 3.11 and Table 3.12 also summarise measured and calculated solubilities in 20 wt% solution. Please note that the measured solubilities at below 278.15 K were not used to tune the CO_2/salt binary interaction parameters.

As reported in Table 3.7 and can be seen in Figure 3.13, model calculations and experimental results are quite closed at 25 °C for solubilities in 20 wt% aqueous solution while for the 10 wt% at pressures higher than 100 bar a deviation of around 8% is observed. Also as presented in Table 3.8, Table 3.10 and Table 3.11, very good agreements were found between models calculation and experimental solubility results in 10 and 20 wt% solutions results at 15 °C, 10 °C and 5 °C with around 5% or less deviation from the experimental data (see Figure 3.14 to Figure 3.16).

Table 3.7 Calculated and measured solubility of CO_2 in 10 wt% NaCl aqueous solutions at 25 °C

P	Measured solubility	Uncertainty	Model calculations			
bar			CPA	PC-SAFT	CPA Deviation	PC-SAFT Deviation
T = 25 °C						
17.93	0.0061	0.0001	0.0060	0.0063	0.88%	2.84%
18.34	0.0064	0.0001	0.0062	0.0064	4.18%	0.59%
40.34	0.0122	0.0001	0.0121	0.0125	0.29%	2.63%
41.52	0.0121	0.0001	0.0124	0.0128	2.40%	5.36%
50.62	0.0136	0.0001	0.0143	0.0147	5.08%	7.91%
68.97	0.0164	0.0002	0.0165	0.0167	0.68%	1.60%
68.97	0.0161	0.0001	0.0165	0.0167	2.65%	3.58%
68.97	0.0158	0.0001	0.0165	0.0167	4.73%	5.69%
108.90	0.0168	0.0002	0.0174	0.0173	3.57%	3.24%
131.03	0.0168	0.0002	0.0177	0.0176	5.67%	4.97%
131.03	0.0169	0.0002	0.0177	0.0176	5.04%	4.35%
182.76	0.0170	0.0002	0.0184	0.0182	8.55%	7.34%
184.14	0.0170	0.0002	0.0185	0.0182	8.64%	7.42%
270.34	0.0179	0.0002	0.0194	0.0192	8.19%	6.77%
270.34	0.0177	0.0002	0.0194	0.0192	9.75%	8.31%
331.79	0.0182	0.0002	0.0200	0.0197	9.97%	8.63%
AAD %					5.02%	5.08%

Table 3.8 Calculated and measured solubility of CO_2 in 10 wt% NaCl aqueous solutions at 14.9°C, 10 °C and 5 °C

P bar	Measured solubility	Uncertainty	Model calculations CPA	PC-SAFT	Deviation CPA	Deviation PC-SAFT
T = 14.9 °C						
16.21	0.0072	0.0001	0.0071	0.0074	1.09%	3.50%
52.41	0.0177	0.0002	0.0181	0.0190	2.31%	7.50%
91.72	0.0180	0.0002	0.0188	0.0190	4.35%	5.43%
127.59	0.0192	0.0002	0.0193	0.0194	0.59%	1.21%
238.76	0.0193	0.0002	0.0206	0.0207	6.73%	6.99%
AAD %					3.01%	4.93%
T = 10 °C						
30.00	0.0136	0.0002	0.0141	0.0145	3.71%	6.65%
30.90	0.0161	0.0002	0.0145	0.0149	10.25%	7.73%
70.34	0.0185	0.0001	0.0196	0.0197	6.13%	6.72%
98.62	0.0186	0.0001	0.0201	0.0201	7.60%	7.80%
142.97	0.0200	0.0001	0.0207	0.0206	3.55%	3.39%
198.97	0.0205	0.0001	0.0213	0.0213	4.34%	4.02%
251.72	0.0213	0.0001	0.0219	0.0218	2.82%	2.53%
AAD %					5.49%	5.55%
T = 5 °C						
9.93	0.0063	0.0001	0.0061	0.0062	2.90%	1.22%
16.83	0.0103	0.0001	0.0101	0.0102	2.52%	1.40%
24.83	0.0147	0.0001	0.0142	0.0143	3.42%	2.82%
30.90	0.0161	0.0001	0.0170	0.0171	5.81%	6.13%
AAD %					3.66%	2.89%

Table 3.9 Calculated and measured solubility of CO_2 in 10 wt% NaCl aqueous solutions at 0 °C, -5 °C and -10 °C

P bar	Measured solubility	Uncertainty	Model Calculation CPA	PC-SAFT	Deviation CPA	Deviation PC-SAFT
T = 0 °C						
6.28	0.0050	0.0001	0.0047	0.0049	6.16%	3.16%
10.14	0.0078	0.0001	0.0075	0.0077	3.41%	0.58%
13.59	0.0102	0.0001	0.0099	0.0101	3.04%	0.52%
AAD %					4.20%	1.42%
T = -5 °C						
2.97	0.0030	0.0001	0.0028	0.0028	6.29%	8.44%
4.41	0.0046	0.0002	0.0042	0.0041	8.26%	10.50%
6.21	0.0061	0.0001	0.0058	0.0057	4.61%	7.09%
AAD %					6.39%	8.68%
T = -10 °C						
2.99	0.0035	0.0002	0.0037	0.0032	5.56%	6.15%

Table 3.10 Calculated and measured solubility of CO_2 in 20 wt% NaCl aqueous solutions at 25 °C and 15 °C

P bar	Measured solubility	Uncertainty	Model calculation		CPA Deviation	PC-SAFT Deviation
			CPA	PC-SAFT		
T = 25 °C						
16.21	0.0041	0.0001	0.0037	0.0038	9.34%	7.94%
39.79	0.0083	0.0001	0.0079	0.0080	4.47%	3.59%
64.97	0.0109	0.0001	0.0107	0.0108	2.22%	1.18%
81.72	0.0113	0.0001	0.0109	0.0108	3.10%	4.35%
119.66	0.0116	0.0001	0.0114	0.0111	1.73%	3.78%
119.66	0.0114	0.0001	0.0114	0.0111	0.33%	2.40%
158.28	0.0120	0.0001	0.0117	0.0114	2.38%	4.79%
236.07	0.0125	0.0001	0.0123	0.0119	2.06%	4.75%
AAD %					3.20%	4.10%
T = 15 °C						
26.62	0.0075	0.0001	0.0071	0.0072	4.58%	3.80%
26.62	0.0072	0.0001	0.0071	0.0072	0.67%	0.13%
47.66	0.0111	0.0001	0.0110	0.0110	0.65%	0.15%
51.17	0.0119	0.0001	0.0114	0.0115	3.95%	3.31%
139.31	0.0125	0.0001	0.0123	0.0120	1.72%	3.81%
247.31	0.0129	0.0001	0.0130	0.0127	1.08%	1.26%
AAD %					2.11%	2.08%

Table 3.11 Calculated and measured solubility of CO_2 in 20 wt% NaCl aqueous solutions at 10 °C and 5 °C

P bar	Measured solubility	Uncertainty	Model Calculation		Deviation	
			CPA	PC-SAFT	CPA	PC-SAFT
T = 10 °C						
13.66	0.0049	0.0001	0.0046	0.0045	8.05%	8.27%
13.66	0.0050	0.0001	0.0046	0.0045	9.17%	9.39%
27.66	0.0088	0.0001	0.0084	0.0083	4.73%	5.49%
45.24	0.0121	0.0001	0.0120	0.0119	0.61%	1.56%
45.24	0.0124	0.0001	0.0120	0.0119	3.40%	4.32%
74.62	0.0127	0.0001	0.0123	0.0120	3.39%	6.05%
74.62	0.0125	0.0001	0.0123	0.0120	1.68%	4.39%
90.90	0.0125	0.0001	0.0125	0.0121	0.05%	2.90%
158.62	0.0130	0.0001	0.0130	0.0126	0.11%	3.25%
158.62	0.0131	0.0001	0.0130	0.0126	0.63%	3.96%
212.41	0.0133	0.0001	0.0134	0.0129	0.42%	3.00%
AAD %					2.93%	4.78%
T = 5 °C						
9.0345	0.0041	0.0001	0.0036	0.0035	12.95%	15.41%
24.4828	0.0096	0.0001	0.0088	0.0085	7.48%	10.76%
39.8621	0.0128	0.0001	0.0127	0.0122	0.52%	4.31%
108.9655	0.0137	0.0001	0.0134	0.0126	2.52%	7.91%
147.9310	0.0140	0.0001	0.0137	0.0129	2.32%	7.85%
147.9310	0.0140	0.0001	0.0137	0.0129	2.64%	8.15%
204.4138	0.0142	0.0001	0.0140	0.0133	0.77%	6.41%
AAD %					4.17%	8.69%

Table 3.12 Calculated and measured solubility of CO_2 in 20 wt% NaCl aqueous solutions at 0 °C, -5 °C and -10 °C

P bar	Measured solubility	Uncertainty	Model Calculation		CPA Deviation	PC-SAFT Deviation
			CPA	PC-SAFT		
T = 0 °C						
16.21	0.0075	0.0001	0.0072	0.0075	4.02%	1.05%
33.72	0.0137	0.0001	0.0131	0.0135	3.87%	1.30%
40.21	0.0139	0.0001	0.0135	0.0152	3.07%	8.67%
67.59	0.0139	0.0001	0.0138	0.0140	0.88%	0.79%
138.90	0.0146	0.0001	0.0143	0.0145	1.78%	0.43%
210.55	0.0152	0.0001	0.0148	0.0150	2.80%	1.43%
AAD %					2.74%	2.28%
T = -5 °C						
3.5172	0.0024	0.0001	0.0021	0.0021	12.70%	14.62%
5.2414	0.0032	0.0001	0.0031	0.0031	0.90%	3.14%
6.2759	0.0041	0.0001	0.0037	0.0037	9.04%	11.16%
AAD %					7.55%	9.64%
T = -10 °C						
2.7586	0.0024	0.0001	0.0022	0.0019	8.79%	18.74%

In general, a good agreement was found between experimental results and model predictions for all solubilities at 0 °C ≤ T ≤ 25 °C. However as reported in Table 3.9 and Table 3.12, measured solubilities differ from model calculations with higher AAD % at T< 0 °C in both brine concentrations which is because the models were tuned to the data range covering 0 °C ≤ T (see also Figure 3.18).

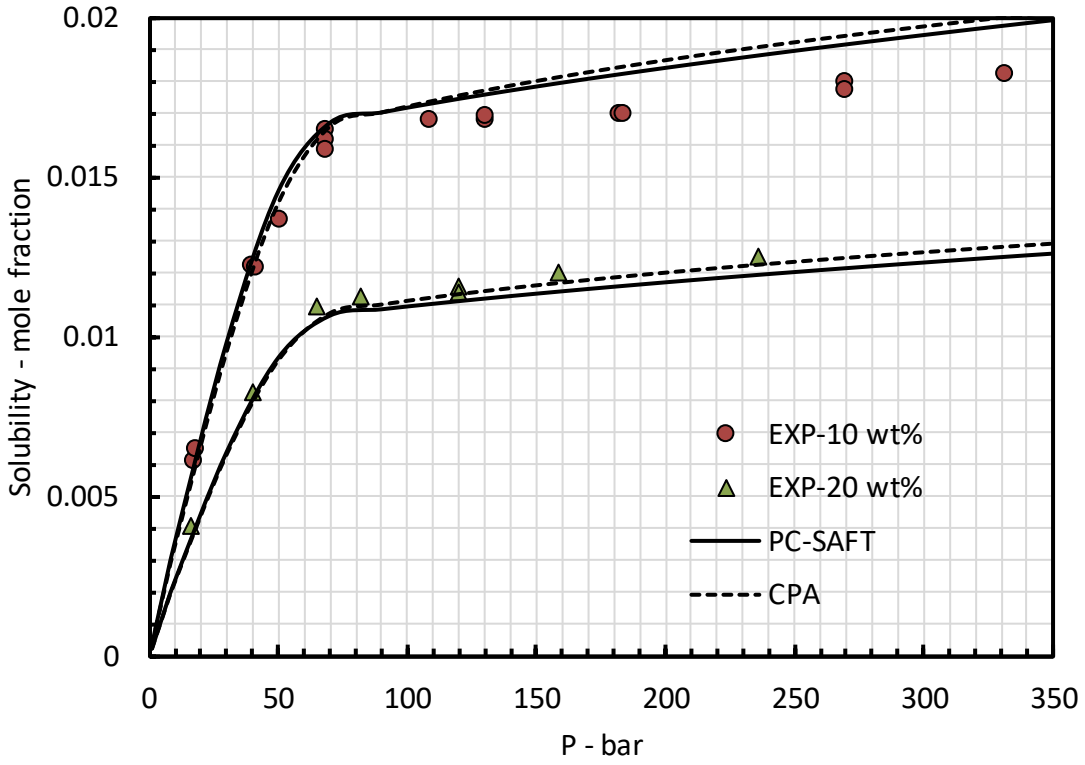

Figure 3.13 Comparison of experimental results of CO_2 solubility in 10 and 20 wt% NaCl aqueous solutions and model calculations using the CPA and the PC-SAFT equation of states at 25 °C.

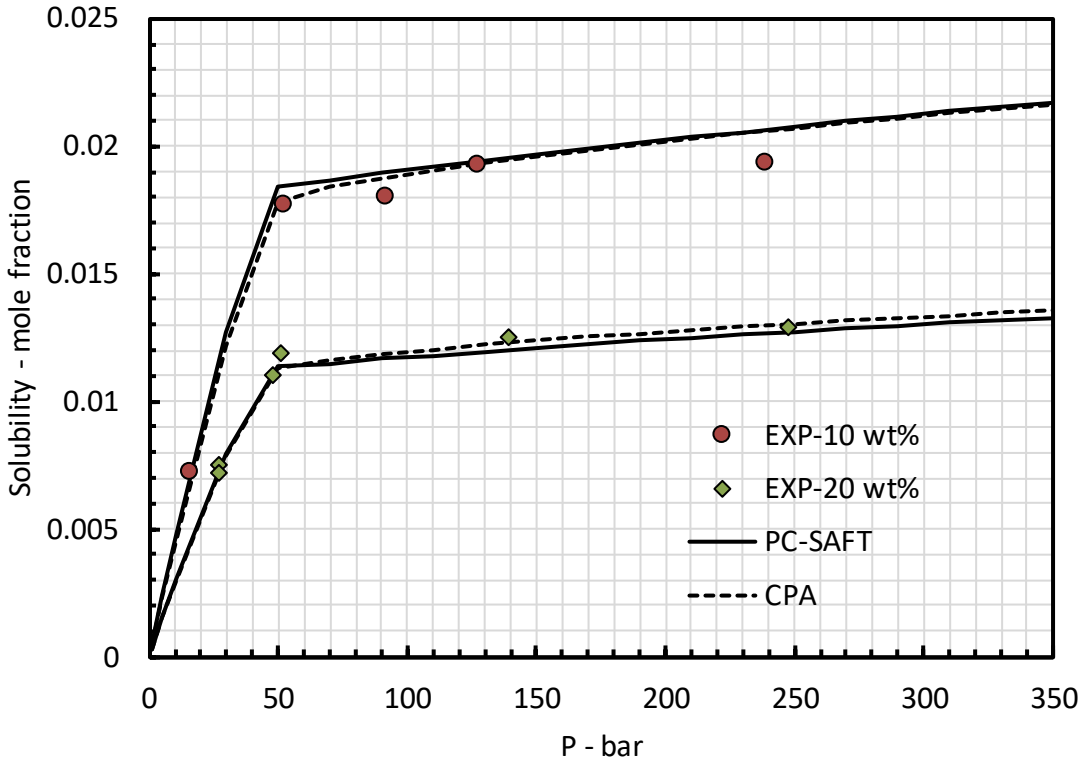

Figure 3.14 Comparison of experimental results of CO_2 solubility in 10 and 20 wt% NaCl aqueous solutions and model calculations using the CPA and the PC-SAFT equation of states at 14.9 °C.

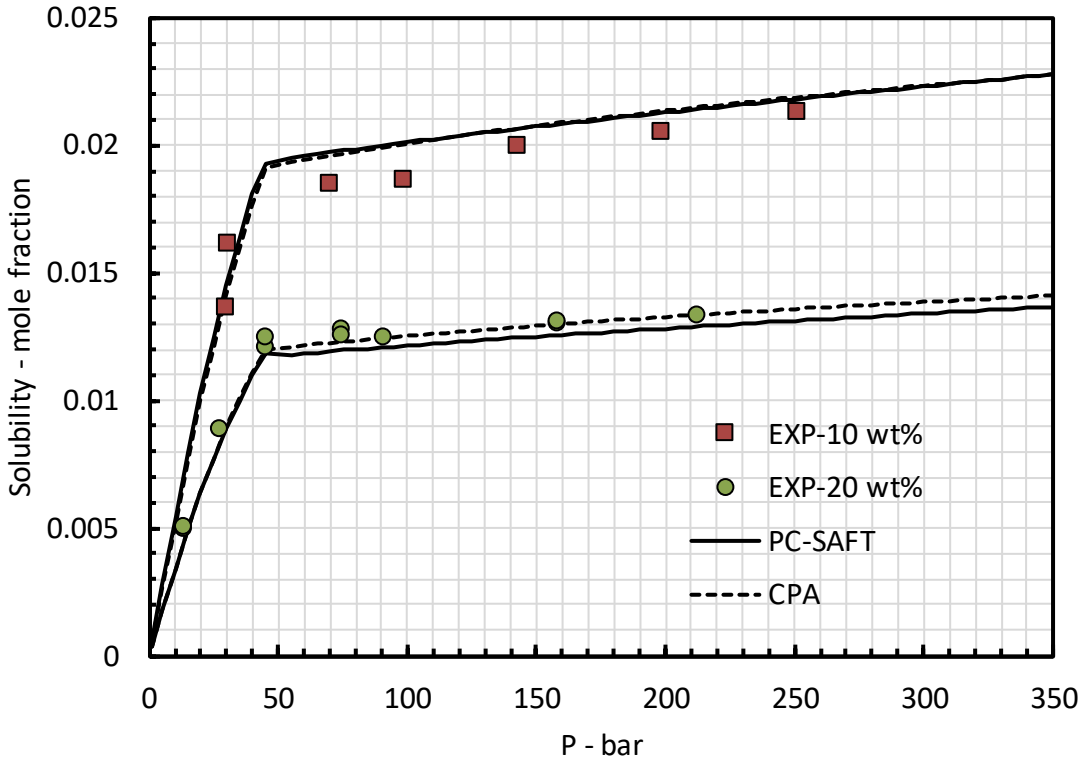

Figure 3.15 Comparison of experimental results of CO_2 solubility in 10 and 20 wt% NaCl aqueous solutions and model calculations using the CPA and the PC-SAFT equation of states at 10 °C.

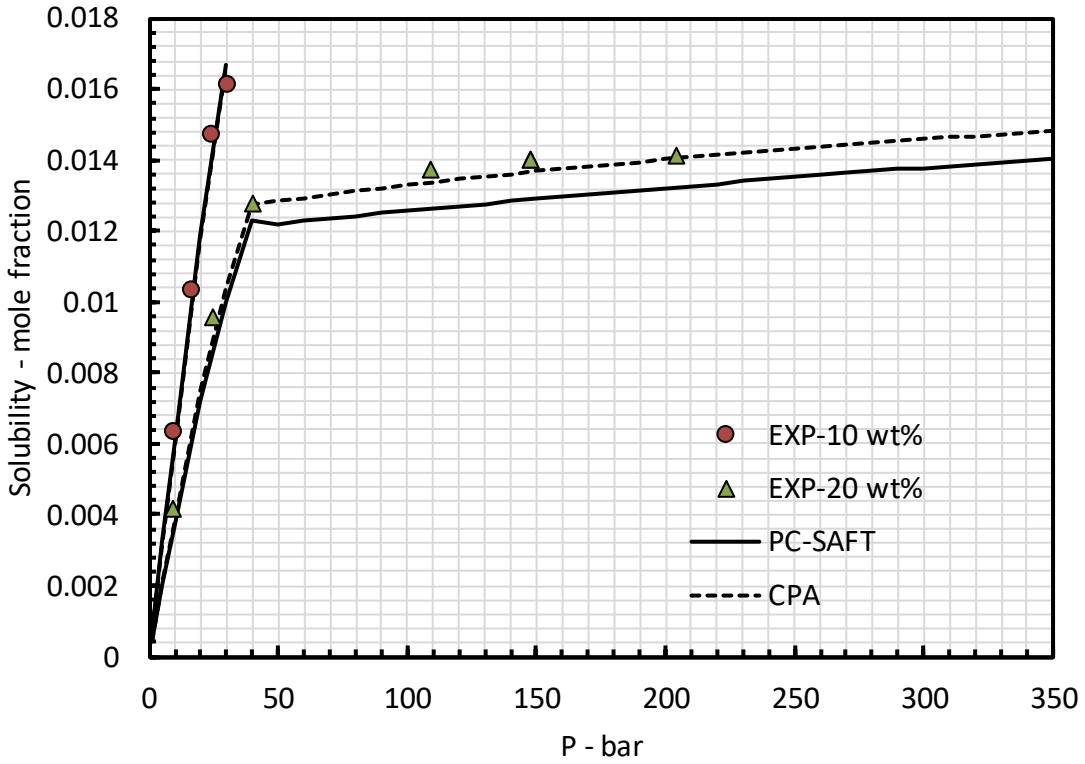

Figure 3.16 Comparison of experimental results of CO_2 solubility in 10 and 20 NaCl aqueous solutions and model calculations using the CPA and the PC-SAFT equation of states at 5 °C.

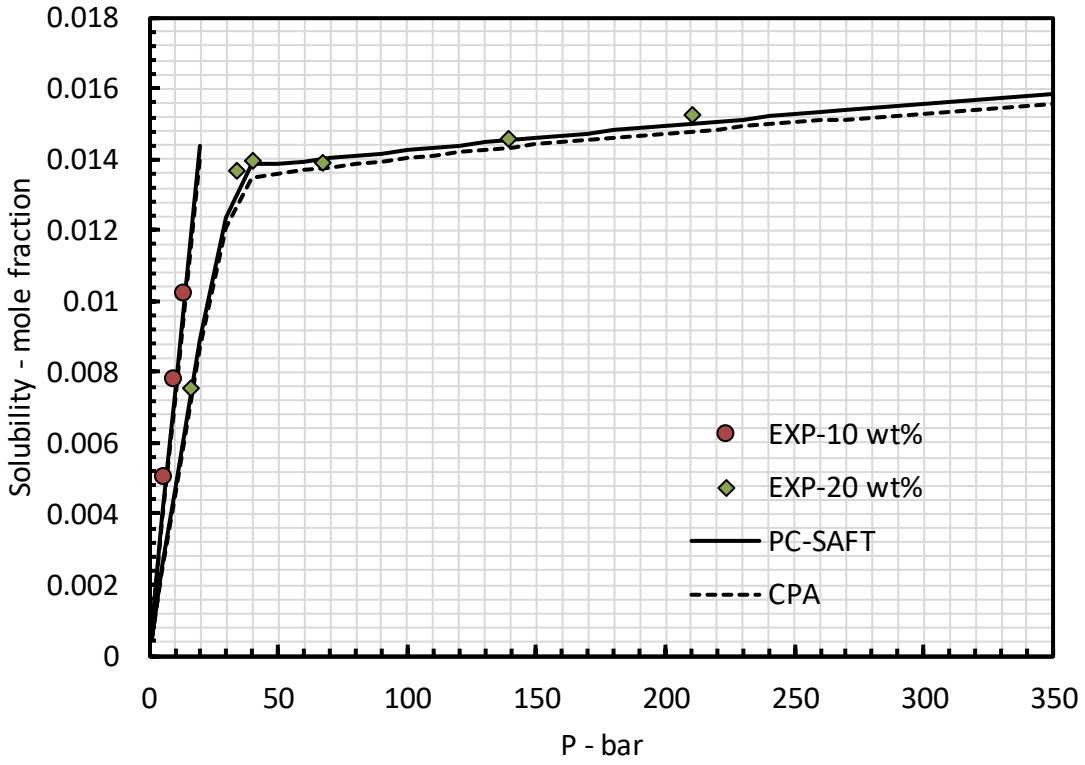

Figure 3.17 Comparison of experimental results of CO_2 solubility in 10 and 20 wt% NaCl aqueous solutions and model calculations using the CPA and the PC-SAFT equation of states at 0 °C.

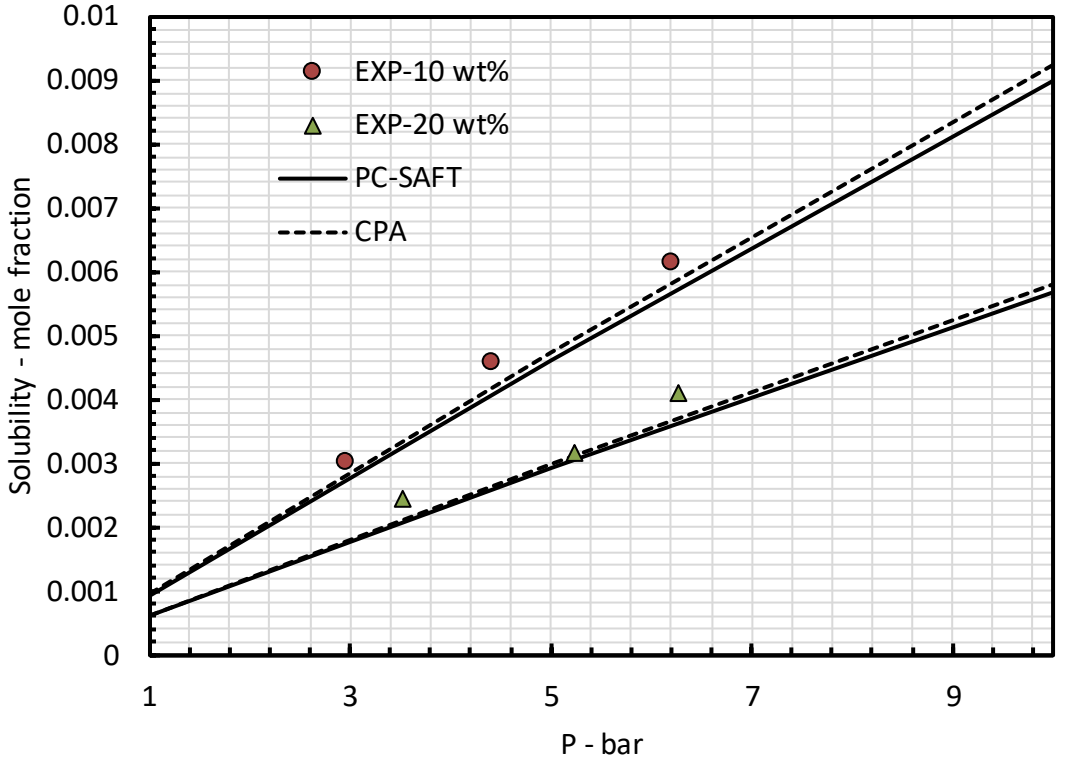

Figure 3.18 Comparison of experimental results of CO_2 solubility in 10 and 20 wt% NaCl aqueous solutions and model calculations using the CPA and the PC-SAFT equation of states at -5 °C.

3.3.2. Solubility of CO_2 in NaCl aqueous solutions at elevated temperatures

The experimental results and calculated CO_2 solubility in 10, 15 and 22 wt% NaCl aqueous solution at elevated temperatures, i.e. 50, 100 and 150 °C are reported in Table 3.13, Table 3.14 and Table 3.15. Both the PC-SAFT and the CPA models correlate the solubilities in 10, 15 and 22 wt% solutions at all test temperatures within an acceptable deviation from the model calculations. However, a considerable deviation from measured data is observed for solubility in 15 wt% solution at 50 °C and 27 bar and in 22 wt% solution at 150 °C and 229 bar.

Table 3.13 Calculated and measured solubility of CO_2 in 10 wt% NaCl aqueous solutions at 50 °C, 100 °C and 150 °C

P	Measured solubility		Model calculations			
bar		Uncertainty	CPA	PC-SAFT	CPA Deviation	PC-SAFT Deviation
T = 50 °C						
122.76	0.0134	0.0001	0.0144	0.0143	7.43%	6.78%
259.31	0.0163	0.0002	0.0167	0.0162	2.35%	0.41%
537.93	0.0198	0.0002	0.0192	0.0188	3.22%	5.32%
AAD %					4.33%	4.17%
T = 100 °C						
148.28	0.0122	0.0002	0.0121	0.0123	1.34%	0.82%
281.38	0.0158	0.0001	0.0159	0.0157	0.50%	0.44%
296.55	0.0158	0.0001	0.0162	0.0160	2.55%	1.45%
407.03	0.0176	0.0001	0.0179	0.0177	1.81%	0.24%
510.34	0.0177	0.0002	0.0192	0.0189	8.27%	6.77%
AAD %					3.28%	2.22%
T = 150 °C						
245.52	0.0158	0.0001	0.0160	0.0163	1.48%	3.30%
373.03	0.0191	0.0002	0.0199	0.0199	3.97%	3.93%
534.48	0.0218	0.0002	0.0232	0.0231	6.19%	5.76%
AAD %					3.88%	4.33%

Figure 3.19 to Figure 3.21 compare the model calculations and experimental results of CO_2 solubilities in NaCl aqueous solutions. As discussed before, the deviation of model calculations from measured solubilities is high at some pressures. As illustrated, experimental results are qualitatively consistent regarding the effect of brine salinity where the solubility of CO_2 is decreased with increasing the salinity of the solution. Also, the CPA and the PC-SAFT EoSs are appeared to perform quite similar in calculating the CO_2 solubilities within the experimental conditions.

Table 3.14 Calculated and measured solubility of CO_2 in 15 wt% NaCl aqueous solutions at 50 °C, 100 °C and 150 °C

P	Measured solubility		Model calculations			
bar		Uncertainty	CPA	PC-SAFT	CPA Deviation	PC-SAFT Deviation
T = 50 °C						
27.86	0.0055	0.0001	0.0046	0.0048	16.86%	14.00%
131.03	0.0112	0.0002	0.0120	0.0120	7.94%	7.38%
356.55	0.0145	0.0002	0.0146	0.0142	0.53%	1.84%
548.97	0.0172	0.0001	0.0158	0.0155	8.10%	9.59%
AAD %					8.36%	8.20%
T = 100 °C						
145.52	0.0113	0.0001	0.0102	0.0105	9.59%	6.47%
371.03	0.0150	0.0002	0.0147	0.0147	1.58%	1.68%
551.72	0.0169	0.0001	0.0165	0.0165	2.12%	1.94%
AAD %					4.43%	3.36%
T = 150 °C						
379.31	0.0166	0.0002	0.0168	0.0168	1.22%	1.01%
572.48	0.0199	0.0002	0.0198	0.0197	0.51%	0.89%
AAD %					0.86%	0.95%

Table 3.15 Calculated and measured solubility of CO_2 in 22 wt% NaCl aqueous solutions at 50 °C, 100 °C and 150 °C

P	Measured solubility		Model calculations			
bar		Uncertainty	CPA	PC-SAFT	CPA Deviation	PC-SAFT Deviation
T = 50 °C						
217.24	0.0105	0.0001	0.0101	0.0099	3.94%	5.48%
572.41	0.0118	0.0001	0.0120	0.0119	2.29%	1.34%
AAD %					3.11%	3.41%
T = 100 °C						
531.03	0.0129	0.0001	0.0128	0.0131	0.35%	1.60%
T = 150 °C						
229.66	0.0116	0.0001	0.0103	0.0104	11.03%	9.77%
409.66	0.0145	0.0002	0.0136	0.0135	6.14%	6.73%
544.83	0.0154	0.0002	0.0152	0.0151	1.50%	2.14%
AAD %					6.22%	6.21%

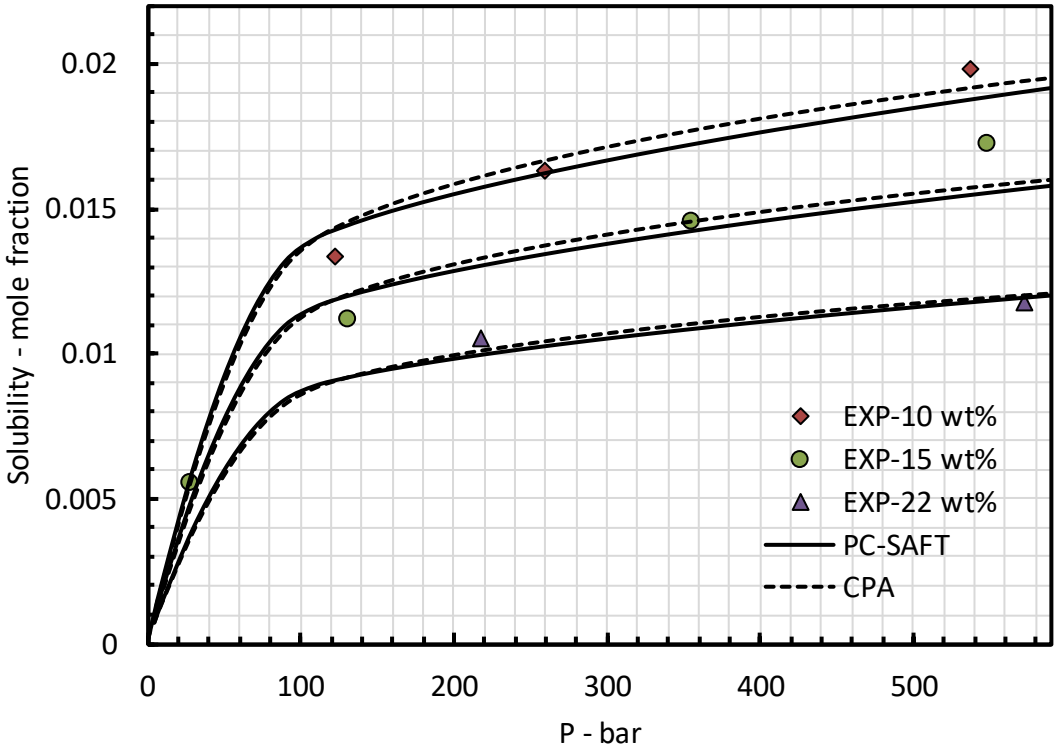

Figure 3.19 Comparison of experimental results of CO_2 solubility in 10, 15 and 22 wt% NaCl aqueous solutions and model calculations using the CPA and the PC-SAFT equation of states at 50 °C.

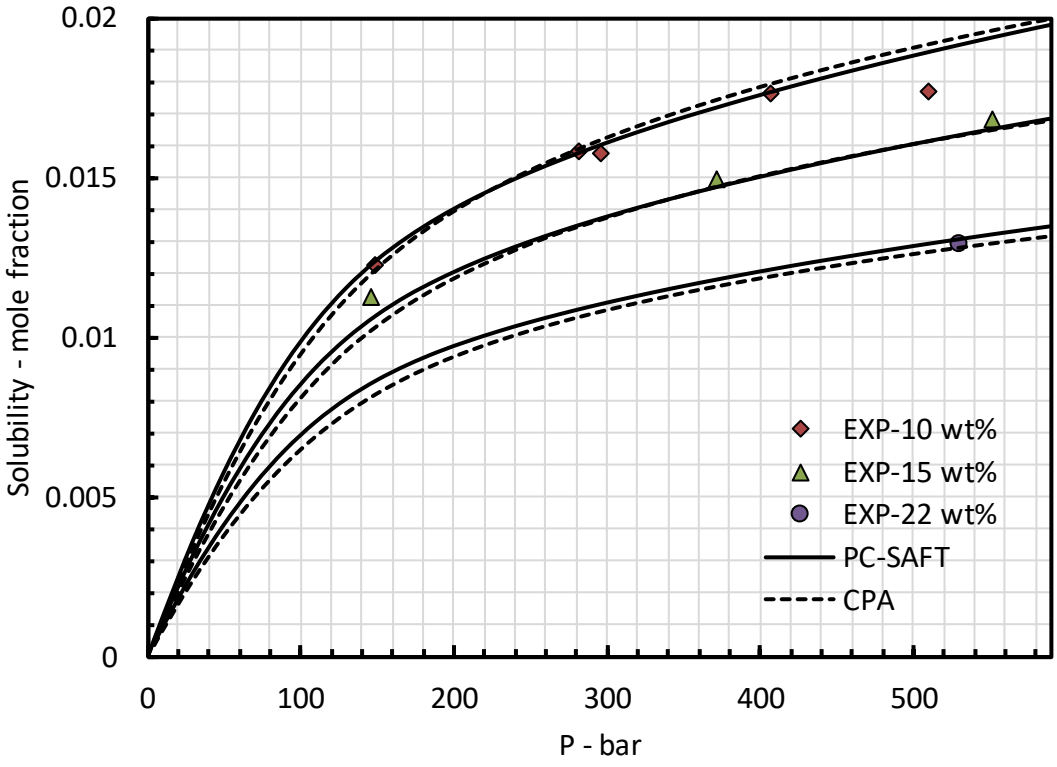

Figure 3.20 Comparison of experimental results of CO_2 solubility in 10, 15 and 22 wt% NaCl aqueous solutions and model calculations using the CPA and the PC-SAFT equation of states at 100 °C.

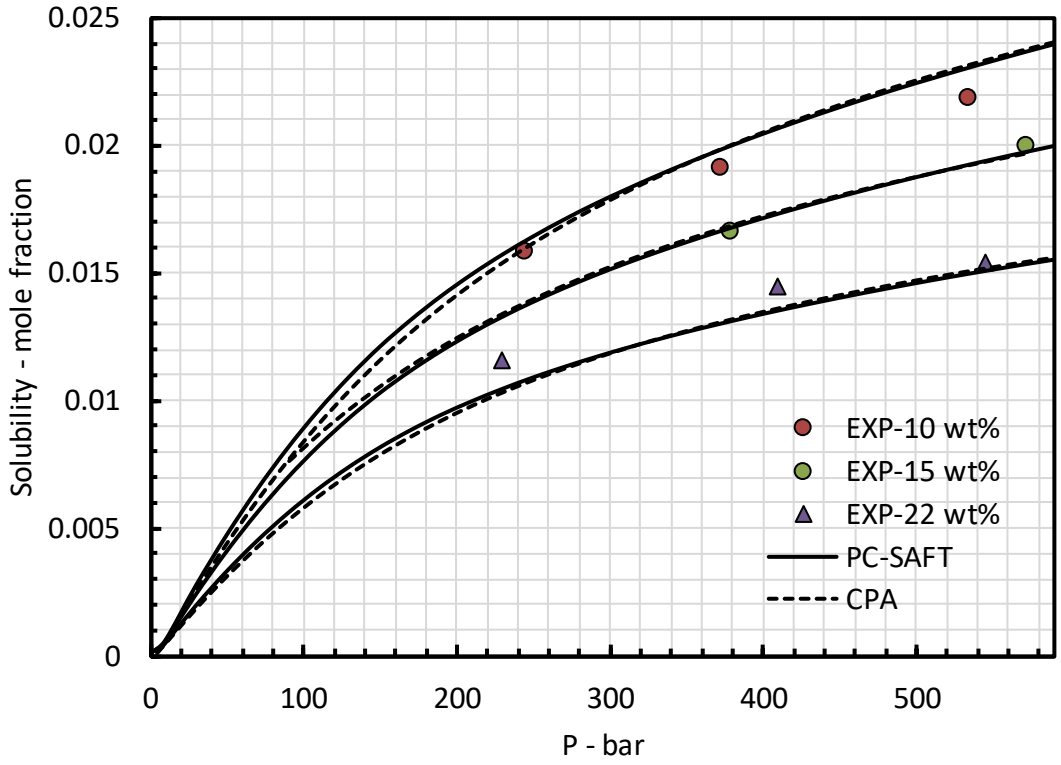

Figure 3.21 Comparison of experimental results of CO_2 solubility in 10, 15 and 22 wt% NaCl aqueous solutions and model calculations using the CPA and the PC-SAFT equation of states at 150 °C.

3.3.3. Solubility of CO_2 in KCl aqueous solutions at elevated temperatures

The CO_2 solubility measurement results in KCl aqueous solutions are presented in this section. Table 3.16, Table 3.17 and Table 3.18 summarise the measured and calculated CO_2 solubilities in 10, 15 and 22 wt% KCl aqueous solutions respectively. The solubility measurements were made at 50 °C, 100 °C and 150 °C and pressures up to 548 bar to cover a broad range of temperature and pressure. The binary interaction parameters of CO_2 and KCl systems were then adjusted to the solubility data measured in this work using both CPA and the PC-SAFT models. The tuned model calculation results were then compared with literature to check whether the calculated solubilities (using the models tuned with measured data) agree with literature CO_2 solubility data and validate this work experimental results.

Table 3.16 Calculated and measured solubility of CO_2 in 10 wt% KCl aqueous solutions at 50 °C, 100 °C and 150 °C

P bar	Measured solubility	Uncertainty	Model calculation		CPA Deviation	PC-SAFT Deviation
			CPA	PC-SAFT		
T = 50 °C						
82.07	0.0165	0.0001	0.0158	0.0169	3.86%	2.43%
222.76	0.0207	0.0001	0.0209	0.0213	1.09%	2.96%
400.00	0.0232	0.0001	0.0235	0.0239	1.36%	2.75%
537.72	0.0252	0.0002	0.0250	0.0255	0.82%	1.08%
AAD %					1.78%	2.30%
T = 100 °C						
93.10	0.0118	0.0000	0.0108	0.0118	8.34%	0.20%
259.31	0.0192	0.0001	0.0190	0.0195	1.19%	1.64%
537.93	0.0236	0.0001	0.0242	0.0247	2.77%	4.72%
AAD %					4.10%	2.18%
T = 150 °C						
162.76	0.0156	0.0001	0.0136	0.0145	12.67%	7.00%
337.93	0.0213	0.0002	0.0213	0.0217	0.00%	2.20%
531.03	0.0245	0.0003	0.0261	0.0264	6.51%	8.03%
AAD %					6.39%	5.75%

Table 3.17 Calculated and measured solubility of CO_2 in 15 wt% KCl aqueous solutions at 50°C, 100 °C and 150 °C

P bar	Measured solubility	Uncertainty	Model calculation		CPA Deviation	PC-SAFT Deviation
			CPA	PC-SAFT		
T = 50 °C						
91.31	0.0157	0.0001	0.0156	0.0166	0.16%	6.12%
260.69	0.0195	0.0001	0.0201	0.0205	2.84%	4.84%
537.93	0.0237	0.0001	0.0233	0.0238	1.97%	0.34%
AAD %					1.66%	3.76%
T = 100 °C						
103.45	0.0119	0.0000	0.0110	0.0119	7.26%	0.64%
281.38	0.0173	0.0001	0.0183	0.0188	5.99%	9.05%
548.28	0.0224	0.0001	0.0227	0.0233	1.46%	3.94%
AAD %					4.90%	4.54%
T = 100 °C						
180.00	0.0140	0.0000	0.0131	0.0139	6.72%	0.98%
385.31	0.0204	0.0001	0.0200	0.0205	2.04%	0.36%
531.03	0.0228	0.0002	0.0229	0.0234	0.53%	2.78%
AAD %					3.09%	1.37%

Table 3.18 Calculated and measured solubility of CO_2 in 22 wt% KCl aqueous solutions at 50 °C, 100 °C and 150 °C

P bar	Measured solubility	Uncertainty	Model calculation		CPA Deviation	PC-SAFT Deviation
			CPA	PC-SAFT		
T = 50 °C						
101.38	0.0146	0.0001	0.0148	0.0157	1.04%	7.09%
288.28	0.0183	0.0001	0.0185	0.0190	1.19%	3.56%
AAD %					1.12%	5.32%
T = 100 °C						
117.24	0.0115	0.0000	0.0110	0.0118	4.30%	3.40%
273.79	0.0163	0.0001	0.0165	0.0170	0.86%	4.29%
524.14	0.0202	0.0001	0.0203	0.0209	0.48%	3.37%
AAD %					1.88%	3.69%
T = 150 °C						
318.97	0.0163	0.0001	0.0153	0.0159	5.82%	2.27%
497.24	0.0188	0.0001	0.0186	0.0192	1.01%	2.09%
AAD %					3.42%	2.18%

The model calculation and experimental results are plotted in Figure 3.22 to Figure 3.24. As the experimental data measured in this work, used for tuning, the models correlates the experimental results very well within totally 2% deviation. The model calculations were also compared with the four datasets presented by Kiepe et al. [438], Kamps et al. [446], Liu et al. [434]. Calculated AAD % for each dataset are listed in Table 3.19. Figure 3.25 to Figure 3.28 illustrate the model calculation and literature data of CO_2 solubility in KCl aqueous solutions.

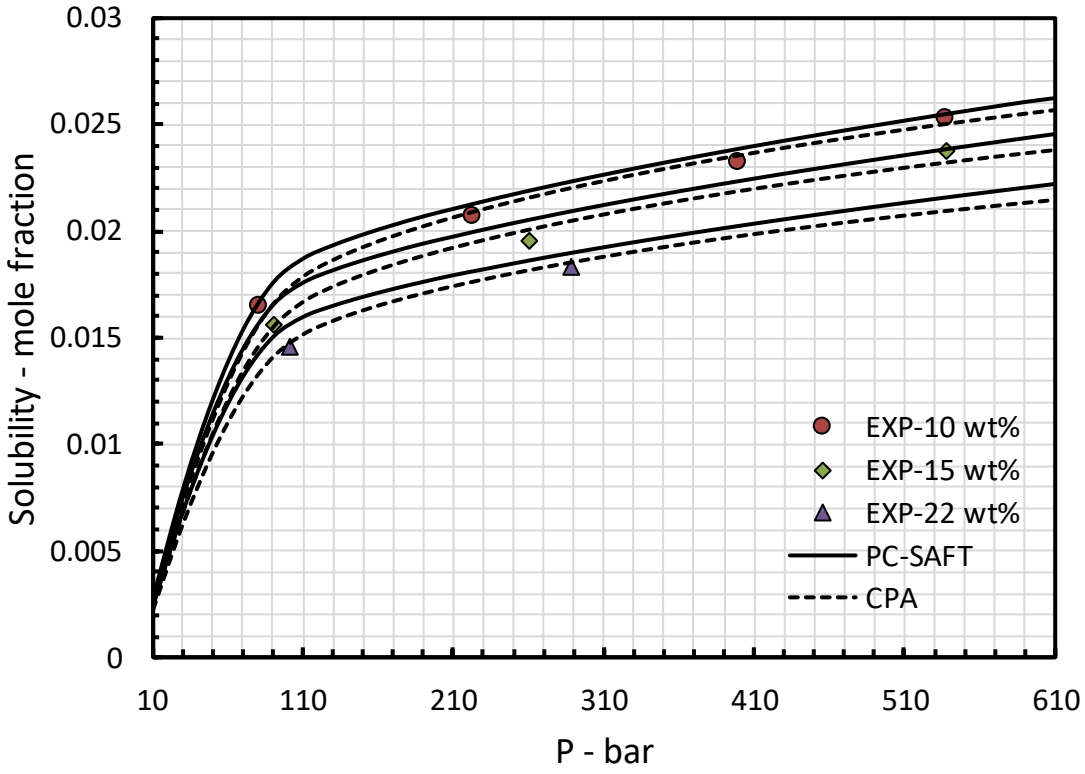

Figure 3.22 Comparison of experimental results of CO_2 solubility in 10, 15 and 22 wt% KCl aqueous solutions and model calculations using the CPA and the PC-SAFT equation of states at 50 °C.

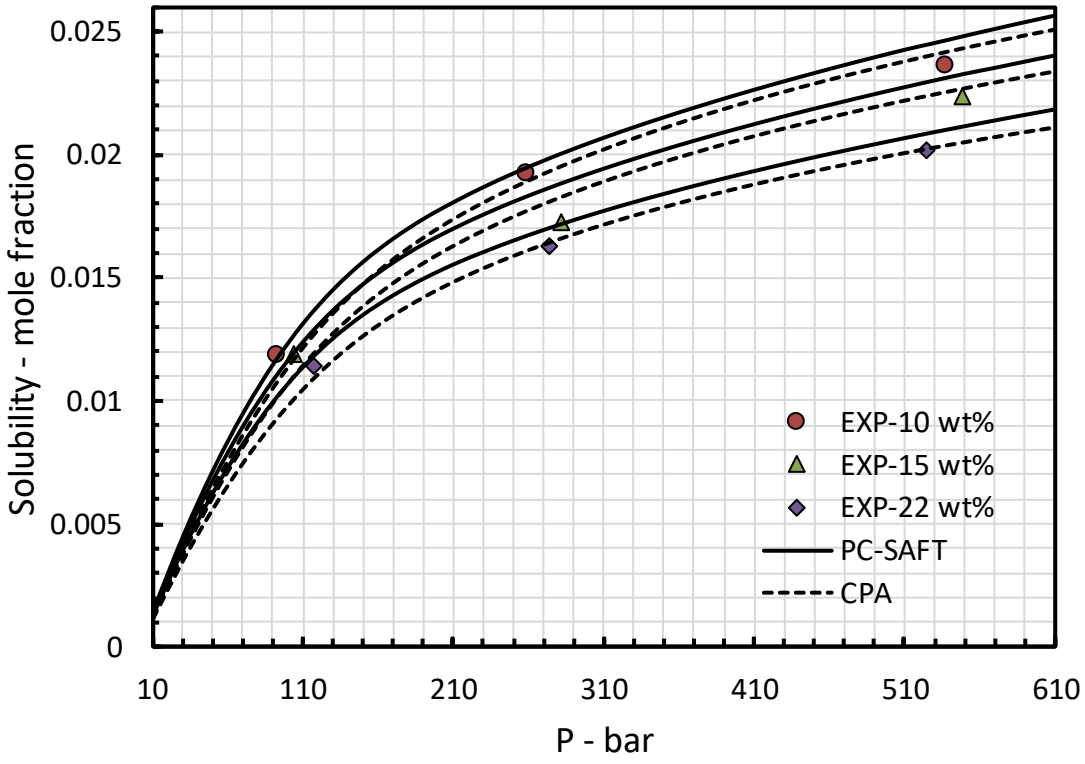

Figure 3.23 Comparison of experimental results of CO_2 solubility in 10, 15 and 22 wt% KCl aqueous solutions and model calculations using the CPA and the PC-SAFT equation of states at 100 °C.

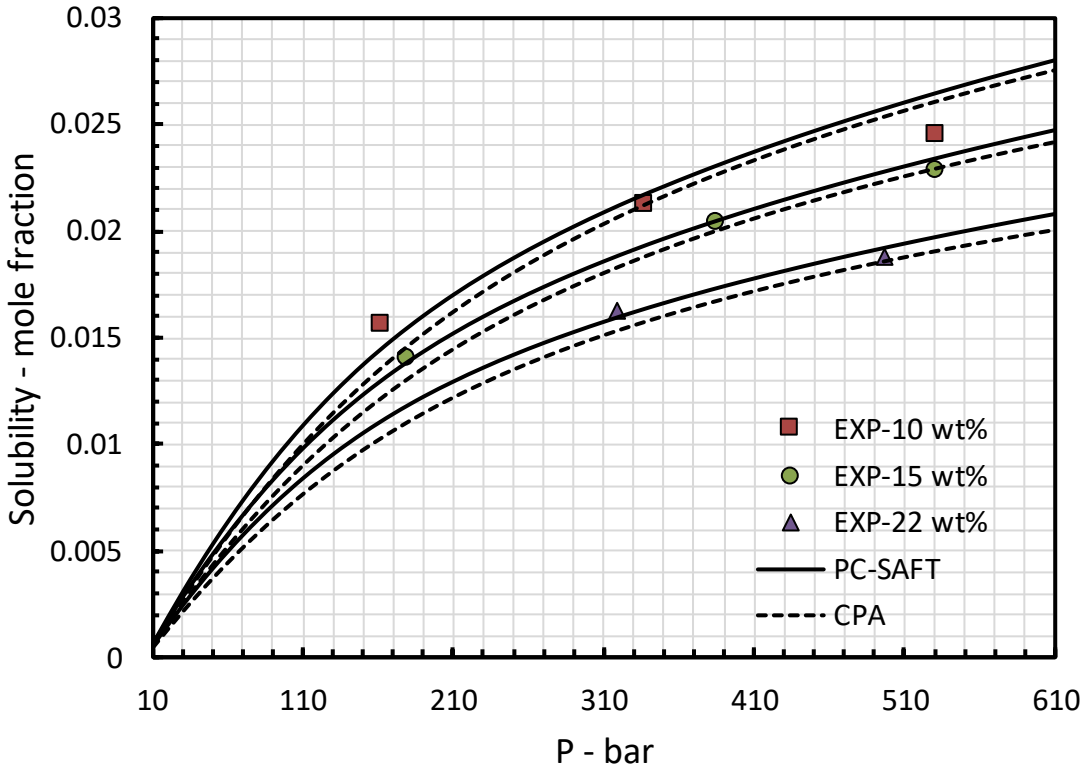

Figure 3.24 Comparison of experimental results of CO_2 solubility in 10, 15 and 22 wt% KCl aqueous solutions and model calculations using the CPA and the PC-SAFT equation of states at 150 °C.

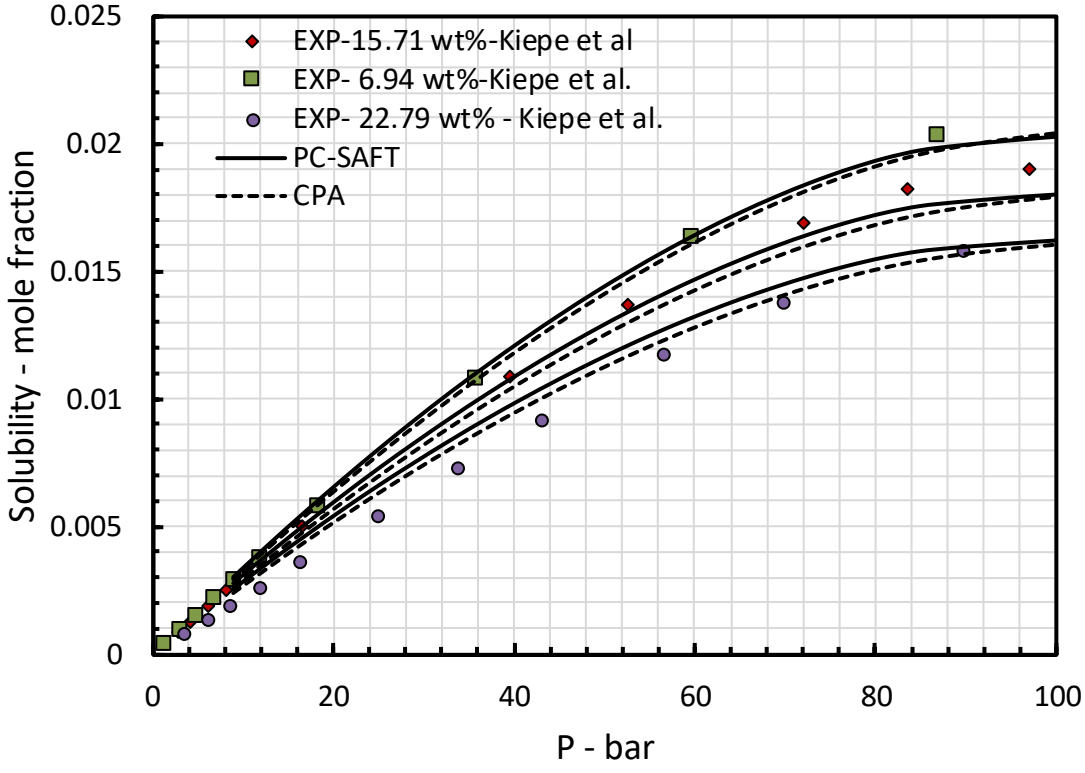

Figure 3.25 Comparison of CO_2 solubility data reported by Kiepe et al. [423] **and model calculations using the CPA and the PC-SAFT equation of states at 313 K.**

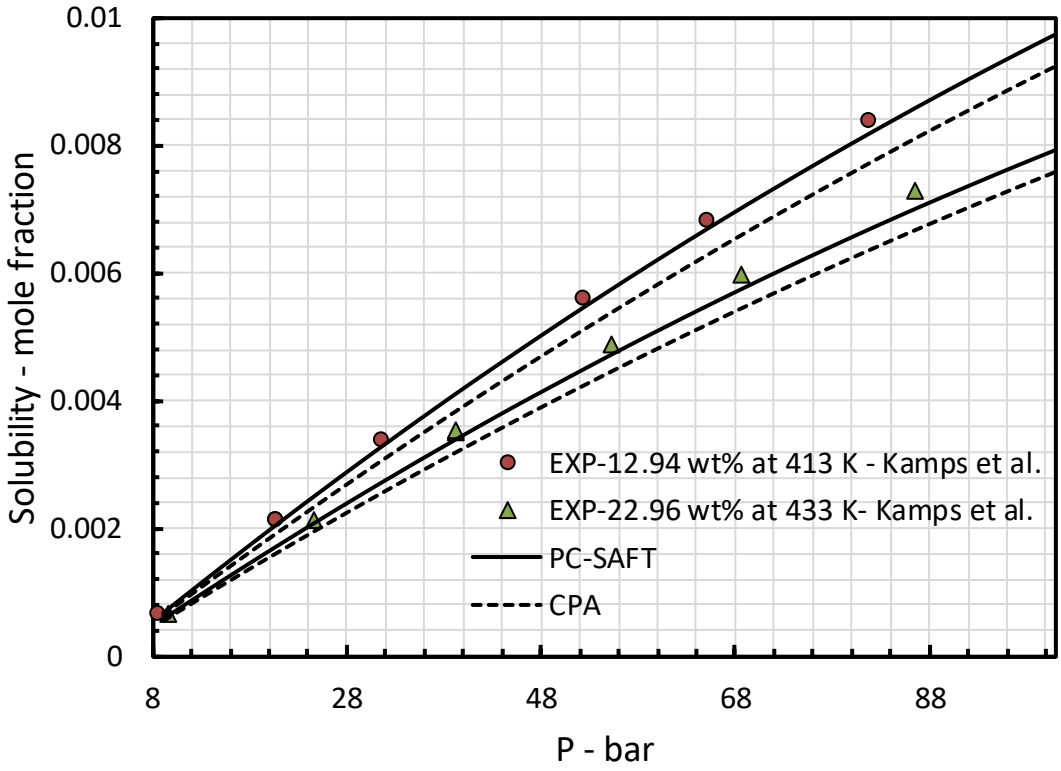

Figure 3.26 Comparison of CO_2 solubility data reported by Kamps et al. [446] **and model calculations using the CPA and the PC-SAFT equation of states at 433 K and 413 K.**

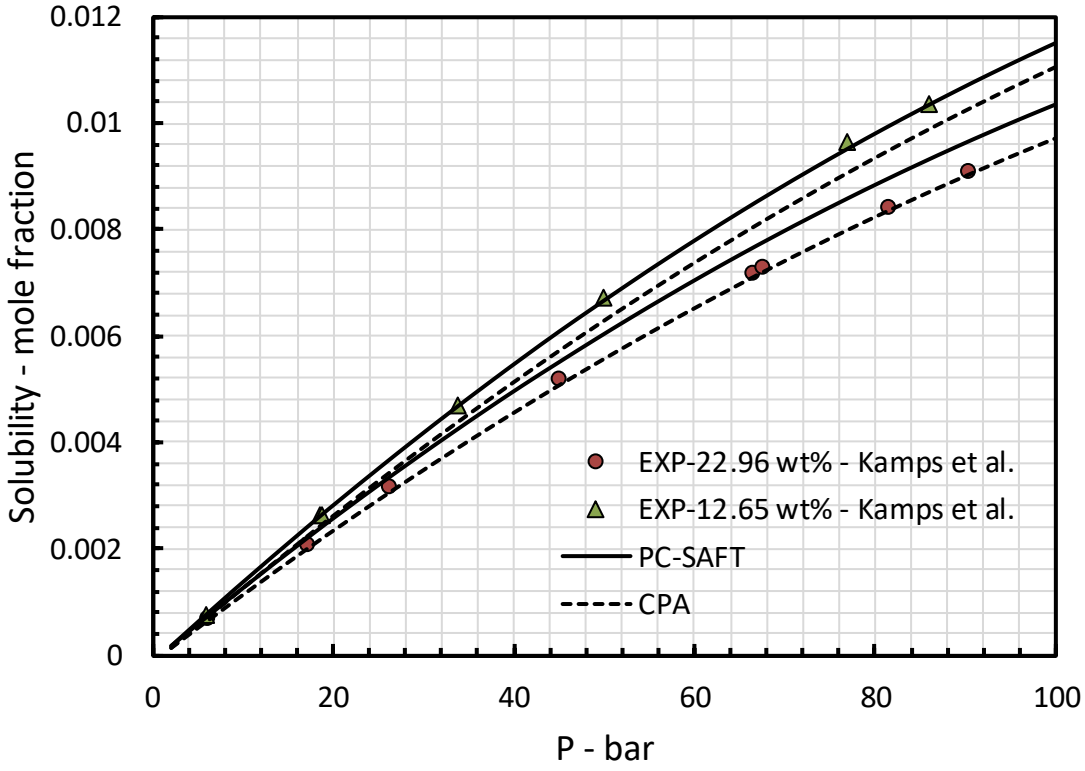

Figure 3.27 Comparison of CO_2 solubility data reported by Kamps et al. [446] **and model calculations using the CPA and the PC-SAFT equation of states at 373 K.**

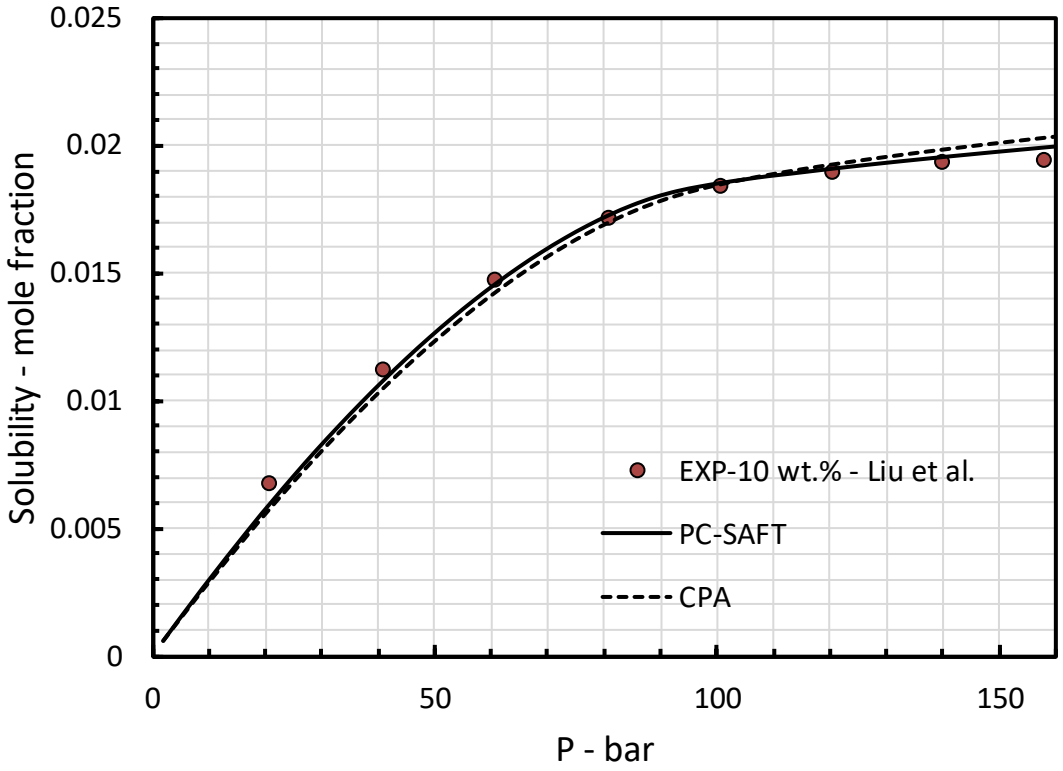

Figure 3.28 Comparison of CO_2 solubility data reported by Liu et al. [434] **and model calculations using the CPA and the PC-SAFT equation of states at 318 K.**

Table 3.19 Average absolute deviations of model calculations with this work experimental results and literature data

wt%	T	P	AAD %	
	K	bar	CPA	PC-SAFT
Kamps et al. [446]				
12.94%	315.8-333.15	7.35-90.16	3.15%	1.11%
12.65%	353-433.1	4.08-54.88	8.91%	2.64%
22.96%	373.05-433.05	6.09-85.97	8.54%	6.98%
23.19%	313.2-353.15	5.88-89.09	1.27%	4.56%
Kiepe et al. [423]				
3.59%	313.31	0.92-82.79	4.97%	2.43%
6.94%	313.31	1.26-86.96	1.89%	4.44%
15.71%	313.16	2.77-97.09	4.65%	1.71%
22.79%	313.37	3.55-89.66	14.36%	18.94%
3.59%	353.08	1.99-99.14	20.63%	17.62%
6.94%	352.55	3.03-94.48	17.63%	13.95%
15.71%	353.09	2.37-105.08	3.88%	2.70%
22.97%	353.4	3.15-95.26	18.98%	28.29%
Liu et al. [434]				
10%	318.15	20.9-158.1	4.32%	2.83%

The AAD % of the models from three solubility datasets reported in the literature are summarised in Table 3.19. As presented in the Table 3.19, the deviations between the calculated and the experimental solubility reported by Kamps et al. [446] is about 5% for both the CPA and the PC-SAFT EoSs (see Figure 3.26 and Figure 3.27). The AAD % of calculated solubilities are 4.3 and 2.8 from the datasets reported by Liu et al. [434] (see Figure 3.28) using the CPA and the PC-SAFT EoSs respectively. However, the deviation of the model calculations from the experimental solubilities reported by Kiepe et al. [438] at high salinities differs considerably.

3.3.4. Solubility of CO_2 in $CaCl_2$ aqueous solutions at elevated temperatures

The measured and calculated solubilities of CO_2 in different salt concentrations of $CaCl_2$ aqueous solutions at 50 °C, 100 °C and 150 °C and pressures up to 595 bar are reported in Table 3.20, Table 3.21, Table 3.22 and Table 3.23. The solubilities were measured in 7.5, 10, 15.7 and 23.4 wt% $CaCl_2$ aqueous solutions. The PC-SAFT and the CPA EoSs were tuned to the solubility data reported by Tong et al. [374] in which a wide range of temperature, pressure and concentrations were covered.

Table 3.20 Calculated and measured solubility of CO_2 in 7.5 wt% $CaCl_2$ aqueous solutions at 50°C, 100 °C

P	Measured solubility	Uncertainty	Model calculation			
bar			CPA	PC-SAFT	CPA Deviation	PC-SAFT Deviation
T = 50 °C						
83.72	0.0136	0.0000	0.0134	0.0136	1.32%	0.15%
263.45	0.0184	0.0001	0.0179	0.0173	2.84%	5.96%
AAD %					2.08%	3.05%
T = 100 °C						
65.17	0.0084	0.0000	0.0070	0.0072	17.15%	14.77%
279.31	0.0156	0.0001	0.0163	0.0157	4.16%	0.55%
AAD %					10.65%	7.66%

Table 3.21 Calculated and measured solubility of CO_2 in 10 wt% $CaCl_2$ aqueous solutions at 50 °C, 100 °C and 150 °C

P	Measured solubility	Uncertainty	Model calculation			
bar			CPA	PC-SAFT	CPA Deviation	PC-SAFT Deviation
T = 50 °C						
135.86	0.0140	0.0000	0.0142	0.0140	1.09%	0.37%
255.79	0.0155	0.0000	0.0161	0.0156	3.88%	0.73%
475.86	0.0175	0.0001	0.0181	0.0176	3.63%	0.70%
564.14	0.0182	0.0001	0.0187	0.0182	2.45%	0.02%
AAD %					2.76%	0.46%
T = 100 °C						
179.31	0.0123	0.0000	0.0124	0.0122	0.76%	0.79%
284.83	0.0147	0.0000	0.0149	0.0143	0.80%	2.71%
416.34	0.0166	0.0000	0.0168	0.0161	1.00%	3.09%
554.28	0.0182	0.0001	0.0182	0.0175	0.12%	3.65%
AAD %					0.67%	2.56%
T = 150 °C						
216.55	0.0147	0.0001	0.0135	0.0136	7.60%	7.50%
387.59	0.0176	0.0001	0.0183	0.0179	4.35%	1.78%
568.97	0.0211	0.0001	0.0214	0.0209	1.74%	0.99%
AAD %					4.56%	3.42%

Table 3.22 Calculated and measured solubility of CO_2 in 15.7 wt% $CaCl_2$ aqueous solutions at 50 °C, 100 °C and 150 °C

P	Measured solubility	Uncertainty	Model calculation		CPA Deviation	PC-SAFT Deviation
bar			CPA	PC-SAFT		
T = 50 °C						
105.52	0.0100	0.0001	0.0107	0.0107	7.43%	7.51%
140.48	0.0111	0.0001	0.0114	0.0113	3.57%	2.08%
246.21	0.0121	0.0001	0.0127	0.0124	4.91%	2.02%
256.28	0.0125	0.0001	0.0128	0.0125	2.39%	0.47%
397.93	0.0139	0.0000	0.0139	0.0135	0.40%	2.40%
554.48	0.0140	0.0001	0.0148	0.0145	5.57%	3.34%
555.86	0.0146	0.0001	0.0148	0.0145	1.64%	0.50%
AAD %					3.70%	2.62%
T = 100 °C						
80.00	0.0066	0.0001	0.0062	0.0063	6.40%	4.61%
124.48	0.0089	0.0001	0.0083	0.0083	6.65%	6.37%
262.07	0.0118	0.0001	0.0117	0.0113	1.11%	4.32%
276.34	0.0120	0.0001	0.0119	0.0115	0.74%	4.13%
409.03	0.0135	0.0001	0.0134	0.0129	0.94%	4.88%
547.59	0.0145	0.0001	0.0146	0.0140	0.15%	3.53%
553.79	0.0147	0.0001	0.0146	0.0141	0.41%	4.06%
AAD %					2.34%	4.56%
T=150 °C						
244.34	0.0118	0.0001	0.0116	0.0114	1.41%	3.47%
406.90	0.0150	0.0001	0.0148	0.0142	1.60%	5.44%
595.86	0.0178	0.0001	0.0171	0.0165	3.62%	7.34%
AAD %					2.21%	5.42%

Table 3.23 Calculated and measured solubility of CO_2 in 23.4 wt% $CaCl_2$ aqueous solutions at 50 °C, 100 °C and 150 °C

P bar	Measured solubility	Uncertainty	Model calculation		CPA Deviation	PC-SAFT Deviation
			CPA	PC-SAFT		
T = 50 °C						
116.55	0.0076	0.0000	0.0082	0.0081	7.76%	7.17%
236.41	0.0085	0.0000	0.0093	0.0091	9.79%	6.97%
385.24	0.0094	0.0000	0.0102	0.0099	8.30%	5.44%
530.21	0.0101	0.0000	0.0108	0.0106	7.01%	4.85%
AAD %					8.22%	6.11%
T = 100 °C						
151.31	0.0071	0.0000	0.0070	0.0069	1.67%	2.67%
292.14	0.0091	0.0000	0.0091	0.0087	0.16%	3.94%
405.59	0.0099	0.0000	0.0100	0.0096	1.69%	2.41%
562.07	0.0110	0.0000	0.0109	0.0105	0.14%	3.79%
AAD %					0.91%	3.20%
T = 150 °C						
246.21	0.0091	0.0000	0.0086	0.0083	5.43%	9.41%
424.14	0.0112	0.0000	0.0111	0.0104	1.23%	6.97%
552.41	0.0123	0.0000	0.0122	0.0115	0.61%	6.35%
AAD %					2.42%	7.57%

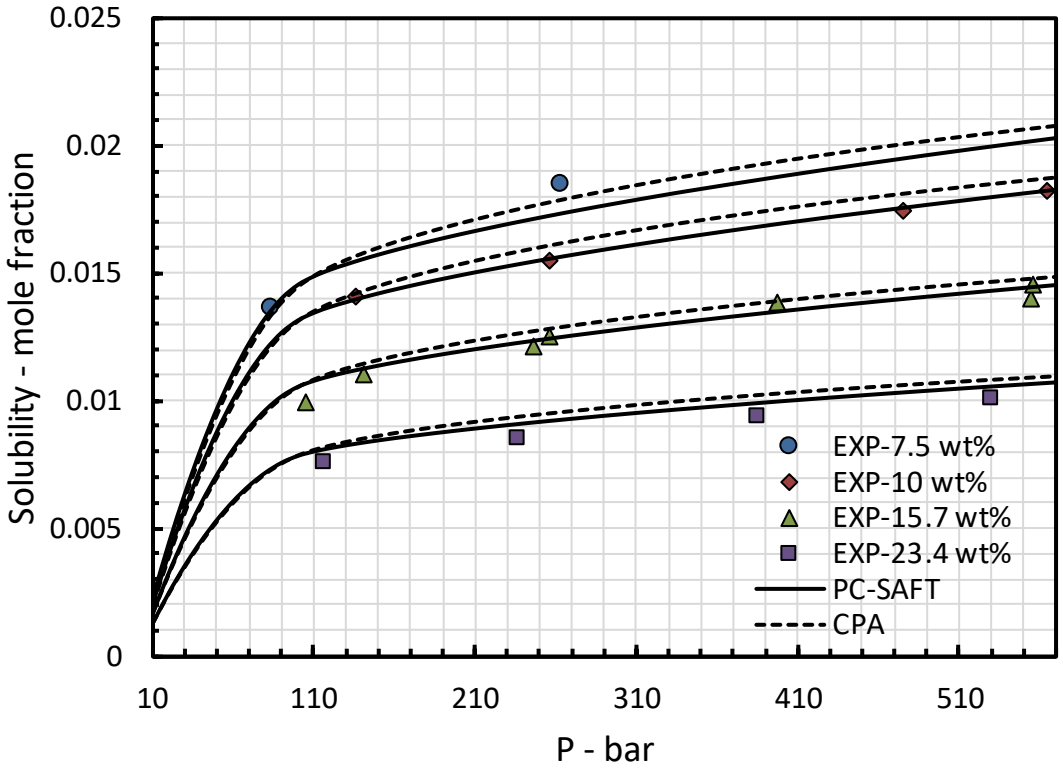

Figure 3.29 Comparison of experimental results of CO_2 solubility in 7.5, 10, 15.7 and 23.4 wt% $CaCl_2$ aqueous solutions and model calculations using the CPA and PC-SAFT models at 50 °C.

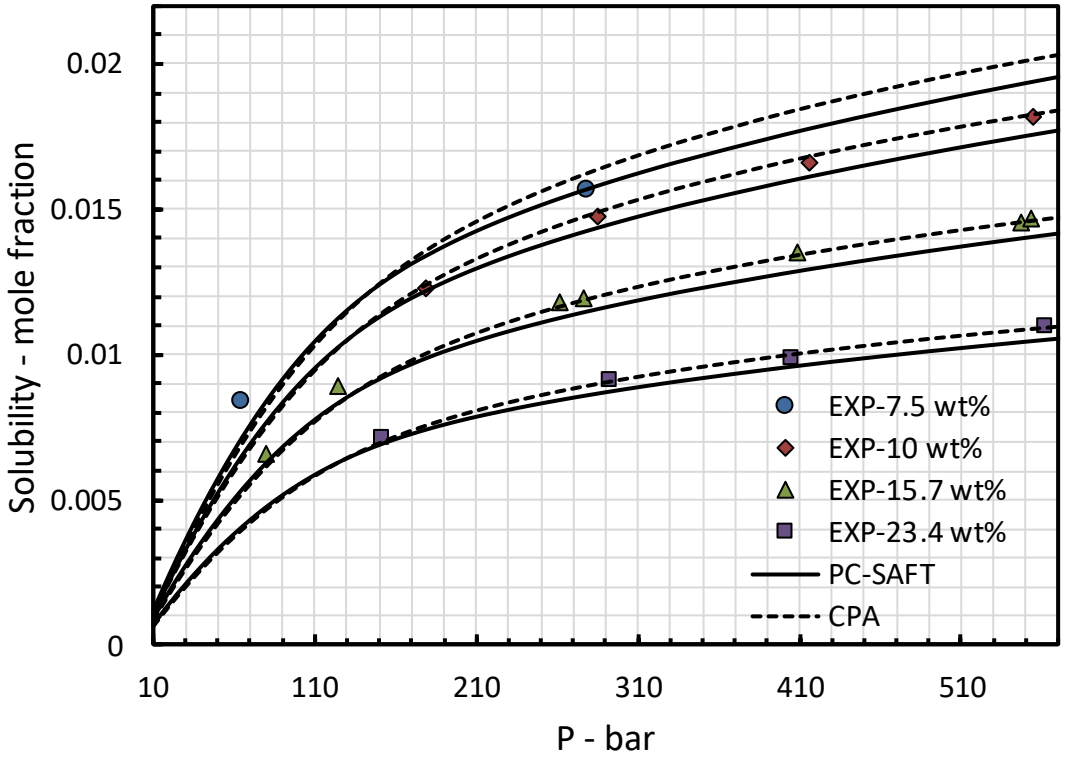

Figure 3.30 Comparison of experimental results of CO_2 solubility in 7.5, 10, 15.7 and 23.4 wt% $CaCl_2$ aqueous solutions and model calculations using the CPA and PC-SAFT models at 100 °C.

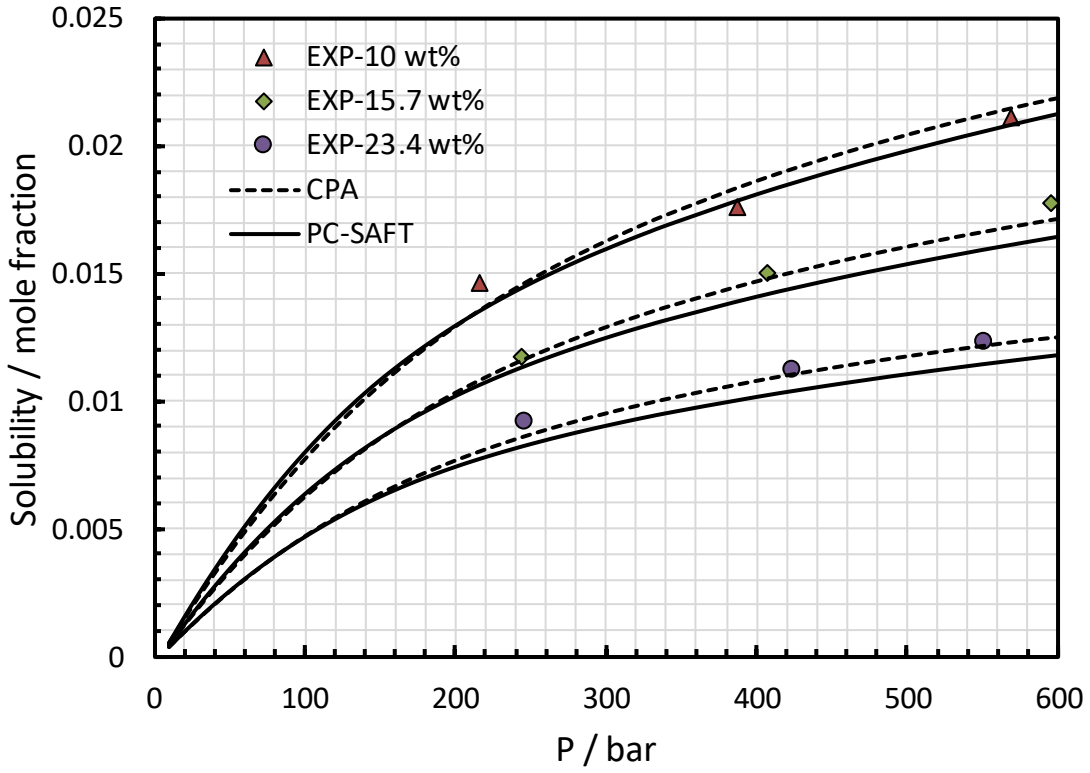

Figure 3.31 Comparison of experimental results of CO_2 solubility in 10, 15.7 and 23.4 wt% $CaCl_2$ aqueous solutions and model calculations using the CPA and PC-SAFT models at 150 °C.

Figure 3.29, Figure 3.30 and Figure 3.31 compare the measured CO_2 solubility in 7.5, 10, 15.7 and 23.4 wt% solutions with the model calculations. As illustrated, the solubility decreases with increasing the salinity of the brine at each given temperature. Also, models correlate the experimental data with AAD % less than 5 at almost all temperatures. However, the deviation between calculated and measured solubilities in 23.4 wt% solution at 50 °C and 150 °C (calculated values using PC-SAFT EoS) differ by less than 8 %. The model calculations were also compared to two sets of literature solubility data to test the model performance further and to compare the deviation of our experimental results and those reported in the literature from model calculations.

Table 3.24 presents the AAD % of the calculated solubilities from the data reported by Prutton et al. [380], Liu et al. [434] and Zhao et al. [375]. The total AAD % of the model calculations from the data reported by Prutton et al. [380] is around 7% using either the PC-SAFT or the CPA EoSs (see Figure 3.32 and Figure 3.33). The absolute average deviation of calculated solubilities using the CPA and the PC-SAFT EoSs from the data reported Zhao et al. [375] are 4.8% and 3.5% respectively (see Figure 3.34). The AAD % values of the model calculations from Liu et al. dataset are 3.97% and 3.61% for the CPA and the PC-SAFT equation of states respectively.

Table 3.24 The average absolute deviation of the models tuned with experimental data reported by Tong et al. [374] **and solubility data reported by Prutton et al.** [380]**, Liu et al.** [434] **and Zhao et al.** [375]

Brine salinity wt%	T - K	P - bar	AAD %	
			CPA	PC-SAFT
Prutton et al.				
10.1	348.65	16.21-628.06	13.46%	10.39%
10.1	374.15	17.22-626.03	10.70%	7.44%
10.1	394.15	21.27-712.14	7.86%	7.07%
20.2	349.15	22.28-607.8	6.76%	1.74%
20.2	374.15	23.30-656.42	7.52%	2.35%
20.2	394.15	25.32-658.45	11.41%	14.76%
30.2	349.15	15.12-633.12	1.90%	14.05%
30.2	374.15	74.96-638.19	3.56%	14.52%
30.2	394.15	84.08-673.64	6.58%	18.56%
Liu et al.				
10	318.15	20.9-158.6	3.97%	3.26%
Zhao et al.				
3.56	323 - 423	15	7.27%	3.85%
6.89	324 - 423	15	6.11%	3.58%
9.99	325 - 423	15	5.52%	3.87%
12.89	326 - 423	15	4.11%	3.31%
15.61	327 - 423	15	2.70%	2.73%
18.16	328 - 423	15	3.13%	3.96%

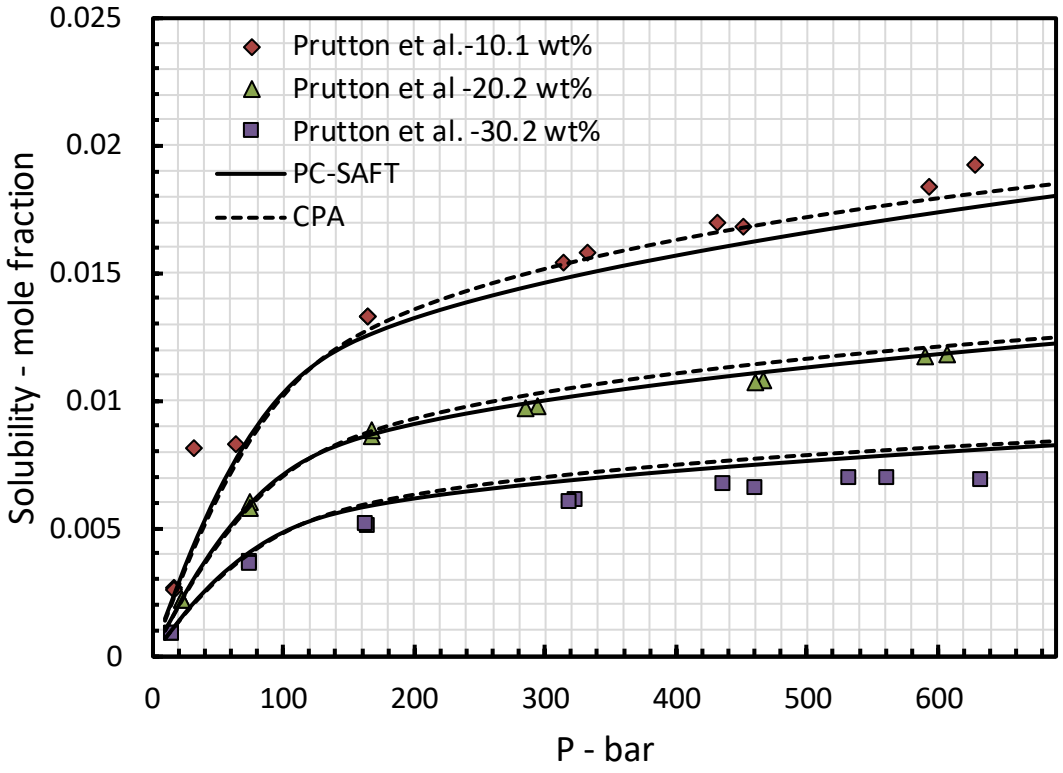

Figure 3.32 CO_2 solubility in $CaCl_2$ aqueous solutions: comparison between experimental data reported by Prutton et al. [380] **and model calculations using the CPA and the PC-SAFT equation of states at 348 K & 349.15 K.**

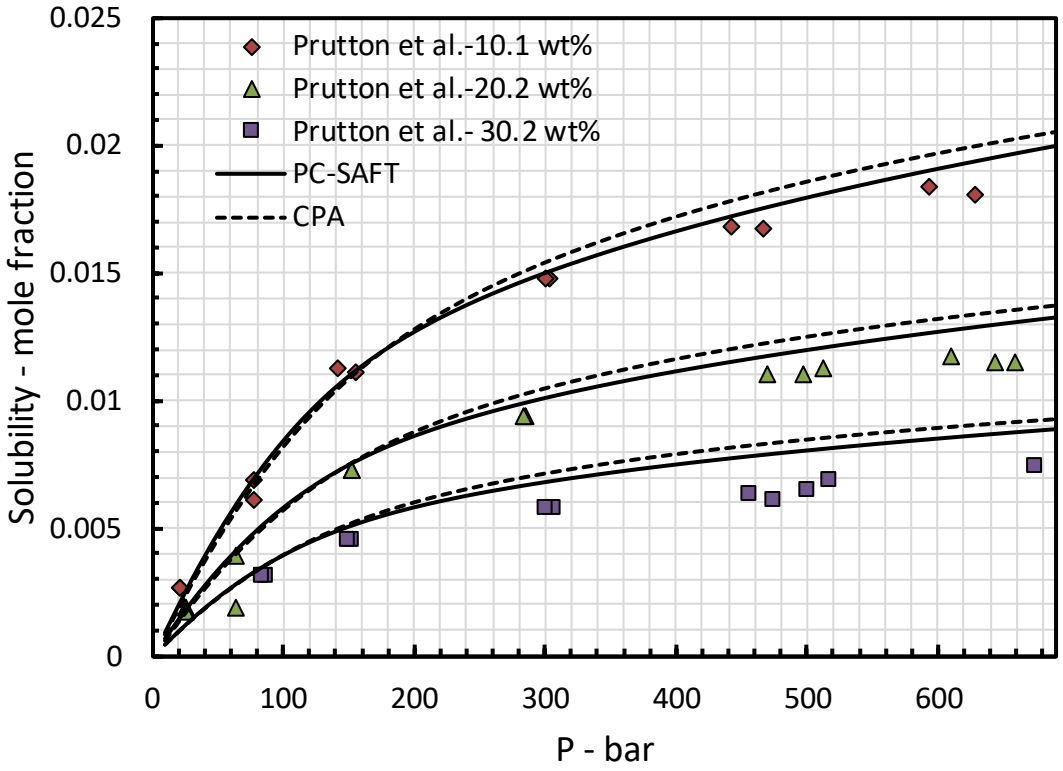

Figure 3.33 CO_2 solubility in $CaCl_2$ aqueous solutions: comparison between experimental data reported by Prutton et al. [380]**and model calculations using the CPA and the PC-SAFT equation of states at 394.15 K.**

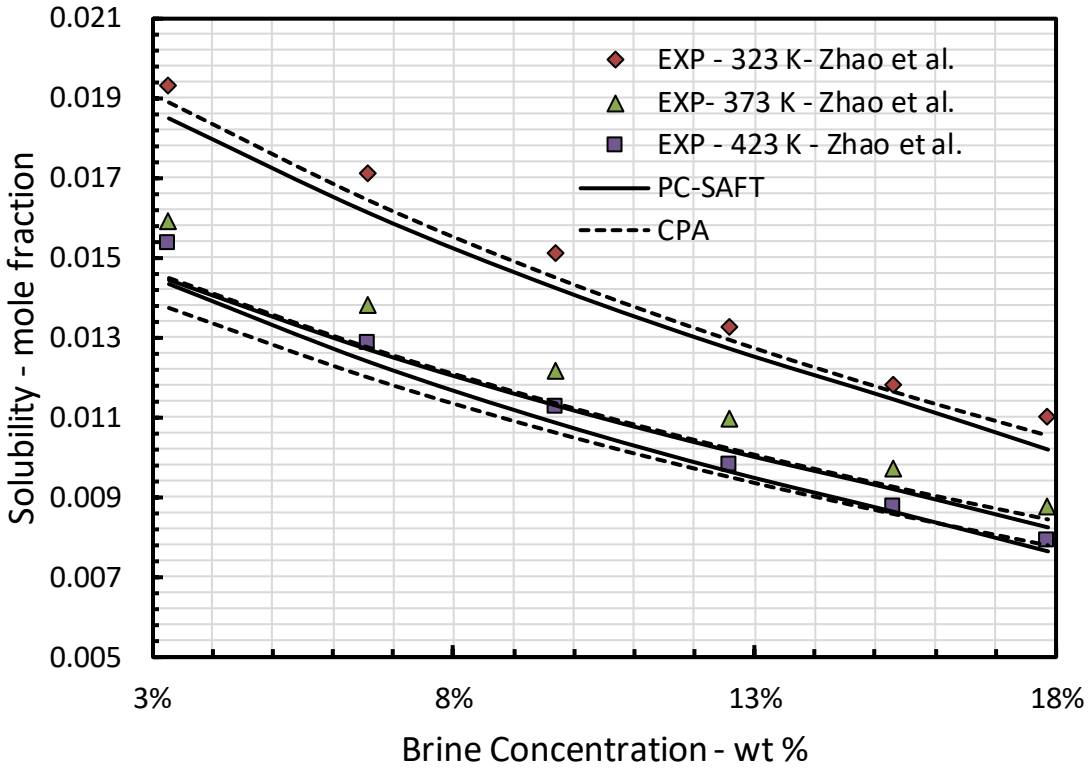

Figure 3.34 CO_2 solubility in $CaCl_2$ aqueous solutions: comparison between experimental data reported by Zhao et al. [375] **and model calculations using the CPA and the PC-SAFT equation of states at 323 K, 373 K and 423 K and 150 bar.**

3.3.5. Solubility of CO_2 in $MgCl_2$ aqueous solutions at elevated temperatures

The solubility of CO_2 in various concentrations of $MgCl_2$ aqueous solution was measured at 50 °C, 100 °C and 150 °C and pressures up to 544 bar. The experimental results are reported in Table 3.25 to Table 3.28. Measured and calculated solubilities using the CPA and the PC-SAFT EoSs are compared graphically through Figure 3.35, Figure 3.36 and Figure 3.37. To validate the experimental results of this study with those reported in the literature, the CPA and the PC-SAFT equation of states were adjusted to the two most recent datasets reported by Tong et al. [374] and Zhao et al. [375]. As declared in Table 3.25 to Table 3.28 excellent agreements were found between model calculations and the experimental results of this work. However, the average deviation between calculated and measured CO_2 solubilities in 29 wt% solution at 100 °C is slightly high using the CPA and the PC-SAFT EoSs.

Table 3.25 Calculated and measured solubility of CO_2 in 6.7 wt% $MgCl_2$ aqueous solutions at 50°C, 100 °C

P	Measured solubility	Uncertainty	Model calculation		CPA	PC-SAFT
bar			CPA	PC-SAFT	Deviation	
T = 50°C						
166.90	0.0161	0.0002	0.0161	0.0159	0.35%	0.99%
379.31	0.0200	0.0002	0.0189	0.0185	5.48%	7.67%
544.83	0.0218	0.0002	0.0203	0.0200	6.72%	8.30%
AAD %					4.19%	5.65%
T = 100°C						
165.52	0.0141	0.0002	0.0133	0.0132	5.78%	6.27%
377.59	0.0183	0.0002	0.0182	0.0175	0.36%	4.00%
544.83	0.0214	0.0002	0.0203	0.0196	4.92%	8.22%
AAD %					3.69%	6.17%

Table 3.26 Calculated and measured solubility of CO_2 in 11 wt% $MgCl_2$ aqueous solutions at 50°C, 100 °C and 150 °C

P bar	Measured solubility	Uncertainty	Model calculation CPA	Model calculation PC-SAFT	CPA Deviation	PC-SAFT Deviation
T=50°C						
82.34	0.0111	0.0001	0.0108	0.0111	2.83%	0.14%
236.55	0.0142	0.0001	0.0142	0.0140	0.11%	1.43%
414.76	0.0164	0.0001	0.0157	0.0155	4.18%	5.50%
538.34	0.0175	0.0002	0.0165	0.0164	5.25%	6.03%
AAD %					3.09%	3.27%
T=100°C						
157.24	0.0109	0.0001	0.0109	0.0109	0.21%	0.30%
283.38	0.0137	0.0001	0.0139	0.0135	1.51%	1.31%
140.69	0.0109	0.0002	0.0103	0.0103	5.57%	5.07%
340.69	0.0150	0.0002	0.0148	0.0143	1.82%	4.91%
533.79	0.0175	0.0001	0.0169	0.0163	3.69%	6.67%
AAD %					2.56%	3.65%
T=150°C						
168.97	0.0110	0.0001	0.0104	0.0104	5.45%	5.51%
298.62	0.0140	0.0001	0.0145	0.0140	3.74%	0.50%
415.72	0.0161	0.0001	0.0168	0.0162	4.61%	0.31%
AAD %					4.60%	2.10%

Table 3.27 Calculated and measured solubility of CO_2 in 18 wt% $MgCl_2$ aqueous solutions at 50 °C, 100 °C and 150 °C

P bar	Measured solubility	Uncertainty	Model calculation CPA	Model calculation PC-SAFT	CPA Deviation	PC-SAFT Deviation
T = 50°C						
164.83	0.0098	0.0001	0.0099	0.0098	0.45%	0.52%
273.10	0.0113	0.0001	0.0108	0.0106	3.95%	5.69%
AAD %					2.20%	3.10%
T = 100°C						
187.24	0.0088	0.0001	0.0091	0.0090	3.04%	2.18%
302.28	0.0106	0.0001	0.0108	0.0105	1.95%	0.69%
416.21	0.0116	0.0001	0.0119	0.0116	2.44%	0.52%
AAD %					2.48%	1.13%
T = 150°C						
208.97	0.0089	0.0001	0.0088	0.0085	1.22%	4.20%
342.00	0.0110	0.0001	0.0113	0.0107	2.29%	2.96%
447.52	0.0123	0.0001	0.0126	0.0119	2.41%	3.35%
542.76	0.0132	0.0001	0.0136	0.0128	2.40%	3.33%
AAD %					2.08%	3.46%

Table 3.28 Calculated and measured solubility of CO_2 in 29 wt% $MgCl_2$ aqueous solutions at 50 °C, 100 °C.

P bar	Measured solubility	Uncertainty	Model calculation CPA	PC-SAFT	Deviation CPA	PC-SAFT
T = 50°C						
82.76	0.0051	0.0001	0.0050	0.0052	1.89%	2.80%
246.90	0.0065	0.0001	0.0064	0.0065	1.61%	0.51%
411.10	0.0072	0.0001	0.0070	0.0071	1.56%	0.36%
532.41	0.0076	0.0001	0.0074	0.0075	2.68%	0.91%
AAD %					1.94%	1.15%
T = 100°C						
135.03	0.0046	0.0001	0.0051	0.0052	10.02%	10.99%
286.76	0.0064	0.0001	0.0069	0.0068	8.10%	5.77%
402.76	0.0071	0.0001	0.0077	0.0075	8.63%	5.90%
544.83	0.0079	0.0001	0.0083	0.0081	5.19%	2.93%
AAD %					7.99%	6.40%

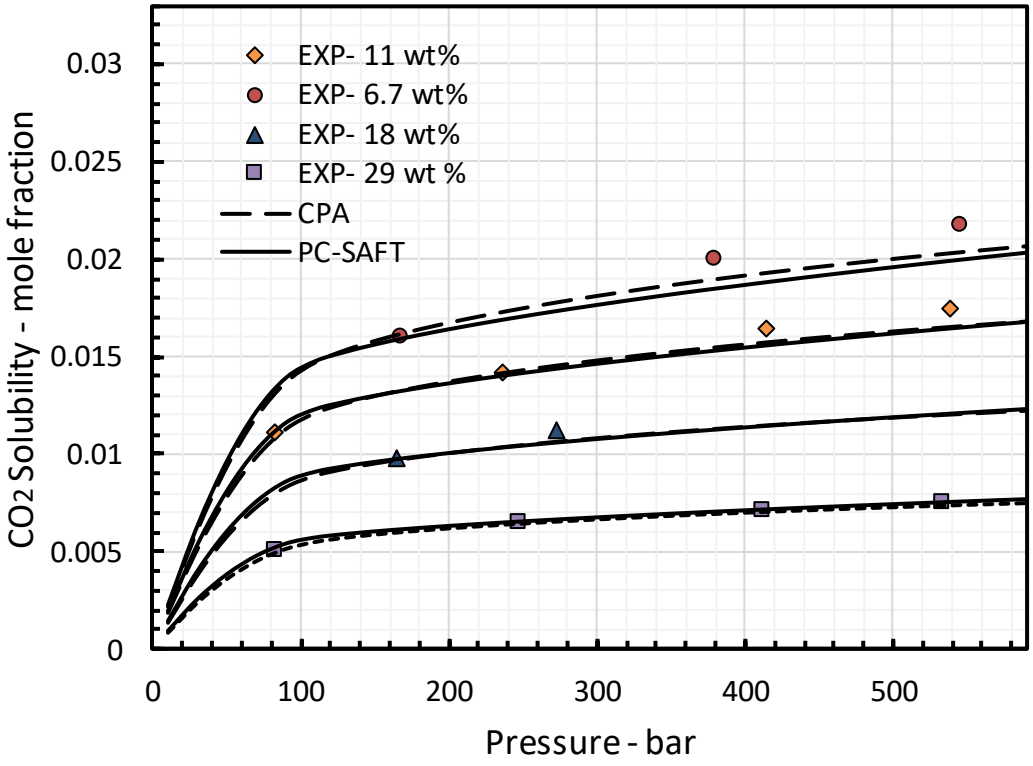

Figure 3.35 Comparison of experimental results of CO_2 solubility in 6.7, 11, 18 and 29 wt% $MgCl_2$ aqueous solutions and model calculations using the CPA and PC-SAFT models at 50 °C.

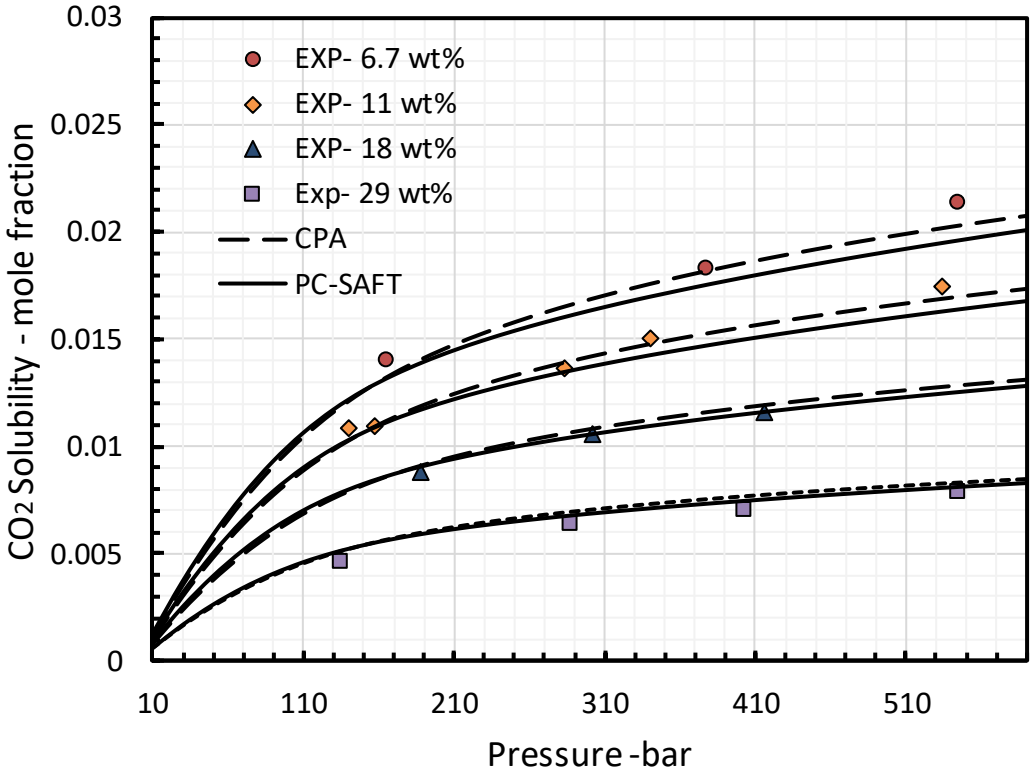

Figure 3.36 Comparison of experimental results of CO_2 solubility in 6.7, 11, 18 and 29 wt% $MgCl_2$ aqueous solutions and model calculations using the CPA and PC-SAFT models at 100 °C.

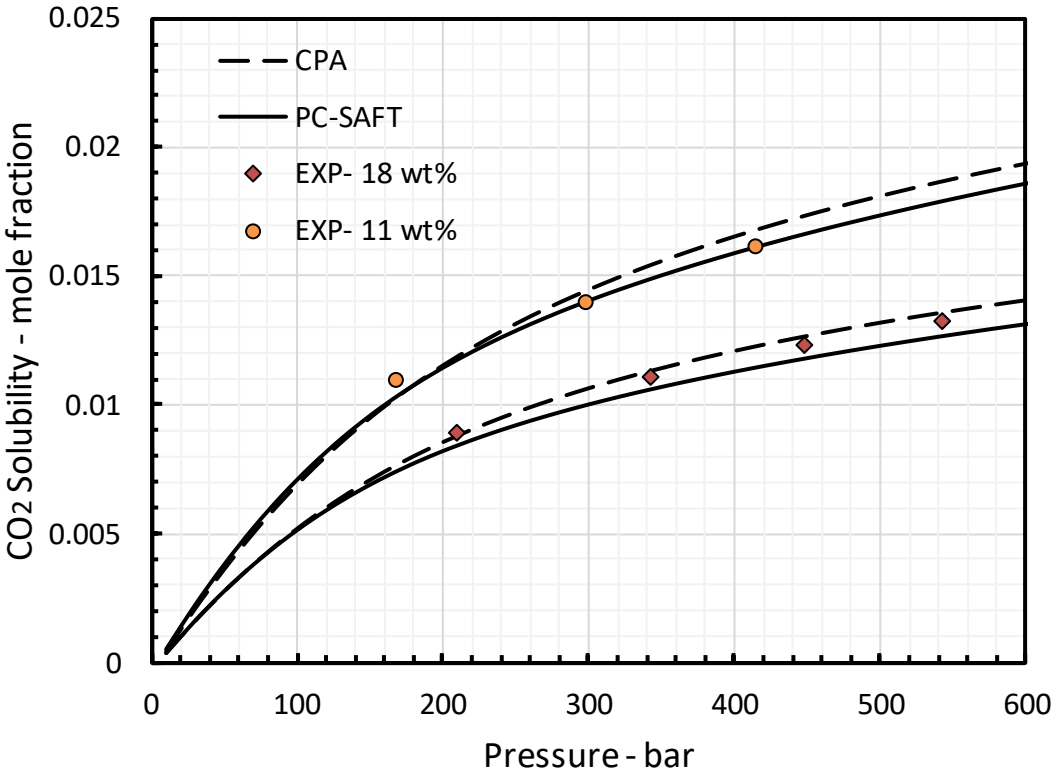

Figure 3.37 Comparison of experimental results of CO_2 solubility in 11 and 18 wt% $MgCl_2$ aqueous solutions and model calculations using the CPA and PC-SAFT models at 150 °C.

3.3.6. Solubility of CO_2 in a mixture of salts aqueous solutions at elevated temperatures

The solubility of CO_2 in a salt mixture aqueous solution was measured at 50 °C, 100 °C and 150 °C and pressures up to 571 bar. The total salinity of the test brine is 23.1 wt%, and it consists of NaCl, $CaCl_2$, KCl and $MgCl_2$. The density of the brine was measured using a 100 ml pyknometer at lab conditions. Table 3.29 presents the composition of the salt mixture and the measured solution density. Using the adjusted binary interaction parameters between single salts and CO_2 in Chapter 2, the solubilities were calculated using the CPA and the PC-SAFT models and are reported in Table 3.30 together with the measured solubility data. The calculated and measured solubilities are also plotted in Figure 3.38 to Figure 3.40.

Table 3.29 Composition of the salt mixture aqueous solution

Salt	g in 1 lit of water	Weight fraction %
NaCl	258.13	19.4
$CaCl_2$	40.09	2.3
$MgCl_2$	31.05	1.1
KCl	3.48	0.3
Total Salinity		23.1%
Density measured		1176.1 gr/lit

As seen, excellent agreements were found between experimental data and model calculations at 50 °C with the AAD % value of 1.15 and 2.03 for the CPA and PC-SAFT EoSs respectively, while at higher temperatures, the deviation is slightly higher especially at low pressures (P< 200 bar). As the salt mixture mainly consists of sodium chloride, with 19.5 wt% NaCl concentration, it is expected to observe a relatively similar AAD % as those reported for solubilities in NaCl aqueous solutions. As reported in Table 3.15, the AAD % values for solubilities in 22 wt% sodium chloride aqueous solutions are 6.20 and 6.21 for the CPA and the PC-SAFT models at 150 °C, which is consistent with the 6.23 and 6.84 AAD % values reported for the mixture of salts aqueous solution reported in this section.

Table 3.30 Measured and calculated CO_2 solubility in the salt mixture aqueous solutions at 50 °C, 100 °C and 150 °C

P bar	Measured solubility	Uncertainty	Model calculation CPA	Model calculation PC-SAFT	Deviation CPA	Deviation PC-SAFT
T=50 °C						
100.21	0.0082	0.0001	0.0082	0.0083	0.52%	0.83%
244.14	0.0098	0.0001	0.0098	0.0097	0.54%	1.14%
398.90	0.0107	0.0001	0.0107	0.0106	0.12%	1.54%
487.59	0.0113	0.0001	0.0111	0.0110	1.34%	2.62%
571.03	0.0118	0.0001	0.0114	0.0113	3.22%	4.03%
AAD %					1.15%	2.03%
T=100 °C						
133.38	0.0083	0.0001	0.0074	0.0077	11.86%	7.63%
160.21	0.0092	0.0001	0.0081	0.0084	12.46%	9.08%
297.38	0.0109	0.0001	0.0103	0.0104	5.42%	4.16%
313.10	0.0114	0.0001	0.0104	0.0106	8.09%	6.96%
420.14	0.0121	0.0001	0.0114	0.0115	5.82%	4.83%
485.31	0.0125	0.0001	0.0119	0.0120	4.80%	3.70%
563.45	0.0130	0.0001	0.0123	0.0125	5.09%	3.69%
AAD %					7.65%	5.72%
T=150 °C						
189.93	0.0096	0.0001	0.0086	0.0087	10.32%	9.09%
212.14	0.0101	0.0001	0.0092	0.0093	9.29%	8.63%
316.55	0.0122	0.0001	0.0113	0.0112	7.38%	8.35%
346.90	0.0125	0.0001	0.0118	0.0117	5.65%	6.90%
438.62	0.0132	0.0001	0.0130	0.0128	1.32%	3.05%
559.59	0.0148	0.0001	0.0143	0.0140	3.39%	4.99%
AAD %					6.23%	6.84%

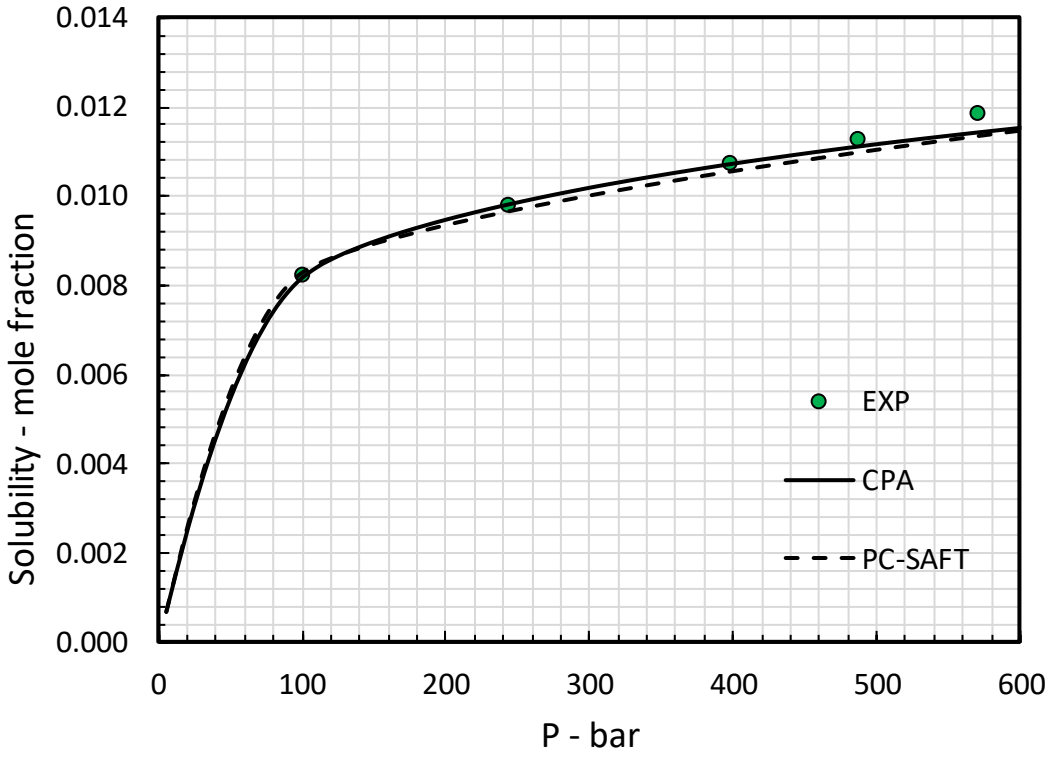

Figure 3.38 Calculated and measured CO_2 solubility in the salt mixture aqueous solution at 50 °C

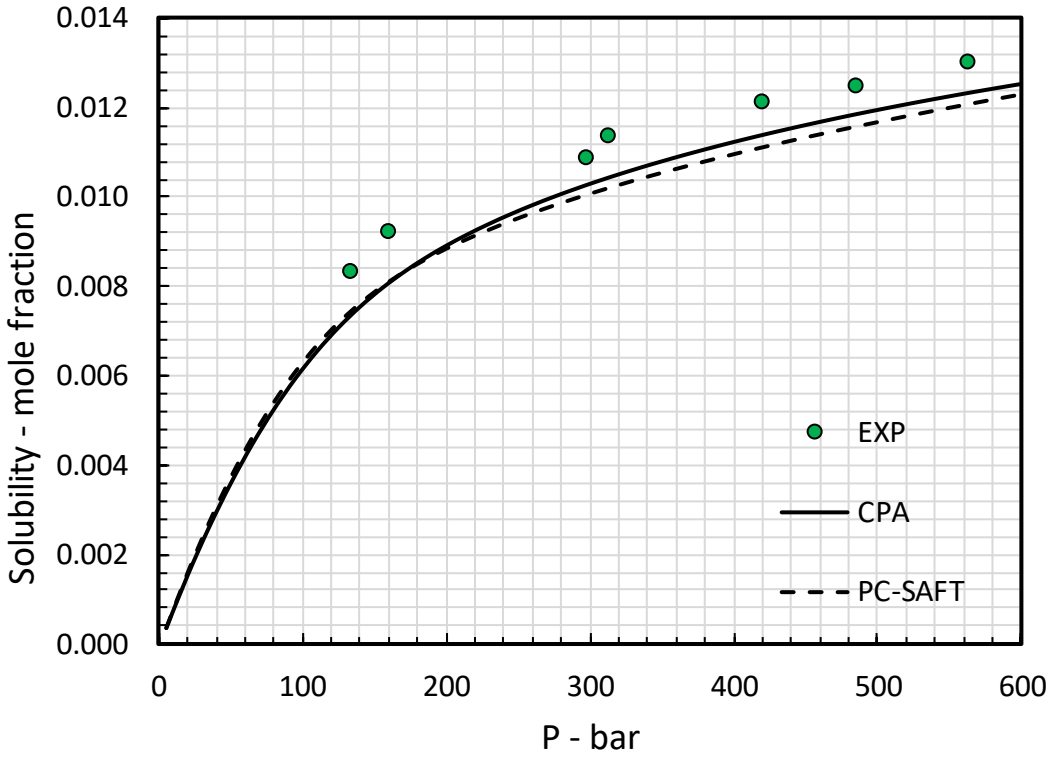

Figure 3.39 Calculated and measured CO_2 solubility in the salt mixture aqueous solution at 100 °C

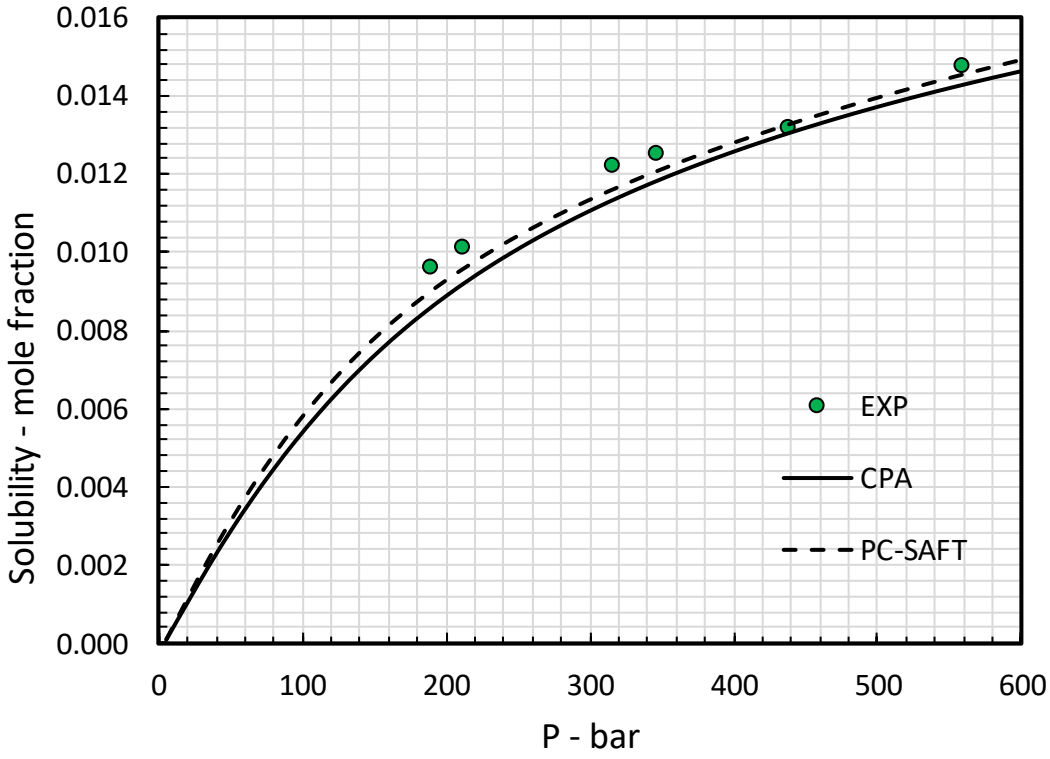

Figure 3.40 Calculated and measured CO_2 solubility in the salt mixture aqueous solution at 150 °C

3.4 Summary and Conclusion

In this chapter, a brief review of the studies involved CO_2 solubility measurements in pure water and/or aqueous solutions of salts was presented, and the gaps in the temperature and the pressure range covered in the literature were recognised. It was shown that the CO_2 solubilities in pure water and aqueous solutions of sodium chloride were studied extensively in the literature. However, the datasets found for solubilities in NaCl aqueous solutions at low temperatures (T<10 °C) were limited to low pressures (atmospheric pressures). Hence, CO_2 solubilities in various concentrations of NaCl aqueous solutions were measured at -10 °C to 150 °C and pressures up to the hydrate dissociation pressure of the system at each test temperature.

Two equation of states, specifically, the PC-SAFT and the CPA, were used to validate the experimental results. The binary interaction parameter of CO_2-NaCl was adjusted to the experimental results of this work and model calculations were compared to predicted solubilities using the Duan model [295] where excellent agreements were found between models calculated solubilities. However, it was observed that the calculated CO_2 solubilities using the PC-SAFT and the CPA EoSs at relatively low temperatures (T<30 °C) and high pressures (P>200 bar) differ from those calculated using Duan model. It was

suggested that as the datasets used for tuning the Duan model at low temperatures were limited to low pressures, the calculated solubilities using the PC-SAFT and the CPA models are closer to the actual behaviour of CO_2-NaCl aqueous solution system at such conditions.

The experimental data of CO_2 solubility in potassium chloride aqueous solutions were found to be reported at broad ranges of temperatures and salinities. However, the pressure range covered was limited to 200 bar. To fill this gap, CO_2 solubility measurements were conducted in 10, 15 and 22 wt% of KCl aqueous solutions at 50 °C < T < 150 °C and pressures up to 548 bar. The PC-SAFT and the CPA EoSs were adjusted to the measured solubilities. It was shown that by employing the BIPs optimised using this work solubility data, the PC-SAFT and the CPA model can correlate the literature solubility data very well.

The experimental results of CO_2 solubility measurements in different concentrations of calcium chloride aqueous solutions at 50 °C < T < 150 ° C and pressure up to 595 bar were reported. The PC-SAFT and the CPA EoSs were adjusted to literature data, and model calculations were compared with this work measured solubilities. Excellent agreements were found between model calculations and experimental results.

Comparing to NaCl, KCl and $CaCl_2$, limited experimental data were found in the literature for CO_2 solubilities in magnesium chloride aqueous solutions. Among totally four solubility datasets obtained in the literature, only one dataset was reported at pressures up to 400 bar. Therefore, CO_2 solubilities in various salinity of $MgCl_2$ aqueous solutions were measured at 50 °C < T < 150 °C at pressures up to 544 bar. The PC-SAFT and the CPA EoSs were adjusted to literature data, and model calculations were compared to measured solubilities. Slight deviations between model calculations and experimental results were obtained indicating the experimental data obtained in this work comply with those reported in the literature.

The solubility of CO_2 in a mixture of salts aqueous solutions were also measured at T=50, 100 and 150 °C and pressure up to 571 bar. Using adjusted models, calculated solubilities were compared to experimental results. Model calculations and experimental results were in good agreement, and the deviations were similar to those observed for CO_2 and 22 wt% NaCl aqueous solution.

Chapter 4

4 –Water Content Measurements

4.1 Introduction

Produced natural gas from underground sources is saturated with water. Natural gas must pass through several pre-treatment stages including gas sweetening and gas dehydration where the sulphur and the moisture content of the gas are removed. H_2S is very toxic and in the presence of free water can be converted to very corrosive acids that severely damage the pipeline. The mositute content of natural gas is removed in the dehydration stage to inhibit hydrate formation and water condensation in the pipelines or in the compressors. The water content of the acid gases in carbon Capture and Storage (CCS) scope of work is one of the critical parameters in flow assurance engineering and equipment design. CO_2 as a hydrate former can form hydrates in the transportation pipelines depending on the transporting conditions and the water content of the CO_2-rich fluid which can result in a reduction of pipeline flow capacities, pipeline blockage or potential damage to process facilities including filters, valves and compressors.

Furthermore, the phase equilibria behaviour of water and acid gases like CO_2 or H_2S are slightly different than conventional hydrocarbons or atmosphere gases like O_2 or N_2. For instance, it has been observed that the water content of CO_2 -rich or H_2S-rich fluids shows a retrograde behaviour with respect to the pressure changes. In other words, by increasing the pressure of the system up to the bubble point pressure of the CO_2-rich phase, the water content of the gas phase decreases. However, for binary systems of CO_2-water, by further pressurising the system above the saturation pressure of the system, when the liquid CO_2-rich phase is formed, the water solubility in the non-aqueous phase is increased as the CO_2-rich phase tends to dissolves more water when it is in a liquid state. Equation of states with conventional mixing rules cannot capture the above-mentioned retrograde behaviour. Hence, as discussed in Chapter 2, to model aforementioned retrograde behaviour, a new parameter is introduced to the association term of the equation of state to be tuned with experimental data of CO_2-water mutual solubilities.

Therefore, a good understanding on the phase equilibria of CO_2-rich or natural gas systems in the presence of pure water or brine is essential in modelling and design of the CCS-related processes.

Mutual solubilities of CO_2-water system have been extensively studied in the literature so far. Numerous experimental datasets have been reported on the CO_2 and water mutual solubility over broad ranges of temperature and pressure. Yan et al. [447] and Zirrahi et al. [448] presented extensive reviews on the CO_2-water phase equilibria measurement studies reported in the literature. In this study, ninetheen datasets with around 376 data points were gathered for the water content of CO_2 in equilibrium with pure water.

Table 4.1 Experimental datasets of pure CO_2 water content in equilibrium with distilled water reported in the literature

Temperature range K	Pressure range bar	Reference
298.15–373.15	17.3–51.5	[342]
285.15–348.15	25.3–709.3	[332]
323.15–348.15	101.33–152	[334]
287.2–318.73	4.6–79.63	[340]
288.75–366.45	6.9–202.7	[294]
323.15–373.15	200–500	[382]
285.15–304.2	6.9–137.9	[449]
373.15	3.2–23.07	[392]
373.15 -413.15	3 - 32	[450]
323.15–353.15	40.5–141.1	[451]
323.15	68.2–176.8	[333]
323.15	101–301	[394]
298.2	36 - 64	[335]
288.15–313.15	60–243	[341]
288.15	20 – 85	[452]
422.98 – 498.35	39 -1290	[337]
348.15	103.4–153.1	[411]
288.15-313.15	51-102	[341]
298.15-448.15	10-170	[336]

The temperature and pressure ranges covered are from 285.15 K to 498.15 K and from 1 bar to 1290 bar respectively. The dataset reported by Valtz et al. [340] includes a broad

range of temperature from 287.2 K to 318.15 K and pressures from 4.6 bar to 79.63 bar while the water content measurements reported by Tabasinejad et al. [337] covers the water contents of CO_2-rich phase at high temperatures i.e. from 422.98 K to 498.35 K and pressures up to 1290 bar. Table 4.1 lists all the experimental datasets gathered together with the temperature and pressure ranges covered by each dataset.

The water content of CO_2-rich phases in equilibrium with pure water has also been investigated in the literature. Examples are, the experimental water content data reported by Yarisson et al. at temperature above 304.15 K at pressures up to 1000 bar for different binary mixtures of CO_2 with methane and ethane [453]. Song and Kobayashi have also measured water content for a mixture of 95% CO_2 and methane [454]. Huang et al. [459] reported the water content in 2 ternary mixtures of CO_2, H_2S and methane at elevated temperatures and pressure. Even though the CO_2 solubility has been widely measured in aqueous solutions of different salt types with various concentrations at a broad range of temperatures and pressures, to our knowledge, there is no experimental data available for the water content of CO_2-brine systems in the literature.

4.2 Experimental Equipment, Materials and Procedures

4.2.1 Materials

High purity research grade CO_2 (99.995%), with less than 49 ppm of impurities, was purchased from Air Products. The 99% pure sodium chloride, has been bought from ALDRICH and Fisher chemistry for CO_2 water content measurements in equilibrium with brines. Deionized water was used for all measurements. For methane water content measurements, research grade methane with a stated purity of 99.99% was used. The synthetic gas mixtures entitled MIX1, MIX6, SYNGAS1 and SYNGAS2 with certified compositions were supplied by Air Products Ltd.

4.2.2 Experimental equipment

- *Low-temperature water Content measurements ($T \leq 25$ °C)*

The experimental setup for low water content measurements is comprised of an equilibrium cell placed on a rocking rig, an HPLC pump and a setup for measuring the water content of equilibrated fluids. The equilibrium cell is a 300 ml, Titanium piston vessel rated to 690 bar. A schematic of the rig is shown in Figure 4.1. The equilibrium cell is housed inside a jacket which is connected to a bath. The bath can maintain the temperature of the circulating fluid through the jacket within ±0.1 °C of the temperature setpoint and can be operated at temperatures between -90 °C and 100 °C. The cell

temperature was monitored using a PRT (Platinum Resistance Thermometer) located in the jacket. Any difference between the temperature of the jacket and the equilibrium cell was accounted for by measuring the temperature variations using a reference probe located in the cell. The temperature probe was calibrated against a platinum resistance probe that has a certificate of calibration issued in accordance with NAMAS Accreditation Standard and NAMAS Regulations. The pressure of the equilibrium cell was monitored using a strain gauge pressure transducer and its accuracy was checked using a Budenberg dead weight tester. A HITACHI MERCK L-6000 pump was also used for injecting the brine into the cell to maintain the pressure of equilibrium cell constant during sampling.

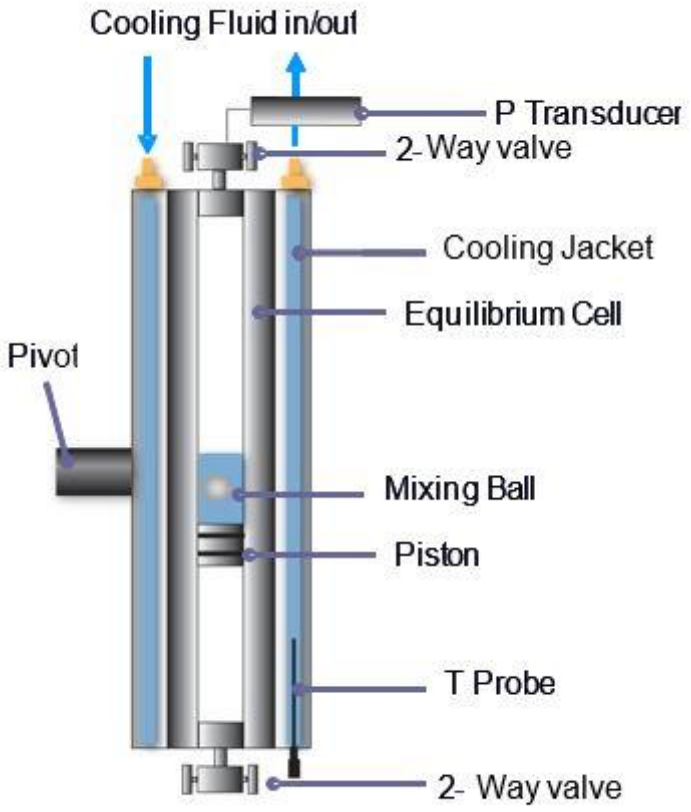

Figure 4.1 Schematic illustration of rocking type rig.

The water content measurement setup used for low-temperature conditions ($T \leq 25$ °C) is comprised of a heated line, a Yokogawa TDLAS and a flow meter as shown in Figure 4.2. TDLAS stands for Tunable Diode Laser Absorption Spectroscopy which is a method for detecting and measuring the amount of some materials (e.g. water) in a gaseous mixture. TDLAS method is based on the capability of gases in the rotational vibrational absorption. When the beam passes through a gas mixture with some moisture content, the water molecules absorbs the energy on the beam which reduces the signal intensity. This

reduction in the energy of the beam is detected at the end of the path by a receiver. The water content of the gas or other properties are then calculated using the Lambert-Beer law [456] which relates the light intensity before and after passing through a gas mixture, with the concentration of the species in the gas mixture at specified temperature and pressure. More details on the TDLAS technique can be found elsewhere [457].

A back-pressure regulator is placed between the TDLAS and the flow meter to maintain the pressure of the gas passing through the TDLAS. The Yokogawa TDLAS must to be operated with gas flowing through at 50 °C and 0.34 barg and can measure water content up to 3000 ppm (This is the reason that this setup was only used for water content measurements at low-temperatures). The accuracy is stated to be ±1% of the reading. A schematic and a picture of the Yokogawa TDLAS set-up is shown in Figure 4.3 and Figure 4.4.

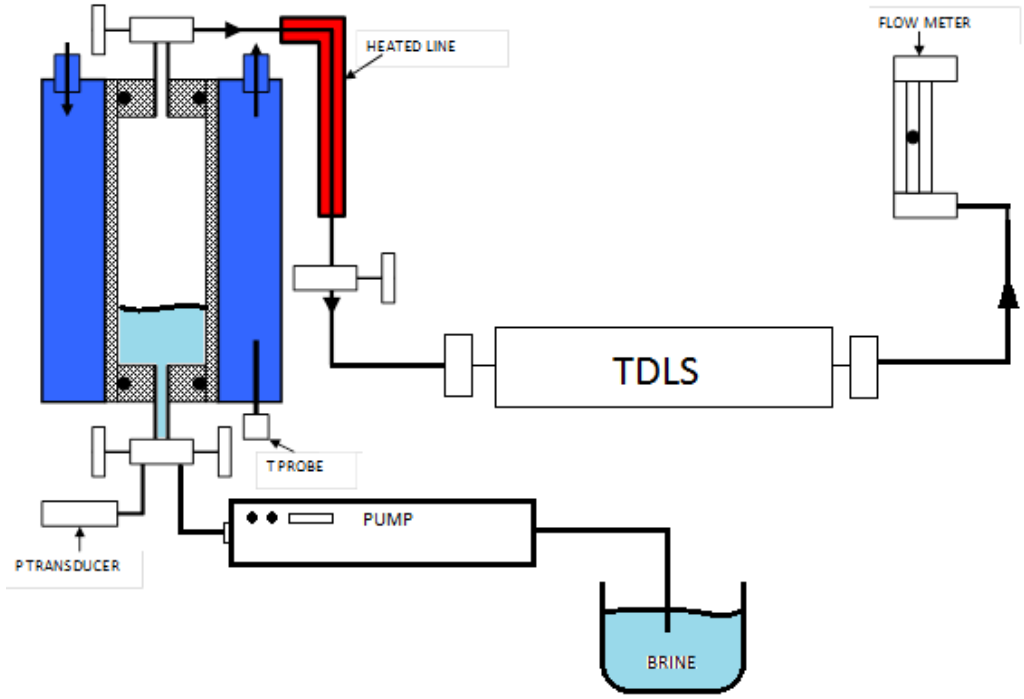

Figure 4.2 Schematic showing equilibrium cell and water content measurement set-up.

Figure 4.3 Picture of Yokogawa TDLAS.

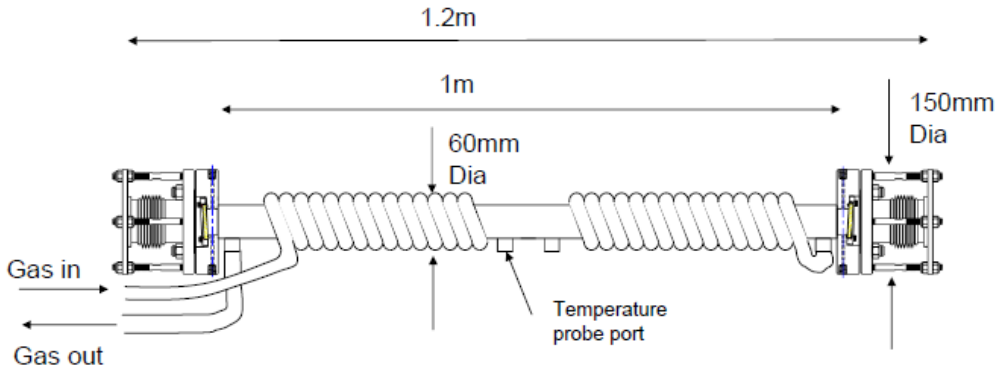

Figure 4.4 Schematic of Yokogawa TDLAS setup.

➢ *High-temperature water content measurements (T ≥ 50 °C)*

The test fluids were equilibrated with water inside a 600 ml titanium piston vessel rated to 690 bar. Another cylinder was also used for high pressure tests which can be used at pressures up to 1380 bar and temperatures up to 204 °C. The cell was placed in the Chandler 3000-GL PVT system (shown in Figure 4.5) to maintain the temperature of the equilibrium cell constant at each test temperature. Samples were taken from the equilibrium cell via a Winkler heated line, maintained at 200 °C to either EdgeTech DewMaster chilled mirror hygrometer (Figure 4.7) or Hewlett Packard 5890 Series II Gas Chromatograph (GC) which is fitted with a Poropak-Q column. The GC is also equipped with a six-port external sample injector (type 1/16) which is placed inside an oven set at 200 °C. The flow rate of the samples through the heated valve was measured using a Platon flow meter. The chilled mirror hygrometer can measure dew/frost point at

temperatures from -75 °C to 100 °C, at pressures up to 20 bar, with a resolution of 0.1 °C and accuracy of ±0.2 °C. A picture of the heated line, external sample injector, and GC and Chandler PVT system picture are shown in Figure 4.5 and Figure 4.6.

4.2.3 Experimental procedure

- *Low-temperature water content measurements ($T \leq 25$ °C)*

Around 2-3 ml of brine was initially loaded into the cell at the beginning of the test. The cell temperature was then reduced to -10 °C and the air inside was evacuated before injecting the test gas. The cell temperature and pressure were then set to the desired test conditions. The cell temperature was then cycled to lower and higher temperatures than the set point over at least 20 hours. To check whether the equilibration time is sufficient for the system to reach equilibrium, the measurements were repeated over a number of days for one test. It was confirmed that the water content remained stable.

Once equilibrium had been achieved the valve at the top of the cell was opened to fill the heated line up to the valve before the TDLAS and at the same time brine with the same concentration as the brine being tested was introduced into the base of the cell to keep the pressure of cell constant. The brine was injected into the cell using a HITACHI MERCK L-6000 pump to prevent the increase of salt concentration in the aqueous solution due to the evaporation of water during the test and maintaining the pressure constant by adjusting a constant flow rate of brine into the cell during the test. In the next step, the valve before the TDLAS was gradually opened to adjust a flow rate of between 0.1 and 0.3 litres per minute through TDLAS. The water content of the gas was then monitored until it was stable for at least 15 minutes. During sampling the heated line was maintained at a temperature of 100 °C to prevent water liquefaction in the line. After each test, the solution was flushed from the bottom of the cell and a fresh solution injected into the cell for a new measurement.

- *High-temperature water content measurements ($50\ °C < T$)*

At the start of the test, the equilibrium cell was loaded with 10 ml of deionized water and evacuated before injecting the test gas. The test fluid was then injected into the cell and the cell was heated to the desired temperature. An equilibration time of at least 24 hours was given for the cell to reach the set temperature and for the fluids to be equilibrated. When the system reached equilibrium, samples were passed through the cell via the

heated line to the GC. To keep the cell pressure constant during the sampling, the hydraulic fluid with adjusted flow rate was injected behind the piston in the equilibrium cell. The flow rate of samples through the heated valve was kept between 200 and 500 ml per minute during measurements.

Figure 4.5 Chandler 3000-GL PVT system

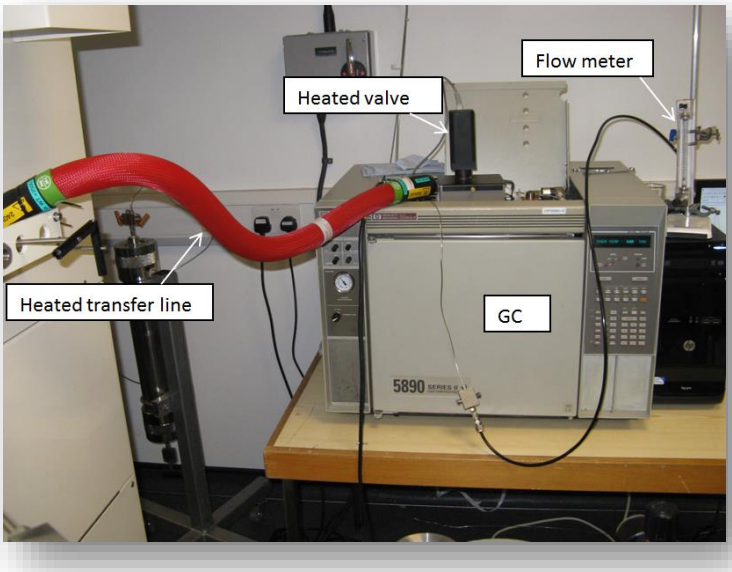

Figure 4.6 Picture showing heated transfer line, heated valve and Hewlett Packard 5890 Series II GC.

Figure 4.7 Picture of EdgeTech DewMaster used to make water content measurements.

- *GC calibration*

Due to the very high moisture content of CO_2-rich systems at high temperatures and based on the on the existing laboratory equipment, the gas chromatography method was chosen to measure the water content of the test fluid at elevated temperatures and pressures. Basically, in gas chromatography, a sample is vapourised (a sample which is chemically stable at vapourising temperature) and injected into a chromatographic column where the compounds are separated. The test fluid is then transported through the column by the flow of an inert gaseous phase called "carrier gas". Helium was used as carrier gas in our measurements. The separated gas is then pass through the detectors where the response of each sensor are sent to the acquisition interface for each exposed compound. As the result, single or multiple peaks with different peak areas and retention times are shown in the acquisition interface for each compound. The carrier gas flow rate was adjusted to 25 ml/min to obtain a maximum sensitivity of the detector (thin peaks), Two detectors were used to analyse the samples, a Thermal Conductivity Detector (TCD) and a Flame Ionization Detector (FID). The TCD measures the variation of the thermal conductivity of the carrier gas continuously while the FID measures the compound capabilities to form ions when it goes through the flame. Because the sample gas is burned in the FID detector, it is located at the outlet of the TCD to prevent the sample components decompositions.

The GC was calibrated for each compound involved in our water content measurement i.e. CO_2, water, and methane. For measuring the content of methane, the FID detector was used and to measure the content of CO_2 and water the TCD detector was used. Figure 4.8,

Figure 4.9 and Figure 4.10 show the calibration curves of CO_2, methane and water respectively.

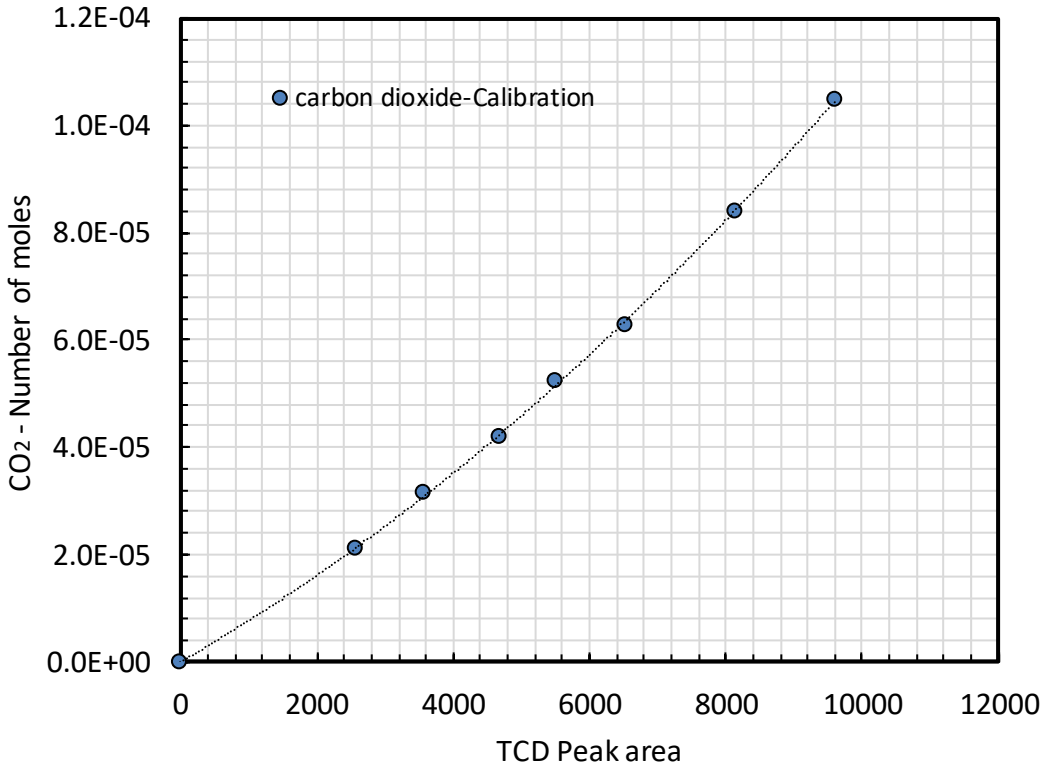

Figure 4.8 TCD CO_2 calibration curve

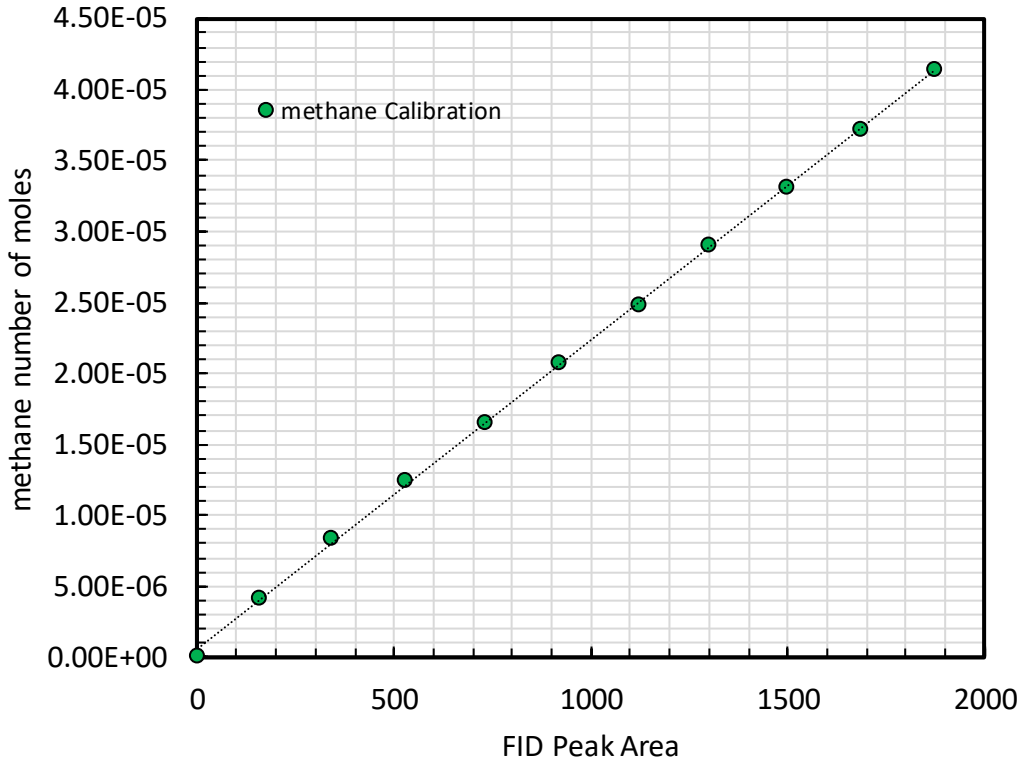

Figure 4.9 FID methane calibration curve

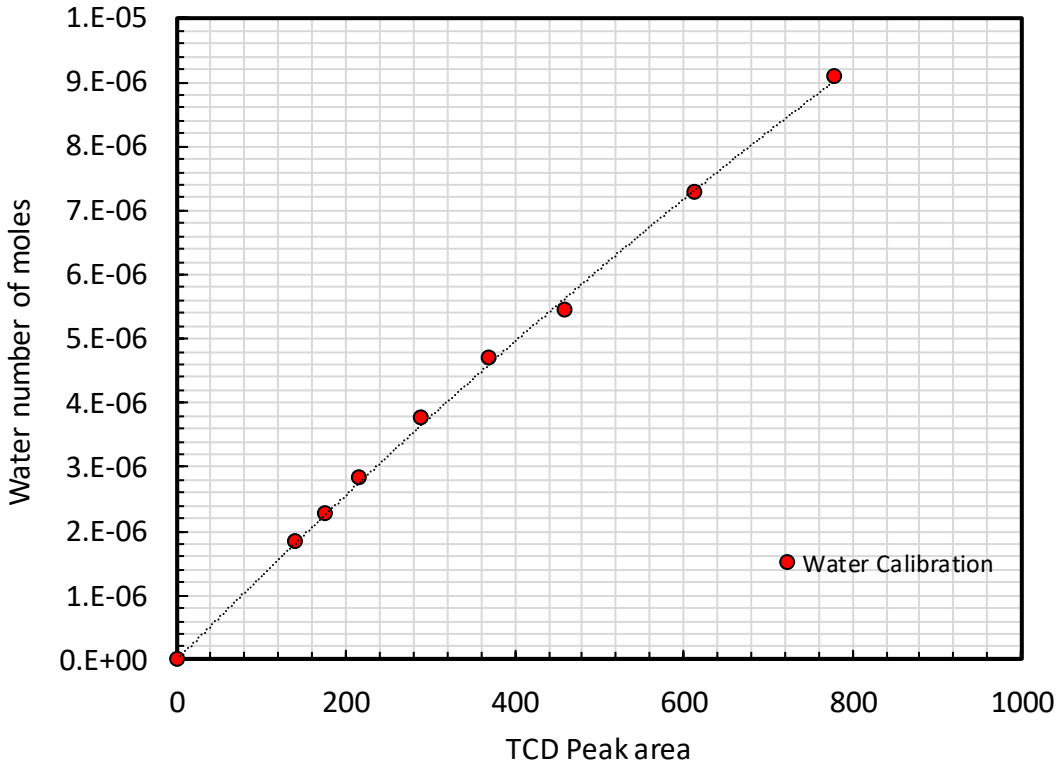

Figure 4.10 TCD water calibration curve

4.3 Experimental Results

In this section, the experimental results of water content measurements are presented. The experimental data are divided into two main sections, the measured water content data at temperatures below 25 °C and temperatures above 50 °C.

4.3.1 Water content measurements at low temperatures (T ≤ 25 °C)

- *Water content of methane measurements results*

To test whether the setup and procedures used for measurements below 25 °C are reliable, the water content of pure methane in equilibrium with distilled water or hydrates were measured. Table 4.2 and Table 4.3 summarize the water content measurement results of methane at temperatures below 15 °C down to -40 °C in the presence of water or hydrates.

The uncertainties for water content data is ±1% or 4 ppm of the reading whichever is greater. As can be seen from Table 4.2 and Table 4.3, with decreasing the temperature the AAD % from model calculations is increased. Also, based on the calculated hydrate dissociation pressure of the methane-water system, the states of the system at each temperature and pressure are specified in Table 4.2 and Table 4.3 as VLE and VHE[1]. At

[1] Vapour-Liquid-Hydrate Equilibrium

-5 °C, -20 ° C and -40 °C temperatures where all test pressures are higher than the hydrate dissociation pressure and methane is in equilibrium with hydrate, the deviation from the model is considerably high.

Table 4.2 Measured and calculated methane water content in the presence of hydrates/water at different conditions

Equilibrium state	Pressure	Measured water content	Model Calculation			
					Deviations	
	bar	ppm	CPA	PC-SAFT	CPA	PC-SAFT
15 °C						
VLE	35.5	550	555	556	0.85%	1.09%
VLE	52.7	378	401	403	6.14%	6.60%
VLE	101	248	258	260	3.86%	5.02%
VHE	138.9	209	218	223	4.17%	6.52%
VHE	207.8	167	182	188	9.17%	12.72%
VHE	276.8	155	165	171	6.61%	10.37%
VHE	380.2	146	149	155	2.32%	5.99%
VHE	483.6	143	138	143	3.37%	0.02%
AAD %					4.56%	6.04%
5 °C						
VLE	18.3	577	518	519	10.15%	10.08%
VLE	35.5	292	289	290	0.90%	0.65%
VHE	52.7	202	207	206	2.61%	2.15%
VHE	101	115	128	126	11.26%	9.74%
VHE	138.9	99	110	107	10.75%	8.32%
VHE	207.8	82	96	94	17.45%	14.10%
VHE	276.8	75	89	87	19.30%	15.85%
VHE	380.2	70	83	80	17.95%	14.60%
VHE	483.6	61	77	75	26.72%	23.24%
AAD %					13.01%	10.97%
-5 °C						
VLE	18.3	262	254	254	3.22%	3.03%
VHE	35.5	127	129	128	1.44%	1.13%
VHE	52.7	88	91	90	2.90%	2.37%
VHE	101	52	59	58	12.75%	11.19%
VHE	138.9	43	52	51	21.27%	18.70%
VHE	207.8	40	48	47	19.49%	16.72%
VHE	276.8	37	45	44	22.84%	20.17%
VHE	380.2	32	43	42	33.81%	31.06%
VHE	483.6	29	41	40	40.05%	37.31%
AAD %					17.53%	15.74%

Table 4.3 Measured and calculated methane water content in the presence of hydrates/water at different conditions

Equilibrium state	Pressure	Measured water content	Model calculation			
					Deviation	
	bar	ppm	CPA	PC-SAFT	CPA	PC-SAFT
-20 °C						
VHE	18.3	69	62	61	10.41%	10.99%
VHE	35.5	35	32	32	7.23%	7.94%
VHE	52.7	21	23	23	11.82%	10.83%
VHE	101	16	17	17	5.19%	3.47%
VHE	138.9	14	16	16	14.94%	12.77%
VHE	207.8	12	16	16	31.79%	30.17%
VHE	276.8	12	16	15	29.83%	28.68%
VHE	380.2	10	15	15	51.32%	50.25%
VHE	483.6	9	15	15	62.53%	61.66%
AAD %					25.01%	24.08%
-40 °C						
VHE	18.3	8.5	7	7	13.18%	15.79%
VHE	35.5	7.6	4	4	46.45%	48.03%
VHE	52.7	4.6	3	3	32.00%	33.93%
VHE	101	1.7	3	3	67.72%	63.12%
VHE	138.9	2.8	3	3	9.81%	8.49%
VHE	276.8	3.3	3	3	2.42%	3.03%
AAD %					28.59%	28.73%

Figure 4.11 demonstrates the water contents of methane at -40 °C to 15 °C as the function of pressure. The hydrate dissociation pressures at each temperature are also displayed to specify the region where methane is in equilibrium with hydrate phase. As seen in Figure 4.11 at each pressure, the water content of methane is decreased with decreasing the temperature and at a constant temperature, the water content of methane is decreased as the pressure incerases.

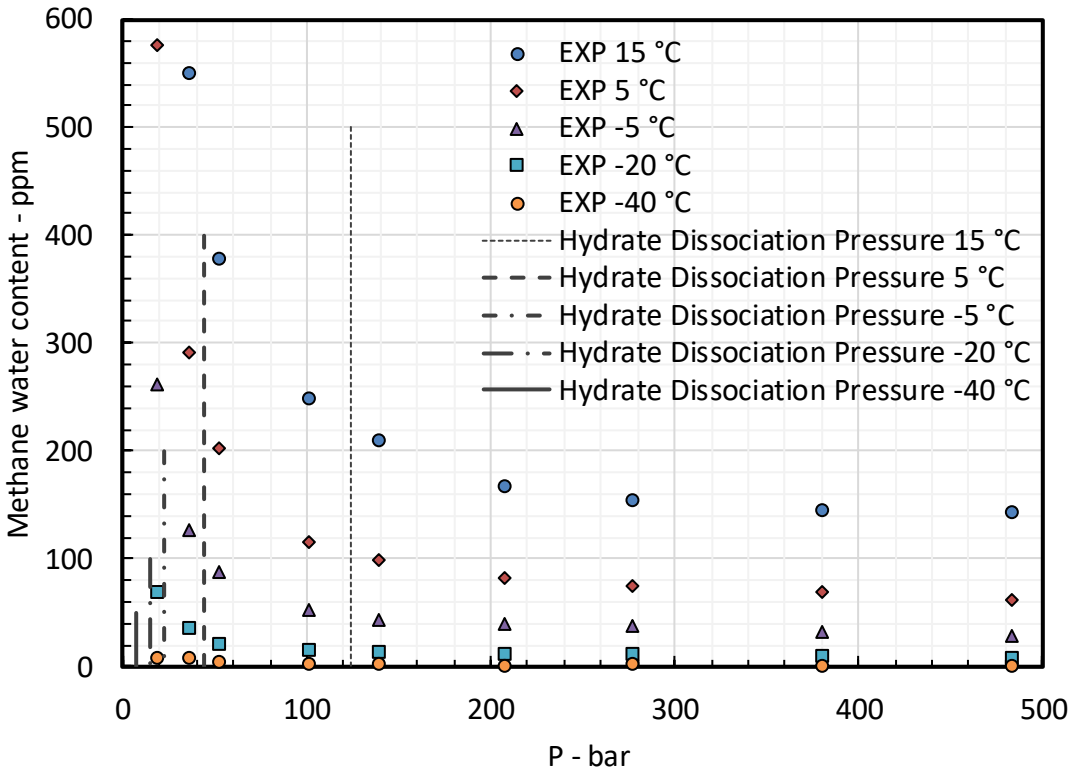

Figure 4.11 Measured methane water content in equilibrium with hydrate/water at -40 °C to 15 °C and pressures up to 500 bar

Figure 4.12 and Figure 4.13 compare the experimental results, literature and calculated water content of methane in equilibrium with water or hydrates. As illustrated in Figure 4.12 and Figure 4.13, the performance of the CPA and the PC-SAFT EoSs are quite similar in calculating the methane water content. Despite the relatively high deviation between model calculation and experimental results at low-water content conditions, i.e. low-temperatures and high pressures where hydrates present (VHE states), model calculations correlate the experimental results of VLE states very well with slight deviations.

The measured methane water contents were also compared with water content data reported by Althaus et al. [458] and Chapoy et al. [459]. As demonstrated by Figure 4.12 and Figure 4.13, at 15 °C, -5 °C and -20 °C where literature data were available, excellent agreements were found between this work experimental results and those reported by others. However, at 15 °C and pressures above 10 bar, measured water contents and literature (the data reported by Chapoy et al.[459]) differ to some extent. As the experimental results of this work agree with calculated water contents using the models that were adjusted to braod ranges of pressures and temperatures, it is concluded that the experimental results of this work are more accurate.

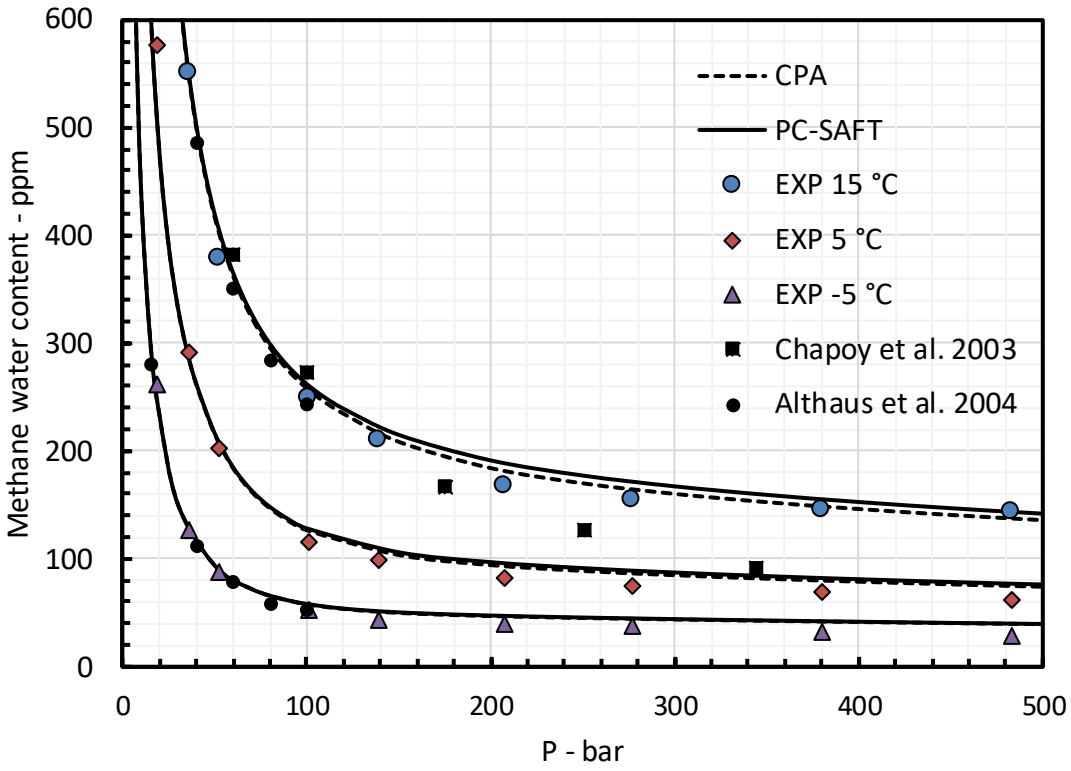

Figure 4.12 Comparison of calculated and measured water content of methane with experimental data reported in the literature (literature experimental data at 15 °C taken from [458], [460]**, at -5 °C from** [458]

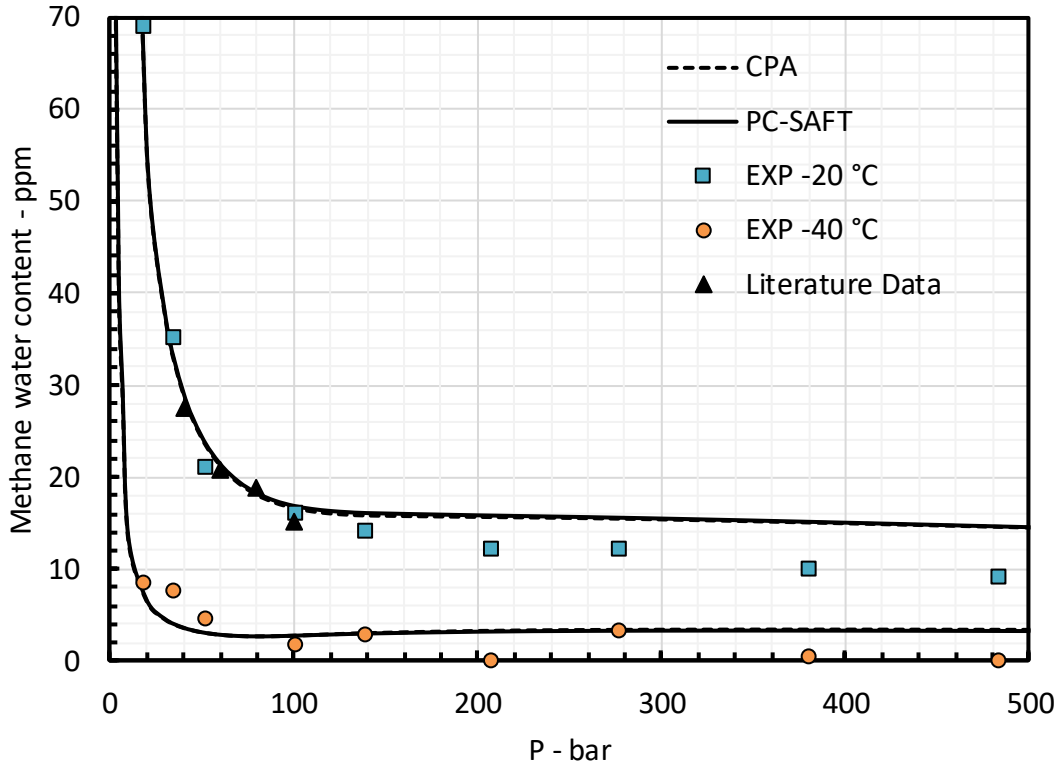

Figure 4.13 Comparison of measured water content of methane with experimental data reported in the literature (literature experimental data at -20 °C taken from [458]**)**

➢ *Water content of CO_2 in equilibrium with brine*

The water content of CO_2 in equilibrium with 10 wt% and 20 wt% of NaCl aqueous solutions were measured at pressures below the hydrate dissociation pressure of the system. The water content of CO_2 in equilibrium with 10 wt% and 20 wt% NaCl solution was measured at 0 °C to 25 °C and -5 °C to 25 °C respectively. Forty-three date points are reported in Table 4.4, Table 4.5 and Table 4.6 together with the calculated water content and hydrate dissociation pressures at each temperature. The uncertainty of measured water content data is ±1% or 4 ppm whichever is greater.

Table 4.4 Measured water content of CO_2 in equilibrium with 10 wt% NaCl aqueous solution. (Temperature error is ±0.1 °C and pressure error is ± 0.4 bar)

T = 25 °C		**T = 15 °C**		**T = 9.8 °C**		**T = 5 °C**		**T = 0 °C**	
Hydrate Dissociation Pressure - bar									
$P_{Dissociation}$>2000		**1300.326**		**544.98**		**72.95**		**20.89**	
P-bar	**y_w - ppm**	**P-bar**	**y_w – ppm**	**P-bar**	**y_w - ppm**	**P-bar**	**y_w - ppm**	**P-bar**	**y_w - ppm**
35.50	1100	38.60	716	18.25	865	18.25	580	17.29	450
57.56	1107	72.74	1801	73.43	1790	27.63	434		
		111.91	2164	103.70	1886	30.25	428		
		140.67	2233	201.70	2012				
		169.98	2274	310.25	2095				
		238.74	2350						
		323.08	2550						
AAD %		**AAD %**		**AAD %**		**AAD %**		**AAD %**	
CPA	*PC-SAFT*	*CPA*	*PC-SAFT*	*CPA*	*PC-SAFT*	*CPA*	*PC-SAFT*	*CPA*	*PC-SAFT*
6.3	8.46	14.47	25.22	11.61	22.13	6.99	14.71	9.76	15.46

Figure 4.14 and Figure 4.15 compare the measured CO_2 water content at various temperatures in equilibrium with 10 wt% and 20 wt% NaCl aqueous solutions respectively. As can be seen from Figure 4.14 and Figure 4.15, at the constant pressure, with decreasing the temperature, the water content of CO_2 in equilibrium with different concentrations of brine is decreased, and the data are qualitatively consistent. Furthermore, as seen in Figure 4.14 and Figure 4.15 the trend of water content with respect to the pressure is changed after the bubble point pressure of CO_2 where more water are dissolved in the CO_2-rich phase.

Table 4.5 Measured water content of CO_2 in equilibrium with 20 wt% NaCl aqueous solution. (Temperature error is ±0.1 °C and pressure error is ± 0.4 bar)

T = 25 °C		T = 15 °C		T = 10 °C	
$P_{Dissociation}$>2000					
P-bar	**y_w - ppm**	**P-bar**	**y_w - ppm**	**P-bar**	**y_w - ppm**
35.50	968	19.50	945	24.19	595
50.67	970	34.94	637	30.53	471
104.46	2360	82.12	1923	207.50	1821
		133.01	2067	332.60	1908
		192.67	2171		
		239.98	2209		
		305.84	2365		
		392.46	2399		
AAD %		**AAD %**		**AAD %**	
CPA	PC-SAFT	CPA	PC-SAFT	CPA	PC-SAFT
10.00	12.78	8.85	19.52	9.59	18.97

Table 4.6 Measured water content of CO_2 in equilibrium with 20 wt% NaCl aqueous solution. (Temperature error is ±0.1 °C and pressure error is ± 0.4 bar)

T = 5 °C		T = 0 °C		T = -5 °C	
945.64		**305.86**		**25.18**	
P-bar	**y_w - ppm**	**P-bar**	**y_w - ppm**	**P-bar**	**y_w - ppm**
20.81	494.19	22.19	384	22.46	276
32.12	431	20.32	428		
205.36	1588	96.53	1313		
321.70	1663	207.50	1379		
		317.98	1430		
AAD %		**AAD %**		**AAD %**	
CPA	PC-SAFT	CPA	PC-SAFT	CPA	PC-SAFT
12.03	20.64	17.43	17.43	22.71	30.13

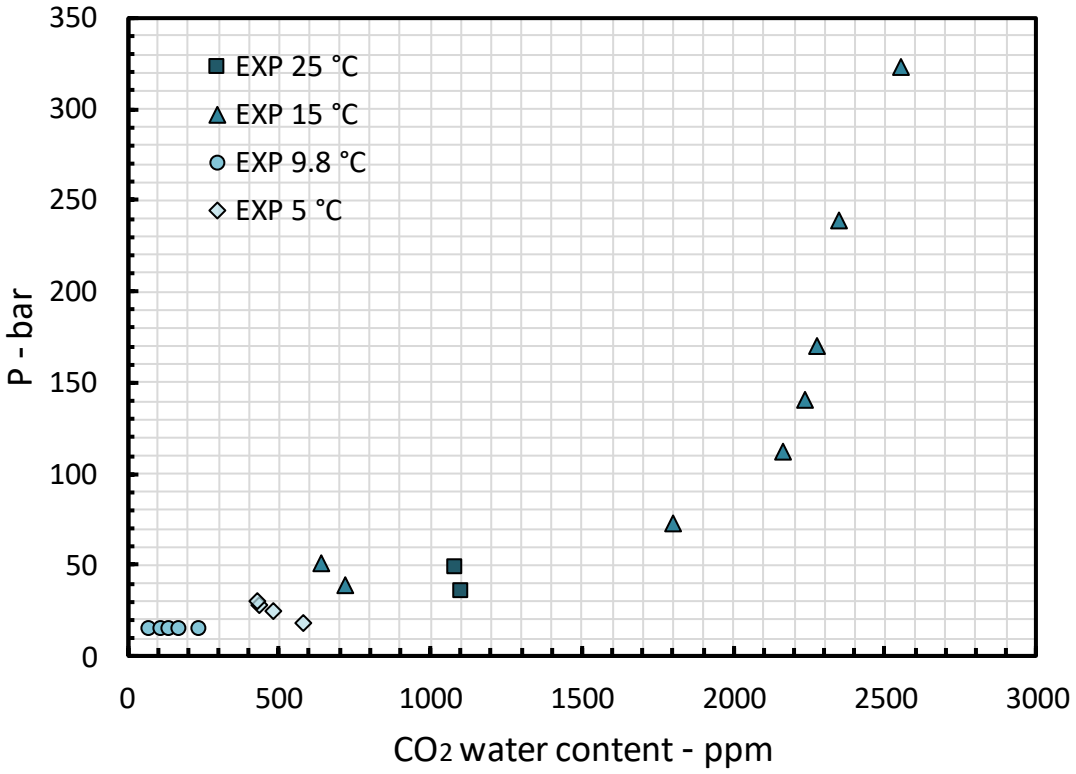

Figure 4.14 Measured CO_2 water content in equilibrium with 10 wt% NaCl aqueous solution at 5 °C to 25 °C

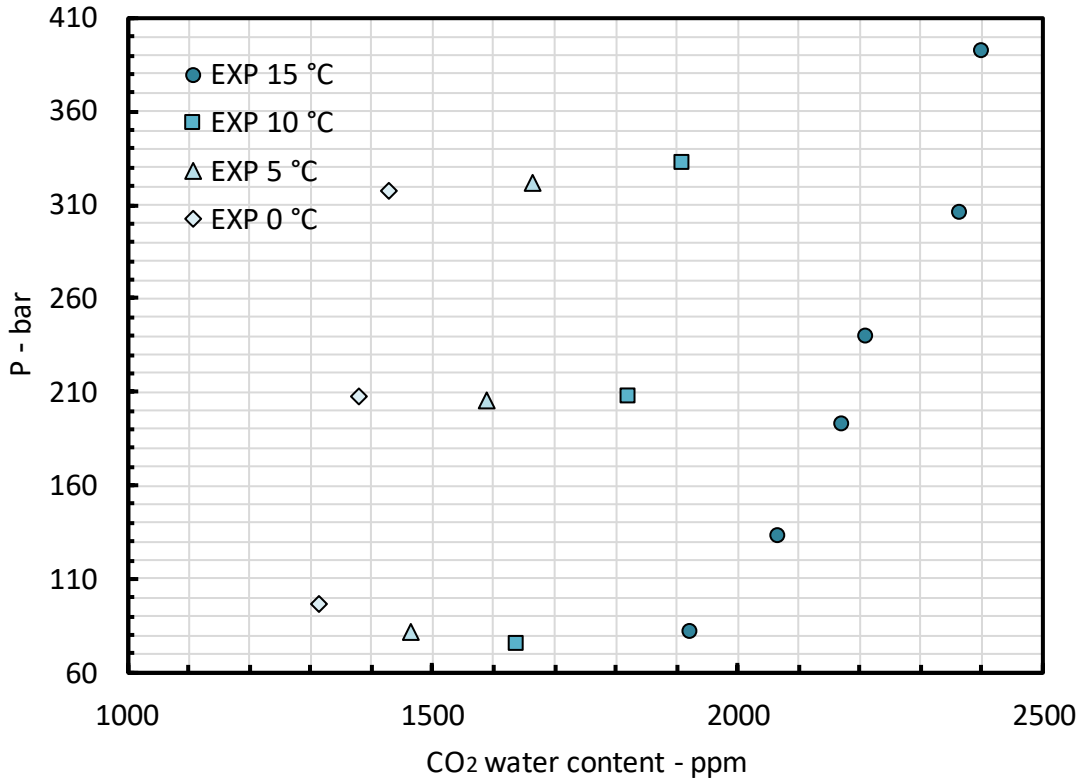

Figure 4.15 Measured CO_2 water content in equilibrium with 20 wt% NaCl aqueous solution at 5 °C to 25 °C

Figure 4.16 compares the experimental results of CO_2 water contents in equilibrium with 10 wt% and 20 wt% NaCl aqueous solutions at the same temperature, 15 °C. As illustrated in Figure 4.13, the water content of CO_2 is lower when the salinity of brine increases due to the decrease in the activity of water in a higher salt concentration brine. This would affect the hydrate dissociation point of the system such that the hydrate dissociation pressure is increased and in the same way the hydrate dissociation temperature of the system is decreased due to the reduction of water available for hydrate formers to form hydrates. Based on our knowledge, there is no data for the water content of pure CO_2 or CO_2-rich phases in equilibrium with brine in the literature so far.

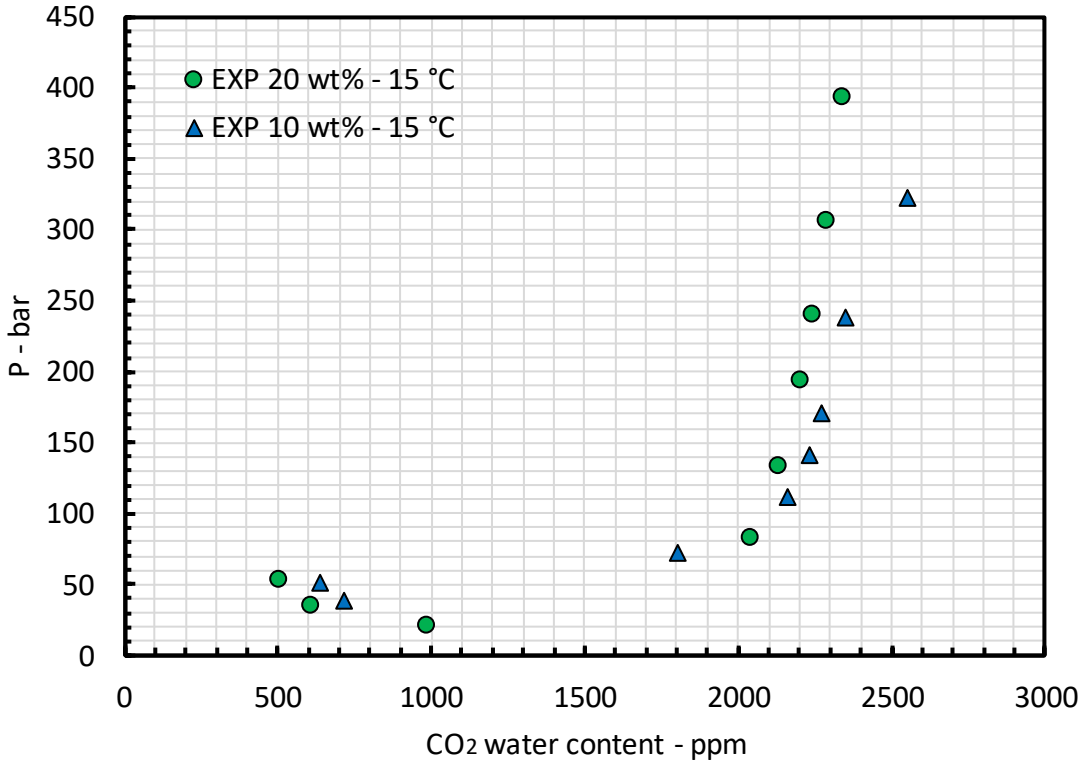

Figure 4.16 Comparisons of the measured water content of CO_2 in equilibrium with 10 wt% and 20 wt% NaCl aqueous solutions at 15 °C

The measured water content reported in Table 4.4 to Table 4.6 are compared with calculated water contents using the PC-SAFT and the CPA equation of states tuned with literature data (See Chapter 2) in Figure 4.17 to Figure 4.25. As displayed, the model can capture the retrograde behaviour of CO_2 water content trend with respect to the pressure at all temperatures and concentrations. Also, the CPA and the PC-SAFT models show relatively similar performance before the bubble point pressure of CO_2. However, the calculated water contents are slightly different at above bubble point pressures using the CPA and the PC-SAFT EoSs. The deviation between model calculations and experimental results are also small at below saturation point pressures, while at higher

saturation pressure of CO_2, the model calculation, and experimental results deviate considerably at all temperatures. The model calculations and experimental data of CO_2 water content in equilibrium with pure water and 10 wt% and 20 wt% NaCl aqueous solutions are compared in Figure 4.19 and Figure 4.22. As seen in Figure 4.19 and Figure 4.22, both calculated (using the same EoS) and measured water contents of CO_2 in equilibrium with brine are less than calculated and experimental CO_2 water contents in equilibrium with pure water which shows that experimental results are qualitatively consistent. Also, the agreement between the experimental and calculated CO_2 water contents in equilibrium with pure water is much better using CPA EoS compared to those calculated using PC-SAFT model. The reason for such an error obtained using PC-SAFT EoS is the temperature range used for tuning the model for CO_2 and water system. As explained in Chapter 2, because of the limited available experimental CO_2 water content data at temperatures below 293.15 K, the BIP and solvation parameter between water and CO_2 were optimised using the experimental data reported at 293.15 K up to 423.15 K. Therefore, it is also concluded that a percentage of the deviation between measured and calculated CO_2 water content in equilibrium with brine using PC-SAFT EoS is due to the error in modelling the phase equilibria of CO_2-water system. It is also suggested that as the solvation parameter (please refer to Chapter 2) was adjusted to the CO_2 and pure water mutual solubilities, the models cannot adequately calculate and capture the retrograde behaviour of CO_2 water content in equilibrium with aqueous solutions of salts.

Moreover, because the accuracy of the experimental setup and procedures we used to measure the CO_2 water content in equilibrium with brine was approved earlier in this chapter and on the other hand considering that excellent agreement obtained between the calculated and measured CO_2 water content below bubble point of CO_2, it is concluded that the measured data are correct but models are not able to correlate the liquid CO_2 water content properly. However, because there is no data available for CO_2 water content in equilibrium with brine, we cannot compare the experimental results with any literature data.

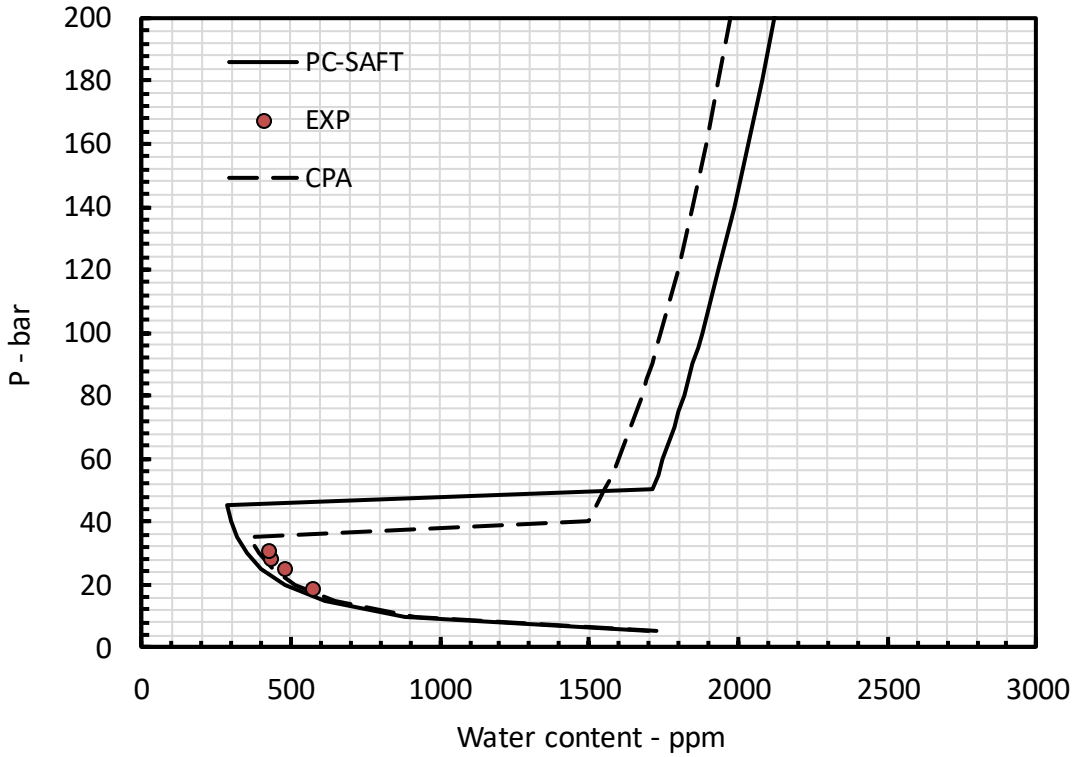

Figure 4.17 Comparison between calculated and measured water content of CO_2 in equilibrium with 10 wt% NaCl aqueous solution at 5 °C

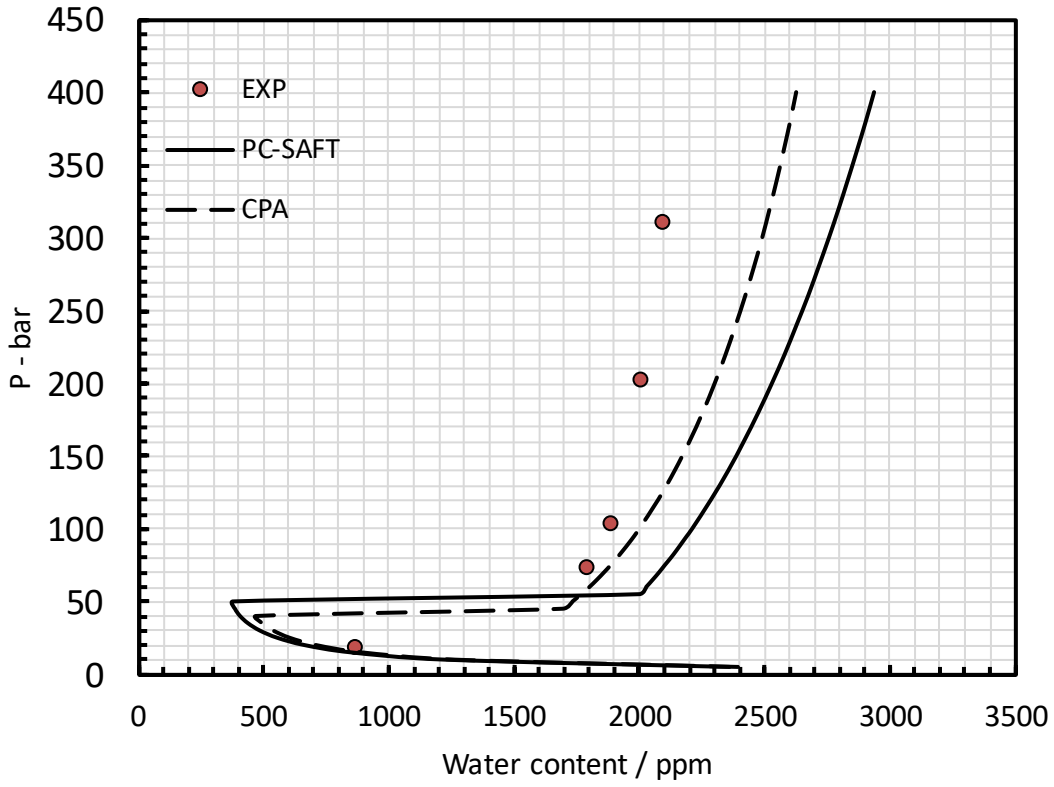

Figure 4.18 Comparison between calculated and measured water content of CO_2 in equilibrium with 10 wt% NaCl aqueous solution at 9.8 °C

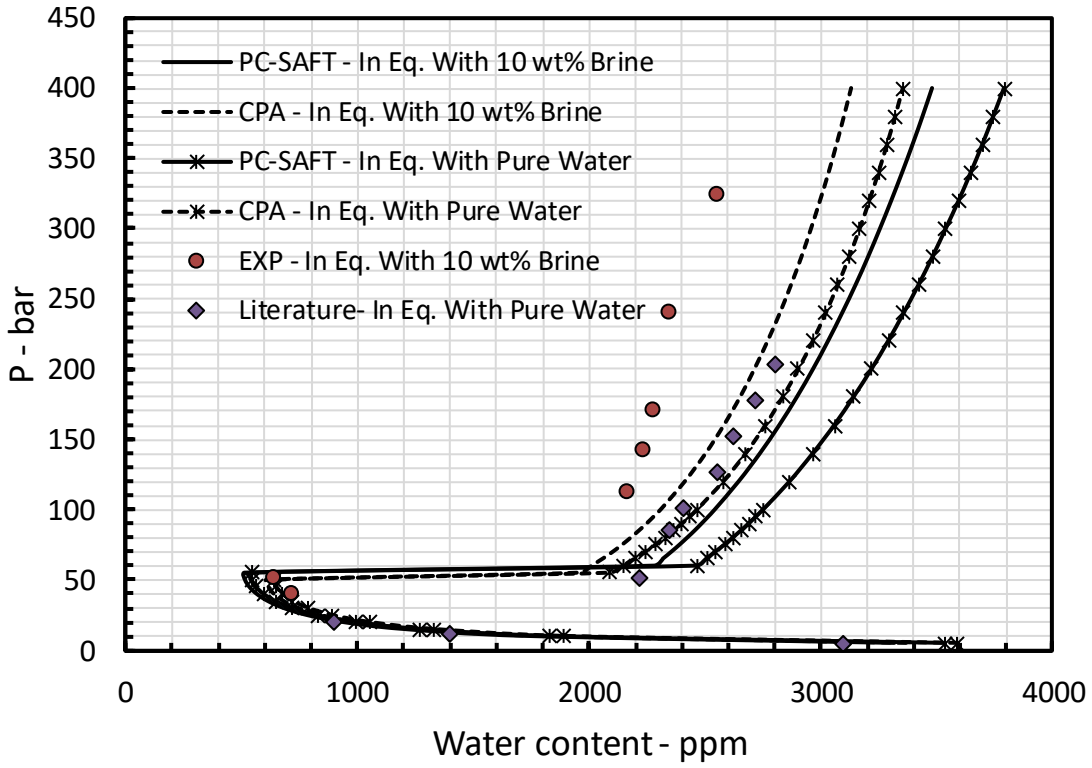

Figure 4.19 Comparison between calculated and measured water content of CO_2 in equilibrium with 10 wt% NaCl aqueous solution at 15 °C (literature experimental data taken from [340], [341]**)**

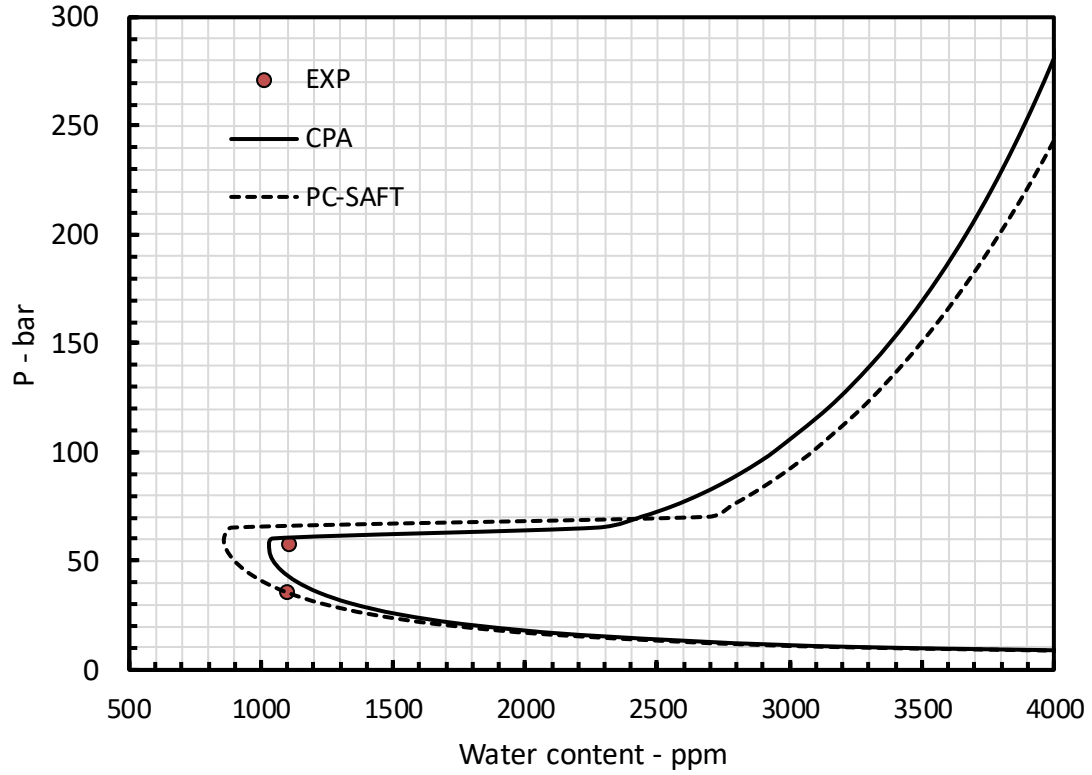

Figure 4.20 Comparison between calculated and measured water content of CO_2 in equilibrium with 10 wt% NaCl aqueous solution at 25 °C

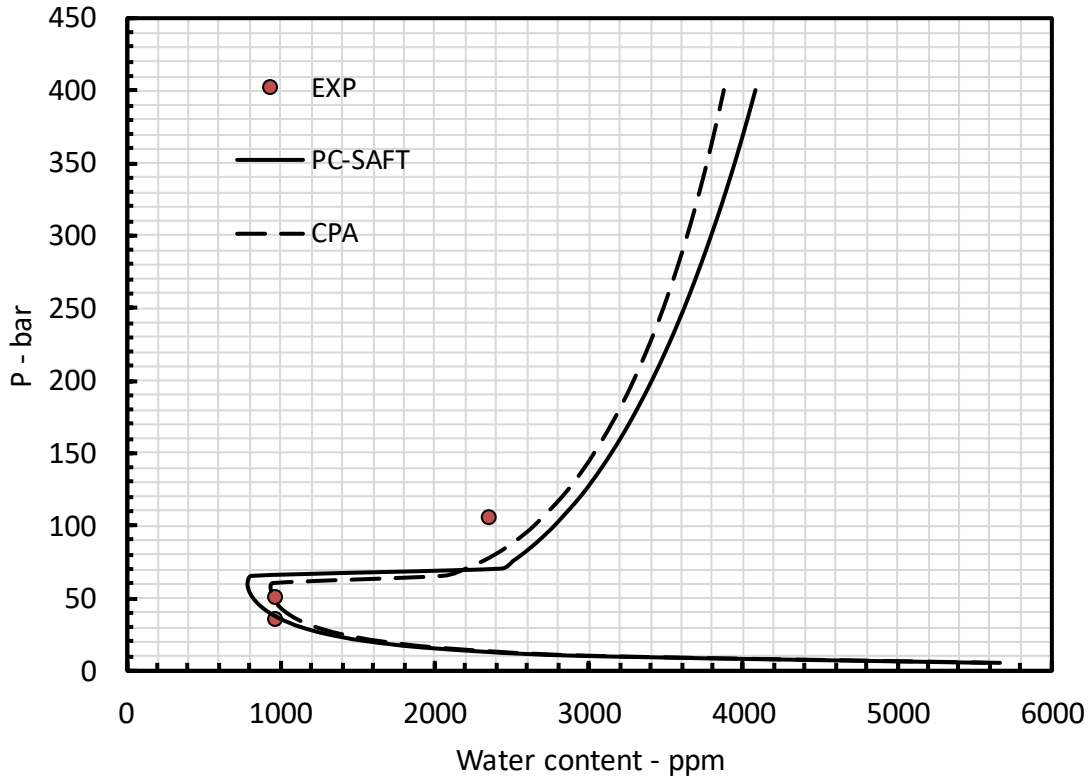

Figure 4.21 Comparison between calculated and measured water content of CO_2 in equilibrium with 20 wt% NaCl aqueous solution at 25 °C

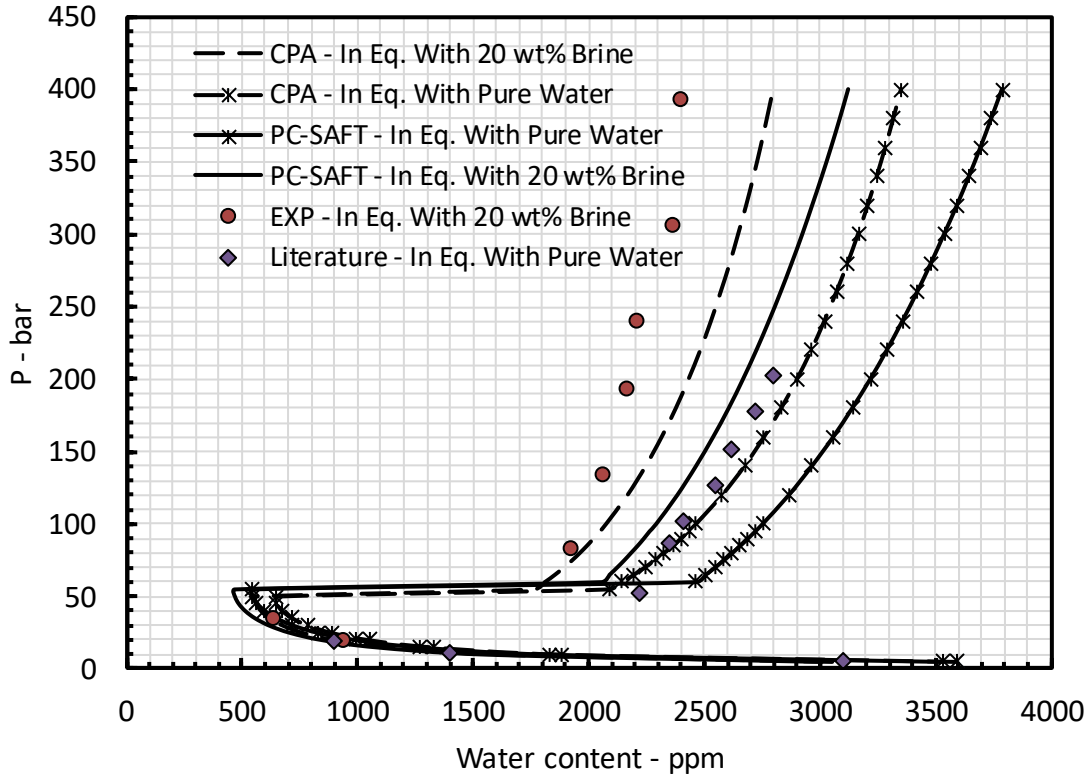

Figure 4.22 Comparison between calculated and measured water content of CO_2 in equilibrium with 20 wt% NaCl aqueous solution at 15 °C (literature experimental data taken from [340], [341]**)**

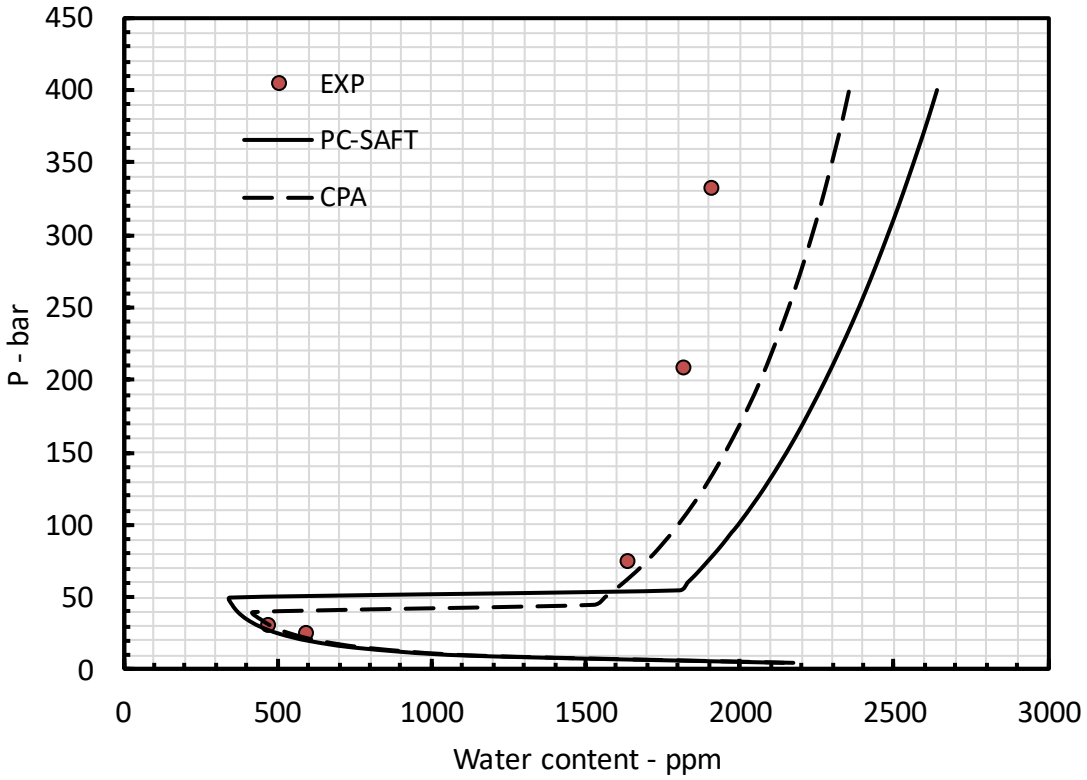

Figure 4.23 Comparison between calculated and measured water content of CO_2 in equilibrium with 20 wt% NaCl aqueous solution at 10 °C

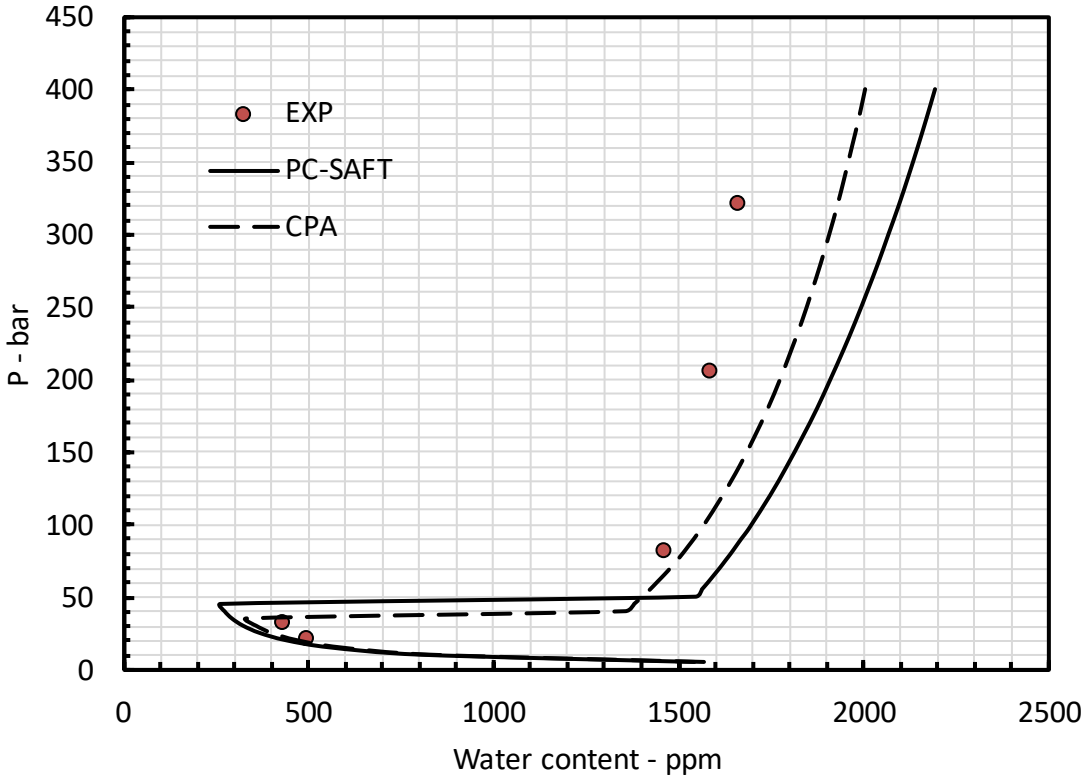

Figure 4.24 Comparison between calculated and measured water content of CO_2 in equilibrium with 20 wt% NaCl aqueous solution at 5 °C

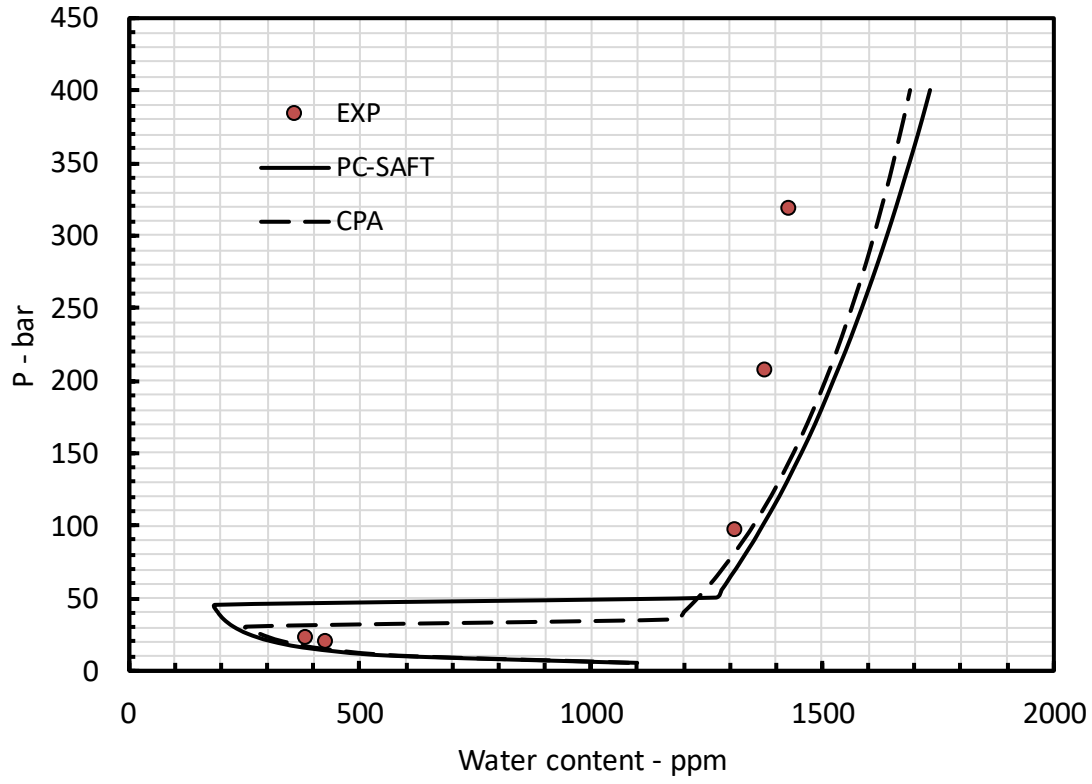

Figure 4.25 Comparison between calculated and measured water content of CO_2 in equilibrium with 20 wt% NaCl aqueous solution at 0 °C

4.3.2 Water Content measurement at elevated temperatures (T ≥ 50 °C)

- *Water content of methane*

Similar to those measurements preformed at low temperatures to check the accuarcy and reliability of water content measurements experimental setup and precedures, the water contents of methane in equilibrium with pure water were measured at 50 °C, 100 °C and 150 °C. The measured water content of methane at three elevated temperatures are reported in Table 4.7 at pressures from 34.5 bar to 827.4 bar. Experimental results are illustrated and compared with literature experimental data in Figure 4.26 and Figure 4.27 where the measured methane water contents are in excellent agreements with the data reported in the literature. The highest water content that is reported is 14.3% water cut with 2% uncertainty was measured at 150 °C and 34.5 bar which shows that using the gas chromatography very high water cut can be measured accurately.

Table 4.7 Experimental results of methane water content at elevated temperatures

T = 150 °C ±0.1 °C			**T = 100 °C ±0.1 °C**			**T = 50 °C ±0.1 °C**		
P-bar ± 0.7	**y_w - ppmV**		**P-bar** ± 0.7	**y_w - ppmV**		**P-bar** ± 0.7	**y_w - ppmV**	
34.5	143872	±2.00%	34.5	31631	±0.94%	27.6	4615	±7.44%
137.9	43177	±0.72%	69.0	16383	±2.52%	69.0	1724	±0.83%
273.7	24686	±3.21%	206.9	6381	±2.16%			
393.0	18650	±1.45%	413.7	4107	±0.81%			
			620.6	3484	±0.19%			
			827.4	3066	±2.03%			
AAD %			**AAD %**			**AAD %**		
CPA	PC-SAFT		CPA	PC-SAFT		CPA	PC-SAFT	
3.44	3.71		5.89	7.40		5.07	5.03	

Measured and calculated water contents are compared graphically in Figure 4.26 and Figure 4.27 where the PC-SAFT and the CPA EoS performances are shown to be similar at all temperatures and pressures. Model calculations also correlate this work and literature experimental results with very slight deviations indicating that the experimental setup used and the procedure followed are reliable for measurement of moderate and very high water contents.

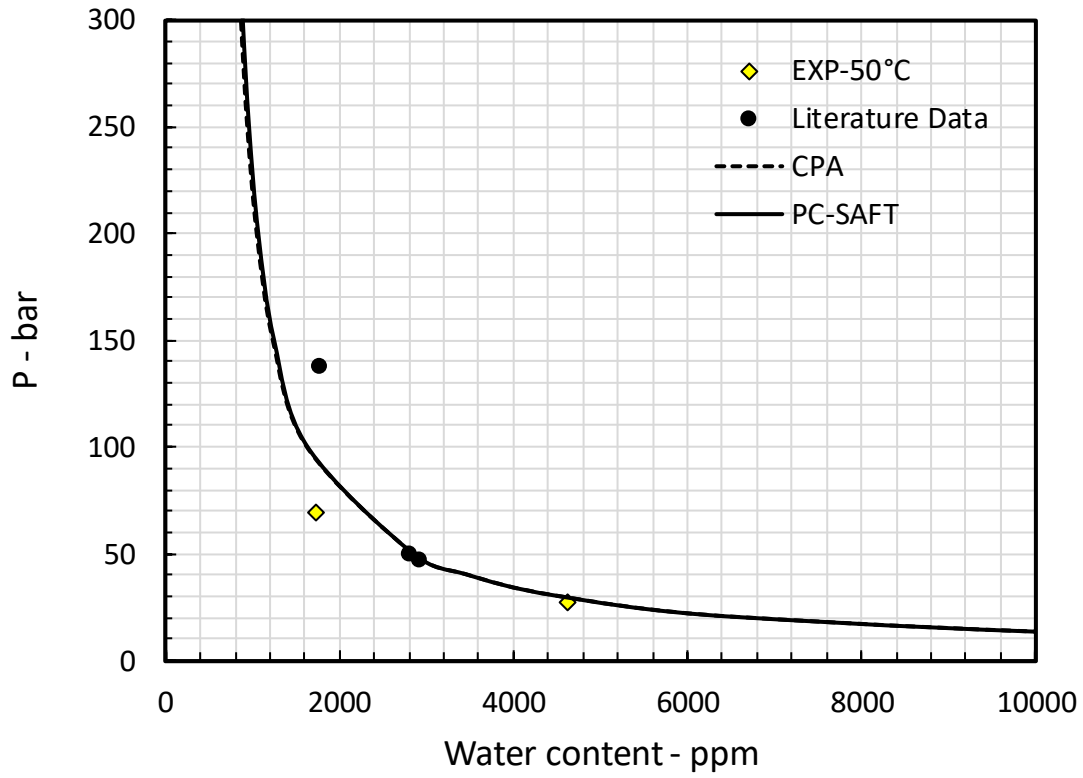

Figure 4.26 Comparison of measured methane water content and literature experimental data at elevated temperatures (50 °C: [461]–[463]**)**

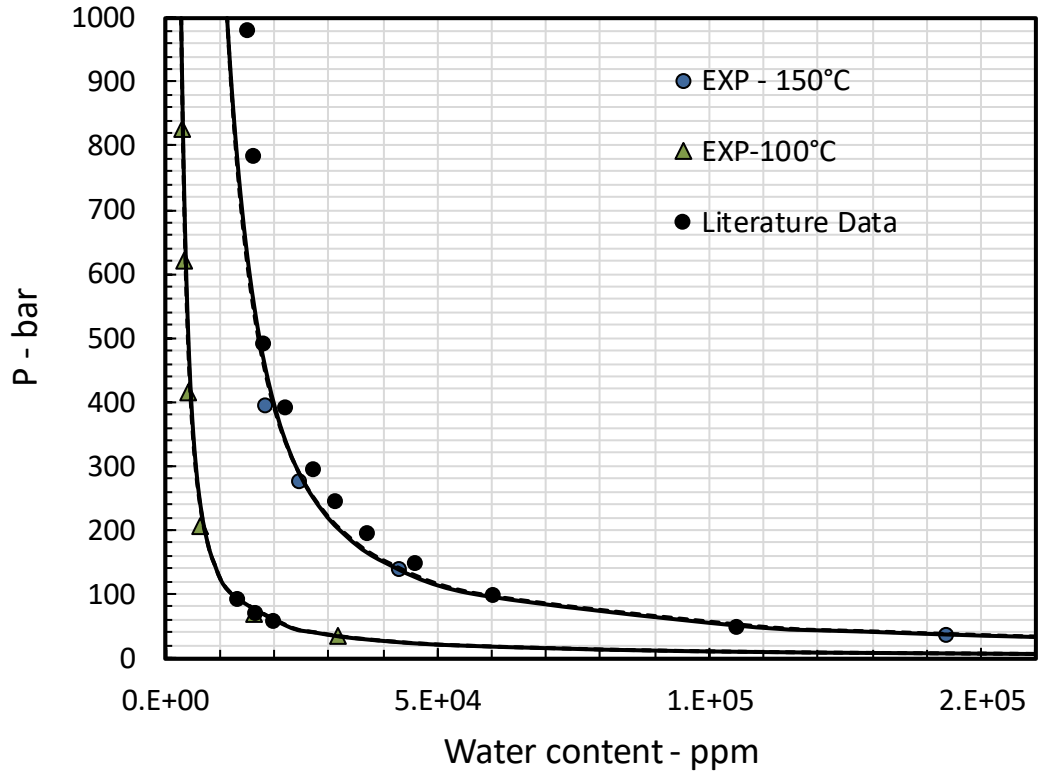

Figure 4.27 Comparison of calculated and measured methane water contents and literature experimental data (100 °C: [461]**, 150 °C:** [464]**)**

➢ *Water content of reservoir fluids*

In this section, the water content of two synthetic reservoir fluids entitled SYNGAS1 and SYNGAS2 (See Table 4.8 for rough compositions of the fluids), in equilibrium with free water at 150 °C at pressures of 34.48, 68.97, 206.90, 413.79, 620.69 and 827.59 bar was measured.

Table 4.8 Rough compositions of SYNGAS1 and SYNGAS2 in terms of mole %

Component	SYNGAS1	SYNGAS2
methane	>70%	>60%
ethane	>4%	>3%
propane	>1%	<1%
iso-butane	<1%	<1%
n-butane	<1%	<1%
N_2	>1%	>2%
CO_2	>5%	>10%

The experimental results of water content of the SYNGAS1 and SYNGAS2 synthetic fluids with and without combination with the stabilized condensates are reported in Table

4.9 to Table 4.12 and plotted in Figure 4.28 to Figure 4.31. water content measurements of each synthetic gas were performed using both GC and chilled mirror hygrometer. However, it was not found possible to make measurements at 34bar with the chilled mirror hygrometer as the reading was not stable due to a significant amount of water present, >140,000 ppm. Water content measurements of synthetic gases recombined with condensates were made using only the GC as the heavy hydrocarbons were condensed on the chilled mirror and made the readings not possible. As can be seen in Table 4.9 to Table 4.12 there is a good agreement between experimental and calculated values for both the synthetic gas and the recombined condensate. As shown in Table 4.9 and Table 4.10 the measured water contents using the GC and the chilled mirror hygrometer are quite close. Comparing the water content of both synthetic gases with those recombined with condensates shows that the calculated and measured water contents are higher for recombined fluids.

Table 4.9 Measured and calculated water content of SYNGAS2 gas at 150 °C and pressures up to 827 bar.

Setup	Pressure	Measured water content		Model Calculation			
	bar	ppm	Uncertainty	CPA	PC-SAFT	Deviations CPA	Deviations PC-SAFT
GC	34.48	161961	2.34%	152641	148741	5.75%	8.16%
	68.97	72109	1.31%	80874	78588	12.16%	8.99%
	206.90	34319	0.50%	33335	32567	2.87%	5.10%
	413.79	20605	3.00%	21717	21652	5.40%	5.08%
	620.69	16871	0.31%	17633	17762	4.52%	5.28%
	827.59	14800	2.21%	15364	15554	3.81%	5.09%
CM	206.90	30200	3%	33335	32567	10.38%	7.84%
	413.79	20300	3%	21717	21652	6.98%	6.66%
	620.69	17700	3%	17633	17762	0.38%	0.35%
	827.59	15800	3%	15364	15554	2.76%	1.56%

Table 4.10 Measured and calculated water content of synthetic SYNGAS1 gas at 150 °C and pressures up to 827 bar.

Setup	Pressure	Measured water content		Model Calculation			
	bar	ppm	Uncertainty	CPA	PC-SAFT	Deviations	
						CPA	PC-SAFT
GC	34.48	150873	3.10%	151836	148305	0.64%	1.70%
	206.90	29584	1.22%	31926	31571	7.92%	6.72%
	413.79	18521	1.39%	19970	20181	7.83%	8.96%
	620.69	14057	1.04%	15722	16027	11.85%	14.02%
	827.59	12187	3.00%	13383	13655	9.81%	12.04%
CM	206.90	29500	3%	31926	31571	8.22%	7.02%
	413.79	18700	3%	19970	20181	6.79%	7.92%
	620.69	15300	3%	15722	16027	2.76%	4.75%
	827.59	13000	3%	13383	13655	2.95%	5.04%

Table 4.11 Measured and calculated water content of synthetic SYNGAS2 + Condensates gas at 150 °C and pressures up to 827 bar.

Setup	Pressure	Measured water content		Model Calculation			
	bar	ppm	Uncertainty	CPA	PC-SAFT	Deviations	
						CPA	PC-SAFT
GC	34.48	155877	6.27%	152744	148767	2.01%	4.56%
	68.96	83322	1.33%	81014	78635	2.77%	5.63%
	206.89	33582	2.52%	33569	32724	0.04%	2.56%
	413.79	21779	3.58%	22000	21872	1.01%	0.42%
	620.68	18793	1.99%	17909	17999	4.71%	4.23%
	827.58	16767	0.69%	15621	15776	6.84%	5.91%

Table 4.12 Measured and calculated water content of synthetic SYNGAS1 gas + Condensates at 150 °C and pressures up to 827 bar.

Setup	Pressure	Measured water content		Model Calculation			
	bar	ppm	Uncertainty	CPA	PC-SAFT	Deviations	
						CPA	PC-SAFT
GC	34.48	168100	2.67%	151937	148330	9.62%	11.76%
	206.90	32300	1.30%	32133	31702	0.52%	1.85%
	413.79	21200	1.70%	20213	20357	4.66%	3.98%
	620.69	17600	3.47%	15960	16221	9.32%	7.84%
	827.59	14600	2.41%	13606	13850	6.81%	5.14%

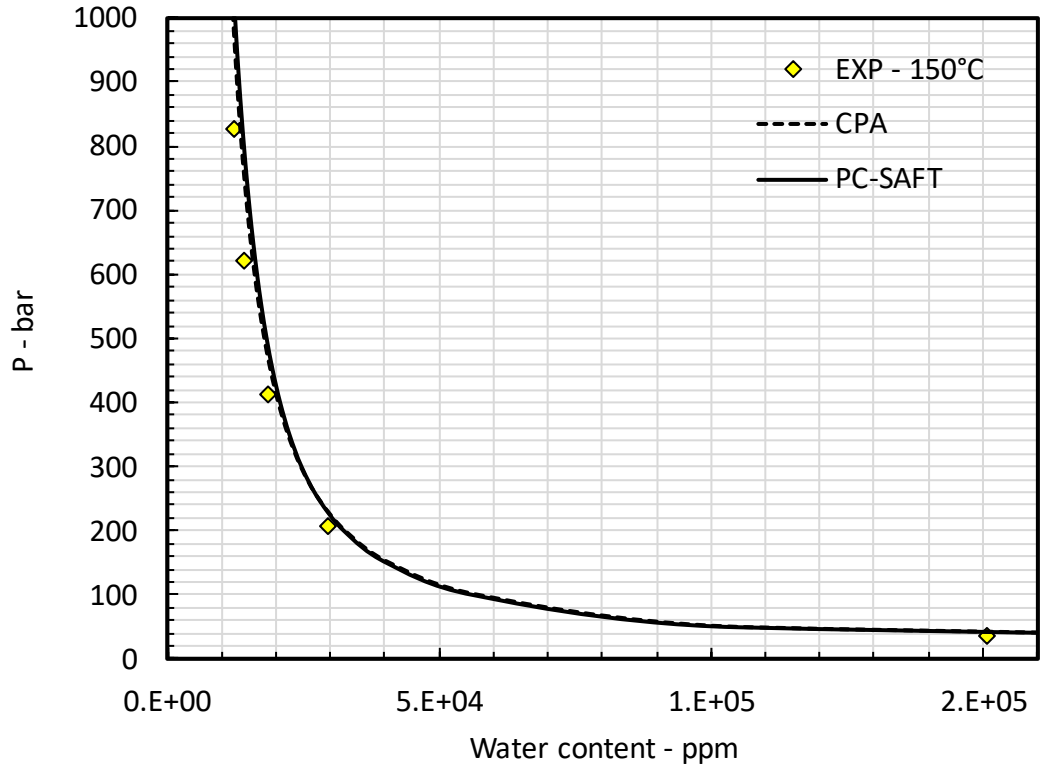

Figure 4.28 Experimental and calculated water contents for SYNGAS1 in equilibrium with water at 150 °C.

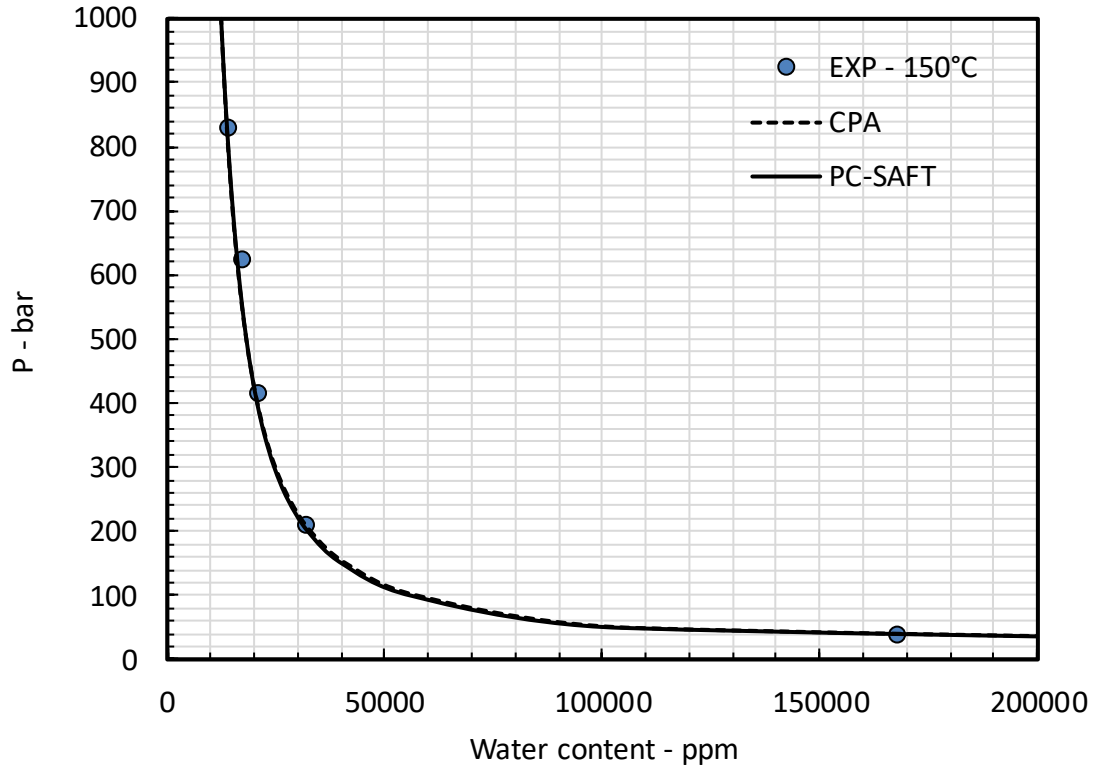

Figure 4.29 Experimental and calculated water contents for SYNGAS1 recombined condensates in equilibrium with water at 150 °C.

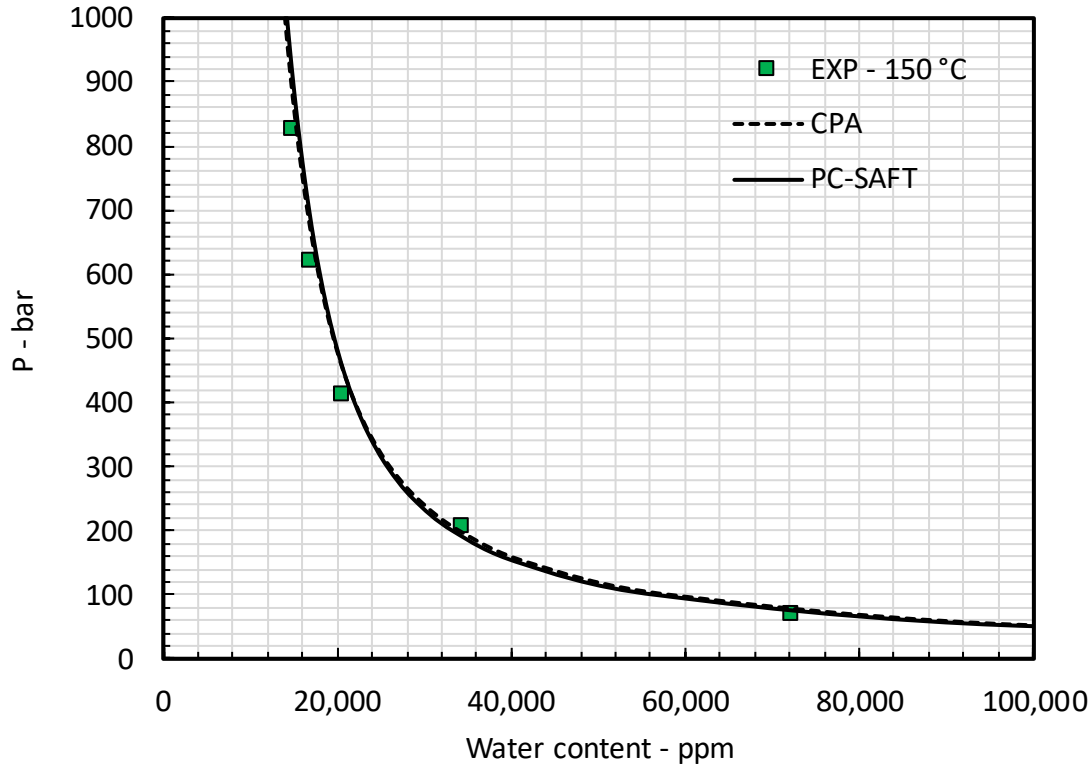

Figure 4.30 Experimental and calculated water contents for SYNGAS2 in equilibrium with water at 150 °C.

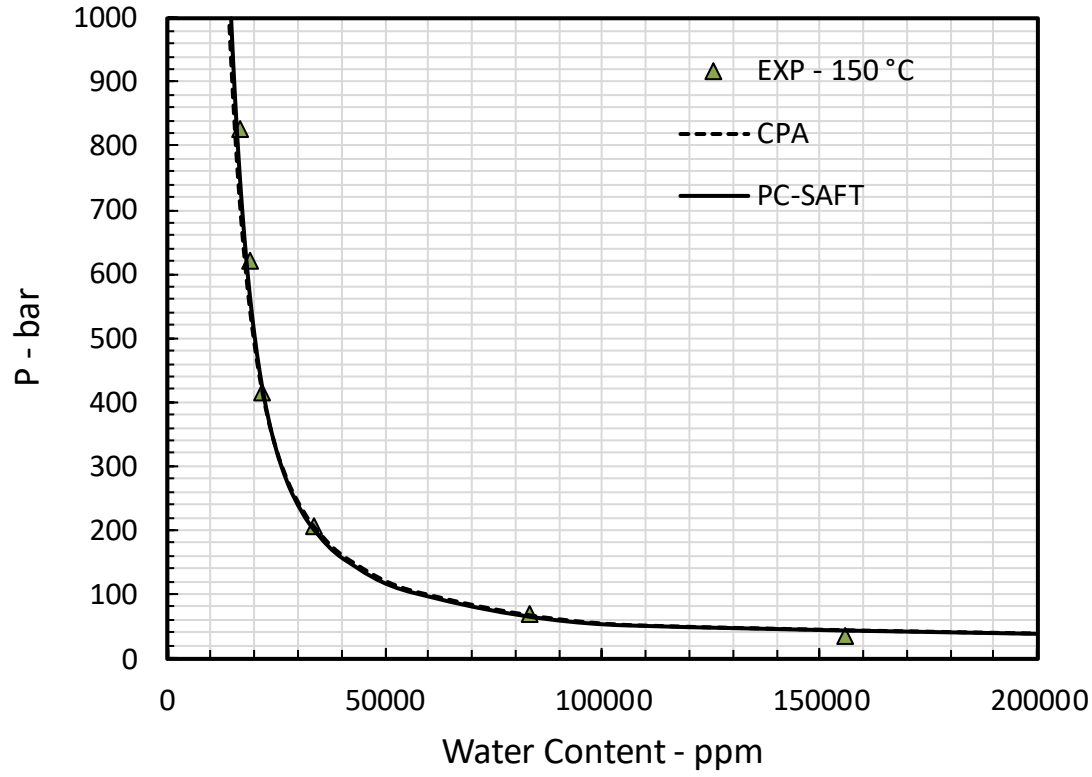

Figure 4.31 Experimental and calculated water contents for SYNGAS2 recombined condensates in equilibrium with water at 150 °C.

- *Water content of pure CO_2 at elevated temperatures*

In the section, the experimental results of CO_2 water content in equilibrium with DM water is reported at 100 °C and 150 °C. The experimental data measured in this work together with calculated CO_2 water contents using the CPA and the PC-SAFT equation of states are summarized in Table 4.13. The AAD % between calculated and measured water contents are 15.91 and 9.6 at 150 °C and 11.65 and 12.2 for the CPA and the PC-SAFT EoSs at 100 °C respectively.

Table 4.13 Measured and calculated water content of pure CO_2 at 100 and 150 °C

P	Measured water content	Model calculation			
		CPA	PC-SAFT	Deviation	
bar ± 0.7		ppm		CPA	PC-SAFT
150 °C ± 0.1					
16.27	247050	314444	306332	27.28%	24.00%
34.47	136035	157874	151662	16.05%	11.49%
51.71	101074	111182	105609	10.00%	4.49%
137.90	49403	56061	51251	13.48%	3.74%
275.79	41808	47141	43600	12.75%	4.29%
413.69	44728	48327	45598	8.05%	1.95%
551.58	46944	50058	47969	6.63%	2.18%
AAD %				15.91%	9.60%
100 °C ± 0.1					
16.27	57560	67925	66042	18.01%	14.74%
34.47	32044	34669	33110	8.19%	3.33%
51.71	23897	24996	23483	4.60%	1.73%
137.90	17498	15219	13667	13.02%	21.89%
275.79	20471	17334	16448	15.32%	19.65%
413.69	21369	19354	18934	11.83%	12.27%
551.58	21474	20622	20603	10.59%	11.77%
AAD %				11.65%	12.20%

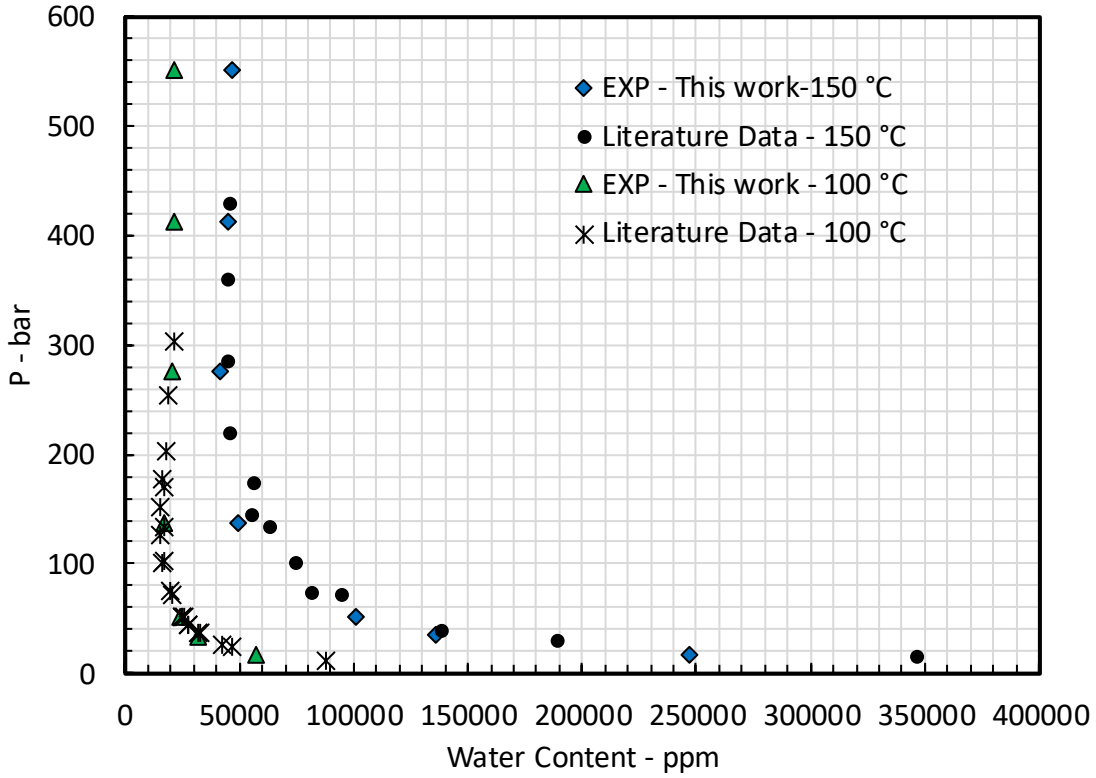

Figure 4.32 Comparison of measured water content of CO_2 at 100 °C and 150 °C with literature data (100 °C: [335], [336], [342]**, 150 °C:** [336], [465]

Measured and literature water content of CO_2 at 100 °C and 150 °C are compared graphically in Figure 4.32. As illustrated in Figure 4.32, at fixed pressure with increasing temperature, the water solubility in the CO_2-rich phase is increased. Furthermore, as shown in Figure 4.32, the experimental results of this work are in excellent agreements with literature at both test temperatures.

Model calculations and experimental results are compared in Figure 4.33 and Figure 4.34. As shown, at each pressure, the calculated water content using the CPA and the PC-SAFT EoSs are quite close. Also as displayed in both Figure 4.33 and Figure 4.34, the measured water contents are in line with those reported in the literature at 100 °C and 150 °C. However, at 100 °C and pressures above 200 bar, the deviation between model calculation and experimental data are higher with respect to those measured at lower pressures despite that this work experimental results and literature data are in excellent agreement.

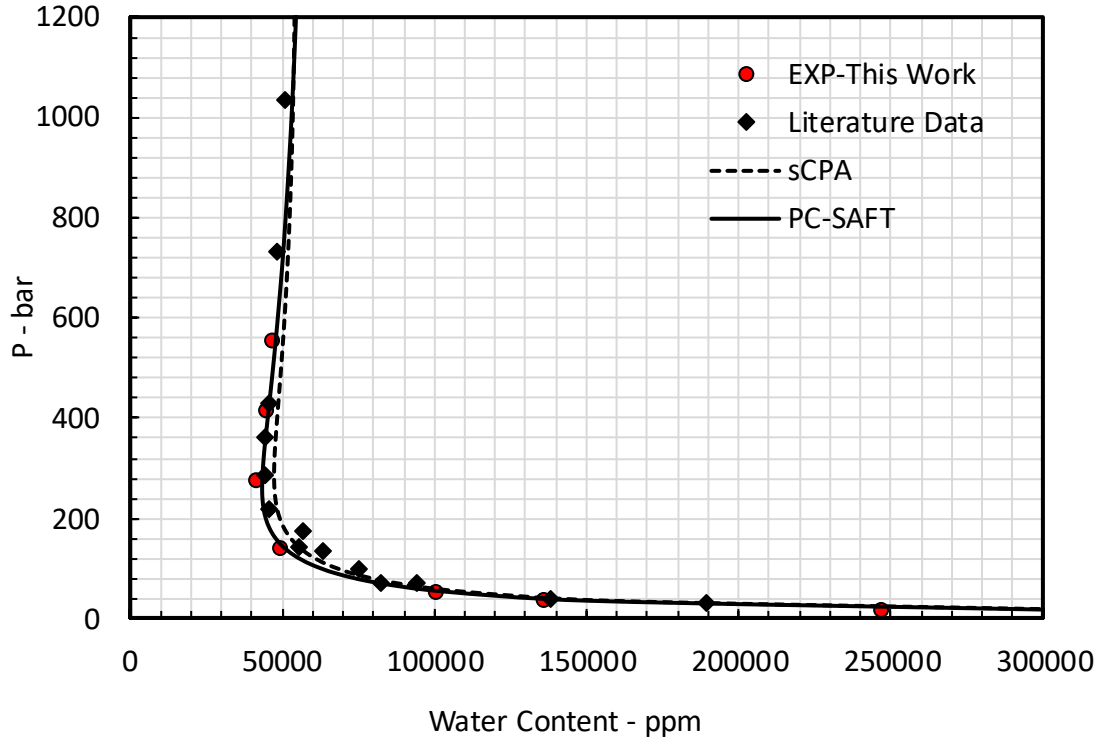

Figure 4.33 Comparison of calculated and measured water content of CO_2 at 150 °C with literature data (150 °C : [336], [465]

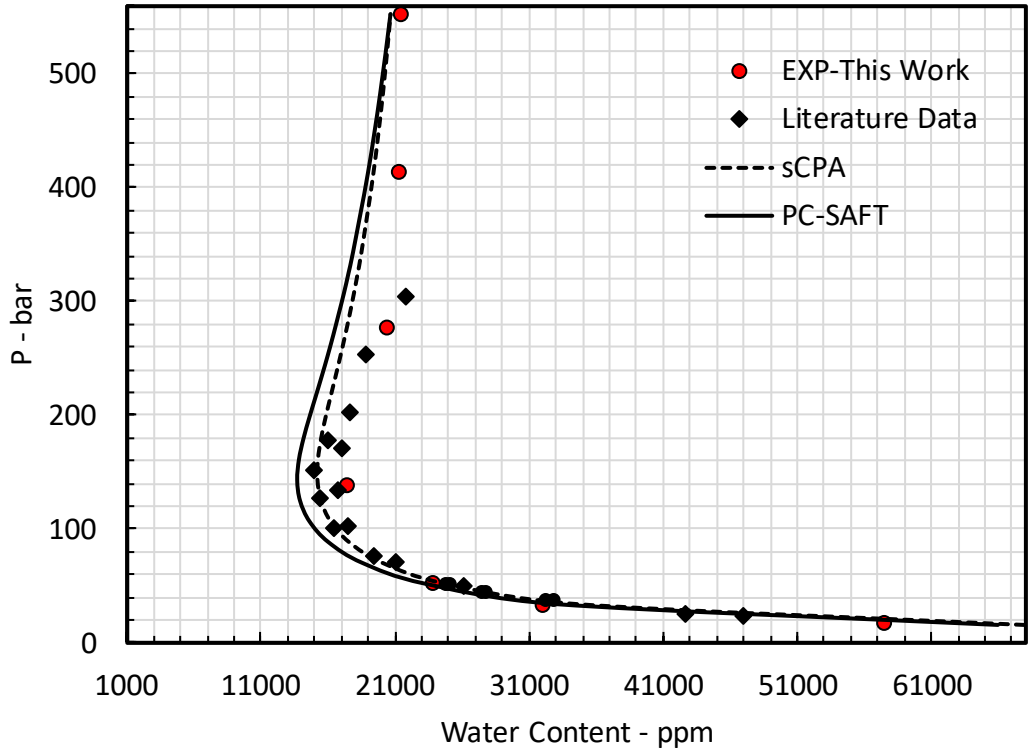

Figure 4.34 Comparison of calculated and measured water content of CO_2 at 100 °C with literature data (100 °C : [335], [336], [342]**)**

- *Water content of CO_2 mixtures at elevated temperatures*

The water contents of two CO_2-rich fluids entitled MIX1 and MIX6 (see Table 4.14 for each fluid composition) in equilibrium with water were measured. Measured water contents of the CO_2-rich fluids are reported in Table 4.15 and Table 4.16 and compared together through Figure 4.35. As can be seen in Table 4.16, good agreements were found between model calculation and experimental results of MIX 1 water content at 150 °C with around 4 AAD %. As illustrated in Figure 4.35, the calculated and measured water content of MIX 6 is lower than MIX 1 at all test pressures as MIX 6 with around 70% CO_2 content has a lower water affinity than MIX 1 with 95% CO_2 content.

Table 4.14 Compositions of the CO_2-rich fluids entitled MIX1 and MIX 6 in terms of mole percent

Components	MIX 1	MIX 6
carbon dioxide	95.64	69.99
methane	0.6261 (±0.031%)	7.901 (±0.040%)
ethane	0	7.015 (±0.036%)
propane	0	4.968 (±0.025%)
n-butane	0	2.067 (±0.0011%)
iso-butane	0	2.049 (±0.0011%)
n-pentane	0	0
nitrogen	1.41 (±0.071%)	6.009 (±0.031%)
hydrogen	0.8175 (±0.041%)	0
oxygen	0.08 (±0.004%)	0
argon	1.21 (±0.061%)	0
carbon monoxide	0.2127 (±0.011%)	0

Table 4.15 Measured and calculated water content of MIX6 at 150 °C

P	Measured water content	Uncertainty	Model calculation			
			CPA	PC-SAFT	Deviation	
bar		ppm			CPA	PC-SAFT
565.52	30966	1.70%	35562	35835	14.84%	15.72%
420.69	31837	2.45%	36945	36356	16.05%	14.20%
282.76	32115	1.46%	39635	37967	23.42%	18.22%
143.45	37768	2.26%	51555	48237	36.51%	27.72%
59.31	91775	1.31%	97349	92803	6.07%	1.12%
37.93	138228	1.72%	143475	138109	3.80%	0.09%
AAD %					16.78%	12.84%

Table 4.16 Measured and calculated water content of MIX1 at 150 °C

P	Measured water content	Uncertainty	Model Calculation			
			CPA	PC-SAFT	Deviations	
bar		ppm			CPA	PC-SAFT
551.72	47338	4.07%	44804	45161	5.35%	4.60%
413.79	46497	5.95%	44020	43328	5.33%	6.82%
275.86	45147	7.65%	44143	42131	2.22%	6.68%
137.93	50893	3.19%	54542	50947	7.17%	0.11%
53.52	108462	5.70%	107191	102510	1.17%	5.49%
35.66	145731	2.91%	152511	147084	4.65%	0.93%
AAD %					4.25%	4.74%

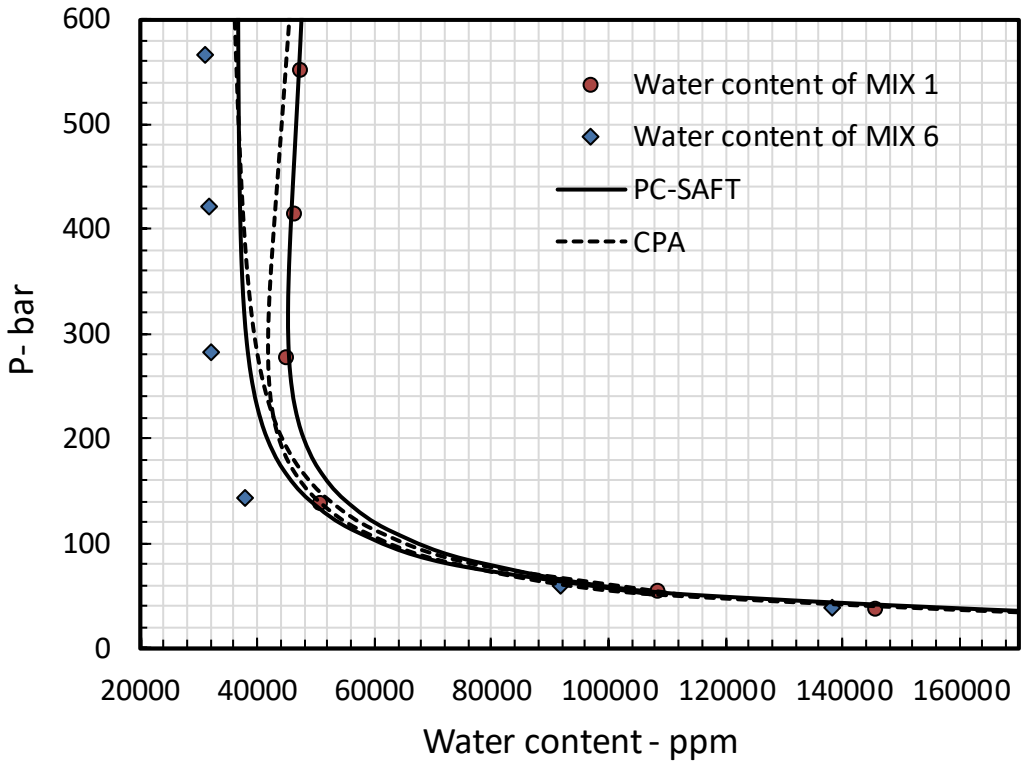

Figure 4.35 Measured water content of MIX1 and MIX6 in equilibrium with distilled water at 150 °C

4.4 Summary and Conclusion

A brief literature survey regarding the studies reported on the solubility of water in CO_2-rich fluids was presented at the beginning in this chapter. It was shown that while the water content of CO_2 in equilibrium with water has been studied extensively over broad ranges of temperature and pressures, there is no data available for the water content of CO_2 in equilibrium with aqueous solutions of salts. To fill this gap, the water content of CO_2 in equilibrium with 10 and 20 wt% NaCl aqueous solutions were measured. Comparing the measured data with model calculation showed an excellent agreement between calculated and measured water contents at below bubble point pressures while higher deviations were calculated between model calculations and experimental results at above bubble point pressures. Despite that there was no data available in the literature to validate the experimental results, the effects of salinity and temperature on the water content of CO_2 were investigated. It was observed that the water content of CO_2 is decreased with increasing the salinity of the brine and is increased with increasing the temperature of the system indicating that the measured data are qualitatively consistent.

Using gas chromatography, the water contents of pure CO_2 and four mixtures with different concentrations of CO_2 in equilibrium with water were measured at elevated temperatures and pressures. It was shown that using the gas chromatography setup used, very high moisture content of CO_2 containing systems can be measured accurately. Slight deviations were found between model calculations and experimental results for both the CPA and the PC-SAFT EoSs.

Chapter 5

5–Summary and recommendations

5.1 Background of the Work

Global warming is nowadays one of the most significant problems that humankind is facing. Global warming is defined as the constant and slight increase in the temperature of the earth which is considered as a severe danger to the life on earth. The main cause of this phenomena is the change in the composition of the atmosphere and increasing the content of greenhouse gases which absorb the heat from the sun and trap it within the atmosphere causing an increase in the earth temperature. Carbon dioxide is mainly produced from consumption of fossil fuels to provide the energy demand. Furthermore, with growing in the global population and entering more consumerism to the lifestyles, this problem is not controlled but is being exacerbated.

To control the situation and to slow down or stop the global warming, CO_2 emissions to the atmosphere must be reduced as much as possible. Therefore, it is recommended to capture the CO_2 from the main emission sources and transport it to sites where CO_2 can be stored by dissolving in large deep down formation without returning to the atmosphere. The processes involved in capturing, transporting and storing CO_2, are known as carbon Capture and Storage (CCS). However, these processes are not trivial, and there are several issues needs to be resolved which does not seem possible without having a sound knowledge of the governing phenomena in these processes. Moreover, to make CCS efficient and cost effective, many engineering problems and difficulties must be resolved as well. For instance, it is usually favourable to transfer the CO_2-rich fluids in a compressed state to a long distance destination where the risk of hydrate formation and pipeline blockage is high. On the other hand, in the storage sector, the main challenge is to find proper storages in which the maximum CO_2 can be stored. Also, it is crucial to make sure that CO_2 is safely stored deep down in the formation and will not be released back into the atmosphere.

In general, engineering, design and control the processes mentioned above, require a good understanding of governing phenomena in all CCS sectors. The aim of this work was to fill the gaps in the available experimental studies regarding the phase equilibria measurements and improving the accuracy and predictive capabilities of the thermodynamic models for modelling such systems.

5.2 Phase Equilibria Modelling Using PC-SAFT Equation of State

5.2.1 PC-SAFT background

An extensive introduction on the background of the molecular-based equation of states with the emphasis on SAFT based models was presented in Chapter 2. The idea and the background of the PC-SAFT model developed by Gross and Sadowski [6], [13] were discussed in Chapter 2.

5.2.2 Investigating the binary mixtures of the main CO_2-rich fluids components

Using the pure compound parameters suggested by Gross and Sadowski [6], the binary interaction parameters of 82 different binary mixtures were tuned to more than thousand literature experimental data points. Comparison of the experimental and calculated VLE of the investigated systems showed that using a single temperature independent binary interaction parameter, the PC-SAFT EoS performs very well and is capable of correlating the phase behaviour of such systems accurately.

5.2.3 Phase equilibria modelling of CO_2-rich fluids/water systems

As stated before, CO_2 is being stored in massive aquifers by dissolving in the brine. Also in the transportation processes, water may be present in the fluid and increases the risk of hydrate formation and pipeline blockage. Therefore, water plays a critical role in either storage sector of the CCS or the flows assurance engineering of transportation processes. To improve the PC-SAFT EoS capability in accurately modelling the PVT and phase equilibria behaviour of such system, a new set of temperature dependent PC-SAFT pure compound parameters were optimised for water and tested against experimental data. The model calculation results showed excellent agreement with experimental VLE data and freezing point of water. Using the set of pure compound parameters tuned in this work, the PC-SAFT EoS appeared to show superior performance over other sets of parameters reported in the literature.

The binary interaction parameters of thirty compounds including, inorganic gases, normal alkanes, aromatics, and noble gases with water were also adjusted to the literature solubility data over a wide range of temperature and pressures. Due to the important role of CO_2 in our study and pseudo retrograde behaviour of the water content of CO_2 in equilibrium with aqueous solutions, another adjusting parameter was also introduced to adjust the association strength between water and CO_2 systems. Excellent agreement was found between the tuned PC-SAFT model and Duan et al. [295] model for calculating the CO_2 solubility in distilled water. The model was also showed a good performance in CO_2

water content calculation and capturing the pseudo retrograde behaviour of the CO_2 water content.

5.2.4 Phase equilibria modelling of hydrate inhibitors/CO_2-rich fluids systems

Water removal or dehydration processes commonly use glycols to remove water from the natural gases in absorption columns. Also, glycols are recently preferred over methanol for hydrate inhibition purposes. New sets of pure compound parameters were developed for MEG, DEG, TEG, TeEG and PG[1] over an extensive range of temperatures. The outcome of the optimisation showed that the model was capable of predicting the vapour pressures and saturate liquid densities of all glycol oligomers with excellent accuracy even at low temperatures where the vapour pressures of some heavy glycols are less than a Pascal. The model calculations using the new sets of parameters were also appeared to be advantageous over those sets of parameters reported in the literature. The binary interaction parameters of glycols and compounds involved in the CCS were also tuned to either available experimental literature or in-house data. Very good agreements were found for all the investigated systems at broad ranges of temperature and pressure.

In continuance of the study on glycols containing systems, the PC-SAFT EoS was applied to model the phase behaviour and thermodynamic properties of methanol, ethanol, 1-propanol and 2-propanol. Gross and Sadowski [214] reported pure compound parameters for several alcohols. However, we found that using the sets of parameters reported by them the vapour pressure of alcohols is not being predicted with the expected accuracy of our modelling purposes. Hence new sets of pure compound parameters were optimised using volumetric data of alcohols to increase the accuracy of the model with an emphasis on low temperatures. Therefore, the new sets of parameter were developed for temperatures up to 373.15 K. Using the new sets of the parameter obtained in this work, the model calculation of vapour pressures and saturated liquid densities of pure alcohols compared with experimental data and model predictions using literature pure compound parameters. In almost all cases the model predictions showed a better performance using this work sets of parameters than using those reported in the literature.

5.2.5 Evaluation of the model in calculating second derivative thermodynamic properties

The performance of equation of states is usually evaluated by their capability in generating accurate phase equilibria results. However, a robust thermodynamic model is

[1] Poly Ethylene Glycol

also expected to predict the second thermodynamic derivative properties like heat capacities, Joule-Thomson coefficients and thermal expansion of complex fluids. Unlike the cubic equation of states, molecular-based models involve more complex equations with the higher non-linearity order. Moreover, SAFT based equation of states use the fraction of non-bonded molecules, X_A, which has to be obtained iteratively for multi component systems. As the above-mentioned thermodynamic properties are calculated by first and second differentiation of residual Helmholtz free energy, one may use numerical differentiation for calculating the derivatives where a single function may be called several times resulting in an increase in the cost of calculations. To resolve this, we developed the first and second derivative of original PC-SAFT equation of state which based on our knowledge so far, has not been reported in the literature. After developing the derivative equations, the model performance was tested for pure propane, dodecane and methanol. Model calculation results show very good agreement with the experimental data of propane and dodecane especially at near or above critical point. The calculated second derivative properties of methanol using the new set of parameter developed in this work and the parameters reported by Gross and Sadowski [214] were also compared with experimental data. No sensible difference in the model performance was observed using two set of parameters.

5.2.6 Electrolytes modelling

CO_2-rich fluids are being stored in underground formation are in equilibrium with brine. To account for the effect of salts on the phase equilibria modelling, the contribution of the electrolytes must be considered in the equation of state. In this study the Debye–Hückel activity model was incorporated with the PC-SAFT EoS for modelling the electrolyte containing systems. For calculating the contribution of the electrolytes in the fugacity coefficients, the binary interaction parameters water/salt and non-associating compounds/salt are obtained by adjusting the model to the volumetric data of water/salts and CO_2/electrolyte systems. To validate the experimental solubility data obtained in this study, we incorporated the water/salt binary interaction parameters reported by Haghighi et al. [372] for the CPA EoS. The CO_2-salt binary interaction parameters were then tuned by employing PC-SAFT EoS and using either this work measured solubility data or literature. It was also shown that as using the new water sets of pure compound parameters, the PC-SAFT and the CPA yields almost identical results for VLE data of water, using the water/salts binary interaction parameters was a reasonable assumption.

5.3 CO_2 Solubility Measurements in Water and Aqueous Salt(s) Solutions

A comprehensive literature survey was conducted for CO_2 solubility in water and aqueous solutions of NaCl, KCl, $CaCl_2$ and $MgCl_2$ to identify the current gaps in literature data. Based on the datasets found, it was observed that the CO_2 solubility in water and aqueous solution of NaCl were studied extensively in the literature, and several datasets were found over wide ranges of temperatures and pressures. However, limited CO_2 solubility data in aqueous solutions of NaCl were found at low temperatures (T<298.15 K) and high pressures. A number of solubility datasets were found in KCl, $CaCl_2$ and $MgCl_2$ aqueous solutions which were either scattered or were reported at conditions not broad enough for modelling and tuning purposes.

To validate whether the experimental setup and procedure, the solubility of CO_2 at 50 °C and 100 °C and pressures up to 500 bar were measured. Experimental results were then compared with literature data and model calculations. As an excellent agreement was found between model calculation and both measured and literature data, it was concluded that the experimental setup and procedure adopted, are reliable for the planned CO_2 solubility measurements. The solubility of CO_2 in aqueous solutions of NaCl, KCl, $CaCl_2$, $MgCl_2$ and a salt mixture were then measured in various concentrations of brine and over wide ranges of temperature and pressure to fill the gaps found in the literature.

The solubility of CO_2 in 10 and 20 wt% aqueous solutions of NaCl were measured at low temperatures (-10 °C ≤ T ≤ 25 °C) and pressures up to the hydrate dissociation pressures of the system at each test temperature. Solubility measurements were also made at elevated temperatures (50 °C ≤ T ≤ 150 °C) in 10, 15 and 22 wt% NaCl aqueous solutions. To validate the experimental data, the PC-SAFT and CPA models were tuned to this work experimental results, and the model calculations were compared to the Duan model [295] predictions. Excellent agreements were found between calculated solubilities using the CPA, the PC-SAFT and the Duan model, indicating that this work experimental results agree with those reported in the literature. However, at low temperatures and high pressures larger deviations are observed between the model calculations and the Duan model predictions. It was suggested that as the Duan model was tuned to the literature data which are limited at low temperatures and high pressures, the CPA and PC-SAFT models are performing better and more accurately.

CO_2 solubilities in aqueous solutions of $CaCl_2$ were measured at 50, 100 and 150 °C in 7.5, 10, 15.7 and 23.4 wt% aqueous solutions. The PC-SAFT and the CPA EoSs were

tuned to the literature solubility data [374] and compared with the experimental data where a very good agreement was found.

CO_2 solubility measurements in 10 wt%, 15 wt% and 22 wt% KCl aqueous solutions were also made at 50 °C, 100 °C and 150 °C and pressures up to 548 bar. Totally nine CO_2 solubility datasets in aqueous solutions of KCl were found in the literature. The maximum pressure at which the solubilities were reported was 200 bar. As the pressure ranges covered in the literature was limited, the CPA and the PC-SAFT models were tuned to the experimental results of this work. Calculated solubilities were then compared to the literature data to validate the experimental results. Excellent agreement was found between the calculated solubilities and the experimental data reported by Kamps et al. [441], Kiepe et al., [438] and Liu et al. [434].

The most extensive solubility datasets that cover broad ranges of temperature and pressure in various concentrations of $MgCl_2$ aqueous solution were reported by Tong et al. [374] and Zhao et al.[375]. Therefore, a set of experiments were conducted to measure the solubility of CO_2 in different concentrations of $MgCl_2$ solutions over extensive temperature and pressure ranges. The CPA and the PC-SAFT EoSs were tuned to the data reported by Tong et al. [374] and Zhao et al. [375], and model calculations were compared to the experimental results obtained in this study. Excellent agreement was observed with the experimental results indicating that the measured solubilities agree with those reported in the literature.

The solubility of CO_2 in a mixture of the aqueous salt solution was also measured at 50 °C, 100 °C and 150 °C. A salt mixture containing 19.4 wt% NaCl, 2.3 wt% $CaCl_2$, 1.1 wt% $MgCl_2$ and 0.3 wt% KCl was prepared, and solubility measurements were made at pressures up to 571 bar. Using the tuned CPA and the PC-SAFT EoSs, the model predictions were compared to the experimental data to validate the measurement results. Good agreement was found between the model calculation and the experimental data with slight deviations.

5.4 Experimental Study of CO_2-Rich Fluid Water Content

A good understanding on the phase equilibria of CO_2-rich or natural gas systems in the presence of distilled water or brine is essential in modelling, design and engineering. An extensive literature survey of the studies on the water content measurements of CO_2-rich fluids was conducted in Chapter 4. Seventeen datasets of CO_2 water content in equilibrium with water were found in the literature. Even though the CO_2 solubility has

been extensively measured in various concentrations of aqueous solutions of salts at a broad range of temperatures and pressures, to our knowledge, there is no experimental data available for the water content of CO_2-brine systems in the literature. To fill the gap, water content of CO_2 in equilibrium with brine at the conditions of flow assurance engineering interests were measured.

To evaluate the reliability of the experimental setup for water content measurements at low temperatures, the water content of methane in equilibrium with demineralised water/hydrate was measured at temperatures from -40 °C to 25 °C. The experimental results were then compared to either literature or calculated CO_2 water contents using the CPA and the PC-SAFT EoSs. Very good agreement was found between literature data and model calculations proving that the setup and procedure adopted for low water content measurements were reliable. Furthermore, the water content of CO_2 in equilibrium with 10 and 20 wt% NaCl aqueous solutions were measured at 0 °C to 25 °C and -5 °C to 25 °C respectively. All the measurements were made at pressures below the hydrate dissociation pressure of each temperature. As no data are available in the literature for the water content of CO_2 in equilibrium with brine, the experimental results were only compared with the model predictions. The experimental results obtained at different temperatures and in different concentration of brine were also compared together. It was observed that the water content decreases with reducing temperature and increasing the salinity of brine which also indicates that the measured data are qualitatively consistent.

To investigate the water solubility in CO_2-rich fluids at higher temperature, the gas chromatography method was adopted. The reliability of the experimental setup and measurement method was checked by measuring the water content of methane and CO_2 at elevated temperatures (100 °C and 150 °C) and comparing the experimental results with literature and model calculations. The measured water contents of CO_2 and methane were completely in line with literature data and were correlated with an excellent agreement with model predictions which showed that using the experimental procedure adopted, the water contents of fluids with very high moisture can be measured precisely. The water content of two synthetic CO_2-rich fluids as well as two reservoir gas fluids were measured at 150 °C. The measured data were then compared with the model calculations. It was shown that the model calculations and experimental data obtained in this work are quite close.

5.5 Recommendations

In continuance with the modelling and experimental results obtained in this dissertation, several prospective are expected in both modelling and experimental sections.

5.5.1 Modelling

It is recommended to investigate more binary mixtures of non-associating compounds and associating compounds involved in CCS and flow assurance. As a shortcoming was observed in predicting the second derivative properties of associating compounds using the equation of states, it is suggested to account these properties in optimising the PC-SAFT pure compound parameters, in addition to volumetric data. Also incorporating the PC-SAFT models with ion based electrolyte models as well as tuning the current model with more non-electrolyte/salts systems seem to be a prosperous plan.

5.5.2 Experimental study

There are still several gaps in the experimental data of CO_2/brine systems to be filled. Examples be the CO_2 solubility in aqueous solutions of $CaCl_2$, KCl, and $MgCl_2$ at low temperatures or the water content of CO_2 in equilibrium with aqueous solutions of above-mentioned salts. It is also recommended to investigate the effect of impurities on the CO_2-rich fluids like O_2, N_2, argon and H_2S on the solubility of CO_2 in water or brine. Another suggestion for future works could be to study the effect of pH on the solubility of CO_2 in aqueous solutions.

6. References

[1] M. R. Raupach, G. Marland, P. Ciais, C. Le Quéré, J. G. Canadell, G. Klepper, and C. B. Field, "Global and regional drivers of accelerating CO_2 emissions.," *Proc. Natl. Acad. Sci. U. S. A.*, 104, 10288–10293, 2007.

[2] "http://www.esrl.noaa.gov/gmd/ccgg/trends/."

[3] J. C. M. Pires, F. G. Martins, M. C. M. Alvim-Ferraz, and M.Simões, "Recent developments on carbon capture and storage: An overview," *Chem. Eng. Res. Des.*, 89, 1446–1460, 2011.

[4] B. Metz, O. Davidson, H. De Coninck, M. Loos, and L. Meyer, "IPCC Special Report on Carbon Dioxide Capture and Storage," *IPCC*, 2005.

[5] S. Solomon, M. Carpenter, and T. A. Flach, "Intermediate storage of carbon dioxide in geological formations: A technical perspective," *Int. J. Greenh. Gas Control*, 2, 502–510, 2008.

[6] J. Gross and G. Sadowski, "Perturbed-Chain SAFT: An Equation of State Based on a Pertubation Theory of Chain Molecules," *Ind. Eng. Chem. Res*, 40, 1244–1260, 2001.

[7] W. G. Chapman, K. E. Gubbins, G. Jackson, and M. Radosz, "SAFT: Equation-of-state solution model for associating fluids," *Fluid Phase Equilib.*, 52, 31–38, 1989.

[8] D.-Y. Peng and D. B. Robinson, "A New Two-Constant Equation of State," *Ind. Eng. Chem. Fundam.*, 15, 59–64, 1976.

[9] G. Soave, "Equilibrium constants from a modified Redlich-Kwong equation of state," *Chem. Eng. Sci.*, 27, 1197–1203, 1972.

[10] M. S. Wertheim, "Fluids with highly directional attractive forces. I. Statistical thermodynamics," *J. Stat. Phys.*, 35, 19–34, 1984.

[11] M. S. Wertheim, "Fluids with highly directional attractive forces. III. Multiple attraction sites," *J. Stat. Phys.*, 42, 459–476, 1986.

[12] W. G. Chapman, G. Jackson, and K. E. Gubbins, "Phase equilibria of associating fluids," *Mol. Phys.*, 65, 1057–1079, 1988.

[13] J. Gross and G. Sadowski, "Application of perturbation theory to a hard-chain

reference fluid: An equation of state for square-well chains," *Fluid Phase Equilib.*, 168, 183–199, 2000.

[14] T. Boublík, "Hard-Sphere Equation of State," *J. Chem. Phys.*, 53, 471, 1970.

[15] G. A. Mansoori, N. F. Carnahan, K. E. Starling, and T. W. Leland Jr., "Equilibrium Thermodynamic Properties of the Mixture of Hard Spheres," *J. Chem. Phys.*, 54, 1523, 1971.

[16] D. Henderson, "Perturbation Theory for a Mixture of Hard Sphere and Squre-well molecules," *J. Chem. Phys.*, 61, 926, 1974.

[17] Y. C. Chiew, "Percus-Yevick integral-equation theory for athermal hard-sphere chains," *Mol. Phys.*, 70, 129–143, May 1990.

[18] H. Gulati and C. Hall, "Fluids and fluid mixtures containing square-well diatomics: Equations of state and canonical molecular dynamics simulation," *J. Chem. Phys.*, 107,3930, 1997.

[19] H. Liu and Y. Hu, "Molecular thermodynamic theory for polymer systems part II. Equation of state for chain fluids," *Fluid Phase Equilib.*, 122, 75–97, 1996.

[20] J. A. Barker, "Perturbation Theory and Equation of State for Fluids. II. A Successful Theory of Liquids," *J. Chem. Phys.*, 47, 4714, 1967.

[21] M. L. Michelsen, J. Mollerup, and M. P. Breil, *Thermodynamic Models: Fundamental & Computational Aspects*. Tie-Line Publications, 2008.

[22] S. P. Tan, H. Adidharma, and M. Radosz, "Generalized Procedure for Estimating the Fractions of Nonbonded Associating Molecules and Their Derivatives in Thermodynamic Perturbation Theory," *Ind. Eng. Chem. Res.*, 43, 203–208, 2004.

[23] W. G. Chapman, K. E. Gubbins, G. Jackson, and M. Radosz, "New reference equation of state for associating liquids," *Ind. Eng. Chem. Res.*, 29, 1709–1721, 1990.

[24] D. Fu, L. Liang, X. S. Li, S. Yan, and T. Liao, "Investigation of vapor-liquid equilibria for supercritical carbon dioxide and hydrocarbon mixtures by perturbed-chain statistical associating fluid theory," *Ind. Eng. Chem. Res.*, 45, 4364–4370, 2006.

[25] F. García-Sánchez, G. Eliosa-Jiménez, G. Silva-Oliver, and R. Vázquez-Román,

"Vapor-liquid equilibria of nitrogen-hydrocarbon systems using the PC-SAFT equation of state," *Fluid Phase Equilib.*, 217, 241–253, 2004.

[26] J. A. Nelder and R. Mead, "A Simplex Method for Function Minimization," *Comput. J.*, 7, 308–313, 1965.

[27] N. I. Diamantonis and I. G. Economou, "Evaluation of statistical associating fluid theory (SAFT) and perturbed chain-SAFT equations of state for the calculation of thermodynamic derivative properties of fluids related to carbon capture and sequestration," *Energy and Fuels*, 25, 3334–3343, 2011.

[28] I. Wichterle and R. Kobayashi, "Vapor-liquid equilibrium of methane-ethane-propane system at low temperatures and high pressures," *J. Chem. Eng.*, 17, 13–18, 1972.

[29] R. Miller, A. Kidnay, and M. Hiza, "Liquid+ vapor equilibria in methane+ ethene and in methane+ ethane from 150.00 to 190.00 K," *J. Chem. Thermodyn.*, 9, 167–178, 1977.

[30] J. Davalos and W. Anderson, "Liquid-vapor equilibria at 250.00. deg. K for systems containing methane, ethane, and carbon dioxide," *J. Chem. Eng. Data*, 21, 81–84, 1976.

[31] M. Gupta and G. Gardner, "Liquid-vapor equilibriums for the N2+ CH4+ C2H6 system from 260 to 280 K," *J. Chem. Eng. Data*, 25, 131–318, 1980.

[32] L. Van Horn and R. Kobayashi, "Vapor-liquid equilibria of light hydrocarbons at low temperatures and elevated pressures in hydrocarbon solvents. Methane-propane-n-heptane, methane-ethane-n-," *J. Chem. Eng. Data*, 12, 294–303, 1967.

[33] S. Chang and B. Lu, "Vapor-liquid equilibriums in the nitrogen-methane-ethane system," *Chem. Eng. Prog., Symp. Ser.;(United States)*, 63, 81, 1967.

[34] H. S. Harned, R. J. Davis, and R. D. Jr., "The ionization constant of carbonic acid in water and the solubility of carbon dioxide in water and aqueous salt solutions from 0 to 50°," *J. Am. Chem. Soc.*, 65, 2030–2037, 1943.

[35] M. Hiza and W. Haynes, "Liquid Mixture Excess Volumes and Total Vapor Pressures Using a Magnetic Suspension Densimeter with Compositions Determined by Chromatographic Analysis:," *Adv. Cryog. Eng.*, 23, 594–601, 1978.

[36] I. Wichterle, P. Chappelear, and R. Kobayashi, “Determination of critical exponents from measurements of binary vapor-liquid equilibrium in the neighborhood of the critical line,” *J. Comput. Phys.*, 7, 606–620, 1971.

[37] M. Wei and T. Brown, “Vapor+ liquid equilibria for the ternary system methane+ ethane+ carbon dioxide at 230 K and its constituent binaries at temperatures from 207 to 270 K,” *J. Chem. Eng. Data*, 40, 726–731, 1995.

[38] H. Reamer, B. Sage, and W. Lacey, “Phase Equilibria in Hydrocarbon Systems. Volumetric and Phase Behavior of the Methane-Propane System.,” *Ind. Eng. Chem*, 42, 534–539, 1950.

[39] B. Sage, W. Lacey, and J. Schaafsma, “Phase Equilibria in Hydrocarbon Systems II. Methane-Propane System,” *Ind. Eng. Chem*, 26, 214–217, 1934.

[40] W. Akers, J. Burns, and W. Fairchild, “Low-temperature phase equilibria: methane-propane system,” *Ind. Eng. Chem*, 46, 2531–2534, 1954.

[41] G. Wilson, “Vapor-liquid equilibria of nitrogen, methane, ethane, and propane binary mixtures at LNG temperatures from total pressure measurements.,” *Adv. Cryog. Eng.;(United States)*, 20, Cryogenic engineering conference, Atlanta, GA, USA, 1975.

[42] H. Cheung and D. Wang, “Solubility of volatile gases in hydrocarbon solvents at cryogenic temperatures,” *Ind. Eng. Chem. Fundam.*, 1964, 355–361, 1964.

[43] H. Kalra and D. Robinson, “An apparatus for the simultaneous measurement of equilibrium phase composition and refractive index data at low temperatures and high pressures,” *Cryogenics (Guildf).*, 1975.

[44] A. R. Price and R. Kobayashi, “Low Temperature Vapor-Liquid Equilibrium in Light Hydrocarbon Mixtures: Methane-Ethane-Propane System.,” *J. Chem. Eng. Data*, 4, 40–52, 1959.

[45] J. Kohn and W. Bradish, “Multiphase and Volumetric Equilibria of the Methane-n-Octane System at Temperatures between-110° and 150° C.,” *J. Chem. Eng. Data*, 9, 5–8, 1964.

[46] P. Rousseaux, D. Richon, and H. Renon, “A static method for determination of vapour—liquid equilibria and saturated liquid molar volumes at high pressures and temperatures using a new variable-volume cell,” *Fluid Phase Equilib.*, 11, 153–

168, 1983.

[47] L. Shipman and J. Kohn, “Heterogeneous Phase and Volumetric Equilibrium in the Methane-n-Nonane System.,” *J. Chem. Eng. Data*, 176–180, 1966.

[48] S. Srivastan and N. Darwish, “Solubility of methane in hexane, decane, and dodecane at temperatures from 311 to 423 K and pressures to 10.4 MPa,” *J. Chem. Eng. Data*, 37, 516–520, 1992.

[49] H. Nourozieh, M. Kariznovi, and J. Abedi, “Vapor–liquid equilibrium measurement and thermodynamic modeling of binary systems (methane+n-tetradecane),” *Fluid Phase Equilib.*, 318, 96–101, 2012.

[50] H.-M. Lin, H. M. Sebastian, and K.-C. Chao, “Gas-liquid equilibrium in hydrogen + n-hexadecane and methane + n-hexadecane at elevated temperatures and pressures,” *J. Chem. Eng. Data*, 25, 252–254, 1980.

[51] N. A. Darwish, J. Fathikalajahi, K. A. M. Gasem, and R. L. Robinson, “Solubility of methane in heavy normal paraffins at temperatures from 323 to 423 K and pressures to 10.7 MPa,” *J. Chem. Eng. Data*, 38, 44–48, 1993.

[52] S. H. Huang, H. M. Lin, and K. C. Chao, “Solubility of carbon dioxide, methane, and ethane in n-eicosane,” *J. Chem. Eng. Data*, 33, 145–147, 1988.

[53] S. Puri and J. P. Kohn, “Solid-liquid-vapor equilibrium in the methane-n-eicosane and ethane-n-eicosane binary systems,” *J. Chem. Eng. Data*, 15, 372–374, 1970.

[54] O. Bloomer and J. Parent, “Liquid-vapor phase behavior of the methane-nitrogen system,” *Chem. Eng. Progr. Symp. Ser.*, 49, 11–18, 1953.

[55] A. Kidnay, R. Miller, W. Parrish, and M. Hiza, “Liquid-vapour phase equilibria in the N2□ CH4 system from 130 to 180 K,” *Cryogenics (Guildf).*, 15, 531–540, 1975.

[56] D. . McClure, K. . Lewis, R. . Miller, and L. A. . Staveley, “Excess enthalpies and Gibbs free energies for nitrogen + methane at temperatures below the critical point of nitrogen,” *J. Chem. Thermodyn.*, 8, 785–792, 1976.

[57] R. Stryjek, P. S. Chappelear, and R. Kobayashi, “Low-temperature vapor-liquid equilibriums of nitrogen-ethane system,” *J. Chem. Eng. Data*, 19, 340–343, 1974.

[58] V. Fastovsky and Y. Petrovsky, “An investigation of the liquid-vapor equilibrium

in the nitrogen-methane system," *Zh. Fiz. Khim*, 31, 2317, 1957.

[59] R. Miller, A. Kidnay, and M. Hiza, "Liquid-vapor equilibria at 112.00 K for systems containing nitrogen, argon, and methane," *AIChE J.*, 19, 145–151, 1973.

[60] S. Fuks and A. Bellemans, "Excess Free Energies and Volumes of two Simple Binary Liquid Mixtures: Methane-Krypton and Nitrogen-Methane," *Bull. des Sociétés Chim. Belges*, 76, 290–299, 1967.

[61] L. Brandt and L. Stroud, "Phase Equilibria in Natural Gas Systems. Apparatus with Windowed Cell for 800 PSIG and Temperatures to 320° F.," *Ind. Eng. Chem.*, 50, 849–852, 1958.

[62] Z. Jin, K. Liu, and W. Sheng, "Vapor-liquid equilibrium in binary and ternary mixtures of nitrogen, argon, and methane," *J. Chem. Eng. Data*, 38, 353–355, 1993.

[63] J. Kohn and F. Kurata, "Heterogeneous phase equilibria of the methane—hydrogen sulfide system," *AIChE J.*, 4, 211–217, 1958.

[64] H. Reamer, B. Sage, and W. Lacey, "Volumetric and phase behavior of the methane-hydrogen sulfide system," *Ind. Eng. Chem*, 1951.

[65] J. Kohn and F. Kurata, "Volumetric Behavior of the Methane-Hydrogen Sulfide System at Low Temperatures and High Pressures.," *J. Chem. Eng. Data*, 4, 33–36, 1959.

[66] N. Yarym-Agaev and L. Afanasenko, "Gas-liquid equilibrium in the methanehydrogen sulfide system below 273 K," *Ukr. Khim. Z*, 10, 25–29, 1991.

[67] A. J. Kidnay, R. C. Miller, W. R. Parrish, and M. J. Hiza, "Liquid-vapour phase equilibria in the N_2-CH_4 system from 130 to 180 K," *Cryogenics (Guildf).*, 15, 531–540, 1975.

[68] H. H. Reamer, B. H. Sage, and W. N. Lacey, "Phase Equilibria in Hydrocarbon Systems. Volumetric and Phase Behavior of the Propane-Carbon Dioxide System," *Ind. Eng. Chem.*, 43, 2515–2520, 1951.

[69] W. W. Akers, R. E. Kelley, and T. G. Lipscomb, "Carbon-Dioxide Propane System," *Ind. Eng. Chem.*, 46, 2535–2536, 1954.

[70] F. H. Poettmann and D. L. Katz, "Phase Behavior of Binary Carbon Dioxide-

Paraffin Systems," *Ind. Eng. Chem.*, 37, 847–853, 1945.

[71] S. E. M. Hamam and B. C. Y. Lu, "Isothermal vapor-liquid equilibriums in binary system propane-carbon dioxide," *J. Chem. Eng. Data*, 21, 200–204, 1976.

[72] M. H. Kunio Nagahama, Hitoshi Konishi, Daisuke Hoshino, "Binary Vapor-Liquid Equilibria of Carbon Dioxide-Light Hydrocarbons At Low Temperature," *J. Chem. Eng. Japan*, 7, 323–328, 1974.

[73] J. C. Acosta, E. Hevia, and S. Leipziger, "Dew and bubble point measurements for carbon dioxide-propane mixtures," *J. Chem. Eng. Data*, 29, 304–309, 1984.

[74] V. Niesen and J. Rainwater, "Critical locus,(vapor+ liquid) equilibria, and coexisting densities of (carbon dioxide+ propane) at temperatures from 311 K to 361 K," *J. Chem. Thermodyn.*, 1990.

[75] H. Kalra, T. R. Krishnana, and D. B. Robinson, "Equilibrium-phase properties of carbon dioxide-butane and nitrogen-hydrogen sulfide systems at subambient temperatures.," *J. Chem. Eng. Data*, 21, 222–225, 1976.

[76] L. A. Weber, "Vapour-liquid equilibria measurements for carbon dioxide with normal and isobutane from 250 to 280 K," *Cryogenics (Guildf).*, 25, 338–342, 1985.

[77] T. S. Brown, V. G. Niesen, E. D. Sloan, and A. J. Kidnay, "Vapor-liquid equilibria for the binary systems of nitrogen, carbon dioxide, and n-butane at temperatures from 220 to 344 K.," *Fluid Phase Equilib.*, 53, 7–14, 1989.

[78] A. D. Leu and D. B. Robinson, "Equilibrium phase properties of the n-butane-carbon dioxide and isobutane-carbon dioxide binary systems," *J. Chem. Eng. Data*, 32, 444–447, 1987.

[79] G. J. Besserer and D. B. Robinson, "A high pressure autocollimating refractometer for determining coexisting liquid and vapor phase densities," *Can. J. Chem. Eng.*, 49, 651–656, 1971.

[80] P. Traub and K. Stephan, "High-pressure phase equilibria of the system CO 2—water-acetone measured with a new apparatus," *Chem. Eng. Sci.*, 45, 751–758, 1990.

[81] N. Nagarajan, K. A. M. Gasem, and R. L. Robinson, "Equilibrium phase

compositions, phase densities, and interfacial tensions for carbon dioxide + hydrocarbon systems. 6. Carbon dioxide + n-butane + n-decane," *J. Chem. Eng. Data*, 35, 228–231, 1990.

[82] S. K. Shibata and S. I. Sandler, "High-pressure vapor-liquid equilibria involving mixtures of nitrogen, carbon dioxide, and n-butane," *J. Chem. Eng. Data*, 34, 291–298, 1989.

[83] M. P. de Fernandez, "Vapor-liquid equilibrium in the binary system carbon dioxide+ n-butane," *J. Chem.& Eng. Data* ,34, 324-328, 1989.

[84] V. Niesen, "(Vapor+ liquid) equilibria and coexisting densities of (carbon dioxide+ n-butane) at 311 to 395 K," *J. Chem. & Eng. Data Thermodyn.*, 21, 915-923, 1989.

[85] E. Levitskaya and K. Pryannikov, "Equilibrium between liquid and vapor in the binary system of hydrogen and ethane," *Zh. Tekh. Fiz*, 9, 1849–1853, 1939.

[86] G. J. Besserer and D. B. Robinson, "Equilibrium-phase properties of n-pentane-carbon dioxide system," *J. Chem. Eng. Data*, 18, 416–419, 1973.

[87] N. Xu, J. Yao, Y. Wang, J. Shi, and B. C.-Y. Lu, "Vapor-liquid equilibria of five binary systems containing R-22," *Fluid Phase Equilib.*, 69, 261–270, 1991.

[88] H. Cheng, M. E. Pozo de Fernandez, J. A. Zollweg, and W. B. Streett, "Vapor-liquid equilibrium in the system carbon dioxide + n-pentane from 252 to 458 K at pressures to 10 MPa," *J. Chem. Eng. Data*, 34, 319–323, 1989.

[89] K. Ohgaki and T. Katayama, "Isothermal vapor-liquid equilibrium data for binary systems containing carbon dioxide at high pressures: methanol-carbon dioxide, n-hexane-carbon dioxide, and benzene-carbon dioxide systems," *J. Chem. Eng. Data*, 21, 53–55, 1976.

[90] Z. Wagner and I. Wichterle, "High-pressure vapour—liquid equilibrium in systems containing carbon dioxide, 1-hexene, and n-hexane," *Fluid Phase Equilib.*, 33, 109–123, 1987.

[91] Y.-H. Li, K. H. Dillard, and R. L. Robinson, "Vapor-liquid phase equilibrium for carbon dioxide-n-hexane at 40, 80, and 120 .degree.C," *J. Chem. Eng. Data*, 26, 53–55, 1981.

[92] G.-I. Kaminishi, C. Yokoyama, and T. Shinji, "Vapor pressures of binary mixtures

of carbon dioxide with benzene, n-hexane and cyclohexane up to 7 MPa," *Fluid Phase Equilib.*, 34, 83–99, 1987.

[93] H. Kalra, H. Kubota, D. B. Robinson, and H.-J. Ng, "Equilibrium phase properties of the carbon dioxide-n-heptane system," *J. Chem. Eng. Data*, 23, 317–321, 1978.

[94] H. Inomata, K. Arai, and S. Saito, "Measurement of vapor-liquid equilibria at elevated temperatures and pressures using a flow type apparatus," *Fluid Phase Equilib.*, 29, 225–232, 1986.

[95] M. King and H. Al-Najjar, "The solubilities of carbon dioxide, hydrogen sulphide and propane in some normal alkane solvents - I: Experimental determinations in the range 15–70° C and," *Chem. Eng. Sci.*, 32, 1247–1252, 1977.

[96] R. J. Wilcock, R. Battino, W. F. Danforth, and E. Wilhelm, "Solubilities of gases in liquids II. The solubilities of He, Ne, Ar, Kr, O_2, N_2, CO, CO_2, CH_4, CF_4, and SF6 in n-octane 1-octanol, n-decane, and 1-decanol," *J. Chem. Thermodyn.*, 10, 817–822, 1978.

[97] W. L. Weng and M. J. Lee, "Vapor-liquid equilibrium of the octane/carbon dioxide, octane/ethane, and octane/ethylene systems," *J. Chem. Eng. Data*, 37, 213–215, 1992.

[98] D. Jennings and R. Schucker, "Comparison of high-pressure vapor-liquid equilibria of mixtures of CO_2 or propane with nonane and C9 alkylbenzenes," *J. Chem. Eng. Data*, 41, 831–838, 1996.

[99] Yun Zhi;Shi Meiren;Shi Jun, "High Pressure Vapor-Liquid Phase Equilibria for Carbon Dioxide-n-Octane and Carbon Dioxide-n-Nonane," *J. Chem. Eng. Chinese Univ.*, 9, 396, 1995.

[100] H. H. Reamer and B. H. Sage, "Phase Equilibria in Hydrocarbon Systems. Volumetric and Phase Behavior of the n-Decane-CO_2 System.," *J. Chem. Eng. Data*, 8, 508–513, 1963.

[101] H. M. Sebastian, J. J. Simnick, H.-M. Lin, and K.-C. Chao, "Vapor-liquid equilibrium in binary mixtures of carbon dioxide + n-decane and carbon dioxide + n-hexadecane," *J. Chem. Eng. Data*, 25, 138–140, 1980.

[102] G. F. Chou, R. R. Forbert, and J. M. Prausnitz, "High-pressure vapor-liquid equilibria for carbon dioxide/n-decane, carbon dioxide/tetralin, and carbon

dioxide/n-decane/tetralin at 71.1 and 104.4.degree. C," *J. Chem. Eng. Data*, 35, 26–29, 1990.

[103] W. Adams, J. Zollweg, W. Streett, and S. Rizvi, "New apparatus for measurement of supercritical fluid-liquid phase equilibria," *AIChE J.*, 34, 1387–1391, 1988.

[104] Y. Iwai, N. Hosotani, T. Morotomi, Y. Koga, and Y. Arai, "High-Pressure Vapor-Liquid Equilibria for Carbon Dioxide + Linalool," *J. Chem. Eng. Data*, 39, 900–902, 1994.

[105] K. A. M. Gasem, P. B. Dulcamara, K. B. Dickson, and R. L. Robinson, "Test of prediction methods for interfacial tensions of CO_2 and ethane in hydrocarbon solvents," *Fluid Phase Equilib.*, 53, 39–50, 1989.

[106] B. Schwarz and J. Prausnitz, "Solubilities of methane, ethane, and carbon dioxide in heavy fossil-fuel fractions," *Ind. Eng. Chem. Res.*,26, 1987.

[107] D. J. Fall, J. L. Fall, and K. D. Luks, "Liquid-liquid-vapor immiscibility limits in carbon dioxide + n-paraffin mixtures," *J. Chem. Eng. Data*, 30, 82–88, 1985.

[108] Y. Sato, Y. Tagashira, D. Maruyama, S. Takishima, and H. Masuoka, "Solubility of carbon dioxide in eicosane, docosane, tetracosane, and octacosane at temperatures from 323 to 473 K and pressures up to 40 MPa," *Fluid Phase Equilib.*, 147, 181–193, 1998.

[109] N. C. Huie, K. D. Luks, and J. P. Kohn, "Phase-equilibriums behavior of systems carbon dioxide-n-eicosane and carbon dioxide-n-decane-n-eicosane," *J. Chem. Eng. Data*, 18, 311–313, 1973.

[110] K. A. M. Gasem and R. L. Robinson, "Solubilities of carbon dioxide in heavy normal paraffins (C20-C44) at pressures to 9.6 MPa and temperatures from 323 to 423 K," *J. Chem. Eng. Data*, 30, 53–56, 1985.

[111] D. J. Fall and K. D. Luks, "Phase equilibria behavior of the systems carbon dioxide + n-dotriacontane and carbon dioxide + n-docosane," *J. Chem. Eng. Data*, 29, 413–417, 1984.

[112] F. N. Tsai and J. S. Yau, "Solubility of carbon dioxide in n-tetracosane and in n-dotriacontane," *J. Chem. Eng. Data*, 35, 43–45, 1990.

[113] M. W. Barrick, J. M. Anderson, and R. L. Robinson, "Solubilities of carbon

dioxide in cyclohexane and trans-decalin at pressures to 10.7 MPa and temperatues from 323 to 423 K," *J. Chem. Eng. Data*, 31, 172–175, 1986.

[114] M. K. Gupta, Y. H. Li, B. J. Hulsey, and R. L. Robinson, "Phase equilibrium for carbon dioxide-benzene at 313.2, 353.2, and 393.2 K," *J. Chem. Eng. Data*, 27, 55–57, 1982.

[115] N. Nagarajan and R. L. Robinson, "Equilibrium phase compositions, phase densities, and interfacial tensions for carbon dioxide + hydrocarbon systems. 3. CO_2 + cyclohexane. 4. CO_2 + benzene," *J. Chem. Eng. Data*, 32, 369–371, 1987.

[116] C.-H. Kim, P. Vimalchand, and M. D. Donohue, "Vapor-liquid equilibria for binary mixtures of carbon dioxide with benzene, toluene and p-xylene," *Fluid Phase Equilib.*, 31, 299–311, 1986.

[117] H. Inomata, K. Arai, and S. Saito, "Vapor- liquid equilibria for CO 2/hydrocarbon mixtures at elevated temperatures and pressures," *Fluid Phase Equilib.*, 36, 107–119, 1987.

[118] P. G. Bendale and R. M. Enick, "Use of carbon dioxide to shift benzene/acetonitrile and benzene/cyclohexane azeotropes," *Fluid Phase Equilib.*, 94, 227–253, 1994.

[119] H.-J. Ng and D. B. Robinson, "Equilibrium-phase properties of the toluene-carbon dioxide system," *J. Chem. Eng. Data*, 23, 325–327, 1978.

[120] H. M. Sebastian, J. J. Simnick, H.-M. Lin, and K.-C. Chao, "Gas-liquid equilibrium in mixtures of carbon dioxide + toluene and carbon dioxide + m-xylene," *J. Chem. Eng. Data*, 25, 246–248, 1980.

[121] U. Wa¨terling, D. Zheng, and H. Knapp, "Vapor—liquid equilibria at high temperatures and pressures in binary mixtures containing H_2, CH_4 and CO_2 with high boiling hydrocarbons: experimental equipment and results," *Chem. Eng. Process. Process Intensif.*, 29, 155–164, May 1991.

[122] S. D. Fink and H. C. Hershey, "Modeling the vapor-liquid equilibria of 1,1,1-trichloroethane + carbon dioxide and toluene + carbon dioxide at 308, 323, and 353 K," *Ind. Eng. Chem. Res.*, 29, 295–306, 1990.

[123] A. L. Muhlbauer and J. D. Raal, "Measurement and thermodynamic interpretation of high-pressure vapour—liquid equilibria in the toluene CO_2 system," *Fluid Phase Equilib.*, 64, 213–236, 1991.

[124] W. O. Morris and M. D. Donohue, “Vapor-liquid equilibria in mixtures containing carbon dioxide, toluene, and 1-methylnaphthalene,” *J. Chem. Eng. Data*, 30, 259–263, 1985.

[125] D. Walther, B. Platzer, and G. Maurer, “High-pressure (vapour + liquid) equilibria of (carbon dioxide + methylbenzene or 1,2-dimethylbenzene or 1,3-dimethylbenzene or 1,4-dimethylbenzene) at temperatures between 313 K and 393 K and pressures up to 17.3 MPa,” *J. Chem. Thermodyn.*, 24, 387–399, 1992.

[126] C. J. Chang, “Volume Expansion Coefficients and Activity Coefficients of High-Pressure Carbon Dioxide Dissolution in Organic Liquids at 298K.,” *J. Chem. Eng. JAPAN*, 25, 164–170, 1992.

[127] C. J. Chang, C.-Y. Chen, and H.-C. Lin, “Solubilities of Carbon Dioxide and Nitrous Oxide in Cyclohexanone, Toluene, and N,N-Dimethylformamide at Elevated Pressures,” *J. Chem. Eng. Data*, 40, 850–855, 1995.

[128] A. Fredenslund and G. A. Sather, “Gas-liquid equilibrium of the oxygen-carbon dioxide system,” *J. Chem. Eng. Data*, 15, 17–22, 1970.

[129] G. Kaminishi and T. Toriumi, “Gas-liquid equilibrium under high pressures. VI. Vapor-liquid phase equilibrium in the CO_2-H_2, CO_2-N_2, and CO_2-O_2 systems,” *Kogyo Kagaku Zasshi*, 69, 175–178, 1966.

[130] G. Zenner and L. Dana, “Liquid-vapor equilibrium compositions of carbon dioxide-oxygen-nitrogen mixtures,” *Chem. Eng. Prog. Symp. Ser.*, 59, 36–41, 1963.

[131] E. Sarashina, Y. Arai, and S. Sasto, “The p-v-t-x relation for the carbon dioxide-argon system,” *J. Chem. Eng. Japan*, 4, 379–381, 1971.

[132] G.-I. Kaminishi, Y. Arai, S. Saito, and S. Maeda, “Vapor-liquid equilibria for binary and ternary systems containing carbon dioxide,” *J. Chem. Eng. Japan*, 1, 109–116, 1968.

[133] C. Coquelet, A. Valtz, F. Dieu, D. Richon, P. Arpentinier, and F. Lockwood, “Isothermal P, x, y data for the argon+carbon dioxide system at six temperatures from 233.32 to 299.21K and pressures up to 14MPa,” *Fluid Phase Equilib.*, 273, 38–43, 2008.

[134] D. P. Sobocinski and F. Kurata, “Heterogeneous phase equilibria of the hydrogen

sulfide–carbon dioxide system," *AIChE J.*, 5, 545–551, 1959.

[135] J. A. Bierlein and W. B. Kay, "Phase-Equilibrium Properties of System Carbon Dioxide-Hydrogen Sulfide," *Ind. Eng. Chem.*, 45, 618–624, 1953.

[136] J. Brewer, N. Rodewald, and F. Kurata, "Phase equilibria of the propane-hydrogen sulfide system from the cricondontherm to the solid-liquid-vapor region," *AIChE J.*, 7, 13–16, 1961.

[137] E. R. Gilliland and H. W. Scheeline, "High-Pressure Vapor-Liquid Equilibrium," *Ind. Eng. Chem.*, 32, 48–54, 1940.

[138] W. B. Kay and G. M. Rambosek, "Liquid-Vapor Equilibrium Relations in Binary Systems - Propane - Hydrogen Sulfide System.," *Ind. Eng. Chem.*, 45, 221–226, 1953.

[139] F. Von Steckel, "Dampf-Flussigkeits-Gleichgewichte einiger binarer, schwefelwasserstoffhaltiger systeme unter Druck," *Sven. Kem. Tidskr.*, 1945.

[140] H. Reamer, B. Sage, and W. Lacey, "Phase equilibria in hydrocarbon systems-volumetric and phase behavior of n-pentane–hydrogen sulfide system," *Ind. Eng. Chem.*, 45, 1805–1809, 1953.

[141] S. Laugier and D. Richon, "Vapor-Liquid Equilibria for Hydrogen Sulfide + Hexane, + Cyclohexane, + Benzene, + Pentadecane, and + (Hexane + Pentadecane)," *J. Chem. Eng. Data*, 40, 153–159, 1995.

[142] K. H. Robinson, DB, *GPA .Res.Rep*, 15, 1975.

[143] B. Eakin and W. DeVaney, "Vapor-liquid equilibria in hydrogen hydrogen sulfide C9 hydrocarbon systems," *AIChE Symp. Ser*, 70, 80–90, 1974.

[144] W. N. Reamer, H. H.; Selleck, F. T.; Sage, B. H.; Lacey, "Phase equilibria in hydrocarbon systems-Volumetric and Phase Behavior of Decane–Hydrogen Sulfide System," *Ind. Eng. Chem*, 45, 1810−1812, 1953.

[145] C. Yokoyama, A. Usui, and S. Takahashi, "Solubility of hydrogen sulfide in isooctane, n-decane, n-tridecane, n-hexadecane and squalane at temperatures from 323 to 523 K and pressures up to 1.6 MPa," *Fluid Phase Equilib.*, 85, 257–269, May 1993.

[146] G. X. Feng and A. E. Mather, "Solubility of hydrogen sulfide in n-eicosane at

elevated pressure," *J. Chem. Eng. Data*, 37, 412–413, 1992.

[147] I. M. Elshayal and B. C. Y. Lu, "Vapor-liquid equilibrium data for nitrogen-argon-oxygen mixtures. Evaluation and correlation," *J. Chem. Eng. Data*, 16, 31–37, 1971.

[148] I. Burn and F. Din, "Liquid-vapour equilibrium of the system argon + oxygen at pressures up to 10 atmospheres," *Trans. Faraday Soc.*, 58, 1341, 1962.

[149] F. Schindler, D. L.; Swift, G. W.; Kurata, "More low temperature VL design data," *Hydro. Process. Pet. Ref*, 45, 205–210, 1966.

[150] L. Grausø, A. Fredenslund, and J. Mollerup, "Vapour-liquid equilibrium data for the systems C_2H_6+ N_2, C_2H_4+ N_2, C_3H8+ N_2, and C_3H_6+ N_2," *Fluid Phase Equilib.*, 1, 13–26, 1977.

[151] H. Kremer and H. Knapp, "Three-phase conditions are predictable," *Hydrocarb. Process. (United States)*, 62, 4, 1983.

[152] F. M. Llave, K. D. Luks, and J. P. Kohn, "Three-phase liquid-liquid-vapor equilibria in the binary systems nitrogen + ethane and nitrogen + propane," *J. Chem. Eng. Data*, 30, 435–438, 1985.

[153] D. Poon and B. Lu, "Phase equilibria for systems containing nitrogen, methane, and propane," *Adv. Cryog. Eng.*, 19, 292–299, 1995.

[154] W. W. Akers, L. L. Attwell, and J. A. Robinson, "Nitrogen-Butane System," *Ind. Eng. Chem.*, 46, 2539–2540, 1954.

[155] L. Roberts and J. McKetta, "Vapor-liquid equilibrium in the n-butane-nitrogen system," *AIChE J.*, 7, 173–174, 1961.

[156] W. R. Lehigh and J. J. McKetta, "Vapor-Liquid Equilibrium in the Ethane-n-Nitrogen System.," *J. Chem. Eng. Data*, 11, 180–182, 1966.

[157] M. K. F. Malewski and S. I. Sandler, "High-pressure vapor-liquid equilibria of the binary mixtures nitrogen + n-butane and argon + n-butane," *J. Chem. Eng. Data*, 34, 424–426, 1989.

[158] H. Kalra, D. B. Robinson, and G. J. Besserer, "The equilibrium phase properties of the nitrogen-n-pentane system," *J. Chem. Eng. Data*, 22, 215–218, 1977.

[159] S. Peter and H. Eicke, "Phase equilibrium in the systems n-heptane-nitrogen,

methylcyclohexane-nitrogen, and n-heptane-methylcyclohexane-nitrogen at high pressure," *Ber. Bunsen-Ges*, 7, 99–104, 1970.

[160] W. Akers, D. Kehn, and C. Kilgore, "Volumetric and Phase Behavior of Nitrogen-Hydrogen Systems: Nitrogen-n-Heptane System," *Ind. Eng. Chem. Research*, 46, 2536–2539, 1954.

[161] P. Figuiere, J. Hom, and S. Laugier, "Vapor-liquid equilibria up to 40,000 KPa and 400° C: A new static method," *AIChE J*, 26, 872–875, 1980.

[162] D. Legret, D. Richon, and H. Renon, "Vapor liquid equilibria up to 100 MPa: A new apparatus," *AIChE J.*, 27, 203–207, 1981.

[163] F. M. Llave and T. H. Chung, "Vapor-liquid equilibria of nitrogen-hydrocarbon systems at elevated pressures," *J. Chem. Eng. Data*, 33, 123–128, 1988.

[164] G. Brunner, S. Peter, and H. Wenzel, "Phase equilibrium in the systems n-heptane-nitrogen, methylcyclohexane-nitrogen and n-heptane-methylcyclohexane-nitrogen at high pressures," *Chem. Eng. J.*, 7, 99–104, 1974.

[165] J. L. Daridon, B. Lagourette, and P. Xans, "Thermodynamic properties of liquid mixtures containing gas under pressure based on ultrasonic measurements," *Fluid Phase Equilib.*, 100, 269–282, 1994.

[166] E. Graham and K. Weale, "The solubility of compressed gases in nonpolar liquids," *Prog. Int. Res. Thermodyn. Transp. Prop. ASME Proc. from 2nd Symp. Thermophys. Prop. Princeton, NJ*, 153–158, 1962.

[167] A. Azarnoosh and J. J. McKetta, "Nitrogen-n-Decane System in the Two-Phase Region.," *J. Chem. Eng. Data*, 8, 494–496, 1963.

[168] Jianfen Tong, Wuzi Gao, A. Robert L. Robinson, Jr., and K. A. M. Gasem, "Solubilities of Nitrogen in Heavy Normal Paraffins from 323 to 423 K at Pressures to 18.0 MPa," *J. Chem. Eng. Data*, 44, 784–787, 1999.

[169] F. Sprow and J. Prausnitz, "Vapor-Liquid equilibria for five cryogenic mixtures," *AIChE J.*, 12, 780–784, 1966.

[170] P. L. Thorpe, "Liquid-vapour equilibrium of the system nitrogen + argon at pressures up to 10 atm," *Trans. Faraday Soc.*, 64, 2273, 1968.

[171] K. . Lewis and L. A. . Staveley, "Excess enthalpies of the liquid mixtures nitrogen

+ oxygen, nitrogen + argon, argon + ethane, and methane + carbon tetrafluoride," *J. Chem. Thermodyn.*, 7, 855–864, 1975.

[172] D. R. Massengill and R. C. Miller, "Temperature dependence of excess volumes for simple liquid mixtures: N_2 + Ar, N_2 + Ar + CH_4," *J. Chem. Thermodyn.*, 5, 207–217, 1973.

[173] I. Elshayal and B. Lu, "Measurement of total pressures for ethylene—propane mixtures," *Can. J. Chem. Eng.*, 53, 83–87, 1975.

[174] G. Narinskii, "Liquid-vapour equilibrium in argon-nitrogen system. i. experimental data and their verification," *Russ. J. Phys. Chem.*, 1966.

[175] and L. A. K. Pool, R. A. H., G. Saville, T. M. Herrington, B. D. C. Shields and Staveley, "Some excess thermodynamic functions for the liquid systems argon+ oxygen, argon+ nitrogen, nitrogen+ oxygen, nitrogen+ carbon monoxide, and argon+," *Trans. Faraday Soc*, 58, 1692, 1962.

[176] F. Dolezalek, "On the theory of binary mixtures vs. vapor tension and molecular constitution of liquid argon and argon–nitrogen mixtures," *Z. Phys. Chem*, 1919.

[177] G. M. Wilson, P. M. Silverberg, and M. G. Zellner, "Argon-oxygen-nitrogen three component system experimental vapor-liquid equilibrium data.," 1964.

[178] P. Uchytil and I. Wichterle, "Liquid-vapour critical region of the most volatile component of a ternary system. I. Vapour-liquid equilibria in the ethane-propane-n-butane system," *Fluid Phase Equilib.*, 15, 209–217, 1983.

[179] J. Mikšovský and I. Wichterle, "Vapour-liquid equilibria in the ethane-propane system at high pressures," *Collect. Czech. Chem. Commun*, 40, 365–370, 1975.

[180] D. E. Matschke and G. Thodos, "Vapor-Liquid Equilibria for the Ethane-Propane System.," *J. Chem. Eng. Data*, 7, 232–234, 1962.

[181] H. Poll, H. Huemer, and F. Moser, "Eine Apparatur zur Bestimmung von Dampf-Flüssigkeits-Gleichgewichten unter erh htem Druck," *Monatshefte for Chemie*, 111, 1159–1164, 1980.

[182] C. J. Blanc and J. C. B. Setier, "Vapor-liquid equilibria for the ethane-propane system at low temperature," *J. Chem. Eng. Data*, 33, 111–115, 1988.

[183] L. Djordjevich and R. A. Budenholzer, "Vapor-liquid equilibrium data for ethane-

propane system at low temperatures," *J. Chem. Eng. Data*, 15, 10–12, 1970.

[184] L. C. Kahre, "Liquid density of light hydrocarbon mixtures," *J. Chem. Eng. Data*, 18, 267–270, 1973.

[185] M. Hirata, S. Suda, T. Hakuta, and K. Nagahama, "Light hydrocarbon vapor-liquid equilibria," *Mem. Fac. Technol., Tokyo Metrop. Univ*, 1969.

[186] V. Skripka, I. Nikitina, L. Zhdanovieh, and A. Sirotin, "Liquid-vapor phase equilibrium at low temperatures in binary systems, components produced from natural gas," *Gazov Promst*, 1970.

[187] V. S. Mehra and G. Thodos, "Vapor-Liquid Equilibrium in the Ethane-n-Butane System.," *J. Chem. Eng. Data*, 10, 307–309, 1965.

[188] V. Lhoták and I. Wichterle, "Vapour-liquid equilibria in the ethane-n-butane system at high pressures," *Fluid Phase Equilib.*, 6, 229–235, 1981.

[189] P. Uchitil and I. Wichterle, "Vapour liquid equilibria in the ethane propane n butane system," *Fluid Phase Equilibr*, 12, 307–309, 1983.

[190] J. Dingrani and G. Thodos, "Vapor-liquid equilibrium behavior of the ethane-n-butane-n-hexane system," *Can. J. Chem. Eng.*, 56, 616–623, 1978.

[191] A. Clark and K. Stead, "VLE of ternary systems ethan carbon dioxide butane and ethane- propane- butane," *J. Chem. Thermodyn.*, 20, 413-428, 1988.

[192] H. H. Reamer, B. H. Sage, and W. N. Lacey, "Phase Equilibria in Hydrocarbon Systems. Volumetric and Phase Behavior of the Ethane-n-Pentane System.," *J. Chem. Eng. Data*, 5, 44–50, 1960.

[193] E. J. Zais and I. H. Silberberg, "Vapor-liquid equilibriums in the ethane-n-hexane system," *J. Chem. Eng. Data*, 15, 253–256, 1970.

[194] W. B. Kay, "Liquid-Vapor Phase Equilibrium Relations in the Ethane-n-Heptane System," *Ind. Eng. Chem.*, 30, 459–465, 1938.

[195] A. B. J. Rodrigues, D. S. McCaffrey, and J. P. Kohn, "Heterogeneous phase and volumetric equilibrium in the ethane-n-octane system," *J. Chem. Eng. Data*, 13, 164–168, 1968.

[196] H. Reamer and B. Sage, "Phase Equilibria in Hydrocarbon Systems. Volumetric and Phase Behavior of the Ethane-n-Decane System.," *J. Chem. Eng. Data*, 8, 508–

513, 1962.

[197] B. A. Bufkin, R. L. Robinson, S. S. Estrera, and K. D. Luks, “Solubility of ethane in n-decane at pressures to 8.2 MPa and temperatures from 278 to 411 K,” *J. Chem. Eng. Data*, 31, 421–423, 1986.

[198] H. Reamer, J. Lower, and B. Sage, “Duffusion Coefficients in Hydrocarbon Systems. Ethane in the Liquid Phase of the Ethane-n-Decane System.,” *J. Chem.& Eng. Data*, 9, 54–59, 1964.

[199] M. Meskel-Lesavre, D. Richon, and H. Renon, “New variable volume cell for determining vapor-liquid equilibriums and saturated liquid molar volumes by the static method,” *Ind. Eng. Chem. Fundam.*, 20, 284–289, 1981.

[200] M. Kariznovi, H. Nourozieh, and J. Abedi, “Measurement and modeling of liquid saturated properties (solubility, density, and viscosity) of (ethane+ n-tetradecane) binary systems,” *J. Chem. Eng. Data*, 56, 3669–3672, 2011.

[201] H. Nourozieh, M. Kariznovi, and J. Abedi, “Experimental Measurement and Equation of State Modeling of Liquid Saturated Properties (Solubility, Density, and Viscosity) of (Ethane+ n-Octadecane) Binary,” *J. Chem. & Eng.Data*, 57, 137–141, 2011.

[202] K. A. M. Gasem, B. A. Bufkin, A. M. Raff, and R. L. Robinson, “Solubilities of ethane in heavy normal paraffins at pressures to 7.8 MPa and temperatures from 348 to 423 K,” *J. Chem. Eng. Data*, 34, 187–191, 1989.

[203] S. Zeck and H. Knapp, “Vapor—liquid and vapor—liquid—liquid phase equilibria for binary and ternary systems for nitrogen, ethane and methanol: Experiment and data reduction,” *Fluid Phase Equilib.*, 25, 303–322, 1986.

[204] T. Brown, E. Sloan, and A. Kidnay, “Vapor-liquid equilibria in the nitrogen+ carbon dioxide+ ethane system,” *Fluid Phase Equilib.*, 1989.

[205] K. Ohgaki and T. Katayama, “Isothermal vapor-liquid equilibrium data for the ethane—carbon dioxide system at high pressures,” *Fluid Phase Equilib.*, 1, 27–32, 1977.

[206] T. S. Brown, A. J. Kidnay, and E. D. Sloan, “Vapor—liquid equilibria in the carbon dioxide-ethane system,” *Fluid Phase Equilib.*, 40, 169–184, 1988.

[207] T. Hakuta, K. Nagahama, and S. Suda, “Binary vapour-liquid equilibria of CO 2-C 2 H 6 hydrocarbons,” *J. Chem. Eng. Japan*, 7, 323–328, 1970.

[208] R. Gugnoni, J. Eldridge, V. Okay, and T. Lee, “Carbon dioxide-ethane phase equilibrium and densities from experimental measurements and the B-W-R equation,” *AIChE J.*, 1974.

[209] A. Fredenslund and J. Mollerup, “Measurement and prediction of equilibrium ratios for the C_2H_6+ CO_2 system,” *J. Chem. Soc. Faraday Trans. 1 Phys. Chem. Condens. Phases*, 70, 1653, 1974.

[210] H. Kalra, D. Robinson, and T. Krishnan, “The equilibrium phase properties of the ethane-hydrogen sulfide system at subambient temperatures,” *J. Chem. & Eng. Data*, 22, 85–88, 1977.

[211] N. Von Solms, M. L. Michelsen, C. P. Passos, S. O. Derawi, and G. M. Kontogeorgis, “Investigating models for associating fluids using spectroscopy,” *Ind. Eng. Chem. Res.*, 45, 5368–5374, 2006.

[212] “https://www.nist.gov,” *Natl. Inst. Stand. Technol.*

[213] C. Held, L. F. Cameretti, and G. Sadowski, “Modeling aqueous electrolyte solutions: Part 1. Fully dissociated electrolytes,” *Fluid Phase Equilib.*, 270, 87–96, 2008.

[214] J. Gross and G. Sadowski, “Application of the Perturbed-Chain SAFT Equation of State to Associating Systems” *Ind. Eng. Chem. Res.*, 41, 5510–5515, 2002.

[215] Z. Duan, N. Møller, J. Greenberg, and J. H. Weare, “The prediction of methane solubility in natural waters to high ionic strength from 0 to 250°C and from 0 to 1600 bar,” *Geochim. Cosmochim. Acta*, 56, 1451–1460, 1992.

[216] Z. Duan, R. Sun, R. Liu, and C. Zhu, “Accurate thermodynamic model for the calculation of H2S solubility in pure water and brines,” *Energy & Fuels*, 21, 2056–2065, 2007.

[217] Z. Duan, N. Møller, J. Greenberg, and J. Weare, “The prediction of methane solubility in natural waters to high ionic strength from 0 to 250 C and from 0 to 1600 bar,” *Geochim. Cosmochim. Acta*, 56, 1451–1460, 1992.

[218] S. Mao, Z. Zhang, J. Hu, R. Sun, and Z. Duan, “An accurate model for calculating

C 2 H 6 solubility in pure water and aqueous NaCl solutions," *Fluid Phase Equilib.*, 238, 77–86, 2005.

[219] A. Chapoy, S. Mokraoui, A. Valtz, D. Richon, A. H. Mohammadi, and B. Tohidi, "Solubility measurement and modeling for the system propane–water from 277.62 to 368.16K," *Fluid Phase Equilib.*, 226, 213–220, 2004.

[220] W. Hayduk, "IUPAC Solubility Data Series, 9," 1982.

[221] W.-Y. Wen and J. H. Hung, "Thermodynamics of hydrocarbon gases in aqueous tetraalkylammonium salt solutions," *J. Phys. Chem.*, 74, 170–180, 1970.

[222] G. C. Kresheck, H. Schneider, and H. A. Scheraga, "The Effect of D 2 O on the Thermal Stability of Proteins. Thermodynamic Parameters for the Transfer of Model Compounds from H_2O to $D_2O_{1,2}$," *J. Phys. Chem.*, 69, 3132–3144, 1965.

[223] G. Barone, V. Crescenzi, B. Pispisa, and F. Quadrifoglio, "Hydrophobic Interactions in Polyelectrolyte Solutions. II. Solubility of some C_3− C_6 Alkanes in Poly (methacrylic acid) Solutions," *J. Macromol. Chem*, 1, 761–771, 1966.

[224] T. J. Morrison and F. Billett, "730. The salting-out of non-electrolytes. Part II. The effect of variation in non-electrolyte," *J. Chem. Soc.*, 3819, 1952.

[225] W. F. Claussen and M. F. Polglase, "Solubilities and Structures in Aqueous Aliphatic Hydrocarbon Solutions," *J. Am. Chem. Soc.*, 74, 4817–4819, 1952.

[226] T. Yano, T. Suetaka, T. Umehara, and A. Horiuchi, "Solubility Data Series (1987), Methane," *Clever, H.L., Young, C.L. (Eds.), Solubility Data Ser. Methane. Pergamon Press. Oxford*, 128, 1974.

[227] D. B. Watlaufer, S. K. Malik, L. Stoller, and R. L. Coffin, "Nonpolar Group Participation in the Denaturation of Proteins by Urea and Guanidinium Salts. Model Compound Studies," *J. Am. Chem. Soc.*, 86, 508–514, 1964.

[228] C. McAULIFFE, "Solubility in Water of C_1–C_9 Hydrocarbons," *Nature*, 200, 4911, 1092–1093, 1963.

[229] A. Wishnia, "The Hydrophobic Contribution To Micelle Formation: the Solubility of Ethane, Propane, Butane, and Pentane in Sodium Dodecyl," *J. Phys. Chem.*, 67, 2079–2082, 1963.

[230] A. Y. Namiot, "Solubility of nonpolar gases in water," *J. Struct. Chem.*, 2, 381–

389, 1961.

[231] E. Rudakov and A. Lutsyk, “Solubility of saturated-hydrocarbons in aqueous-solution of sulfuric-acid,” Zh. Fiz. Khim, 53, 731–733, 1979.

[232] A. Azarnoosh and J. McKetta, “The solubility of propane in water,” *Pet. Refin.*, 37, 275–278, 1958.

[233] A. H. Wehe and J. J. McKetta, “Method for Determining Total Hydrocarbons Dissolved in Water,” *Anal. Chem.*, 33, 291–293, 1961.

[234] K. Sparks and E. Sloan, “Water content of NGL in presence of hydrates,” *GPA Res. Rep. 71; GPA Tulsa, OK*, 1983.

[235] R. Kobayashi and D. Katz, “Vapor-Liquid Equilibria For Binary Hydrocarbon-Water Systems Correlation of Data,” *Ind. Eng. Chem.*, 45, 446–451, 1953.

[236] B. M. Moudgil, P. Somasundaran, and I. J. Lin, “Automated constant pressure reactor for measuring solubilities of gases in aqueous solutions,” *Rev. Sci. Instrum.*, 45, 406–409, 1974.

[237] Y. N. S Umano, “Solubilities of propane and n-butane in water and common-salt solution,” *Kogyo Kagaku Zasshi*, 61, 536–542.

[238] A. Ben-Naim, J. Wilf, and M. Yaacobi, “Hydrophobic interaction in light and heavy water,” *J. Phys. Chem.*, 77, 95–102, 1973.

[239] P. A. Rice, R. P. Gale, and A. J. Barduhn, “Solubility of butane in water and salt solutions at low temperatures,” *J. Chem. Eng. Data*, 21, 204–206, 1976.

[240] W. Denton, N. Taylor, and J. Klaschka, “Experimental studies on the immiscible refrigerant (butane) freezing process,” *Fresh Water from Sea*, 41, 251–264, 1970.

[241] E. Rudakov, A. Lutsyk, and S. Suikov, “Extremal change in solubility of non-electrolytes in the water-sulfuric acid system (0-100% H_2SO_4). Modification of the Sechenov equation,” *Russ. J. Phys. Chem*, 61, 601–607, 1987.

[242] R. W. Cargill and D. E. MacPhee, “A phase separation caused by the solubility of butane in 2-methylpropan-2-ol–water mixtures,” *J. Chem. Soc. Faraday Trans. 1 Phys. Chem. Condens. Phases*, 85, 2665, 1989.

[243] W. Brooks, G. Gibbs, and J. M. Jr, “Mutual solubilities of light hydrocarbonwater systems,” *Pet. Refin.*, 30, 118–120, 1951.

[244] J. Le Breton and J. M. Jr, “Low-pressure solubility of n-butane in water,” *Hydrocarb. Proc. Petr. Ref*, 43, 136–138, 1964.

[245] A. Danneil, K. Tödheide, and E. U. Franck, “Verdampfungsgleichgewichte und kritische Kurven in den Systemen Äthan/Wasser und n-Butan/Wasser bei hohen Drücken,” *Chemie Ing. Tech. - CIT*, 39, 816–822, 1967.

[246] “IUPAC-NIST Solubility Database.”

[247] J. Polak and B. C.-Y. Lu, “Mutual Solubilities of Hydrocarbons and Water at 0 and 25 °C,” *Can. J. Chem.*, 51, 4018–4023, 1973.

[248] S. Pavlova, S. Pavlova, L. Serafimov, and L. Kofman, “Mutual solubility of C5 hydrocarbons and water,” *Promyshlennost Sint. Kauchuka (Industry Synth. Rubber)*, 3, 18–25, 1966.

[249] C. McAuliffe, “Solubility in water of paraffin, cycloparaffin, olefin, acetylene, cycloolefin, and aromatic hydrocarbons,” *J. Phys. Chem.*, 70, 1267–1275, 1966.

[250] L. C. Price, “Aqueous Solubility of Petroleum as Applied to Its Origin and Primary Migration,” *Am. Assoc. Pet. Geol. Bull.*, 60, 213–244, 1976.

[251] T. Morrison and N. Johnstone, “Solubilities of the inert gases in water,” *J. Chem. Soc.*, 3441, 1954.

[252] A. Lannung, “The solubilities of helium, neon and argon in water and some organic solvents,” *J. Am. Chem. Soc.*, 52, 68–80, 1930.

[253] M. Celeste, C. Serra, J. A. P. Coelho, J. C. G. Calado, and A. M. F. Palavra, “Solubility of Argon in Micellar Aqueous Solutions of Sodium Dodecyl Sulfate,” *J. Colloid Interface Sci.*, 173, 278–283, 1995.

[254] Y. A. Purwanto, S. Oshita, Y. Seo, and Y. Kawagoe, “Concentration of liquid foods by the use of gas hydrate,” *J. Food Eng.*, 47, 133–138, 2001.

[255] H. Clever, “Solubility Data Series: Argon,” *Solubility Data Ser. Pergamon Press New York*, 2, 1979.

[256] A. Naim and S. Baer, “Method for measuring solubilities of slightly soluble gases in liquids,” *Trans. Faraday Soc.*, 59, 2735, 1963.

[257] R. Crovetto, “Solubilities of inert gases and methane in H_2O and in D_2O in the temperature range of 300 to 600 K,” *J. Chem. Phys.*, 76, 561–568, 1982.

[258] R. W. Cargill and T. J. Morrison, “Solubility of argon in water + alcohol systems,” *J. Chem. Soc. Faraday Trans. 1 Phys. Chem. Condens. Phases*, 71, 618, 1975.

[259] H. Fuhner, “Water-Solubility in Homologous Series,” *Ber. Dtsch. Chem. Ges*, 57B, 510–515, 1924.

[260] H. Nelson and C. De Ligny, “The determination of the solubilities of some n-alkanes in water at different temperatures, by means of gas chromatography,” *Recl. des Trav. Chim. des Pays-Bas*, 1968.

[261] “Solubility of paraffin hydrocarbons in fresh and salt waters,” *Pet. Chem.*, 13, 267–270, 1973.

[262] P. J. Leinonen and D. Mackay, “The multicomponent solubility of hydrocarbons in water,” *Can. J. Chem. Eng.*, 51, 230–233, 1973.

[263] D. Mackay and W. Y. Shiu, “The determination of the solubility of hydrocarbons in aqueous sodium chloride solutions,” *Can. J. Chem. Eng.*, 53, 239–242, 1975.

[264] L. Budantseva, T. Lesteva, and M. Nemstov, “Deposited Doc.(1976), VINITI 437−476,” *Zh. Fiz. Khim*, 1976.

[265] J. Å. Jönsson, J. Vejrosta, and J. Novák, “Air/water partition coefficients for normal alkanes (n-pentane to n-nonane),” *Fluid Phase Equilib.*, 9, 279–286, 1982.

[266] C. Tsonopoulos and G. Wilson, “High-temperature mutual solubilities of hydrocarbons and water. Part I: Benzene, cyclohexane and n-hexane,” *AIChE J.*, 29, 990–999, 1983.

[267] C. McAuliffe, “Solubility in Water of Normal C9 and C10, Alkane Hydrocarbons,” *Science.*, 163, 478-479, 1969.

[268] S. Banerjee, “Water solubility and octanol/water partition coefficients of organics. Limitations of the solubility-partition coefficient correlation,” *Environ. Sci. Technol.*, 14, 1227–1229, 1980.

[269] I. Sanemasa, M. Araki, T. Deguchi, and H. Nagai, “Solubilities of benzene and the alkylbenzenes in water-method for obtaining aqueous solutions saturated with vapours in equilibrium with organic liquids,” *Chem. Lett.*, 10, 225–228, 1981.

[270] H. . F. Bittrich, H. J.; Gedan, “Solubility of hydrocarbons in water,” *Z. Phys. Chem. Leipzig*, 260, 1009–1013, 1979.

[271] F. P. Schwarz, “Measurement of the solubilities of slightly soluble organic liquids in water by elution chromatography,” *Anal. Chem.*, 52, 10–15, 1980.

[272] I. Sanemasa, M. Araki, T. Deguchi, and H. Nagai, “Solubility measurements of benzene and the alkylbenzenes in water by making use of solute vapor,” *Bull. Chem. Soc. Jpn.*, 55, 1054–1062, 1982.

[273] V. Udovenko and L. Aleksandrova, “Vapor pressures of 3-component systems. 4. formic acid-benzene-water,” *Zh. Fiz. Khim*, 37, 52–56, 1963.

[274] R. S. Bradley, M. J. Dew, and D. C. Munro, “The solubility of benzene and toluene in water and aqueous salt solutions under pressure,” *High Temp. -High Press.*, 5, 169–176, 1973.

[275] R. Brown and S. Wasik, “A method of measuring the solubilities of hydrocarbons in aqueous solutions,” *J. Res. NBS A*, 78, 453–460, 1974.

[276] A. E. Hill, “The system, silver perchlorate-water-benzene,” *J. Am. Chem. Soc.*, 44, 1163–1193, 1922.

[277] J. Barbaudy, “The distillation of heterogeneous ternary mixtures: I the system water+ benzene+ toluene,” *J. Chim. Phys*, 23, 289–291, 1926.

[278] P. Gross and J. Saylor, “The solubilities of certain slightly soluble organic compounds in water,” *J. Am. Chem. Soc.*, 53, 1744–1751, 1931.

[279] H. Klevens, “The Solubilization of Polycyclic Hydrocarbons.,” *J. Phys. Chem.*, 54, 283–298, 1950.

[280] D. Donahue and F. Bartell, “The boundary tension at water-organic liquid interfaces,” *J. Phys. Chem.*, 56, 480–484, 1952.

[281] W. McDevit and F. Long, “The activity coefficient of benzene in aqueous salt solutions,” *J. Am. Chem. Soc.*, 52, 119–124, 1952.

[282] M. Hayashi and T. Sasaki, “Measurement of solubilities of sparingly soluble liquids in water and aqueous detergent solution using non-ionic surfactant,” *Bull. Chem. Soc. Jpn.*, 29, 857–859, 1956.

[283] D. Arnold and C. Plank, “Solubility of Benzene in Water.,” *Chem. Eng. Data Ser.*, 253–256, 1958.

[284] A. Brady and H. Huff, “The Vapor Pressure of Benzene over Aqueous Detergent

Solutions," *J. Phys. Chem.*, 62, 644–649, 1958.

[285] D. Alexander, "The solubility of benzene in water," *J. Phys. Chem.*, 63, 1021–1022, 1959.

[286] A. Guseva and E. Parnov, "The solubility of aromatic hydrocarbons in water," *Vestn. Mosk. Univ. Ser. 2 Khim*, 18, 76–79, 1963.

[287] J. C. De Hemptinne, H. Delepine, C. Jose, and J. Jose, "Aqueous Solubility of Hydrocarbon Mixtures," *Rev. l'Institut Français du Pétrole*, 53, 409–419, 1998.

[288] C. Rebert and W. Kay, "The phase behavior and solubility relations of the benzene-water system," *AIChE J.*, 5, 285–289, 1959.

[289] T. O'Grady, "Liquid-liquid equilibriums for the benzene-n-heptane-water system in the critical solution region," *J. Chem. Eng. Data*, 12, 9–12, 1967.

[290] *,† Céline Marche, † Hervé Delépine, ‡ and Corinne Ferronato, and J. Jose†, "Apparatus for the On-line GC Determination of Hydrocarbon Solubility in Water: Benzene and Cyclohexane from 70 °C to 150 °C," 2003.

[291] T. Rettich, R. Battino, and E. Wilhelm, "The solubility of Gases in Liquids. 15. High-Precision Determination of Henry Coefficients for Carbon Monoxide in Liquid Water at 278 to 323 K," *Berichte der Bunsengesellschaft für Phys. Chemie*, 86, 1128–1132, 1982.

[292] R. Bunsen, "Ueber das Gesetz der Gasabsorption," *Justus Liebigs Ann. Chem.*, 93, 1–50, 1855.

[293] L. Winkler, "Die Löslichkeit der Gase in Wasser.," *Eur. J. Inorg. Chem.*, 24, 89–101, 1901.

[294] G. M. Gillespie, P. C.; Wilson, "Vapor−liquid and liquid−liquid equilibria: water−methane, water−carbon dioxide, water−hydrogen sulfide, water−n-pentane, water−methane−n-pentane," *Res. Rep. RR48; Gas Process. Assoc. Tulsa, OK*, 1982.

[295] Z. Duan and R. Sun, "An improved model calculating CO_2 solubility in pure water and aqueous NaCl solutions from 273 to 533 K and from 0 to 2000 bar," *Chem. Geol.*, 193, 257–271, 2003.

[296] V. Ipat'ev and V. Teodorovich, "Solubility of hydrogen in water under pressure at

elevated temperatures Zhur," *J. Gen. Chem*, 395, 1934.

[297] G. Kling and G. Maurer, "The solubility of hydrogen in water and in 2-aminoethanol at temperatures between 323 K and 423 K and pressures up to 16 MPa," *J. Chem. Thermodyn.*, 23, 531–541, 1991.

[298] R. Dohrn and G. Brunner, "Phase equilibria in ternary and quaternary systems of hydrogen, water and hydrocarbons at elevated temperatures and pressures.," *Fluid Phase Equilib.*, 29, 535–544, 1986.

[299] "Solubility of water in compressed hydrogen," *Russ. J. Phys. Chem*, 50, 240–243, 1976.

[300] H. Pray, "Solubility of hydrogen, oxygen, nitrogen, and helium in water at elevated temperatures," *Ind. Eng. Chem.*, 44, 1146–1151, 1952.

[301] R. Wiebe and V. L. Gaddy, "The Solubility of Hydrogen in Water at 0, 50, 75 and 100 °C from 25 to 1000 Atmospheres," *J. Am. Chem. Soc.*, 56, 76–79, 1934.

[302] V. Ugrozov, "Equilibrium compositions of vapor-gas mixtures over solutions," *Russ. J. Phys. Chem.*, 70, 1240–1241, 1996.

[303] P. Gillespie and G. Wilson, "Research Report RR-41: Vapour–Liquid Equilibrium Data on Water-Substitute Gas Components: N_2–H_2O, H_2–H_2O, CO–H_2O," 60, 609–640, 1980.

[304] D. K. Jr and B. Benson, "The solubility and isotopic fractionation of gases in dilute aqueous solution. IIa. Solubilities of the noble gases," *J. Solution Chem.*, 18, 823–872, 1989.

[305] R. Strang, "The measurement of the Ostwald solubility coefficient of krypton in blood and oculr tissue (relevant to blood flow measurement)," *Phys. Med. Biol.*, 20, 1025–1028, 1975.

[306] H. Clever, "Krypton, Xenon and Radon} Gas Solubilities. Solubility Data Series., 2. International Union of Pure and Applied Chemistry," *Int. Union Pure Appl. Chem. Pergamon Press. Oxford*, 2, 1979.

[307] A. Guseva and E. Parnov, "Isothermal sections in the systems cyclanes-water," *Vestn. Mosk. Univ., Ser. II, Khim*, 19, 77–81, 1964.

[308] J. Clarke, "Kinetics of absorption of cardon dioxide in monoethanolamine

solutions at short contact times," *Ind. Eng. Chem. Fundam.*, 3, 239–245, 1964.

[309] N. Haimour and O. Sandall, "Absorption of carbon dioxide into aqueous methyldiethanolamine," *Chem. Eng. Sci.*, 39, 1791–1796, 1984.

[310] H. Al-Ghawas, "Physicochemical properties important for carbon dioxide absorption in aqueous methyldiethanolamine," *J. Chem. Eng. Data*, 34, 385–391, 1989.

[311] E. Rinker and O. Sandall, "Solubility of nitrous oxide in aqueous solutions of methyldiethanolamine, diethanolamine and mixtures of methyldiethanolamine and diethanolamine," *Chem. Eng. Commun.*, 85–94, 1996.

[312] R. A. Davis and B. J. Pogainis, "Solubility of Nitrous Oxide in Aqueous Blends of N-Methyldiethanolamine and 2-Amino-2-methyl-1-propanol," *J. Chem. Eng. Data*, 40, 1249–1251, 1995.

[313] Y. Wang, S. Xu, F. Otto, and A. Mather, "Solubility of N_2O in Alkanolamines and in Mixed Solvents," *Chem. Eng. J.*, 48, 31–40, 1992.

[314] E. Sada, H. Kumazawa, and N. Tsubol, "Absorption of nitric oxide in aqueous ferrous sulfate solutions," *Ind. Eng. Chem. Process Des. Dev.*, 17, 321–324, 1978.

[315] G. Browning and R. Weiland, "Physical solubility of carbon dioxide in aqueous alkanolamines via nitrous oxide analogy," *J. Chem. Eng. Data*, 39, 817–822, 1994.

[316] S. Mao and Z. Duan, "A thermodynamic model for calculating nitrogen solubility, gas phase composition and density of the N 2–H 2 O–NaCl system," *Fluid Phase Equilib.*, 248, 103–114, 2006.

[317] M. Geng and Z. Duan, "Prediction of oxygen solubility in pure water and brines up to high temperatures and pressures," *Geochim. Cosmochim. Acta*, 74, 5631–5640, 2010.

[318] E. F. G. Herington, "The solubility of aromatic hydrocarbons in water," *J. Am. Chem. Soc.*, 73, 5883–5884, 1951.

[319] J. Connolly, "Solubility of Hydrocarbons in Water Near the Critical Solution Temperatures.," *J. Chem. Eng. Data*, 11, 13–16, 1966.

[320] C. Sutton and J. Calder, "Solubility of alkylbenzenes in distilled water and sea water at 25.0. deg.," *J. Chem. Eng. Data*, 1975.

[321] T. Krzyzanowska and J. Szeliga, “Water solubility of individual hydrocarbons,” *Nafta*, 1978.

[322] F. Chernoglazova and Y. Simulin, “Mutual solubility in the system m-xylene-water,” *Zh. Fiz. Khim*, 1976.

[323] L. Andrews and R. Keefer, “IV. The argentation of aromatic hydrocarbons,” *J. Am. Chem. Soc*, 1949.

[324] F. Franks, “Solute–water interactions and the solubility behaviour of long-chain paraffin hydrocarbons,” *Nature*, 210, 87–88, 1966.

[325] H. Becke and G. Quitzsch, “Das phasengleichgewichtsverhalten ternarer sysQuitzschteme der art C4-alkohol− wasser− kohlenwasserstoff,” *Chem. Tech.(Leipzig)*, 29, 49–51, 1977.

[326] T. Cremont, “Prévision de la solubilité des hydrocarbures dans l’eau en fonction de la température et de la pression,” Clermont-Ferrand, 2002.

[327] C. Sutton and J. Calder, “Solubility of higher-molecular-weight normal-paraffins in distilled water and sea water,” *Environ. Sci. Technol.*, 8, 654–657, 1974.

[328] E. Baker, “Origin and Migration of Oil,” *Science (80-.).*, 129, 871–874, 1959.

[329] A. Austegard and E. Solbraa, “Thermodynamic models for calculating mutual solubilities in H_2O–CO_2–CH_4 mixtures,” *Chem. Eng. Res. Des.*, 84, 781–794, 2006.

[330] A. Valtz, A. Chapoy, C. Coquelet, P. Paricaud, and D. Richon, “Vapour–liquid equilibria in the carbon dioxide–water system, measurement and modelling from 278.2 to 318.2K,” *Fluid Phase Equilib.*, 226, 333–344, 2004.

[331] A. K. Jr and C. Coan, “Solubility of water in compressed carbon dioxide, nitrous oxide, and ethane. Evidence for hydration of carbon dioxide and nitrous oxide in the gas phase,” *J. Am. Chem. Soc.*, 93, 1815–1862, 1971.

[332] R. Wiebe and V. Gaddy, “Vapor phase composition of carbon dioxide-water mixtures at various temperatures and at pressures to 700 atmospheres,” *J. Am. Chem. Soc.*, 63, 475–477, 1941.

[333] J. A. Briones, J. C. Mullins, M. C. Thies, and B.-U. Kim, “Ternary phase equilibria for acetic acid-water mixtures with supercritical carbon dioxide,” *Fluid Phase*

Equilib., 36, 235–246, 1987.

[334] R. D'souza, J. R. Patrick, and A. S. Teja, "High pressure phase equilibria in the carbon dioxide - n -Hexadecane and carbon dioxide - water systems," *Can. J. Chem. Eng.*, 66, 319–323, 1988.

[335] I. Sidorov, Y. Kazarnovskii, and A. Goldman, "Solubility of water in compressed gases," *Tr. Gos. Naucn. ˇ i Proektn. Instituta Azotn. Prom.*, 48–67, 1953.

[336] S.-X. Hou, G. C. Maitland, and J. P. M. Trusler, "Measurement and modeling of the phase behavior of the (carbon dioxide+water) mixture at temperatures from 298.15K to 448.15K," *J. Supercrit. Fluids*, 73, 87–96, 2013.

[337] F. Tabasinejad and R. Moore, "Water solubility in supercritical methane, nitrogen, and carbon dioxide: measurement and modeling from 422 to 483 K and pressures from 3.6 to 134 MPa," *Ind. Eng. Chem. Res.*, 50, 4029–4041, 2011.

[338] S. . Malinin, "The system water-carbon dioxide at high temperatures and pressures," *Geokhimiya*, 3, 292–306, 1959.

[339] R. Wiebe and V. Gaddy, "The Solubility in Water of Carbon Dioxide at 50, 75, and 100 C at Pressure to 70 Atmospheres," *J. Am. Chem. Soc.*, 1940.

[340] A. Valtz, A. Chapoy, C. Coquelet, P. Paricaud, and D. Richon, "Vapour-liquid equilibria in the carbon dioxide-water system, measurement and modelling from 278.2 to 318.2 K," *Fluid Phase Equilib.*, 226, 333–344, 2004.

[341] M. B. King, A. Mubarak, J. D. Kim, and T. R. Bott, "The mutual solubilities of water with supercritical and liquid carbon dioxides," *J. Supercrit. Fluids*, 5, 296–302, 1992.

[342] C. R. Coan and a. D. King Jr., "Solubility of water in compressed carbon dioxide, nitrous oxide, and ethane. Evidence for hydration of carbon dioxide and nitrous oxide in the gas phase," *J. Am. Chem. Soc.*, 93, 1815–1862, 1971.

[343] C. Giavarini and K. Hester, *Gas hydrates: immense energy potential and environmental challenges*. 2011.

[344] A. Grenner, G. M. Kontogeorgis, N. von Solms, and M. L. Michelsen, "Application of PC-SAFT to glycol containing systems PC-SAFT towards a predictive approach," *Fluid Phase Equilib.*, 261, 248–257, 2007.

[345] S. O. Derawi, M. L. Michelsen, G. M. Kontogeorgis, and E. H. Stenby, “Application of the CPA equation of state to glycol/hydrocarbons liquid–liquid equilibria,” *Fluid Phase Equilib.*, 209, 163–184, 2003.

[346] S. O. Derawi, G. M. Kontogeorgis, M. L. Michelsen, and E. H. Stenby, “Extension of the cubic-plus-association equation of state to glycol-water cross-associating systems,” *Ind. Eng. Chem. Res.*, 42, 1470–1477, 2003.

[347] G. K. Folas, S. O. Derawi, M. L. Michelsen, E. H. Stenby, and G. M. Kontogeorgis, “Recent applications of the cubic-plus-association (CPA) equation of state to industrially important systems,” *Fluid Phase Equilib.*, 228–229, 121–126, 2005.

[348] S. H. Huang and M. Radosz, “Equation of state for small, large, polydisperse and associating molecules,” *Ind. Eng. Chem. Res.*, 29, 2284–2294, 1990.

[349] X. Li and P. Englezos, “Vapor−Liquid Equilibrium of Systems Containing Alcohols Using the Statistical Associating Fluid Theory Equation of State,” *Ind. Eng. Chem. Res.*, 42, 4953–4961, 2003.

[350] G. N. I. Clark, A. Galindo, G. Jackson, S. Rogers, and A. N. Burgess, “Modeling and Understanding Closed-Loop Liquid−Liquid Immiscibility in Aqueous Solutions of Poly(ethylene glycol) Using the SAFT-VR Approach with Transferable Parameters,” *Macromolecules*, 41, 6582–6595, 2008.

[351] S. Dufal, A. Galindo, G. Jackson, and A. J. Haslam, “Modelling the effect of methanol, glycol inhibitors and electrolytes on the equilibrium stability of hydrates with the SAFT-VR approach,” *Mol. Phys.*, 110, 1223–1240, 2012.

[352] N. Pedrosa, J. C. Pàmies, J. a P. Coutinho, I. M. Marrucho, and L. F. Vega, “Phase Equilibria of Ethylene Glycol Oligomers and Their Mixtures,” *Ind. Eng. Chem. Res.*, 44, 7027–7037, 2005.

[353] N. Pedrosa and L. F. Vega, “Modeling the Phase Equilibria of Poly (ethylene glycol) Binary Mixtures with soft-SAFT EoS,” *Ind. Eng. Chem. Res*, 46, 4678–4685, 2007.

[354] N. Von Solms, M. L. Michelsen, and G. M. Kontogeorgis, “Computational and physical performance of a modified PC-SAFT Equation of State for Highly Asymmetric and Associating Mixtures,” *Ind. Eng. Chem. Res.*, 42, 1098–1105, 2003.

[355] A. H. Tafazzol and K. Nasrifar, “Thermophysical Properties of Associating Fluids in Natural Gas Industry Using Pc-Saft Equation of State,” *Chem. Eng. Commun.*, 198, 1244–1262, 2011.

[356] L. K. Wang, G. J. Chen, G. H. Han, X. Q. Guo, and T. M. Guo, “Experimental study on the solubility of natural gas components in water with or without hydrate inhibitor,” *Fluid Phase Equilib.*, 207, 143–154, 2003.

[357] D. D.-Q. Zheng, W. W. W.-D. Ma, R. Wei, and T. T. Guo, “Solubility study of methane, carbon dioxide and nitrogen in ethylene glycol at elevated temperatures and pressures,” *Fluid Phase Equilib.*, 155, 277–286, 1999.

[358] F. Jou, F. D. Otto, and a E. Mather, “Solubility of Methane in Glycols at Elevated Pressures,” *Can. J. Chem. Eng.*, 72, 130–133, 1994.

[359] J.CHR. Gjaldbek and H.Niemann, “The solubility of nitrogen, argon and ethane in alcohols and water,” *Acta Chem. Scand.*, 12, 1015–1023, 1958.

[360] F.-Y. Jou, F. D. Otto, and A. E. Mather, “The solubility of propane in 1,2-ethanediol at elevated pressures,” *The Journal of Chemical Thermodynamics*, 25, 37–40, 1993.

[361] G. K. Folas, “Modeling of Complex Mixtures Containing Hydrogen Bonding Molecules,” DTU, 2006.

[362] S. Derawi, E. Stenby, and G. Kontogeorgis, *Modeling of phase equilibria containing associating fluids*. 2002.

[363] F. Jou, F. Otto, and A. Mather, “Solubility of H_2S and CO_2 in diethylene glycol at elevated pressures,” *Fluid Phase Equilib.*, 2000.

[364] and A. E. M. Fang-Yuan Jou, Kurt A. G. Schmidt, “Solubility of Ethane in Diethylene Glycol,” *J. Chem. Eng. Data*, 50, 6, 2005.

[365] A. Bahadori, H. B. Vuthaluru, and S. Mokhatab, “Analyzing solubility of acid gas and light alkanes in triethylene glycol,” *J. Nat. Gas Chem.*, 17, 51–58, 2008.

[366] Y. Yu, J. Liu, and G. Gao, “Isobaric vapor–liquid equilibria of three aromatic hydrocarbon-tetraethylene glycol binary systems,” *Fluid Phase Equilib.*, 1999.

[367] E. S. Jr and C. Koh, *Clathrate hydrates of natural gases*. 2007.

[368] A. J. de Villiers, C. E. Schwarz, A. J. Burger, and G. M. Kontogeorgis, “Evaluation

of the PC-SAFT, SAFT and CPA equations of state in predicting derivative properties of selected non-polar and hydrogen-bonding compounds," *Fluid Phase Equilib.*, 338, 1–15, 2013.

[369] B. Younglove, N. Frederick, and R. McCarty, "Speed of sound data and related models for mixtures of natural gas constituents," *Tech. Rep. Speed sound data Relat. Model. Mix. Nat. gas Const.*, PB-93-2008, 1993.

[370] E. A. Macedo, P. Skovborg, and P. Rasmussen, "Calculation of phase equilibria for solutions of strong electrolytes in solvent—water mixtures," *Chem. Eng. Sci.*, 45, 875–882, 1990.

[371] Al. F. Cameretti, G. Sadowski, and J. M. Mollerup, "Modeling of Aqueous Electrolyte Solutions with Perturbed-Chain Statistical Associated Fluid Theory," *Ind. Eng. Chem. Res.*, 44, 3355–3362, 2005.

[372] H. Haghighi, A. Chapoy, and B. Tohidi, "Freezing Point Depression of Electrolyte Solutions: Experimental Measurements and Modeling Using the Cubic-Plus-Association Equation of State," *Ind. Eng. Chem. Res.*, 47, 3983–3989, 2008.

[373] H. Haghighi, A. Chapoy, R. Burgess, and B. Tohidi, "Experimental and thermodynamic modelling of systems containing water and ethylene glycol: Application to flow assurance and gas processing," *Fluid Phase Equilib.*, 276, 24–30, 2009.

[374] D. Tong, J. Trusler, and D. Vega-Maza, "Solubility of CO_2 in aqueous solutions of CaCl2 or MgCl2 and in a synthetic formation brine at temperatures up to 423 K and pressures up to 40 MPa," *J. Chem. Eng. Data*, 58, 2116–2124, 2013.

[375] H. Zhao, R. M. Dilmore, and S. N. Lvov, "Experimental Studies and Modeling of CO 2 Solubility in High Temperature Aqueous $CaCl_2$, $MgCl_2$, Na_2SO_4 , and KCl Solutions," *AIChE J.*, 61, 2286–2297, 2015.

[376] I. Kritschewsky, N. Shaworonkoff, and V. Aepelbaum, "Combined solubility of gases in liquids under pressure: I. Solubility of carbon dioxide in water from its mixtures with hydrogen of 20 and 30 8C and total pressure of 30 kg/cm2," *Z. Phys. Chem., A*, A175, 232–238, 1935.

[377] Y. Zel'vinskii, "Measurements of carbon dioxide solubility in water," *Zhurn. Khim. Prom*, 14, 1250–1257, 1937.

[378] R. Wiebe and V. L. Gaddy, “The Solubility in Water of Carbon Dioxide at 50, 75 and 100°, at Pressures to 700 Atmospheres,” *J. Am. Chem. Soc.*, 61, 315–318, 1939.

[379] R. Wiebe and V. Gaddy, “The solubility of carbon dioxide in water at various temperatures from 12 to 40 and at pressures to 500 atmospheres. critical phenomena*,” *J. Am. Chem. Soc.*, 315, 61–63, 1940.

[380] C. F. Prutton and R. L. Savage, “The Solubility of Carbon Dioxide in Calcium Chloride-Water Solutions at 75, 100, 120° and High Pressures1,” *J. Am. Chem. Soc.*, 67, 1550–1554, 1945.

[381] E. Bartholomé and H. Friz, “Löslichkeit von Kohlendioxyd in Wasser bei höheren Drucken,” *Chemie Ing. Tech.*, 28, 706–708, 1956.

[382] E. U. Tödheide, K., Franck, “Das Zweiphasengebiet und die kritische Kurve im System Kohlendioxid-Wasser bis zu Drucken von 3500 bar,” *Zeitschrift für Phys. Chemie*, 37, 387–401, 1963.

[383] S. Takenouchi and G. C. Kennedy, “The binary system H_2O-CO_2 at high temperatures and pressures,” *American Journal of Science*, 262, 1055–1074, 1964.

[384] J. Matouš, J. Šobr, J. P. Novák, and J. Pick, “Solubility of carbon dioxide in water at pressures up to 40 atm,” *Collect. Czechoslov. Chem. Commun.*, 34, 3982–3985, 1969.

[385] S. Malinin and N. Kurovskaya, “Investigation of CO_2 solubility in solutions of chlorides at elevated-temperatures and pressures of CO_2,” *Geokhimiya*, 4, 547–551, 1975.

[386] N. I. Malinin, S.D., Savelyeva, “The solubility of CO_2 in NaCl and $CaCl_2$ solutions at 25, 50, and 75°C under elevated CO_2 pressures,” *Geokhimiya*, 6, 643–653, 1972.

[387] S. Drummond, “Boiling and mixing of hydrothermal fluids: chemical effects on mineral precipitation,” Pennsylvania State University, 1981.

[388] a. Zawlsza and B. Maleslnska, “Solubility of carbon dioxide in liquid water and of water in gaseous carbon dioxide in the range 0 . 2-5 MPa and at temperatures up to 473 K,” *J. Chem. Eng. Data*, 26, 388–391, 1981.

[389] R. Shagiakhmetov and A. Tarzimanov, “Measurements of CO_2 solubility in water

up to 60 MPa," *Depos. Doc. SPSTL 200khp-D81-1982*, 1981.

[390] P. Gillespie and G. Wilson, "Vapor-Liquid and Liquid-Liquid Equilibria: Water-Methane, Water-Carbon Dioxide, Water-Hydrogen Sulfide, Water-n-Pentane, Water-Methane-n-Pentane," *Gas Process. Assoc. Tulsa, OK*, Research R, 1982.

[391] P. Oleinik, "Method of evaluating gases in liquids and volumetric properties of solutions under pressure," *Neftepromysl. Delo*, 1986.

[392] G. Müller, E. Bender, and G. Maurer, "Das Dampf-Flüssigkeitsgleichgewicht des ternären Systems Ammoniak-Kohlendioxid-Wasser bei hohen Wassergehalten im Bereich zwischen 373 und 473 Kelvin," *Berichte der Bunsengesellschaft für Phys. Chemie*, 92, 148–160, 1988.

[393] J. A. Nighswander, N. Kalogerakis, and A. K. Mehrotra, "Solubilities of carbon dioxide in water and 1 wt. % sodium chloride solution at pressures up to 10 MPa and temperatures from 80 to 200.degree.C," *J. Chem. Eng. Data*, 34, 355–360, 1989.

[394] R. Dohrn, A. P. Bünz, F. Devlieghere, and D. Thelen, "Experimental measurements of phase equilibria for ternary and quaternary systems of glucose, water, CO_2 and ethanol with a novel apparatus," *Fluid Phase Equilib.*, 83, 149–158, 1993.

[395] H. Teng and A. Yamasaki, "Solubility of Liquid CO_2 in Synthetic Sea Water at Temperatures from 278 K to 293 K and Pressures from 6.44 MPa to 29.49 MPa, and Densities of the Corresponding Aqueous Solutions," *J. Chem. Eng. Data*, 43, 2–5, 1998.

[396] D.-Q. Zheng, T.-M. Guo, and H. Knapp, "Experimental and modeling studies on the solubility of CO_2, $CHC1F_2$, CHF_3, $C_2H_2F_4$ and $C_2H_4F_2$ in water and aqueous NaCl solutions under low pressures," *Fluid Phase Equilib.*, 129, 197–209, 1997.

[397] a Dhima, J. De Hemptinne, and J. Jose, "Solubility of hydrocarbons and CO_2 mixtures in water under high pressure," *Ind. Eng. Chem. Res.*, 38, 3144–3161, 1999.

[398] A. Bamberger, G. Sieder, and G. Maurer, "High-pressure (vapor+liquid) equilibrium in binary mixtures of (carbon dioxide+water or acetic acid) at temperatures from 313 to 353 K," *J. Supercrit. Fluids*, 17, 97–110, 2000.

[399] S. O. Yang, S. H. Cho, H. Lee, and C. S. Lee, “Measurement and prediction of phase equilibria for water + methane in hydrate forming conditions,” *Fluid Phase Equilib.*, 185, 53–63, 2001.

[400] R. Rosenbauer, “An experimental approach to CO_2 sequestration in saline aquifers: application to Paradox Valley, CO,” *Am. Geophys. Union, Fall Meet.*, 2001.

[401] P. Servio, “Effect of temperature and pressure on the solubility of carbon dioxide in water in the presence of gas hydrate,” *Fluid Phase Equilib.*, 190, 127–134, 2001.

[402] G. K. Anderson, “Solubility of carbon dioxide in water under incipient clathrate formation conditions,” *J. Chem. Eng. Data*, 47, 219–222, 2002.

[403] S. Bando, F. Takemura, M. Nishio, E. Hihara, and M. Akai, “Solubility of CO_2 in aqueous solutions of NaCl at (30 to 60)°C and (10 to 20) MPa,” *J. Chem. Eng. Data*, 48, 576–579, 2003.

[404] a. Chapoy, a. H. Mohammadi, a. Chareton, B. Tohidi, and D. Richon, “Measurement and Modeling of Gas Solubility and Literature Review of the Properties for the Carbon Dioxide−Water System,” *Ind. Eng. Chem. Res.*, 43, 1794–1802, 2004.

[405] S. Wroblewski, “The solubility of carbon dioxide in water,” *Ann. Phys. Chem*, 18, 290 – 308, 1883.

[406] W. Sander, “Über die Löslichkeit der Kohlensäure in Wasser und einigen anderen Lösungsmitteln unter höheren Drucken,” 78, 513–549, 1911.

[407] O. Hahnel, “Solubility of carbon dioxide in water,” *Centr. Min. Geol*, 25, 25–32, 1920.

[408] R. Vilcu and I. Gainar, “Loslichkeit der gase unter druck in flussigkeiten. i. das system kohlendioxid-wasser,” *Rev. Roum. Chim.*, 12, 181–189, 1967.

[409] P. B. Stewart and P. Munjal, “Solubility of carbon dioxide in pure water, synthetic sea water, and synthetic sea water concentrates at -5˚C to 25˚C and 10 to 45 Atm,” *J. Chem. Eng. Data*, 15, 67–71, 1970.

[410] G. Houghton, A. M. McLean, and P. D. Ritchie, “Compressibility, fugacity, and water-solubility of carbon dioxide in the region 0–36 atm. and 0–100°c,” *Chem. Eng. Sci.*, 6, 132–137, 1957.

[411] T. Sako, T. Sugeta, N. Nakazawa, T. Okubo, M. Sato, T. Taguchi, and T. Hiaki, "Phase equilibrium study of extraction and concentration of furfural produced in reactor using supercritical carbon dioxide," *Journal of chemical engineering of Japan*, 24, 449–455, 1991.

[412] R. Jacob and B. Z. Saylor, "CO_2 solubility in multi-component brines containing NaCl, KCl, $CaCl_2$ and $MgCl_2$ at 297K and 1–14MPa," *Chem. Geol.*, 424, 86–95, 2016.

[413] B. Rumpf, H. Nicolaisen, C. Ocal, and G. Maurer, "Solubility of carbon dioxide in aqueous solutions of sodium chloride: Experimental results and correlation," *J. Solution Chem.*, 23, 431–448, 1994.

[414] P. D. R. G. Houghton, A.M. McLean, "Compressibility, fugacity, and water-solubility of carbon dioxide in the region 0–36 atm. and 0–100°c," *Chem. Eng. Sci.*, 6, 132–137, 1957.

[415] A. E. Markham and K. A. Kobe, "The Solubility of Carbon Dioxide and Nitrous Oxide in Aqueous Salt Solutions," *Am. Chem. Soc.*, 63, 449–454, 1941.

[416] A. J. Ellis and R. M. Golding, "The solubility of carbon dioxide above 100 degrees C in water and in sodium chloride solutions," *Am. J. Sci.*, 261, 47–60, 1963.

[417] S. Takenouchi and G. C. Kennedy, "The solubility of carbon dioxide in nacl solutions at high temperatures and pressures," *Am. J. Sci.*, 263, 445–454, May 1965.

[418] K. Onda, E. Sada, and T. Kobayashi, "Salting-out parameters of gas solubility in aqueous salt solutions," *J. Chem. Eng. Japan*, 3, 18–24, 1970.

[419] N. A. Malinin, S.D., Kurovskaya, "Investigation of CO_2 solubility in a solution of chlorides at elevated temperatures and pressures of CO_2," *Geokhimiya*, 4, 547–551, 1975.

[420] M. Gehrig, "Phasengleichgewichte und PVT-daten ternarermischungen aus wasser, kohlendioxid und natriumchloridbis 3 kbar and 550 8C," *PhD thesis, Univ. Karlsruhe, Freibg.*

[421] J. a Nighswander, N. Kalogerakis, and a K. Mehrotra, "Solubilities of carbon dioxide in water and 1 wt % NaCl solution at pressures up to 10 MPa and temperatures from 80 to 200 °C," *J. Chem. Eng. Data*, 34, 355–360, 1989.

[422] H. Nicolaisen, “Phase equilibria in aqueous electrolyte solutions,” Technical University of Denmark, 1994.

[423] J. Kiepe, S. Horstmann, K. Fischer, and J. Gmehling, “Experimental Determination and Prediction of Gas Solubility Data for CO_2 + H_2O Mixtures Containing NaCl or KCl at Temperatures between 313 and 393 K and Pressures up to 10 MPa,” *Ind. Eng. Chem. Res.*, 41, 4393–4398, 2002.

[424] J. Setschenow, “Uber die konstitution der salzlosungenauf grund ihres verhaltens zu kohlensaure,” *Z. Phys. Chem*, 4, 25–32, 1889.

[425] W. Rosenthal, “Contribution a l’étude de la solubilité des gaz dans quelques solvants et solutions,” 45, 1954.

[426] S.-Y. Yeh and R. E. Peterson, “Solubility of Carbon Dioxide, Krypton, and Xenon in Aqueous Solution,” *J. Pharm. Sci.*, 53, 822–824, 1964.

[427] J. Gerecke, “Ein Beitrag zur Gaslöslichkeit in Elektrolytlösungen: Untersucht am Beisp. d. Löslichkeit v. H_2, CO_2 und NH_3 in Wasser und wässrigen Salzlösungen,” 119, 1969.

[428] a Yasunishi and F. Yoshida, “Solubility of carbon dioxide in aqueous electrolyte solutions,” *J. Chem. Eng.*, 24, 13–16, 1979.

[429] S. Cramer, “The solubility of methane, carbon dioxide, and oxygen in brines from 0 to 3000 c,” 8706, 1–14, 1982.

[430] S. He and J. W. Morse, “The carbonic acid system and calcite solubility in aqueous Na-K-Ca-Mg-Cl-SO4 solutions from 0 to 90°C,” *Geochim. Cosmochim. Acta*, 57, 3533–3554, 1993.

[431] G. Vazquez and F. Chenlo, “Solubility of CO_2 in aqueous-solutions of nacl, cuso4, kl and nabr,” *J. Peaguda, Anal. Quim*, 90, 324–328, 1994.

[432] S. Bando, F. Takemura, M. Nishio, E. Hihara, and M. Akai, “Solubility of CO_2 in Aqueous Solutions of NaCl at (30 to 60) °C and (10 to 20) MPa,” *J. Chem. Eng. Data*, 48, 576–579, May 2003.

[433] D. Koschel, J. Y. Coxam, L. Rodier, and V. Majer, “Enthalpy and solubility data of CO_2 in water and NaCl(aq) at conditions of interest for geological sequestration,” *Fluid Phase Equilib.*, 247, 107–120, 2006.

[434] Y. Liu, M. Hou, G. Yang, and B. Han, “Solubility of CO_2 in aqueous solutions of NaCl, KCl, CaCl 2 and their mixed salts at different temperatures and pressures,” *J. Supercrit. Fluids*, 56, 125–129, 2011.

[435] H. Zhao, R. Dilmore, D. E. Allen, S. W. Hedges, Y. Soong, and S. N. Lvov, “Measurement and modeling of CO_2 solubility in natural and synthetic formation brines for CO_2 sequestration.,” *Environ. Sci. Technol.*, 49, 1972–80, 2015.

[436] A. Bastami, M. Allahgholi, and P. Pourafshary, “Experimental and modelling study of the solubility of CO_2 in various $CaCl_2$ solutions at different temperatures and pressures,” *Pet. Sci.*, 11, 569–577, 2014.

[437] A. E. Markham and K. A. Kobe, “The solubility of carbon dioxide and nitrous oxide in aqueous salt solutions,” *J. Am. Chem. Soc.*, 63, 449–454, 1941.

[438] J. Kiepe, S. Horstmann, K. Fischer, and J. Gmehling, “Experimental Determination and Prediction of Gas Solubility Data for CO_2 + H_2O Mixtures Containing NaCl or KCl at Temperatures between 313 and 393 K and Pressures up to 10 MPa,” *Ind. Eng. Chem. Res.*, 41, 4393–4398, 2002.

[439] G.Geffcken, “Beitrage zur Kenntnis der Loslichkeitsbeeinflussun,” *Ph.D. Diss. Leipzig Univ.*, 1904.

[440] A. Findlay and B. Shen, “The influence of colloids and fine suspensions on the solubility of gases in water. Part II. Solubility of carbon dioxide and of hydrogen,” *J. Chem. Soc. Trans.*, 101, 1459, 1912.

[441] Á.P.S. Kamps E. Meyer, B. Rumpf, G. Maurer, and A. Thermodynamics, “Solubility of CO_2 in Aqueous Solutions of KCl and in Aqueous Solutions of,” *Engineering*, 817–832, 2007.

[442] K. A. Kobe and J. S. Williams, “Confining liquids for gas analysis: Solubility of carbon dioxide in salt solutions,” *Ind. Eng. Chem. Anal. Ed.*, 7, 37–38, 1935.

[443] A. Chapoy, A. H. Mohammadi, D. Richon, and B. Tohidi, “Gas solubility measurement and modeling for methane-water and methane-ethane-n-butane-water systems at low temperature conditions,” *Fluid Phase Equilib.*, 220, 113–121, 2004.

[444] A. Zawisza and B. Malesinska, “Solubility of carbon dioxide in liquid water and of water in gaseous carbon dioxide in the range 0. 2-5 mpa and at temperatures up

to 473 K.," *Journal of Chemical and Engineering Data*, 26, 388–391, 1981.

[445] G. Müller, E. Bender, and G. Maurer, "Das Dampf-Flüssigkeitsgleichgewicht des ternären Systems Ammoniak-Kohlendioxid-Wasser bei hohen Wassergehalten im Bereich zwischen 373 und 473 Kelvin," *Berichte der Bunsengesellschaft für Phys. Chemie*, 92, 148–160, 1988.

[446] Álvaro Pérez-Salado Kamps, Eckehard Meyer, and Bernd Rumpf, and G. Maurer*, "Solubility of CO_2 in Aqueous Solutions of KCl and in Aqueous Solutions of K_2CO_3," 2007.

[447] W. Yan, S. Huang, and E. H. Stenby, "Measurement and modeling of CO2 solubility in NaCl brine and CO_2–saturated NaCl brine density," *Int. J. Greenh. Gas Control*, 5, 1460–1477, 2011.

[448] M. Zirrahi, R. Azin, H. Hassanzadeh, and M. Moshfeghian, "Mutual solubility of CH_4, CO_2, H_2S, and their mixtures in brine under subsurface disposal conditions," *Fluid Phase Equilib.*, 324, 80–93, 2012.

[449] K. Song and R. Kobayashi, "Water content of CO_2 in equilibrium with liquid water and/or hydrates," *SPE Form. Eval.*, 1987.

[450] T. Nakayama, H. Sagara, K. Arai, and S. Saito, "High pressure liquid liquid equilibria for the system of water, ethanol and 1,1-difluoroethane at 323.2 K," *Fluid Phase Equilib.*, 38, 109–127, 1987.

[451] a. Bamberger, G. Sieder, and G. Maurer, "High-pressure (vapor+liquid) equilibrium in binary mixtures of (carbon dioxide+water or acetic acid) at temperatures from 313 to 353 K," *J. Supercrit. Fluids*, 17, 97–110, 2000.

[452] A. Chapoy, R. Burgass, B. Tohidi, J. Austell, and C. Eickhoff, "Effect of common impurities on the phase behavior of carbon-dioxide-rich systems: minimizing the risk of hydrate formation and two-phase flow," *SPE J.*, 16, SPE-123778-PA, 2011.

[453] M. Yarrison, "Water Content of High Pressure, High Temperature Methane, Ethane and Methane+ CO_2, Ethane+ CO_2," *Gas Process. Assoc. Tulsa, OK*, 2008.

[454] K. Song and R. Kobayashi, "The Water Content of CO_2-rich Fluids in Equilibrium with Liquid Water or Hydrate," *Gas Process. Assoc. Res. Rep. RR-80*, 19, 1984.

[455] S. Huang, A. Leu, H. Ng, and D. Robinson, "The phase behavior of two mixtures

of methane, carbon dioxide, hydrogen sulfide, and water," *Fluid Phase Equilib.*, 19, 21–32, 1985.

[456] Beer, "Bestimmung der Absorption des rothen Lichts in farbigen Flüssigkeiten," *Ann. der Phys. und Chemie*, 162, 78–88, 1852.

[457] C. S. Goldenstein, J. B. Jeffries, and R. K. Hanson, "Diode laser measurements of linestrength and temperature-dependent lineshape parameters of H_2O-, CO_2-, and N_2-perturbed H_2O transitions near 2474 and 2482nm," *J. Quant. Spectrosc. Radiat. Transf.*, 130, 100–111, 2013.

[458] K. Althaus, "Relationship Between Water Content and Water Dew Point Keeping in Consideration the Gas Composition in the Field of Natural Gas. Fortschritt-Berichte," *Tech. Monogr.*, 14, 2004.

[459] A. Chapoy, C. Coquelet, and D. Richon, "Solubility measurement and modeling of water in the gas phase of the methane/water binary system at temperatures from 283.08 to 318.12 K and pressures up to 34.5," *Fluid Phase Equilib.*, 214, 101–117, 2003.

[460] A. Chapoy, C. Coquelet, and D. Richon, "Solubility measurement and modeling of water in the gas phase of the methane/water binary system at temperatures from 283.08 to 318.12 K and pressures up to 34.5 MPa," *Fluid Phase Equilib.*, 214, 101–117, 2003.

[461] M. Rigby and J. Prausnitz, "Solubility of water in compressed nitrogen, argon, and methane," *J. Phys. Chem.*, 72, 330–334, 1968.

[462] P. Gillespie, G. Wilson, and G. P. Association, "Vapor-liquid and liquid-liquid equilibria: water-methane, water-carbon dioxide, water-hydrogen sulfide, water-npentane, water-methane-npentane," 1982.

[463] C. Yokoyama and S. Wakana, "Vapor-liquid equilibria in the methane-diethylene glycol-water system at 298.15 and 323.15 K," *J. Chem. Eng. Data*, 33, 274–276, 1988.

[464] R. Sultanov, V. Skripka, and A. Namiot, "Moisture content of methane at high temperatures and pressures," *Gazov. Promst*, 6, 4372–4387, 1971.

[465] F. Tabasinejad, R. G. Moore, S. A. Mehta, K. C. Van Fraassen, Y. Barzin, J. A. Rushing, and K. E. Newsham, "Water Solubility in Supercritical Methane,

Nitrogen, and Carbon Dioxide: Measurement and Modeling from 422 to 483 K and Pressures from 3.6 to 134 MPa," *Ind. Eng. Chem. Res.*, 50, 4029–4041, 2011.